UNIVERSITÀ DEGLI STUDI DI PADOVA

DIPARTIMENTO DI COSTRUZIONI E TRASPORTI

SCUOLA DI DOTTORATO DI RICERCA IN SCIENZE
DELL'INGEGNERIA CIVILE ED AMBIENTALE – CICLO XXI
Sede Amministrativa: Università degli Studi di Padova

COMPOSITE STEEL TRUSS AND CONCRETE BEAMS AND BEAM-COLUMN JOINTS FOR SEISMIC RESISTANT FRAMES

Modelling, numerical analysis and experimental verifications

Direttore della Scuola:	Ch.mo Prof. **STEFANO LANZONI**
Supervisore:	Ch.mo Prof. **RENATO VITALIANI**
Controrelatore	Ch.mo Prof. **FILIP C. FILIPPOU**

Dottorando: **LEOPOLDO TESSER**

FEBBRAIO 2009

Contents

Contents I

Summary VII

Sommario XI

1 Structural typology, Italian Code and Eurocode frameworks 1

1.1 Introduction 1

1.2 Composite Steel Truss and Concrete Typology 2

1.3 Italian Code and Eurocode framework 7

1.4 Merit vs. defect valuation 8

2 Nonlinear analysis of Reinforced Concrete frames 13

2.1 Introduction 13

2.2 Concrete damage model 15

2.3 Reinforcing steel buckling and steel damage model 17

2.4 Global Damage Indexes 20

2.5 LDIs and GDIs in the beam fibre model 21

2.6 Validation examples 22

2.6.1 Validation test N.1 23

2.6.2 Validation test N.2 25

2.6.3 Validation test N.3 26

2.6.4 Conclusions to the validation tests 27

2.7 Nonlinear analyses of an high ductility RC frame 27
2.7.1 Building design 27
2.7.2 Nonlinear static analysis of the frame 28
2.7.3 Nonlinear dynamic analysis of the frame 30
2.7.4 GDIs and performance levels 33
2.8 Nonlinear analyses of an existing RC frame 34
2.8.1 Building characterization 34
2.8.2 Nonlinear static analysis of the frame 35
2.8.3 GDIs and performance levels 35
2.9 Conclusions 36

3 Composite Steel Truss and Concrete beam mechanics 41
3.1 Introduction 41
3.2 General principles on the CSTC mechanics 42
3.2.1 Simplified analysis of creep effects 42
3.2.2 Effective width of flanges for shear lag 43
3.3 First phase ultimate and serviceability limit states 44
3.4 Second phase bending Ultimate Limit State 46
3.4.1 Positive bending Ultimate Limit Sate 46
3.4.2 Negative bending Ultimate Limit State 48
3.5 Second phase shear Ultimate Limit State 49
3.6 Second phase connection Ultimate Limit State 51
3.7 Second phase Serviceability Limit States 52
3.7.1 Simplified analysis of shrinkage effects 52
3.7.2 Stress Serviceability Limit State 53
3.7.3 Deformation Serviceability Limit State 53
3.7.4 Concrete cracking Serviceability Limit State 54
3.8 Complete analysis of stresses, shrinkage and creep effects 59
3.9 Conclusions 61

4 Composite Steel Truss and Concrete beam experimental tests 65

4.1 Introduction 65

4.2 Lab equipment and measure instruments 66

4.3 REP®-NOR beams 68

4.3.1 Experimental test design 68

4.3.2 Material characterization tests 71

4.3.3 Experimental test results and analyses 72

4.3.4 Nude trusses 1 73

4.3.5 Nude trusses 2 74

4.3.6 Composite beams 3 76

4.3.7 Composite beams 4 77

4.4 Ecotrave® Raftile® Beams 80

4.4.1 Experimental test design 80

4.4.2 Material characterization tests 85

4.4.3 Experimental test results and analyses 85

4.4.4 Nude trusses 102n 86

4.4.5 Composite beams 101 88

4.4.6 Composite beams 102 91

4.4.7 Composite beams 103 93

4.5 PREREP® beams 96

4.5.1 Experimental test design 96

4.5.2 Material characterization tests 106

4.5.3 Experimental test results and analyses 106

4.6 Conclusions 111

5 Reinforced Concrete beam-column joints 115

5.1 Introduction 115

5.2 Reinforced Concrete joints 116

5.2.1 General criteria 116

5.2.2 Column behaviour 118
5.2.3 Joint shear forces 119
5.2.4 Effects of column axial compression 124
5.2.5 Evaluation of the two resistant mechanisms 125
5.2.6 Observations 126
5.3 RC joint Code prescription comparison 127
5.3.1 General criteria 127
5.3.2 Depth of member in interior joint 128
5.3.3 Flexural strength of column 129
5.3.4 Shear force acting on the joint 129
5.3.5 Shear strength of joint 130
5.3.6 Effective joint area 132
5.3.7 Nominal shear stress of the joint 132
5.3.8 Design of shear reinforcement 133
5.3.9 Horizontal shear reinforcement 133
5.3.10 Vertical shear reinforcement 135
5.3.11 Detailing for shear reinforcement 135
5.3.12 Observations 136
5.4 Joint test structural design 137
5.4.1 Test joint static scheme 137
5.4.2 Design of the RC joint 138
5.5 Numerical models 141
5.5.1 Mesh properties 141
5.5.2 Material properties 141
5.5.3 Solution algorithm 142
5.5.4 Verification of finite element model 142
5.6 Numerical analysis 144
5.6.1 Two-dimension analyses 144

5.6.2 Three-dimension analyses 147
5.7 Conclusions 152

6 Composite Steel Truss and Concrete beam-column joints 157
6.1 Introduction 157
6.2 CSTC beam-column joint theory and design 157
6.2.1 General criteria 158
6.2.2 Resistant mechanism evaluation 160
6.2.3 CSTC joint design 163
6.3 Numerical analyses of CSTC beam-column joint 173
6.3.1 Two-dimensional numerical models 173
6.3.2 Three-dimensional numerical models 177
6.4 Conclusions 183

7 A new joint between CSTC beams and CFT columns 187
7.1 Introduction 187
7.2 Composite joint theory and design 188
7.2.1 General criteria 188
7.2.2 CSTC beam-CFT column joint description 190
7.2.3 CSTC beam-CFT column joint design 194
7.3 Numerical analyses 197
7.3.1 Numerical model 197
7.3.2 Analysis results 200
7.4 Conclusions 210

8 Conclusions 213

Acknowledgment

Summary

The Composite Steel Truss and Concrete (CSTC) beams and beam column joints are the subject of the present work. The CSTC beam are composed by prefabricated steel trusses embedded in cast in place concrete. The main features of the steel trusses are that they can bear their own weight and the weight of the slabs without any provisional support during the first phase and then they can collaborate with the cast in place concrete. The recent Italian Code DMLLPP 14/01/2008 mentions the composite steel truss and concrete structures and establishes that the use of this typology requires the authorization of the Italian Superior Council of Public Works without any other specification. The CSTC type isn't included in any other existing construction type of Italian or International Codes and it needs particular design rules. The research aims are the verification of their efficiency, the development of a reliable calculation method, the application of the composite steel truss beams for seismic resistant frame, the design and the verification of innovative joints with all the necessary good seismic performance requirements.

Firstly it has been focused on the reinforced concrete seismic resistant frames in order to fully understand the solicitations, that they have to withstand, and to underscored all the characteristics that can determine their behaviour in terms of stiffness, strength and ductility. In the framework of continuum damage theory, a new two-parameter damage model for concrete has been proposed. In particular, a new concrete compressive damage evolution law has been developed to evaluate the effect of confining reinforcement in RC structure better. With the aim of describing, in a unitary approach, the steel behaviour, specific steel damage indexes have been formulated, taking into account the plastic strain development and the possibility of rebar buckling. A new methodology to estimate the critical buckling load has been formulated, which turned out to be in good agreement with experimental results. An improved and generalized definition of the global damage indexes has finally been proposed, in order to obtain powerful tools to estimate the performance and the state of a RC structure. The improved model has been implemented into a fibre research FEM code, which has been used to carry out nonlinear analyses of tests examples and of a RC concrete frame structure. In particular, the reliability of the model has been demonstrated by comparison with trusted experimental tests on RC column axially loaded and subjected to

imposed transversal displacements, some of which had presented the rebar buckling. The static and dynamic nonlinear analyses of two RC frames, respectively one designed in high ductility class and one with weak-columns at the ground floor, have been carried out and the model has demonstrated its ability to describe the dynamic behaviour, the failure mechanism and the energy dissipation of both frames efficiently and accurately. The RC frames investigated with the fibre approach have been studied with a concentrated plastic hinge approach as suggested by FEMA 356. A clear correlation between the GDIs here proposed and the Performance Level proposed by FEMA has been demonstrated for the test examples.

The CSTC beam mechanics have been analyzed and a new calculation method has been proposed in the Limit State assessment method framework. Every Ultimate and Serviceability Limit Sates have been defined and correlated to the beam performances. The hardening of the completion concrete cast distinguishes two phases in the life of the CSTC beam that are characterized by distinct resistant sections and different mechanics. During the first phase the beam behaves as a prefabricated steel truss. In the second phase the steel truss collaborates with the hardened concrete. The mechanics of the CSTC beam have been studied for the first and second phases.

The developed method has been used to predict and analyze the experimental tests carried out in the Department of Construction and Transportation of the University of Padua. Three sets of experimental tests, conduced on composite steel truss and concrete beams, have been presented and their results analyzed. In particular eight REP®-NOR beams, six ECOTRAVE® RAFTILE® and two PREREP® beams have been designed and tested. The global deformability, the bending and the shear resistant mechanisms, the global ductility, the cracking phenomena have been studied. The results have been compared to those obtained by means of the calculation method presented. The beam mechanics have been confirmed and the method has demonstrated to be efficient and precise to assess the behaviour of the CSTC beams even with very different and innovative solutions. The experimental results have demonstrated the efficiency of the proposed design method and the interesting features of the studied structural type like its strength and ductility properties.

The reinforced concrete joint mechanics have been exposed, recalling the main theory and their recent development. Two resistant mechanisms have been evaluated, the concrete strut one and the diagonal compressed field or truss one. Their contribution for the total joint shear strength has been investigated. The theory can then explain all the Code prescriptions and be applied to generalized joint problem. The Eurocode, similar to the Italian code, and ACI 318M code provisions have been compared and the main points have been underlined. A test structural joint element has been defined and designed according to the actual Italian and European Code in high seismicity region. The problem of the accurate numerical analysis of reinforced concrete has been faced. The validation examples have been

carried out comparing the numerical results with the experimental ones. Using two dimensional and three dimensional models, it has been possible to evaluate efficiently and accurately the behaviour of the designed reinforced concrete test joint. The numerical analyses have shown all the features and the issues underlined by the theory. The numerical results have been compared qualitatively and quantitatively with the ones obtained by theoretical simplified schemes showing a good agreement.

Starting from theoretical considerations a new CSTC joint has been proposed. The main aim is to reach an adequate stiffness, strength and ductility in sight of the application on seismic resistant frames. The similarity of the resisting mechanisms has permitted the extension of the RC theory to the joint shear resistant of the CSTC structural type. The calculation of the proposed joint started with the investigations of possible admissible stress distribution within the joint and it follows with their quantitative evaluations. By means of the numerical model studied and validated on the RC structures, the analysis of the designed joint have been carried out. Both two dimensional and three dimensional analysis results have been presented along with their comparison with the RC joint ones. The numerical analysis showed the achievement of important targets as the joint stiffness, the joint strength and the joint ductility. The capacity of dissipating energy has been also assessed and compared with the RC one. The results confirm the efficiency of the proposed CSTC joint.

An innovative composite beam-column joint has been studied for applications in medium-low seismicity regions. The joint connects composite steel truss and concrete beams and concrete filled steel tube columns. The main concept of this joint is to conserve the continuity of the column steel tube between one storey and the following one by means of blind cold connection. Additional elements, which passes through the joint to restore the beam continuity, have been proposed. The proposed connections require little manpower work in the construction site reducing the number of operations and the working time. The resulting joint is a special kind of composite steel and concrete structure in which the steel and the concrete collaborate to sustain the solicitations. The assessment of the joint has been made using the Eurocode 3 and 4. The verification of the joint behaviour has been done by means of numerical analyses and a finite element method program has been used with different modelling solutions. The results confirmed the efficiency of the proposed composite beam-column joint.

Sommario

L'oggetto della presente Tesi di Dottorato riguarda lo studio delle travi tralicciate composte acciaio e calcestruzzo e dei nodi trave pilastro ideati per l'impiego di tale tipologia strutturale. Le travi tralicciate composte sono costituite da tralicci di acciaio prefabbricati conglobati in getti di calcestruzzo comunemente realizzati in cantiere. Le principali caratteristiche dei tralicci di acciaio sono l'autoportanza nei confronti del peso proprio e di quello del solaio senza alcun ulteriore supporto provvisionale e la collaborazione con il getto di calcestruzzo quando esso indurisce. La recente norma italiana DMLLPP 14/01/2008 fa menzione della tipologia strutturale tralicciata composta e stabilisce che il suo impiego richiede la preventiva autorizzazione del Consiglio Superiore dei Lavori Pubblici senza fornire alcuna altra specifica. L'assenza quindi di normativa Italiana e Internazionale a riguardo richiede la formulazione di regole di progetto specifiche. Gli scopi della ricerca sono la verifica dell'efficienza di questo sistema strutturale, lo sviluppo di un metodo di calcolo attendibile, l'applicazione delle travi tralicciate composte in telai sismo resistenti, il progetto e la verifica di innovativi nodi trave-pilastro con adeguate prestazioni anti sismiche.

Come primo obiettivo, si sono focalizzati i telai in cemento armato sismo resistenti per comprendere a pieno le sollecitazioni a cui sono soggetti e per analizzare tutte le caratteristiche che possono condizionare il loro comportamento in termini di rigidezza, resistenza e duttilità. Nel quadro della teoria del danno continuo, è stato proposto un nuovo modello di danno a due parametri per il calcestruzzo. In particolare è stata sviluppata una nuova legge di evoluzione del danno a compressione per il calcestruzzo per una migliore valutazione degli effetti delle armature di confinamento nelle strutture di cemento armato. Allo scopo di descrivere il comportamento dell'armatura in un approccio unitario, sono stati formulati specifici indici di danno per l'acciaio, prendendo in considerazione lo sviluppo della deformazione plastica e il fenomeno dell'instabilità delle barre compresse. È stata inoltre formulata una nuova metodologia per stimare il carico critico delle barre che risulta in ottimo accordo con i risultati sperimentali. Infine è stata proposta una migliore e generalizzata definizione degli indici di danno globali con lo scopo di ottenere strumenti efficaci nella caratterizzazione delle prestazioni di strutture in cemento armato. Il modello sviluppato è stato implementato in un codice di ricerca agli elementi finiti con modello a

fibre, il quale è stato validato mediante la comparazione di analisi non lineari di strutture sottoposte a prove sperimentali. In particolare, è stata dimostrata l'affidabilità del modello mediante la comparazione con i risultati di esperimenti condotti in colonne di cemento armato alcune delle quali hanno presentato l'instabilità delle barre compresse. Sono state condotte analisi statiche e dinamiche non lineari di telai in cemento armato progettati con o senza i criteri di alta duttilità e il modello si è dimostrato in grado di descrivere in modo efficiente ed accurato il comportamento dinamico, i meccanismi di collasso e l'energia dissipata. Gli stessi telai sono stati poi studiati mediante un approccio a cerniere plastiche concentrate così come proposto dalla normativa Americana FEMA 356. È stata proposta e indagata una correlazione tra i livelli di prestazione contenuti nella normativa FEMA e gli indici di danno globali.

La meccanica delle travi tralicciate composte è stata analizzata ed è stato proposto un innovativo metodo di calcolo nell'ambito del metodo Semiprobabilistico agli Stati Limite. Ogni Stato Limite Ultimo e di Esercizio è stato definito e correlato alle prestazioni delle travi. L'indurimento del getto di completamento distingue due fasi nella vita delle travi tralicciate che sono caratterizzate da differenti sezioni resistenti e conseguentemente da una meccanica differente. Durante la prima fase le travi si comportano come tralicci di acciaio prefabbricati, mentre nella seconda i tralicci di acciaio collaborano con il calcestruzzo indurito. Per entrambe le fasi sono stati proposti metodi di calcolo e verifica del comportamento delle travi.

Il metodo così sviluppato è stato impiegato per predire e analizzare le prove sperimentali condotte presso il Laboratorio di Prove sui Materiali da Costruzione del Dipartimento di Costruzioni e Trasporti dell'Università di Padova. Sono presentate tre serie di prove sperimentali su travi tralicciate con le relative analisi dei risultati ottenuti. In particolare sono state progettate e sottoposte a prova: otto travi REP®-NOR, sei travi ECOTRAVE® RAFTILE® e due travi PREREP®.Sono stati studiati la deformabilità globale, i meccanismi resistenti a flessione e taglio e i fenomeni di fessurazione e decompressione. I risultati sono stati comparati con quelli ottenuti per mezzo del metodo di calcolo presentato. La meccanica delle travi è stata così confermata e il metodo di calcolo si è dimostrato efficiente e preciso nella valutazione del comportamento di travi tralicciate, alcune delle quali presentavano soluzioni costruttive distinte ed innovative.

La meccanica del nodo trave pilastro in cemento armato è stata poi analizzata, richiamando le principali teorie e i loro recenti sviluppi. Sono stati valutati i due meccanismi di resistenza del nodo ovvero quello del puntone di calcestruzzo e quello a traliccio d'armatura. È stato investigato il loro contributo nell'assorbire il taglio totale che sollecita il nodo per effetto di azioni sismiche. Sono state così chiaramente esplicitate tutte le prescrizioni contenute nelle normative di merito in vista dell'applicazione a nodi di

geometrie e caratteristiche distinte. Sono state quindi confrontate le prescrizioni dell'Eurocodice e della normativa Americana ACI 318M nei loro apsetti fondamentali. È stato poi definito un nodo trave-colonna da impiegarsi come struttura di riferimento ed è stato progettato in cemento armato secondo la vigente normativa Europea e Italiana. Si è affrontato di seguito il problema dell'analisi numerica accurata di tale nodo. I modelli numerici proposti sono stati validati tramite confronti con risultati sperimentali. Tramite l'impiego di analisi bi- e tri- dimensionali è stato possibile valutare in modo appropriato il comportamento del nodo progettato. Lo sviluppo teorico ha così trovato conferma nelle analisi numeriche sia qualitativamente che quantitativamente.

Partendo da considerazioni teoriche, è stato proposto un innovativo nodo per travi tralicciate miste. Lo scopo principale è stato quello di raggiungere adeguate rigidezza, resistenza e duttilità in telai sismo-resistenti. La similarità dei meccanismi resistenti ha permesso di estendere la teoria dei nodi di cemento armato alla tipologia tralicciata mista. Il calcolo dei nodi proposti parte dallo studio di distribuzioni di tensioni staticamente ammissibili all'interno del nodo e segue con la loro valutazione quantitativa. Per mezzo degli strumenti di analisi numerica studiati e validati con le strutture di cemento armato, sono state eseguite le analisi dei nuovi nodi progettati. Anche in questo caso analisi bi- e tri-dimensionali sono presentate assieme al loro confronto con le corrispettive dei nodi in cemento armato. Le analisi numeriche mostrano il raggiungimento di obiettivi importanti quali la rigidezza del nodo, la sua resistenza e la sua duttilità. È stata altresì verificata la capacità del nodo di dissipare energia confrontandola con quella del nodo in cemento armato. I risultati confermano l'efficienza della soluzione di nodo in tipologia tralicciata mista proposta.

Infine, è stato studiato un innovativo nodo di tipologia strutturale composta per applicazioni in zone a medio-bassa sismicità. Il nodo è stato pensato per connettere travi tralicciate composte e pilastri di calcestruzzo con camicia esterna di acciaio. Il principale spunto del nodo è quello di conservare la continuità della camicia di acciaio attraverso il nodo per mezzo di connessioni a freddo con bulloni ciechi. Sono stati quindi proposti elementi strutturali aggiuntivi, che oltrepassano la colonna in corrispondenza del nodo, con il compito di ripristinare la continuità. Le connessioni proposte richiedono un limitato impiego di manodopera in cantiere riducendo così il numero di lavorazioni e i tempi di costruzione. Il nodo risultante è un tipo speciale di struttura composta acciaio e calcestruzzo, collaborando l'acciaio con il calcestruzzo nel sostenere le sollecitazioni. Il progetto del nodo è stato condotto secondo le prescrizioni della vigente normativa Italiana ed Europea. La verifica del comportamento del nodo composto è stata eseguita per mezzo di analisi numeriche con programmi agli elementi finiti valutando differenti soluzioni di modellazione. I modelli numerici hanno tenuto conto della limitazione delle tensioni di

trazione all'interfaccia tra camicia di acciaio e calcestruzzo delle travi. Grazie a tale accurata modellazione, i relativi risultati possono essere considerati affidabili e precisi. Le analisi hanno quindi confermato l'efficienza del nodo trave-pilastro proposto in struttura mista acciaio e calcestruzzo.

Chapter 1

Structural typology, Italian Code and Eurocode frameworks

1.1 Introduction

Nowadays in Italy composite steel truss and concrete beams, also called hybrid truss beams, have been more and more used because they allow high construction speed, minimum site labour and economical convenience. These beams are composed by prefabricated steel trusses embedded in cast in place concrete. The main features of the steel trusses are that they can bear their own weight and the weight of the slabs without any provisional support during the first phase and then they can collaborate with the cast in place concrete. The concrete doesn't have any other longitudinal or web transverse reinforcement. The inventor of these beams was Salvatore Leone, who patented them in 1967 and deposited his own production rules and assessment methods in the Italian Superior Council of Public Works. The last decade showed an increasing number of constructions using this structural typology in Italy, whereas the only similar structures abroad are the one called concrete composite truss, with the evident difference that their webs are made only by diagonal members and not by concrete solid webs [1] ÷ [3].

The composite truss typology is outlined in between the reinforced concrete and the composite steel concrete ones since it has some peculiar characteristics of both of them. This fact causes the issue of the right placing in the Italian Code [4] and in the Eurocode [5] ÷ [7] frameworks [8] ÷ [10]. As consequences a recent series of theoretical and experimental works has been made to fully understand this typology behaviour and its resistant mechanisms in order to create a solid background to base its design and assessment methods [8], [11] ÷

[17].

This structural typology has been applied to isostatic beams and now the development is in progress for the hyperstatic ones. The new research field is the application of the composite steel truss beams for seismic resistant frame. In fact the first sets of experimental tests carried out have demonstrated that this beam typology can show an useful plastic behaviour under certain conditions and with accurate details [8], [9], [11], [17]. Then, the next step is to conceive a joint with all the necessary good seismic performance requirements and also with the further characteristic of being easy to assemble [9], [10], [18]. Towards this direction, innovative beam-column joints, that allow the employment of the composite steel truss and concrete beams even in seismic resistant frames, are presented. The new joints are designed to obtain a resisting strength higher than the demanding one, to control the deformability both in the Serviceability and Ultimate Limit States, to eliminate brittle mechanisms, to promote ductile ones and above all to confine concrete. The design of these joints has been made by means of the application of the study of the RC resistant mechanisms on the new structural elements starting from Paulay [19]. The proposed joints have also been simulated under static and dynamic conditions by means of nonlinear numerical analysis, using improved finite element programs. These analyses were carried out in order to highlight three important key parameters that are the cracking, associated with a first distinct stiffness change, the steel yielding, associated with another stiffness change and the maximum strength response, related to the concrete crushing phenomena. Particular efforts were made towards the joint versatility. As a result, they can be profitably used in conjunction with various column typologies such as concrete filled steel tube ones. The design of the joints and the analyses have been made in view of the successive experimental tests in which the performance of the new composite steel truss and concrete joints will be compared with high ductility reinforced concrete beam-column one.

1.2 Composite Steel Truss and Concrete Typology

Since the invention of the REP® beams by S. Leone in early 60s, the development of this beam type has followed different path leading to very different products. Not only the first brand REP® have proposed distinct evolutions but even other companies, copying the main idea, have launched many other beams that differ substantially from the original one. The researchers understood immediately that these beams cannot be treated as reinforced concrete beam even if they have many characteristics in common. The purpose of this paragraph is to propose an English name to this typology, since it has become popular only

in Italy, and to draw a definition. Hence it is necessary to outline their essential characteristics.

The Italian common name varies between typology "*reticolare composta*" or "*tralicciata mista*" "*acciaio-calcestruzzo*" with possible word interchanges. These name can find a translation in English in "composite steel truss and concrete" (hereinafter also CSTC) typology that is similar to the already existent "concrete composite truss" [1] ÷ [3] (see also Fig. 1.1 and Fig. 1.2).

Fig. 1.1: Composite steel and concrete truss bridges: Yamaguragawa Bridge (Japan) and Kinogawa Bridge (Japan)

Fig. 1.2: Pedestrian composite steel and concrete truss bridge of Arsenal's Emirates Stadium (United Kingdom)

The similarity is the presence of a steel truss in a composite steel and concrete structure. The immediate difference is that in the concrete composite truss typology the truss remain nude giving the whole structure a truss shape, whereas in the composite steel truss and concrete one the truss is surrounded by a concrete cast that determines the external shape of the structure. Another important difference is that, in the composite truss typology, even only the truss constitute a structure on its own and it is supposed to carry all the loads applied before the concrete hardening without any provisional support. Exactly this second property leads to the distinction of two phases in the life of a composite steel truss and concrete structure. The first one considers the structure made only by the truss while the

second phase concerns the structure composed also by the hardened concrete cast. The writer's opinion is that these two principal characteristics can define the composite steel truss and concrete typology.

It is necessary to explain better what steel truss stands for, since various types of beam truss were developed without changing its mechanics. In fact the original beam truss is made by welding steel elements that are plates, straight and curved bars (see Fig. 1.3).

Fig. 1.3: Leone's original composite steel truss and concrete beams with the inferior steel plate (Italy)

The typical assembly was the plate as the bottom chord, two or more straight bars as top chord and one or more sequences of curved bars to from the diagonal truss members. These last diagonal bars are usually convergent in the top chord in such a way to give the truss a typical triangle section to provide it with stiffness against the torsion and the out of plane buckling. The bottom chord has been thought out to support the slab. Different kind of bottom chord were developed creating a concrete base at the place of the steel plate (see Fig. 1.4).

Fig. 1.4: Leone's composite steel truss and concrete beams with the inferior concrete base (Italy)

In this case the diagonal bars are welded to some lower straight bars embedded in a prefabricated reinforced concrete base. This kind of beam truss maintains the original concept of the steel truss even if the bottom chord is not made by steel only and behaves differently from the local point of view. Similar considerations can be drawn for other types

of bottom chord i.e. the one made by "S" section profiled steel plates where the particular shape is used to support a lower clay tile that constitutes the bottom finish of the beam (see Fig. 1.5). Since the global behaviour of these beam types is similar they should be comprised in the composite steel truss and concrete typology and the name can be justified seeing that the skeleton of the truss is made by steel in all the cases.

Fig. 1.5: Tecnostrutture's composite steel truss and concrete beams with the inferior clay tile (Italy)

A composite steel truss and concrete element necessitates of an huge welding amount. This is the reason why the original trusses were made with structural steel (usually S355). The later apparition of weldable reinforcing steel even ribbed let the choice of the steel material. The weldability requirement is based on the maximum contents of chemical elements (C, P, S, N) and verified by chemical analyses both for the casting and for the final product.

The Italian Code gives the following limitations for the maximum contents of chemical elements (%)

Chemical element	final product analysis	casting analysis
Carbon (C)	0.24	0.22
Phosphorous (P)	0.055	0.050
Sulphur (S)	0.055	0.050
Copper (Cu)	0.85	0.80
Nitrogen (N)	0.014	0.012
Equivalent Carbon (C_{eq})	0.52	0.50

where the equivalent carbon is computed with the following formula:

$$C_{eq} = C + Mn/6 + (Cr + Mo + V)/5 + (Ni + Cu)/15$$

Another requirement for the weldability is the absence in the productive process of

hardening by means of cold plastic deformation. In fact when the material is leaded to the fusion in a certain region close to the welding point, it loses its mechanical characteristics due to the previous hardening process.

The benefit of having ribbed bars is the better bond between the steel bar and the concrete. But some considerations are necessary. The first one is that the reinforcing steel ribs make the welding process difficult. The second one is that the fabrication of the truss often needs to bend the diagonal members and their integrity should be verified. In general that brings to a restriction for the minimum bending diameter depending on the bar diameter. The production rules of the REP® beams deposited at the Italian Superior Council of Public Works [20], that uses only structural steel, declares a minimum bending diameters equal of four times the bar diameter. For the reinforcing steel B450C, The Italian Code [4] and Eurocode 2 [5] prescribe bending and rebending tests after which the specimen shall not have any clique. The minimum bending diameter is prescribed as follows:

bar diameter	minimum bending diameter: Italian Code	Eurocode 2
$\phi < 12$ mm	4 ϕ	4 ϕ
$12 \leq \phi \leq 16$ mm	5 ϕ	4 ϕ
$16 < \phi \leq 25$ mm	8 ϕ	7 ϕ
$25 < \phi \leq 40$ mm	10 ϕ	7 ϕ

If a medium size truss web bars are bent respecting these limitations the subsequent eccentricities of the resulting truss joints can become very disadvantageous in the design. Another consideration is that a classical joint of a typical steel truss provide concrete with supports by which the transmission of the solicitation between the two material is possible and efficient. This fact reduces the importance of increasing the bond resistance all along the steel bar. All these reasons have been yielded the structural steel the most applied and preferred material even if other choice can be possible. The welding method are the manual Shielded Metal Arc Welding, also known as Manual Metal Arc Welding, and the automatic, or semi-automatic, Gas Metal Arc Welding that can be Metal Inert Gas using Argon or Metal Active Gas using Carbon Dioxide. The wire electrodes have to be adequate to the steel type and to the shielding gas according to the in force Codes.

For what concerns the concrete material, there can be a lot of freedom in the choice of its characteristics. The fact that the completion cast is usually done in place conditions the possibility to have an high strength one from the economical point of view. Whereas the truss concrete base, especially if pre-stressed, belongs to higher classes. In the case of truss with concrete base, the packing reinforcement is of reinforcing steel and its percentage is usually very low. The possible pre-stressing steel is the usual high strength one, that respect

the code requirements, in wires, bars or strands.

1.3 Italian Code and Eurocode framework

The recent Italian Code [4] mentions the composite steel truss and concrete structures in the paragraph 4.6 that is under "*other material constructions*". It establishes that the use of this typology requires the authorization of the Italian Superior Council of Public Works and it doesn't contain any other specification. It means that the composite steel truss and concrete structures are considered outside from reinforced concrete, steel, composite steel and concrete construction types and the Code doesn't provide any design methods. Some preliminary considerations can be drawn. During the first phase the steel truss, if it is made only by steel, has to be considered a steel construction and can be designed according with the corresponding rules. The completed composite steel truss and concrete member cannot be considered a reinforced concrete construction since the steel truss cannot usually be anchored only by bond forces, although the truss in the second phase can be seen as a system of particular concrete reinforcements. In fact the welded joints of the truss can be considered as connectors. In the same Code the definition of the composite steel and concrete structure writes: "*the composite structures are formed by structural steel parts and by reinforced concrete ones (ordinary or pre-stressed) made collaborating by means of a connection system accurately designed*" and the connection system as "*the device suitable for the transmission of the tangential forces*".

The Eurocode 4 [6] doesn't mention the CSTC type. It defines a composite member as "*a structural member with components of concrete and of structural steel or cold-formed steel, interconnected by shear connection so as to limit the longitudinal slip between concrete and steel and the separation of one component from the other*" and the shear connection as "*an interconnection between the concrete and the steel components of a composite member that has sufficient strength and stiffness to enable the two components to be designed as parts of a single structural member*".

The definition of the composite steel and concrete constructions seems match quite well with the composite steel truss and concrete ones both for the Italian Code and the Eurocode, even if the typical constructions of the first type usually has the steel member with solid web. The truss bars are similar to concrete reinforcements especially seeing that the composite steel truss and concrete member doesn't have any additional reinforcement for the cast in place concrete. Instead the bottom plate of the truss can be considered as a steel part connected to the concrete by the truss web bars. It can be noted that, if this connection type could be considered as rigid, the CSTC global mechanics in the second phase would be very

similar to the reinforced concrete ones.

The effects of the two construction phases that induce internal stresses need adequate analysis in order to determine the satisfaction of both the Serviceability and the Ultimate Limit States requirements. From this point of view we can find similarities with the composite steel and concrete structures.

Therefore it is reasonable that the CSTC type isn't included in any other existing construction type and needs particular design rules. The institution by the Italian National Research Council of a national committee with the task to deal with the CSTC construction type is hopeful, although the published theoretical and experimental research studies are still few even for the beams that were the original members with which this structural typology was born.

1.4 Merit vs. defect valuation

The inventor of this construction type, S. Leone, decided the original brand name that is an acronym standing for *Rapidity*, *Efficiency*, *Practicalness*. The owner of the patent had to choose an attractive name to merchandize his product but the success of the REP® beams testify that this type showed its actual suitability in many applications. Getting further in the description of the CSTC type, some peculiar characteristics can be drawn trying also to evaluate its main merits and defects. It has been focused on the CSTC beams that is the original member and the mainly used one. The principal characteristic of this beam type is that the prefabricated truss can bear its own weight, the slab and the concrete cast and, at the same time, its base can be the formwork for the concrete cast. Any other provisional support is not necessary in the first phase. The most efficient application of the CSTC beams is in pair with prefabricated self bearing slabs (see Fig. 1.6).

Fig. 1.6: Pictures of the use of CSTC beams with first phase self bearing slab (Italy)

In this case the use of provisional support is totally avoided. Moreover all the delicate

constructive processes, as the steel cut and welding, are prefabricated. Because of the previous reasons the need of manpower in place is reduced and the construction speed can notably increase. To make that possible the steel truss contains an adequate amount of steel both at the top and at the bottom, that is usually higher than the one of a reinforced concrete beam designed to support similar second phase loads. On the other hand, in general, the higher percent of steel, in a fixed concrete section, can produce higher flexural stiffness, strength and ductility.

The fabrication of the steel truss requires an huge amount of cuts, bends and welds. All these operations are very delicate needing a lot of checks and condition the efficiency of the final product. The possible presence of defects in the steel truss can determine early failure of the structure both in the first and in the second phase. Although the eccentricities on the steel truss are always present and determine the rise up of bending moments on the truss members, rough bends and assemblies make this effect worse. The presence of the steel plate at the beam bottom makes the plastering difficult and it turns out as a possible condensation surface. Therefore the use of steel base is not very common in residential buildings. Whereas the concrete base usually is out of the floor slab depth, being its upper level the support of the slab elements. To overcome this drawbacks a particular base has been proposed and patented as ECOTRAVE® RAFTILE® by the Italian producing company Tecnostrutture srl. It is made by a couple of "S" shaped cold formed steel plates supporting a lower clay tile (see Fig. 1.1). These beams are used together with the classical Italian reinforced concrete slab lightened by perforated brick tiles. In this case the plastering can be very uniform even more than the one using reinforced concrete beams.

Last years have seen an increasing use of the CSTC beams on the bridge engineering field as primary or secondary beams. In fact, in such applications the CSTC self bearing capacity can be extremely convenient. The possibility to have curved or arch shapes, modelling the steel trusses, permits also different architectural and engineering solutions maintaining its benefits (see Fig. 1.7).

Fig. 1.7: Curved and arch steel truss examples (Italy)

References

1. Noritsune T, Yamazaki K, Kusaga A, Kuwano M. Composite truss bridge using suspension structure – Seiun Bridge. *Japan Prestressed Concrete Engineering Association National Report for the Second fib Congress* 2006, 41-44.
2. Kimura Y, Ono T, Minami H, Yamamura M, Seto K. Kinokawa Bridge. *Japan Prestressed Concrete Engineering Association National Report for the Second fib Congress* 2006, 45-48.
3. Katsuragi Y, Shoji A, Osugi T, Kondo T. Monitoring measurement of Kamantani bridge (PC truss bridge) during the construction. *Japan Prestressed Concrete Engineering Association National Report for the Second fib Congress* 2006, 53-56.
4. D M LL PP 14 Jan 2008. Norme Tecniche per le Costruzioni (Construction Technical Codes). *Gazzetta Ufficiale* 04 Feb 2008.
5. CEN. *Eurocode 2: Design of concrete structures Part 1-1: General rules and rules for buildings*. Comité Européen de Normalisation: Bruxelles, 2003.
6. CEN. *Eurocode 4: Design of composite steel and concrete structures Part 1-1: General rules and rules for buildings.* Comité Européen de Normalisation: Bruxelles, 2004.
7. CEN. *Eurocode 8: Design of structures for earthquake resistance Part 1: General rules, seismic actions and rules for buildings*. Comité Européen de Normalisation: Bruxelles, 2003.
8. Scotta R, Tesser L. Preliminary experiences and basic concepts on the structural performance of hybrid trussed beams. *4th Spec. Conference on The Conceptual Approach to Structural Design,* Venice, 2007.
9. Sassone M, Bigaran D, Massa S. Le travi composte nel nuovo quadro normativo (The composite beams in the new code framework). *XVI CTE Congress*, Parma, 2007, 715-723.
10. Petrovich F. *Un nuovo sistema strutturale per edifici multipiano in zona sismica realizzato mediante elementi tralicciati misti acciaio-calcestruzzo: analisi numerica e sperimentale* (A new structural system for multi-storey building in seismic zone made by composite steel truss and concrete elements: numerical and experimental analyses). Ph.D. Thesis, University of Trieste, 2008.
11. Scotta R, Tesser L. Sperimentazione su travi tralicciate miste REP® – NOR (Experimental tests on composite truss beams REP® – NOR). *VII Italian Workshop on Composite Structures*, Benevento, 2008.

12. Puhali R, Smotlack I. Relazione sulle prove di push-out atte a determinare le leggi di carico-scorrimento delle travi in sistema composto REP (Report on the push-out tests fit for the determination of load-slip laws of REP composite truss beams). *Science of Constructions Institute Acts*, University of Trieste, 1980.

13. Giordano G, Spadea G. Stato Ultimo in flessione di travi in cemento armato con doppia armatura tipo REP: ricerca sperimentale (Flexural ultimate state of reinforced concrete beams with double reinforcement REP type: experimental research). *Report n. 65*, Structural Department of University of Calabria, 1983.

14. Giordano G, Ombres L, Spadea G. Modellazione teorica e controllo sperimentale del comportamento a rottura di travi inflesse di tipo REP (Theoretical modelling and experimental verification of the collapse behaviour of REP type bended beams). *L'Industria Italiana del Cemento* 1987, **617**.

15. Di Marco R. Sperimentazione su travi continue REP con traliccio tipo TR (Experimental tests on hyperstatic REP beams with TR truss type). *Internal Report University IUAV of Venice*, 2004.

16. Borri A, Grazini A. Analisi del comportamento di travi tralicciate in c.a. per il miglioramento della risposta sismica degli edifici (Analysis of the reinforced concrete truss beam behaviour for the improvement of the building seismic capacity). *XII ANIDIS Convention*, Pisa, 2007.

17. Scotta R, Tesser L. Sperimentazione su travi tralicciate miste (Experimental tests on composite truss beams). *XVII CTE Congress*, Rome, 2008.

18. Ceccoli C, Mazzotti C, Savoia M, Vincenzi L, Ferrari M. Comportamento dei nodi di un sistema di prefabbricazione (Behaviour of a prefabricated system joints). *XVI CTE Congress*, Parma, 2007, 705-714.

19. Paulay T. Equilibrium Criteria for reinforced concrete beam column joints. *ACI Structural Journal* 1989, **86**: 635-643.

20. Edis® Srl. Norme di produzione per travi REP® (REP® beam production rules). *EDIS-Elaborazione Dati per l'Ingegneria Strutturale ed Infrastrutturale* 1998, NOR 007.

Chapter 2

Nonlinear analysis of Reinforced Concrete frames

2.1 Introduction

The accurate prediction of the structural response of RC buildings subject to strong earthquakes has necessarily to be performed by means of numerical nonlinear analyses. In such analyses, the behaviour of each structural member and of the structure on the whole, even beyond the elastic field, must be described accurately.

The beam fibre approach, [1] ÷ [3], is gathering increasing interest as an alternative to the concentrated plastic hinge procedure to perform non linear analysis of framed R.C. structure, *e.g.* for the seismic hazard assessment of existing buildings (dynamic and pushover analyses). The appeal of using a fibre approach is that neither the preliminary positioning of the plastic hinge, nor the definition of their moment-rotation characteristic curves are needed, even if the number of unknowns remains far lower than that of the classical finite element model. Some problems could arise, with fibre approach, when dealing with the localization problem and the mesh dependency of the solutions [4]. The models based on damage mechanics have shown both the numerical efficiency and the accuracy necessary for a description of brittle materials behaviour, and in particular of concrete ([5] ÷ [13]).

The recent seismic standards associate the achievement of structural performance with compliance with the prescribed levels of structural damage. In particular, FEMA 356 [14] defines the Immediate Occupancy (IO), the Life Safety (LS) and the Collapse Prevention (CP) levels. These damage levels are often evaluated as limiting values of some generalized

deformations that involve each structural member or the structure as a whole. It must be underscored that the concept of Performance Levels, as proposed in FEMA 356 [14] to assess the seismic safety of buildings, cannot be applied when a distributed damage model (like the fibre one) is adopted in substitution for a plastic hinge model. Within a strain-based continuum damage approach, the deformation development is connected with the material damaging in nonlinear field. Therefore the definition of a suitable correlation between the displacement capacity, in any limit state, of the structure and its damage level may be potentially useful to draw reliable technical and economical considerations on the seismic safety of buildings. DiPasquale and Çakmak [15] proposed an objective global damage index defined as a function of the variation of the structure fundamental frequency. This formulation can be applied to an entire structure but not to any of its substructure. Besides, the calculation of the fundamental frequency is not always possible and requires high computational costs. Hanganu *et al.* [12] developed a local and global damage assessment methodology for R.C. structures based on a concrete damage model. According to this work, the global damage indexes were computed as average of the local ones weighted by the elastic energy. In the last work the knowledge of the damage state of a R.C. structure seems incomplete since the damage indexes referred only to the concrete material. In fact, when the structural behaviour is determined by steel yielding, the concrete damage indexes alone cannot give a real description of the performance of the structure itself [16].

In this paper, an effective and reliable method to perform nonlinear analyses of reinforced concrete frame systems has been developed, based on the theory of damage mechanics to describe the materials behaviour and on the fibre approach to model the structural behaviour. An improved two-parameter plastic damage law for concrete, derived from the works by Faria *et al.* [7] and Saetta *et al.* [9]-[10]. As for the reinforcing steel, a specific index, named "steel damage index", is proposed to measure the plastic strain development in steel, that is, to measure the ductility level required of the steel. The reinforcement constitutive law accounts also for the possibility of buckling of the compressed longitudinal bar, *e.g.* [17] ÷ [21]. The concept of Global Damage Indexes (GDIs) is introduced as a measure of the overall structural conditions. Their formulation has been improved according to the new proposed damage model to summarize the performance level of the entire structure efficiently. Some acceptance criteria, usable with a distributed damage model, are proposed starting from the definition of suitable global structural performance indexes. Using the proposed approach, some preliminary numerical tests have been carried out to validate the proposed model in comparison with available experimental results. Some nonlinear analysis of a reinforced concrete frame structure, one of which designed in accordance to the European seismic provisions [22], have been performed in both static and dynamic conditions. A comparison with FEMA 356 [14] in characterizing the frame

performance level is finally presented. The obtained results confirm the reliability of the proposed method and the effectiveness of the GDIs for a careful description of the structural state [37].

2.2 Concrete damage model

The readers can refer to the works by Faria *et al.* [7] and Saetta *et al.* [9]-[10] for an exhaustive explanation of the basic damage model formulation and notations.

The following expression summarizes the constitutive law adopted for concrete:

$$\sigma_{ij} = \left(1 - d^{+}\right)\overline{\sigma}_{ij}^{+} + \left(1 - d^{-}\right)\overline{\sigma}_{ij}^{-} \tag{1}$$

where σ_{ij} is the damaged Cauchy stress tensor, derived from the positive part $\overline{\sigma}_{ij}^{+}$ and negative part $\overline{\sigma}_{ij}^{-}$ of the effective (i.e. elastic) stress tensor, as corrected, respectively, by two independent local damage parameters d^{+} and d^{-}, named, respectively, Tensile and Compressive Local Damage Indexes (LDIs), which are null for the virgin material and approach the unit as damage increases up to complete degradation.

In the previous works by the same authors [9]-[10] the following damage parameter evolution laws were proposed:

$$d^{+} = 1 - \frac{r_0^{+}}{\overline{\tau}^{+}} \exp\left[A^{+}\left(1 - \frac{\overline{\tau}^{+}}{r_0^{+}}\right)\right] \text{ and } d^{-} = 1 - \frac{r_0^{-}}{\overline{\tau}^{-}}\left(1 - A^{-}\right) - A^{-} \exp\left[B^{+}\left(1 - \frac{\overline{\tau}^{-}}{r_0^{-}}\right)\right] \tag{2}$$

where r_0^{+} and r_0^{-} are initial damage thresholds, A^{+}, A^{-} and B^{-} are suitable material parameters, $\overline{\tau}^{+}$ and $\overline{\tau}^{-}$ are, respectively, the tensile and compressive uniaxial stresses equivalent to $\overline{\sigma}_{ij}^{+}$ and $\overline{\sigma}_{ij}^{-}$

In particular the parameter A^{+} depends on the tensile fracture energy G_f of the material through the following expression:

$$A^{+} = \left[\left(G_f E\right)/\left(l_{ch} {f_0^{+}}^2\right) - 0.5\right]^{-1} \tag{3}$$

where f_0^{+} is the peak tensile strength of the material and l_{ch} is the "characteristic length", which depends on the size of the finite elements adopted within an approximate energy correction approach [10].

Between others, the evolution of d^{-} depends on the two parameters A^{-} and B^{-} that have to be chosen by making the numerical curve fit the experimental or analytical constitutive curve in uniaxial compression. Besides the uncertainties arising from the fact that parameters A^{-} and B^{-} don't have a physical meaning, it turned out that the constitutive law is excessively sensitive to the value of B^{-} which appears in the exponential

of the formula.

To overcome these drawbacks, an innovative formulation of the compressive damage parameter d^- is proposed as an improvement of the second of (2). It takes inspiration from the classical constitutive law for concrete proposed by Kent and Park [23], which requires only parameters of clear physical meaning. In uniaxial condition it writes:

$$\sigma = f_{cc}\left[2\frac{\varepsilon}{\varepsilon_{c0}} - \left(\frac{\varepsilon}{\varepsilon_{c0}}\right)^2\right] \qquad \text{for} \qquad 0 \geq \varepsilon > \varepsilon_{c0} \tag{4}$$

$$\sigma = f_{cc}\frac{\varepsilon - \varepsilon_{cu}}{\varepsilon_{c0} - \varepsilon_{cu}} \qquad \text{for} \qquad \varepsilon_{c0} \geq \varepsilon \geq \varepsilon_{cu} \tag{5}$$

$$\sigma = 0 \qquad \text{for} \qquad \varepsilon_{cu} > \varepsilon \tag{6}$$

where f_{cc} is the uniaxial compressive strength of the confined concrete evaluated according to Mander *et al.* [24], ε_{c0} is the corresponding strain and ε_{cu} is the ultimate deformation for which the proposal by Paulay and Priestley [25] has been adopted:

$$\varepsilon_{cu} = -0.4\% - 1.4 \cdot \rho_s \cdot \frac{f_y}{|f_{c0}|} \cdot \varepsilon_{sm} \tag{7}$$

with ρ_s the geometric transverse reinforcement ratio, f_y the transverse reinforcement tensile yield strength, ε_{sm} the corresponding steel ultimate deformation and f_{c0} the uniaxial unconfined peak compressive concrete strength.

Since in this work we are focused on a fibre approach, the description of the new damage formulation for compressed concrete is given only for uniaxial stress states.

As usual the concrete constitutive law in the compression field writes:

$$\sigma = \left(1 - d^-\right)\overline{\sigma}^- \tag{8}$$

being $\overline{\sigma}^- = E_0\,\overline{\varepsilon} = E_0\left[\varepsilon - \varepsilon_p\right]$ the elastic or effective stress corresponding to the reversible part $\overline{\varepsilon}$ of total strain through $E_0 = 2f_{cc}/\varepsilon_{c0}$, that is the initial elastic modulus of concrete.

According to Faria et al. [7], the plastic strain evolution is given by:

$$\dot{\varepsilon}^p = \beta \cdot H\left(\dot{d}^-\right) \cdot \dot{\varepsilon} \qquad \text{with} \qquad \begin{cases} \beta = \beta_0 \dfrac{\varepsilon}{\varepsilon_{c0}} & \text{for} \quad 0 > \varepsilon \geq \varepsilon_{c0} \\ \beta = \beta_0 & \text{for} \quad \varepsilon_{c0} \geq \varepsilon \end{cases} \tag{9}$$

where the material parameter $\beta \geq 0$ has been enhanced by taking into account its dependence on the strain level, and $H\left(\dot{d}^-\right)$ is the Heaviside function computed for the compressive damage rate (i.e. plastic strain accumulates only when an increase of damage takes place). Finally, the following expression of the damage evolution law in compression is

proposed:

$$d^- = 1 - \frac{1}{(2-\beta)}\left[2 - \frac{\overline{\sigma}^-}{\overline{\sigma}_0^-}\right] \qquad \text{for} \qquad 0 > \overline{\sigma}^- \geq \overline{\sigma}_0^- \tag{10}$$

$$d^- = 1 - \frac{1}{(2-\beta)}\frac{\overline{\sigma}_0^-}{\overline{\sigma}^-}\left[\frac{\overline{\sigma}_u^- - \overline{\sigma}^-}{\overline{\sigma}_u^- - \overline{\sigma}_0^-}\right] \quad \text{for} \qquad \overline{\sigma}_0^- > \overline{\sigma}^- \geq \overline{\sigma}_u^- \tag{11}$$

$$d^- = 1 \qquad \text{for} \qquad \overline{\sigma}_u^- > \overline{\sigma}^- \tag{12}$$

where $\overline{\sigma}_0^-$ and $\overline{\sigma}_u^-$ are the equivalent stresses corresponding respectively to the total strains ε_{c0} and ε_{cu}.

Eqs. (8) to (12) can be easily extended to generic 2D or 3D stress cases.

It should be noted that the newly proposed constitutive and damage evolution laws depend only on material parameters whose meanings are well known and are obtainable by standard experimental tests. A characteristic of the new approach is that the compressive concrete LDI at the peak strength point ε_{c0} depends only upon the parameter β_0: for example $d^- = 0.286$ for the value β_0=0.6 that has been assumed in all the numerical analyses presented in following.

2.3 Reinforcing steel buckling and steel damage model

In the numerical procedure it has been assumed that the reinforcing steel bars inside the concrete are subjected to uniaxial stress state and that the flexural stiffness of rebars can be neglected. An elastic-plastic kinematic hardening constitutive law has been assumed for the reinforcing steel. The bars fail when a prescribed plastic strain accumulation limit is achieved. Such ultimate limit is the one recorded in a monotonic, or low-fatigue cyclic, experimental test. Starting from this assumption, two distinct indexes measuring the amount of plastic strain developed in tension and in compression have been introduced. Such indexes, respectively named "*tensile and compressive steel damage indexes*", in analogy with the concrete ones, are defined as follows:

$$d_s^{+(-)} = \left(1 - \frac{W^{+(-)}}{\overline{W}^{+(-)}}\right) \Big/ \left(1 - \frac{W_u^{+(-)}}{\overline{W}_u^{+(-)}}\right) \tag{13}$$

In Eq. (13) W is the work necessary to deform the elastic-plastic material, while $\overline{W}$ is the corresponding work for hypothetical elastic behaviour (elastic strain energy). The constants W_u and $\overline{W}_u$ are the same quantities at the ultimate limit strain of the material. As

usual, suffixes "+" and "–" refer to the tensile and compressive strain state, respectively.

In the initial elastic field, the steel damage parameters are null. The unitary value is reached when the bar strain exceeds the ultimate plastic limit strain in tension or in compression: in this case the bar breaks irreversibly and both the damage parameters are permanently set equal to 1.

A different condition for which the compressive steel damage index d_s^- can temporary assume a unitary value is when a compressed bar buckles, as explained below.

The buckling phenomenon takes place when longitudinal reinforcing bars inside R.C. members undergo lateral deformation when subjected to compressive strain. It is mainly associated with geometrical nonlinearity and can reduce the ultimate strength and ductility of the whole structure considerably, *e.g.* [17].

The critical buckling load depends on the bar's lateral restraints, *i.e.* on ties arrangement, cover and core concrete and on their damage conditions.

Based on the work by Bresler and Gilbert [18], Pantazopoulou [21] has proposed the following expression for the critical load:

$$P_E = \left(4\pi^2 E_r I_b\right)/ L_b^2 + \alpha k L_b^2 \tag{14}$$

where I_b is the moment of inertia of the bar, $\alpha = \left(\pi^2 + 4\right)/\left(16\pi^2\right)$ is a constant coefficient, L_b is the wave length of the buckled bar that may span several tie spacings and $k = K/S$ is a fictitious distributed tie stiffness equal to the ratio between the stiffness of the system of stirrups K and the tie spacing S. The symbol E_r stands for the "reduced modulus" assumed equal to the steel hardening modulus in the stress-strain path.

In the case of a longitudinal bar, the stiffness K can be calculated considering the axial or the flexural resistance of stirrups, depending on the rebar arrangement and on the geometrical and mechanical properties of the stirrups themselves. The wave length was calculated by minimization of P_{cr} with respect to L_b, leading to:

$$L_b = \left[4\pi^2 E_r I_b /\left(\alpha k\right)\right]^{1/4} \tag{15}$$

rounded to a multiple of actual tie spacing S.

An alternative estimate of the wave length was proposed by Dhakal and Maekawa [17]. The value of the tie stiffness K_n, necessary to stabilize the longitudinal bar in the n^{th} buckling mode, that is, having $L_n = nS$, was obtained by searching the minimum of the potential energy with respect to the maximum amplitude.

In all the previously cited works, the direct interaction between the longitudinal bar and the concrete core has been disregarded, except for the modification introduced in the tie

stiffness. Actually, a certain interaction may take place, since the longitudinal and transversal reinforcements act as a net that opposes the transverse concrete core expansion of axially loaded members due to the Poisson effect and to the cracking phenomena. Bayrak and Sheikh [26] have accounted for this interaction considering an equivalent distributed load that the core concrete exerts on the rebar in order to evaluated their lateral deflection, but disregarding the second order effect due to axial load in the longitudinal bars.

Due to the different simplifications assumed, most of the proposed formulas, when applied to experimental tests in which rebars had actually buckled, frequently give a prediction of critical axial stress even greater than the steel's ultimate strength.

In general, the buckling phenomenon depends on the slenderness of the compressed member. For very slender bars, the critical buckling load tends towards the theoretical Euler buckling load, whereas the ultimate steel compressive strength condition gives the ultimate load of short bars. In most practical cases, considering the usual diameter of reinforcing bars, and stirrups spacing and diameter, the slenderness assumes an intermediate value and, therefore, the critical buckling load is highly influenced by several aspects that are neglected in the existing theories, such as initial imperfection, shear distortion, local hardening of the steel material and the interaction with the compressed core concrete. Tests conducted on bare bars cannot account for these phenomena, while the available tests of R.C. members often do not report the critical buckling stresses of the bars, but only parameters referring to the onset of the buckling phenomenon. Other tests are therefore needed, to validate the existing formulations for the critical buckling load estimation, or to develop new ones.

In this paper, the procedure by Dhakal and Maekawa [17] has been adopted for the evaluation of the wave length. The slenderness of the bar was assessed by taking into account the reinforcement arrangement and the tie stiffness, then the linear buckling load P_E was determined by means of Eq. (14).

Finally the expected critical load P_{cr} and the corresponding critical stress have been obtained by dividing the linear buckling load P_E by a coefficient ω that accounts for all the simplifications assumed in the calculation:

$$P_{cr} = P_E / \omega \tag{16}$$

In general, the value of ω should depend on the bar slenderness and imperfections and materials characteristics and it should be obtained by statistical analysis of experimental observations.

Examining the laboratory tests available in literature, where the longitudinal reinforcing bar slenderness was in the range between 32 and 44, the authors have found that a good correspondence with the experimental results was assured, assuming $E_r = 20$ GPa and

$\omega = 2.0$. Such values have been used in all the numerical tests presented in this paper.

In the numerical procedure it is assumed that, when in a compressed bar the critical stress is reached, the bar buckles and instantaneously loses its bearing capacity. At that moment, the compressive steel damage index is set at $d_s^- = 1.0$, its axial stiffness is zeroed and the accumulated plastic strain fixed. If the external force changes in sign and the stresses turn out to be positive, i.e. the total strain exceeds the accumulated plastic strain, the previous buckled rebar is expected to return in straight position and be able to support tensile stresses (Monti and Nuti [20]). Hence, the bar's compressive damage index is again a function of the accumulated plastic strain and in the subsequent load steps the bar can sustain compressive stresses until it buckles once more. Obviously, this assumption can hold only for a few cycles after the first buckling, because during the process there is a heavy accumulation of plastic strain due to the flexural deformation, which is not accounted for in the model. The typical stress-strain curve that can be obtained in a bar alternatively stressed beyond the yielding material limits is represented in Fig. 2.1.

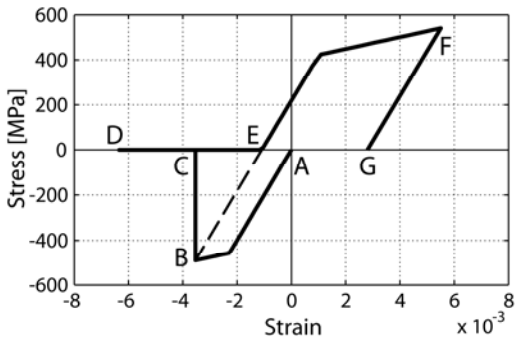

Fig. 2.1: Rebar stress-strain curve including buckling and post-buckling behaviour

2.4 Global Damage Indexes

For large scale problems it is necessary to define indexes able to monitor the effect of the distribution of the local damage indexes throughout a structure, in order to assess its overall state. Saetta *et al.* [10] and Hanganu *et al.* [12] proposed the definition of global damage indexes (GDIs) as the suitably weighted average of the local damage indexes over a certain finite volume of a structure. The following formula represents the extension of such a proposal to the case of two materials and two local damage parameters [16]:

$$D_i^{+(-)} = 1 - \frac{W_i^{+(-)}}{\overline{W}_i^{+(-)}} = 1 - \frac{\int_V \left(1 - d_i^{+(-)}\right) \Psi_{0,i}^{+(-)} \, dV}{\int_V \Psi_{0,i}^{+(-)} \, dV} = \frac{\int_V d_i^{+(-)} \, \Psi_{0,i}^{+(-)} \, dV}{\int_V \Psi_{0,i}^{+(-)} \, dV} \qquad (17)$$

where index *i* stands for the different materials, that is, *c* for concrete or *s* for reinforcing steel, $\overline{W}_i^{+(-)}$ is the total elastic strain energy due to the positive (negative) strains, $W_i^{+(-)}$ is the total actual potential energy due to the same strains in the damaged material, Ψ_0 is the elastic strain energy density, V is the integration volume.

Conceptually, the GDIs assume the significance of the unit complement of the ratio between the potential energy of the actual damaged structure and the hypothetical potential energy of an elastic structure undergoing the same displacement field. They approach the unit as strain localizes inside a limited zone, transforming the structures into a kinematism.

It has to be stressed that only in the case of a fixed load pattern monotonically increasing, the global damage indexes are as irreversible as the local ones. Whereas, in a generic load path, since the elastic strain energies are not increasing functions, also the global damage indexes are not always monotonically increasing. Nevertheless, the statement that global damage indexes approaching 1.0 means the crisis of the structure still holds.

Eq. (17) defines four distinct global damage indexes, *i.e.* D_c^+, D_c^-, D_s^+ and D_s^- that are tensile and compressive damage indexes for concrete and reinforcing steel, respectively.

The D_c^- parameter gives an overall measure of compressive concrete damaging and therefore is related with the loss of load-carrying capacity of the structure due to excessive compression in concrete. In particular, D_c^- approaches the unit as strain localizes inside the compressive damaged zones, up to the formation of a kinematic mechanism of the whole structure, or part of it.

The D_c^+ parameter measures the tensile concrete damaging and its cracking level. Since the tensile stresses are usually supported by the reinforcing bars, D_c^+ doesn't represent a safety index, but offers only useful indications on the serviceability limit state requirements.

Definition of further global indexes can be thought out similarly, such as a unique global damage index D weighted over all the different materials forming the structure.

2.5 LDIs and GDIs in the beam fibre model

The damage evolution laws previously defined have been implemented into a research numerical code using the standard Finite Element Method. This code deals with 2D frames described by beam fibre elements. Preservation of plain section is assumed, implying a perfect bonding between the reinforcement bars and the surrounding concrete. The damage parameters are evaluated in each fibre, at the node and in the middle of each element. The integral of Eq. (17), appropriate for continuous media, reduces to a sum when applied to finite elements:

$$D_i^{+(-)} = 1 - \frac{\sum_e a^T \int_{V(e),i} B^T \sigma^{+(-)} dV}{\sum_e a^T \int_{V(e),i} B^T \overline{\sigma}^{+(-)} dV} \tag{18}$$

In these equations $V(e),i$ indicates the volume of the beam element *e* of the material *i*. The sums are extended to the elements of the whole structure, or any part of it and **a** and **B** are the usual nodal displacements vector and matrix **B** = **LN** of Finite Element approach.

Besides the GDIs, in a beam fibre approach, the damage indexes of a single section of each element (hereinafter SDI = Section Damage Index) can also be defined. In this case, the LDIs of the considered section are averaged over a unitary beam length. Considering the potential energy due to the axial and flexural internal forces separately, more specific SDI could be formulated to state whether the damage distribution in the considered section and for a specific load combination produces more effect in the flexural or in the axial strength of the member. The SDIs allow easy monitoring, in every instant of the load process, of the state of the more critical sections of the structure in a way similar to that proposed by FEMA 356 for concentrated hinges approach.

In order to avoid loss of objectivity due to strain softening localization issues [13], the minimum length of the damaged zone (the plastic hinge length) should be pre-set, and the suitable beam element size be selected accordingly. In this work, the empirically validated expression of Paulay and Priestley [25] has been used:

$$L_p = 0.08 \cdot L + 0.022 \cdot f_y \cdot d_b \tag{19}$$

where L is the length between the end of the member and the point of contraflexure, d_b and f_y are respectively the diameter of the longitudinal reinforcing bars and the yield strength.

2.6 Validation examples

The ability of the new FEM damage model to simulate the real behaviour of R.C. structures has been proved by numerical simulation of some experimental test results.

The tests available at the site of the PEER Structural Performance Database [27], which has been instituted to provide researchers with the necessary information to evaluate and develop R.C. seismic models, have been used. For each test the PEER site provides the data on the materials, the longitudinal and transversal reinforcement characteristics, the test geometry configuration, the failure classification, the force-deflection history and the relative displacements, the axial load and the observed damage.

In particular, tests which showed a flexure critical behaviour and also the appearance of rebar buckling have been considered. This is due to the fact that the main aim of this work is the development of global indexes for axial and flexural collapse phenomena. Therefore, all the selected test examples deal with structures specifically designed to avoid other modes of failure, e.g. involving shear, torsion, anchorage. However, since fibre models are potentially able to handle such different failure phenomena, (as demonstrated for example in [28], [29] for shear, in [30], [31] for bond slip and in [32] for torsion), future developments of the proposed model will consider the possibility of different failure mechanisms and then it could be applied to a structure that was actually tested, that had members with other modes of failure than the flexural and axial ones.

2.6.1 Validation test N.1

The first test example was carried out by Gill *et al.* [33]. It deals with an axially loaded cantilever subjected to imposed horizontal displacements at the top (Fig. 2.2a).

The column has a square section 550 mm x 550 mm and length 1,200 mm. The compressive axial load is 1,815 kN and the axial load ratio is about 0.260. The cylindrical strength of the concrete is equal to 23.1 MPa and the steel yield stress is equal to 297 MPa for stirrups and to 375 MPa for the longitudinal reinforcement. The latter has a failure strength of 636.6 MPa and the ultimate plastic strain is assumed equal to about 1.0%. The column reinforcements consist of 12#24 longitudinal bars with a 40 mm clear cover and stirrups 4#10@80 mm.

The critical buckling stress evaluated with the proposed method is about 1,075 MPa, that is greater than the tensile strength, therefore rebar buckling is not expected.

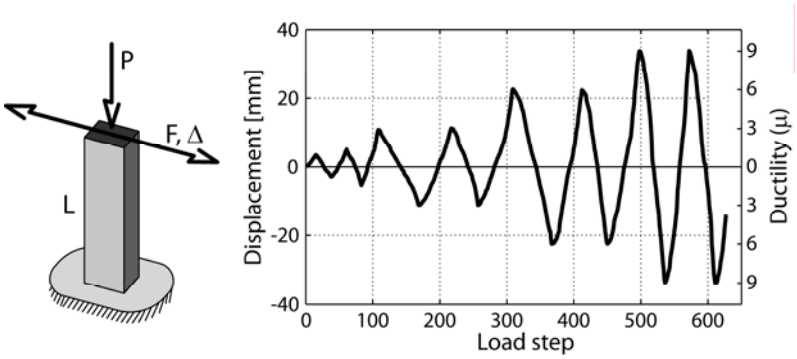

Fig. 2.2: Test 1 (Gill et al. [33]) - scheme of the cantilever (a) and top imposed displacements history (b)

Fig. 2.2b shows the horizontal displacement history imposed at the top of the column.

Named $\Delta y_p = 3.75$ mm the displacement at which the first yielding of the longitudinal reinforcement occurs, the ratio $\mu = \Delta y / \Delta y_p$ represents the ductility, i.e. the measure of

penetration into the plastic field. The history of imposed horizontal displacement, consists of an initial cycle between $\mu = \pm 1.0$, then the cycle size increases up to a final value $\mu = \pm 9.0$. The bending moment-base curvature diagram (Fig. 2.3a) and the force-top displacement diagram (Fig. 2.3b) are particularly significant. Both diagrams highlight the initial elastic phase in which the steel has not yet yielded, followed by the phases of steel yielding evidenced by the stiffness reduction.

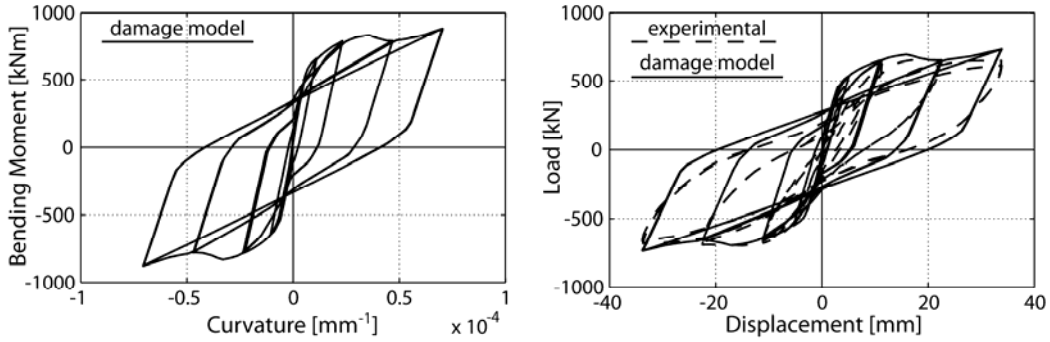

Fig. 2.3: Test 1 - numerical bending moment - base curvature diagram (a) and experimental and numerical force - top displacement diagrams comparison (b)

At the level $\mu = 3.0$ the bending moment-curvature diagram shows, in the unloading path, a weakness around the value M=200 kNm, followed by stiffness recovery immediately after the inversion of the curvature sign. This fact, which has been observed also in the experimental tests, can be explained considering that at $\mu = 3.0$ cycle the first strong plasticization of the steel in traction occurs and therefore an appreciable crack opening and damage appears in the compressed concrete side. At the successive displacement inversion, the steel previously in traction is initially compressed, without the concrete contribution because the cracks are still open, and yields. By increasing the displacement, the crack closes back, allowing the concrete to be recompressed. At this point the section shows a stiffness recovery and the bending moment value reaches the same level of the previous cycle. The same mechanism can explain the parts of the diagram with an intermediate slope at $\mu = 6.0$ cycles. During the first of these cycles the compressed concrete is further damaged and so the bending moment value is slightly reduced. The same conclusions can be even better testified by the shape of the load-top displacement diagram in Fig. 2.3b. It can be appreciated how the numerical results fit the experimental data closely. The obtained results can be used to evaluate the stiffness reduction experienced by the column with the increase of the displacement cycles. The stiffness is calculated as the ratio between the load value, at the maximum and the minimum point of the load history, and the related displacement value. Fig. 2.4a shows the stiffness reduction vs. load cycles diagram, evidencing the sudden reduction of the section stiffness as soon as the yield displacement is exceeded. The evolution of the tension and compression global damage indexes is represented in Fig. 2.4b, for

concrete and steel. In this figure, the GDIs appear to be not decreasing quantities, since they are evaluated only at the load steps in which a relative maximum of the top displacement are reached. As expected D_c^- increases with the imposed displacement and for the level of $\mu = 9$ it approaches the unit. The residual stiffness for $\mu = 9$ is given only by the steel reinforcements, since the concrete, at this load level, is almost completely damaged.

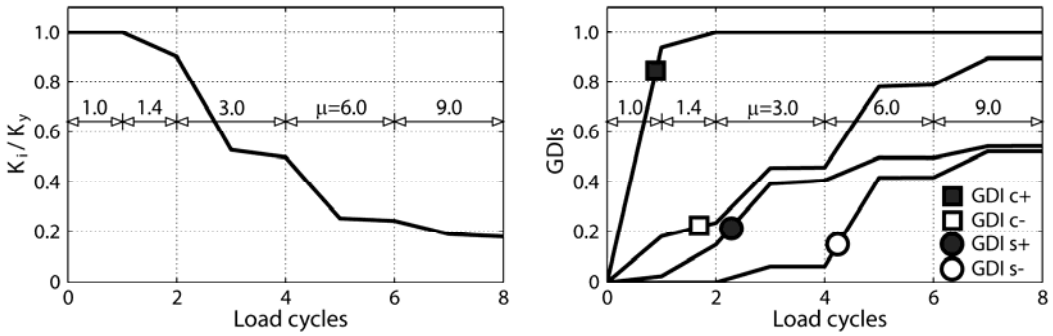

Fig. 2.4: Test 1 - column stiffness reduction (a) and GDIs evolution (b)

2.6.2 Validation test N.2

The second example demonstrates the importance of considering the bar buckling in a R.C. column to estimate its strength and ductility correctly.

The test has been carried out by Saatcioglu et al. [34]. As in the first case, it deals with an axially loaded cantilever subjected to imposed horizontal displacements at the top.

The column has a 350 mm x 350 mm square section and length 1,645 mm. The compressive axial load is 961 kN and the axial load ratio is about 0.231. The concrete cylindrical strength is equal to 34 MPa and steel yield stress is equal to 580 MPa for stirrups and to 455.6 MPa for the longitudinal reinforcement. The latter has a 660.0 MPa tensile strength. The ultimate plastic strain is assumed equal 1.0%.

The column reinforcements consist of 12#19.5 longitudinal bars with a 29 mm clear cover and stirrups 4#6.6@76 mm. The predicted wave length is equal to 228 mm, that is 3 times the hoop spacing and the critical buckling stress is about 490 MPa.

The top horizontal yield displacement is about 14 mm.

Two nonlinear static analyses have been conducted with the proposed damage model. Both analyses assume the amplitude of the horizontal displacement monotonically increasing. The first one disregards, while the second includes, the possibility of bar buckling. The numerical and experimental results are compared in Fig. 2.5a in terms of load-displacement diagrams: the improvement of the analysis when the buckling phenomenon is taken into account is clearly proved.

Fig. 2.5b depicts the evolution of the GDIs for the analysis with the buckling effect included. It can be observed that the concrete under compression starts to damage almost immediately due to the combined effects of the axial and flexural solicitations. After few load steps, the first external concrete fibre suffers the initiation of crushing. The steel rebars yield initially in traction and then in compression. When in the compressive rebars the critical buckling stress is achieved the corresponding GDI shows a sudden increase. At this step the tensile stresses are supported by the intermediate rebar but their distance from the compressive concrete fibres decreases, so causing progressive strength decay.

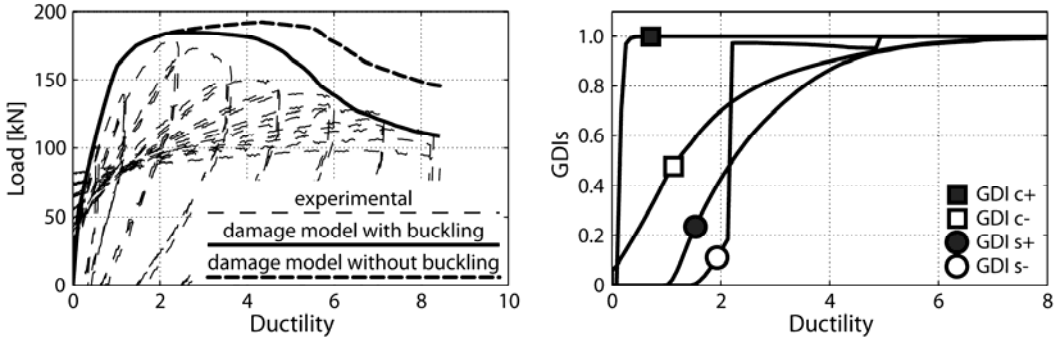

Fig. 2.5: Test 2 [34] – force - top displacement diagram (a) and evolution of GDIs in the analysis including bar buckling (b)

The GDIs evolution can also explain the significant difference between the models with and without buckling: actually when the first rebar buckling occurs, the corresponding concrete damage index is not yet close to unit value and the concrete section can sustain further compressive stresses, but the column stiffness and strength without the contribution of the compressed rebars are far reduced.

2.6.3 Validation test N.3

The third validation analysis reproduces the test by Tanaka and Park [35] and, similarly to the previous tests 1 and 2, deals with an axially loaded cantilever subject to imposed horizontal displacements at the top. The column has a 400 mm x 400 mm square section and length 1,600 mm. The compressive axial load is 819 kN and the axial load ratio is about 0.2. The measured cylindrical strength of the concrete is equal to 25.6 MPa and the steel yield stress is equal to 333 MPa for the stirrups and to 474 MPa for the longitudinal reinforcement. The latter has a 721 MPa tensile strength and the ultimate plastic strain is assumed equal to about 1.0%.

The column is reinforced with 8#20 mm longitudinal bars with a 40 mm clear cover and 3#12@80 mm stirrups. The predicted wave length is equal to 160 mm, that is, 2 times the hoop spacing, and the estimated rebar's critical buckling stress is about 620 MPa. In the

experiment the longitudinal reinforcement buckling had caused the decay of the strength and the column collapse in the last cycle.

Even in this test, experimental and numerical results show a good correspondence in terms of force-top displacement diagrams (Fig. 2.6a). The evolution of maximum GDIs is represented in Fig. 2.6b. Damage indexes grow significantly as a greater penetration in the ductility field is imposed to structure. Thanks to the different GDIs, it is easy to understand which material and which stress state (tension of compression) are more critical for the structure. Also, in this example the GDIs assume unit values at the end of the test when the structure collapse has been recorded.

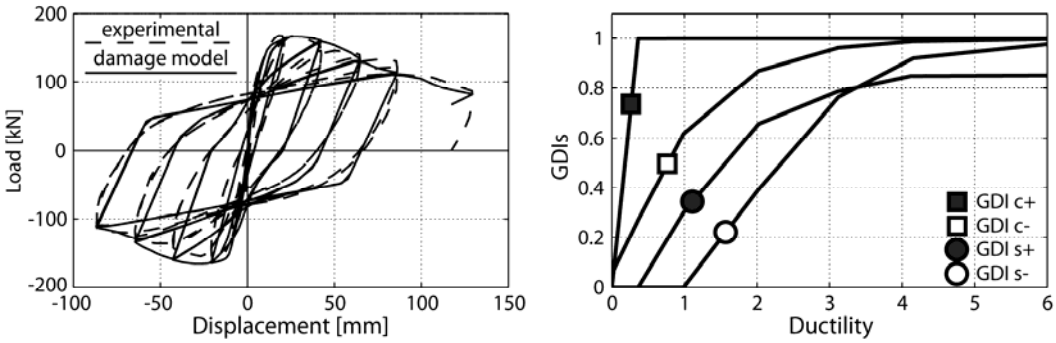

Fig. 2.6: Test 3 [35] –force- top displacement (a) and evolution of GDIs (b) diagrams

2.6.4 Conclusions to the validation tests

In all the performed validation analyses it has been demonstrated that the proposed model carefully reproduces the concrete characteristics and accurately describes the peculiar behaviour of the reinforced concrete members. The global damage indexes appear to be effective compact measures of the structural integrity and failure mode.

2.7 Nonlinear analyses of an high ductility RC frame

2.7.1 Building design

In this section, the nonlinear static and dynamic analyses of a R.C. building carried out with the developed numerical code are presented. The aim is to prove the ability of the proposed model to describe the nonlinear behaviour of the designed R.C. frame and to test the efficacy of SDIs and GDIs. The analyses deal with the typical transversal frame of a R.C. four-storey structure, framed in two orthogonal directions with symmetrical plan configurations, designed according to European Standards EC2 [36] and EC8 [22]. The

structure is designed as belonging to high ductility class (DCH) and fulfils both the vertical and horizontal regularity requirements. The frame geometry is shown in Fig. 2.7.

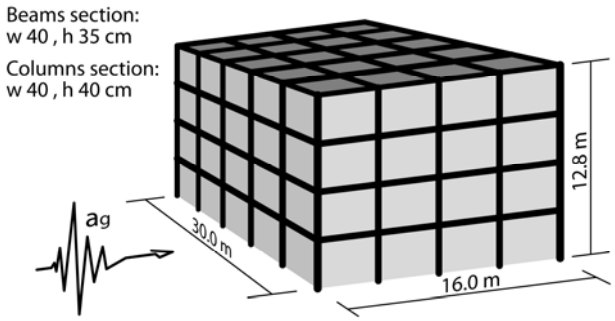

Fig. 2.7: Building's typical floor and frame geometry

The frame is 16.40 m wide and 12.80 m high, the inter-storey height is 3.20 m. The interspace between the bearing frames is 6.0 m. The columns have 40x40 cm cross-section and are reinforced symmetrically with about 2.36% longitudinal reinforcement ratio; the beams section is w40xh35 cm, with longitudinal reinforcement ratio varying between 1.86% for the first floor and 1.29% for the others. The stirrups are arranged according to the EC8 prescriptions and the maximum transverse reinforcement ratios are about 0.50% for the column and about 0.63% for the beams. The elementary load conditions are: self-weight and permanent loads 7.0 kN/m^2, live load 2.0 kN/m^2. A seismic design spectrum for ground type B and PGA=0.35g is considered. The importance factor γ_I chosen is equal to 1.0 and the behavioural factor q=5.85 is assumed for the DCH frame. The materials characteristics are f_{ck}=25.0 MPa for concrete and f_{yk} = 430 MPa for reinforcing steel. The corresponding mechanical characteristic properties, according to the EC8 prescription for new structures properties, are introduced in the fibre damage model. For each different type of confining reinforcement, different values of ultimate concrete strain and strength are chosen according to Eq. (7). Referring to the column's longitudinal rebars, the critical buckling stress is evaluated, after verifying that the designed stirrups remain elastic under the axial and transverse static and seismic internal forces. The critical buckling stress of the ground floor column's rebars results to be about 1,190 MPa, greater than the steel yield strength, hence the steel buckling was not expected.

2.7.2 Nonlinear static analysis of the frame

Two nonlinear static analysis of the designed frame have been carried out, considering two different load patterns applied to the frame: the uniform one, *i.e.* proportional to the mass, and the modal one, *i.e.* proportional to the 1st modal shape. For the uniform load pattern, Fig. 2.8a shows the results in terms of the capacity curve with superimposed the

evolutions of global damage indexes averaged on the entire structure. It is worth noting that D_c^- starts from a non-zero value. This starting damage level is due to the vertical loads, which have been considered as acting on the structure before the beginning of pushover analysis. For the same reason, D_c^+ starts from a value already approaching the unit, the concrete being almost completely cracked under the vertical load alone.

The first element yielding is identified by the appearance of a non-zero value of the tensile steel GDI for a top displacement of 78 mm.

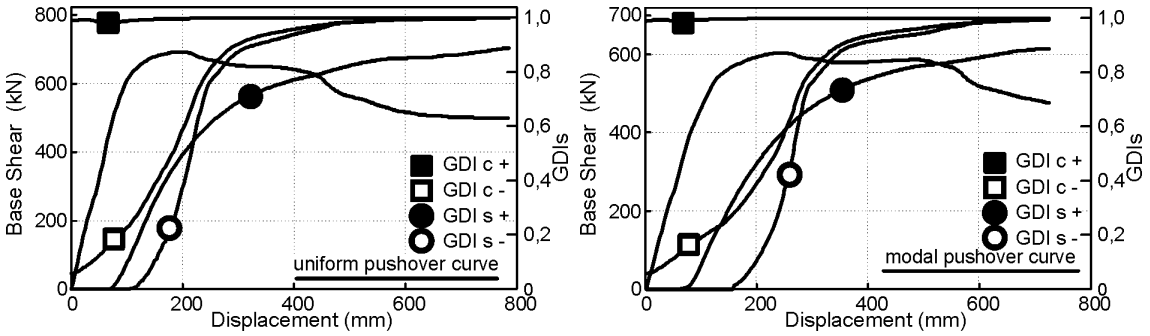

Fig. 2.8: Capacity curves and evolutions of GDIs: uniform (a) and modal (b) pushover analyses

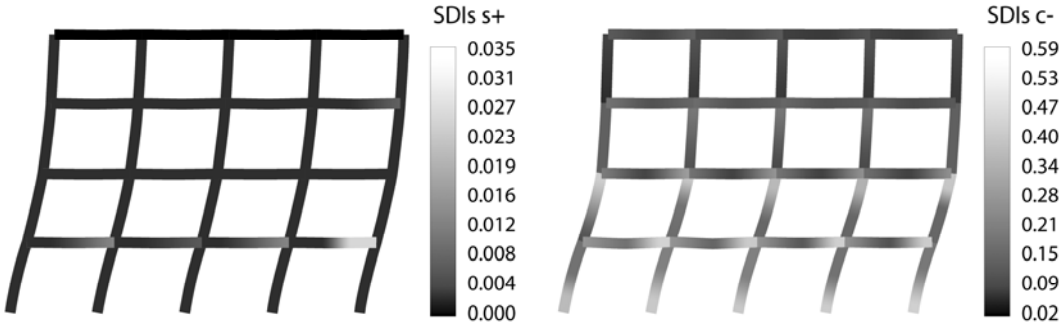

Fig. 2.9: Uniform pushover analysis - deformed shape and contour of tensile steel SDI at δ=200 mm (a) and compressive concrete SDI at failure δ=625 mm (b)

The maximum base shear is equal to about 700 kN corresponding to about 200 mm top displacement. Then the structure shows a softening phase during which the compressive concrete and steel global damage indexes quickly grow. The 80% of the residual peak strength is reached at about 524 mm top displacement. In the subsequent strength decrease, both compressed concrete and steel GDIs tend to the unit value. The formation of a plastic hinge at the peak force step can be easily identified by means of the contour map of the tensile steel SDI in Fig. 2.9a. The first and main bar yielding takes place on the right section of the 1st floor's 4th beam. All the beams of the 1st floor enter in the non linear field, since in all their right sections there is appearance of damage index.

For the uniform pushover analysis, the distribution of d_c^- SDI is depicted in Fig. 2.9b, at the imposed top displacement of 625 mm close to structure failure. It shows clearly that the

maximum damage accumulates at the bases of the ground floor columns: therefore, it can be concluded that the failure of the structure occurs by concrete crushing in those members, due to excessive compressive stresses. Similar considerations can be drawn for the modal pushover analysis, whose main results are summarized in Fig. 2.8b, in terms of base shear-top displacement curve and GDIs evolution curves.

2.7.3 Nonlinear dynamic analysis of the frame

In this section, the results obtained by the nonlinear dynamic analysis of the frame subjected to a set of spectrum-compatible seismic excitations are presented. 18 different spectrum-compatible accelerograms with 0.35 PGA have been generated. Half of them have a duration of 10 s, the other of 20 s. The proof of the compatibility of the 18 accelerograms' average spectrum with the EC8 design spectrum is shown in Fig. 2.10. Thereby the response of the structure subjected to each accelerogram has been evaluated, mainly in terms of Global Damage Indexes.

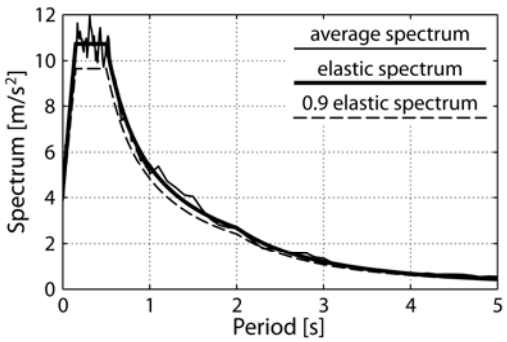

Fig. 2.10: Check of compatibility of simulated earthquake accelerograms with EC8 elastic spectrum

For the sake of brevity, the complete results, in terms of displacements, GDIs histories, damage patterns and bending moment–curvature diagrams, are reported for only one of the accelerograms, with a duration of 20 s, even if the analysis has been extended for further 10 s.

Fig. 2.11a shows the time-displacement histories of each floor. During the oscillations the frame reaches a maximum top displacement value of about 159 mm after 16.9 s from the beginning of the analysis. At the end the frame settles in a new equilibrium configuration, characterized by residual displacements.

The evolution of the GDIs versus time is depicted in

Fig. 2.11b. Each time that the structure achieves an increase of maximum displacement, the peak of GDIs grows: after 16.9 s of analyses, the maximum values of D_c^- =0.43 and D_s^+ =0.33, are reached as well.

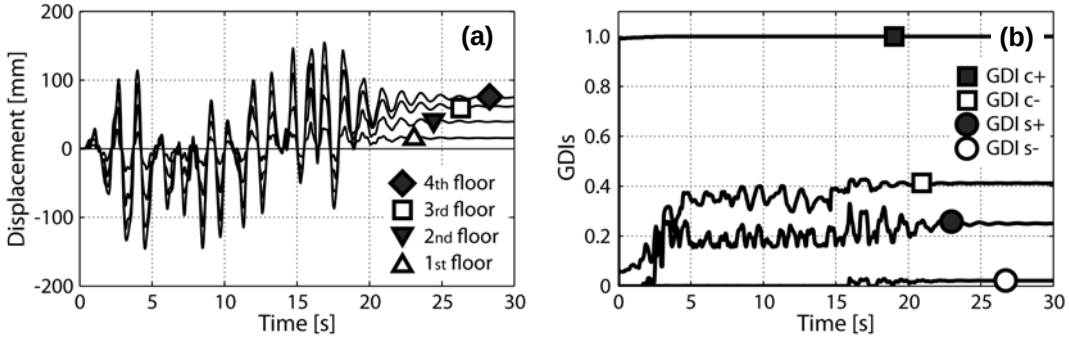

Fig. 2.11: Horizontal displacement time histories (a) and evolution of GDIs for a 20 s accelerogram (b).

These values of the peak of GDIs testify that the frame is only partially damaged from the earthquake. The contours of the SDIs identify the section where the steel plasticization starts. Fig. 2.12a, which shows the d_s^+ SDI at 1.7 s when the first relative maximum of storey left displacement took place, shows that the sections that yielded first are the left ones of the 3rd floor's beams.

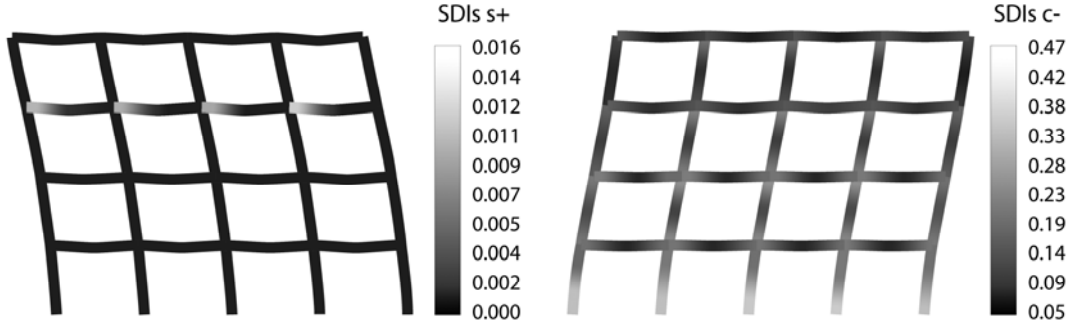

Fig. 2.12: Contour of d_s^+ SDI after 1,7 s (a) and of d_c^- SDI after 16,9 s (b)

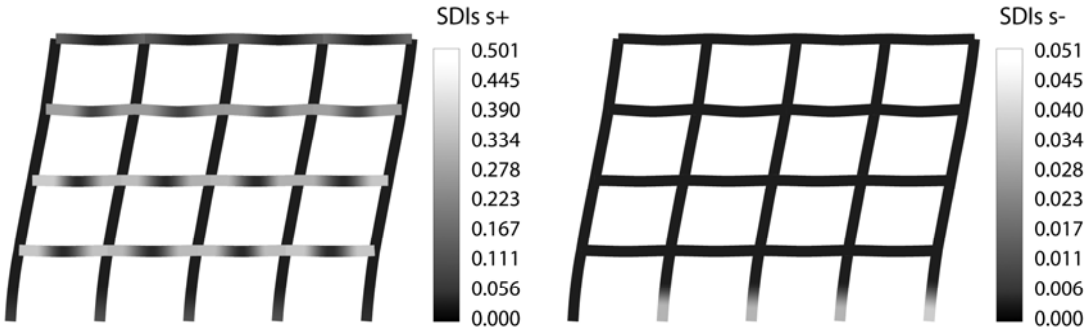

Fig. 2.13: Contour of d_s^+ SDI (a) and of d_s^- SDI (b) after 16,9 s

The maximum values of d_c^-, and d_s^+ and d_s^- SDIs are reached after 16.9 s from the beginning of the analyses. Their distributions are depicted in Fig. 2.12b, Fig. 2.13a and Fig. 2.13b, respectively, and make it possible to appreciate how the plastic hinge are well distributed all over the beam end sections accordingly with the hierarchy criteria of the high

ductility class for which the structure has been designed. The greater values of the d_c^- SDI are located at the base of the ground columns, these elements being subject to the most severe combination of axial and flexural internal forces. The higher values of d_s^+ SDI occur in the first and second floor beams' end sections, while smaller values of d_s^- SDI are in the base sections of the ground floor's columns.

The results obtained by the 18 dynamic analyses, represented by means of the maximum base shear-maximum displacement points, are compared in Fig. 2.14 with the capacity curves obtained from the pushover analyses. It can be noted that almost all of the 18 points from NLD analyses fall within the two pushover curves corresponding to uniform and linear distribution of forces. It has to be remarked that the maximum top displacements from the NLD are all lower than the value of about 600 mm that the pushover analyses indicate as the point of structural failure. This result matches the observation that the maximum values of GDIs obtained from NLD are far lower than the unit and indicates that the level of assumed PGA can be safely sustained by the frame, even though with considerable damaging. In other words, it is possible to affirm that the compliance with the Collapse Prevention Limit of FEMA 356 has been verified.

From the NLD analyses results it possible to say that each accelerogram requires different values of ductility, even if the maximum base shear is almost constant, being limited by the maximum strength of the frame.

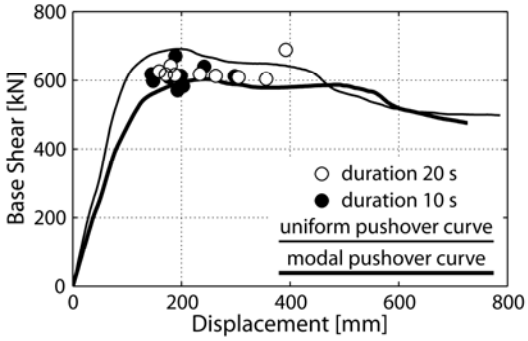

Fig. 2.14: Comparison between pushover curve and nonlinear dynamic maximum results

Fig. 2.15 also proves that the maximum displacement experienced by the frame increases, on average, as the seismic duration increases, from 10 s to20 s. In particular, the maximum top displacement increases from 145 mm for the group of 10 s duration excitations to 392 mm for the 20 s group. The good correlation between the maximum displacement level and the maximum values of GDIs reached during the time history is demonstrated in Fig. 2.15a-c. For the specific analyzed frame, there is a fairly linear proportion between the maximum top displacement and the steel and compressed concrete GDIs. The well-balanced design of the frame is testified by the fact that the steel's tensile

GDI and the concrete's compressive GDI evolve in similar way with displacements. Obviously, such considerations cannot be immediately generalized, but hold only for the considered frame, at least until after considerable more analyses are performed. In the authors' experience, the statement that the D_c^+ GDI is not useful to assess the structural performance at ultimate limit state, since it always tends towards the unit value, even with low displacement levels, is generally valid.

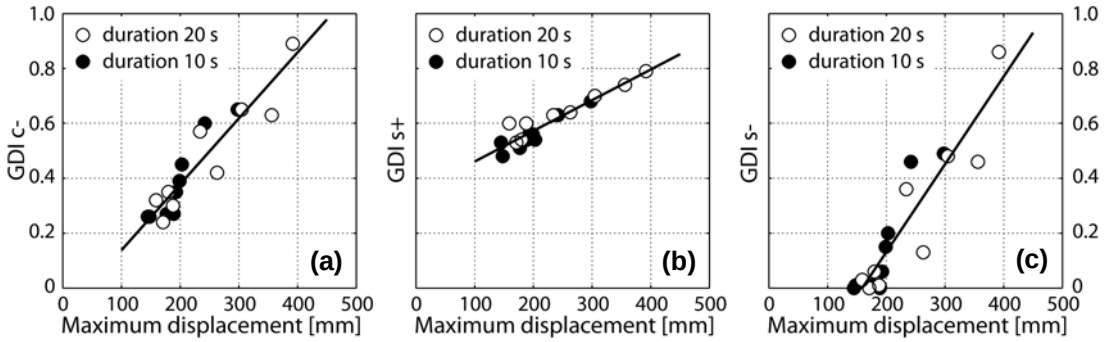

Fig. 2.15: Maximum D_c^- GDI (a), D_s^+ GDI (b) and D_s^- GDI (c) versus maximum top displacement

2.7.4 GDIs and performance levels

On the basis of the preliminary studies presented in this section, a comparison between the GDIs, as proposed within the fibre damage model approach, and the Performance Levels defined in FEMA 356, although the latter applies to existing buildings only, is presented. To make such a comparison possible, nonlinear pushover analyses of the R.C. frame with a concentrate plasticity model have also been performed. The yielding and ultimate bending moment and the yielding rotation of the plastic hinges have been evaluated according with the prescription of EC2. The ultimate rotation capacity of the plastic hinges for the newly designed buildings have been assuming a value which is double the one provided by FEMA 356 for existing buildings.

Fig. 2.16a (for uniform load pattern) and Fig. 2.16b (for modal load pattern) demonstrate that with such assumptions the two distinct methods to performs the pushover analyses, *i.e.* the fibre beam approach and the concentrate hinge one, agree, the respective capacity curves being very close together.

In the same figures, the evolution of the GDIs with top displacement and the FEMA 356 performance level limits are also plotted to demonstrate the ability of the proposed GDIs to describe both the structure's status and performance. First of all, it is possible to verify that the Immediate Occupancy performance level effectively corresponds to the onset of non-zero values of the tensile steel GDI. This result has a general validity, since the IO level is defined as the occurrence of first rebar yielding in some point of the structure. At IO

level, the compressive concrete GDI ranges between 0.15 and 0.2 with the proposed damage model. With regard to the LS level, it corresponds to both D_c^- and D_s^- GDIs within the interval 0.75÷0.80, whereas the D_s^+ GDI is around 0.65. Finally, at the CP level, the D_c^- and D_s^- GDIs fall in the interval 0.9÷1.0, *i.e.* they approach the unit, and the D_s^+ GDI is around 0.80.

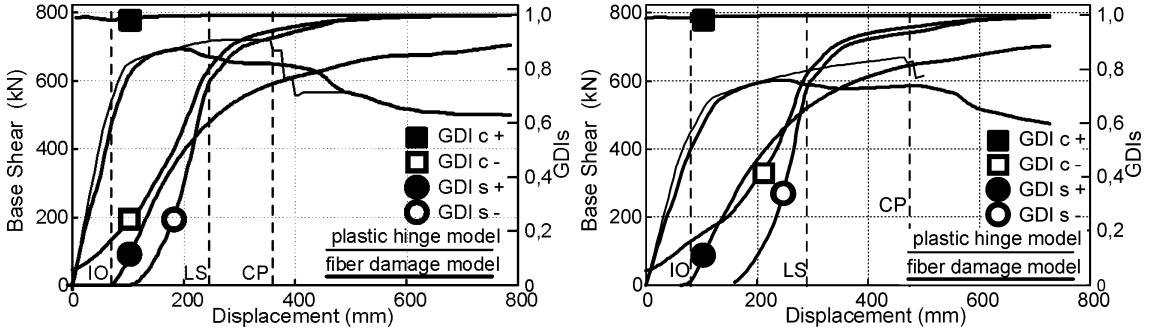

Fig. 2.16: Comparison between plastic hinge model and fibre damage model: uniform (a) and modal (b) pushover analysis

It must be remarked that the values of the GDIs must always be judged in relation to the definition and evolution laws adopted for LDIs. To give general validity to the proposed methodology, more tests need to be performed, both on new and existing structures.

2.8 Nonlinear analyses of an existing RC frame

2.8.1 Building characterization

This section shows the application of the proposed damage model to a weak-columns RC frame, corresponding to an existing building. To accomplish this aim, the DCH frame analyzed in the previous section has been modified by reducing both the transversal and the longitudinal steel bars of the ground floor columns, keeping the same concrete section sizes. Referring to the FEMA 356, and according to typical existing building details, the longitudinal reinforcement ratio is assumed equal to 1.51% and the transverse reinforcement ratio has been kept constant along the column length and equal to 0.25%. Therefore, the design of the first storey columns has been made disregarding the capacity hierarchy provisions.

The reduction of the longitudinal rebar ratio changes the cracked stiffness and the strength of the selected sections, whereas the lower transverse reinforcement ratio induces a reduction of the ultimate strain and strength of the concrete material model according to Eq. (7). For this reinforcement arrangement, the critical buckling stress of the column's longitudinal rebar is about 374 MPa, that is equal to the yield strength. This is due to the

fact that a sudden fall of the Young modulus appears at that point. Hence, steel buckling can be expected during the analysis.

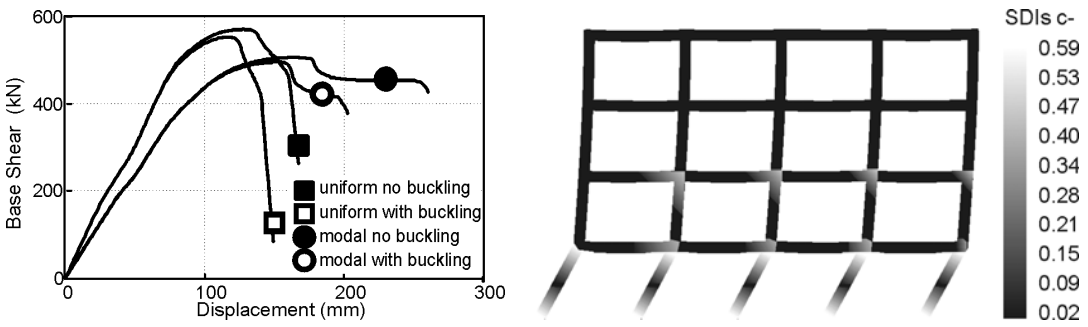

Fig. 2.17: Pushover analyses: different model capacity curves (a) and contour of D_c^- SDI at δ=180 mm (b)

2.8.2 Nonlinear static analysis of the frame

To illustrate the difference between the damage model including, and the one disregarding the buckling model, the capacity curves obtained with the two hypotheses, for uniform and modal load patterns, respectively, are presented in Fig. 2.17a. The model that doesn't take into account the buckling phenomenon shows a capacity curve with higher peak strength, as well as higher ductility, as against the model that takes buckling into account. Such increases are not justified by the validation examples and by the literature. Concerning the fibre damage model including the buckling phenomenon, the deformed shape and the D_c^- SDI contour map corresponding to the collapse state of the modal pushover analysis are presented in Fig. 2.17b. It can be noted how the failure of the entire structure is due to a local collapse, since the compressive concrete damage is mostly concentrated in the ground floor column.

2.8.3 GDIs and performance levels

This section shows the comparison between the GDIs evaluated by using the fibre damage model including the buckling phenomena, and the FEMA 356 Performance Levels evaluated by using a concentrated plasticity approach. As for the plastic hinge model used in the previous section, all the plastic hinges of the ground floor columns have been modified according to the new reinforcement ratio, and the ultimate rotational capacity has been directly obtained from the FEMA 356 provisions for existing building. Fig. 2.18a (for uniform load pattern) and Fig. 2.18b (for modal load pattern) show the results in terms of capacity curves with the evolutions of global damage indexes averaged on the entire structure superimposed, and compared with the FEMA performance level limits.

The pushover curves display a low ductility behaviour of the frame and both analyses show a failure due to a weak storey mechanism that occurred at the ground floor. In this

case, the structural damage is concentrated in a limited part of the structure and the local collapse causes global collapse.

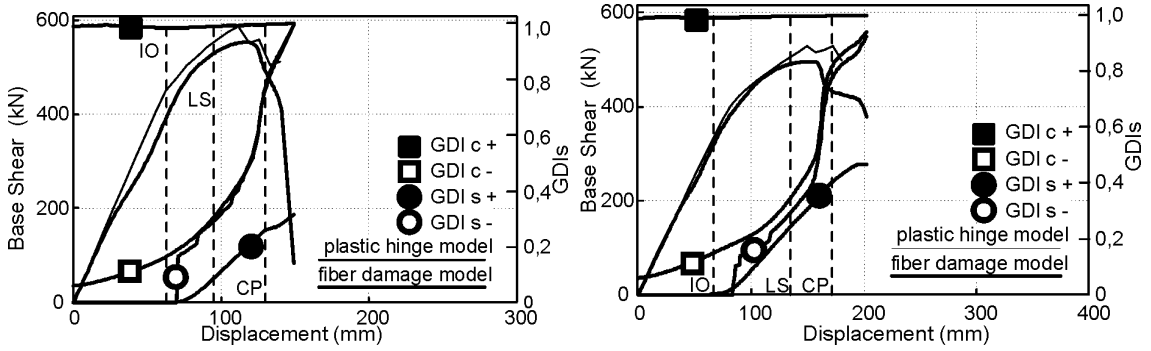

Fig. 2.18: Comparison between plastic hinge model and fibre damage model: uniform (a) and modal (b) pushover analysis

Nonetheless, being the GDIs weighted average of LDIs, assuming the elastic energy as weight, the GDIs themselves grow up to values close to 1, even if only some parts of the structure collapse and the other parts remain nearly elastic. In this example, the first non-zero values of D_s^+ and the values of about 0.2 of the D_c^- GDIs characterize the IO limits, similarly to the previous example designed in high ductility. The maximum gradients of D_c^- and D_s^- GDIs correspond to the peak strength of the capacity curves. At this point, the GDI values range between 0.6 and 0.7 and indicate the LS level. The LS limit calculated by the FEMA is slightly anticipated. In this case such a limit is very close to the main bar buckling occurrences and the D_c^- and D_s^- maximum gradients. The final D_c^- and D_s^- GDIs values, which range between 0.8 and 1.0, sanction the global collapse of the structure and the achievement of the CP performance level. It is worth noting that the ultimate values of D_s^+ vary between 0.35 and 0.45, demonstrating the low energy dissipation capacity of the weak-columns frame compared to the DCH one. Every sudden increase of the D_s^- GDI means that the buckling phenomenon has occurred at least in one element section. This section can be easily identified with the aim of the D_c^- SDI contour maps.

2.9 Conclusions

In the framework of continuum damage theory, a new two-parameter damage model for concrete has been proposed. In particular, a new concrete compressive damage evolution law has been developed to evaluate the effect of confining reinforcement in R.C. structure better. With the aim of describing, in a unitary approach, the steel behaviour, specific "steel damage indexes" have been formulated, taking into account the plastic strain development and the possibility of rebar buckling. A new methodology to estimate the critical buckling load has

been formulated, which turned out to be in good agreement with experimental results. An improved and generalized definition of the global damage indexes has finally been proposed, in order to obtain powerful tools to estimate the performance and the state of a R.C. structure.

The improved model has been implemented into a fibre research FEM code, which has been used to carry out nonlinear analyses of tests examples and of a R.C. concrete frame structure. In particular, the reliability of the model has been demonstrated by comparison with trusted experimental tests on R.C. column axially loaded and subjected to imposed transversal displacements, some of which had presented the rebar buckling.

The static and dynamic nonlinear analyses of two R.C. frames, respectively one designed in high ductility class and one with weak-columns at the ground floor, have been carried out and the model has demonstrated its ability to describe the dynamic behaviour, the failure mechanism and the energy dissipation of both frames efficiently and accurately. In particular, the GDIs have demonstrated that they can interpret the development of the overall structural decaying correctly. The contour maps of SDIs have made it possible to evaluate the damage distribution all over the structure.

Finally, the two R.C. frames investigated with the fibre approach have been studied with a concentrated plastic hinge approach as suggested by FEMA 356. A clear correlation between the GDIs here proposed and the Performance Level proposed by FEMA has been demonstrated for the test examples. Even though more analyses and comparisons have to be performed, especially with regard to existing buildings, the method proposed here appears to be a tool that could be used profitably for the structural seismic safety assessment, when distributed non linear models are employed. Further efforts have to be spent to extend the proposed approach in three-dimensional codes and to keep into account failure mechanism of the beams related to shear and torsion solicitations, as well as to failure of anchorage.

References

1. Lai S, Will G, Otani S. Model for inelastic biaxial bending of concrete members. *ASCE Journal of Structural Engineering* 1984, **110**: 2563-2584.
2. Spacone E, Filippou FC, Taucer FF. Fiber Beam-Column Model for Nonlinear Analysis of R/C Frames. I: Formulation. *Earthquake Engineering and Structural Dynamics* 1996, **25**: 711-725.
3. Spacone E, Filippou FC, Taucer FF. Fiber Beam-Column Model for Nonlinear Analysis of R/C Frames. II: Applications. *Earthquake Engineering and Structural Dynamics* 1996, **25**: 727-742.
4. Coleman J, Spacone E. Localization Issues in Nonlinear Force-Based Frame Elements. *ASCE Journal of Structural Engineering* 2001; **127**: 1257-1265.
5. Lubliner J, Oliver J, Oller S, Oñate E. A plastic-damage model for concrete. *Elsevier International Journal of Solids and Structures* 1989, **25**: 299-326.
6. Mazars J, Pijaudier-Cabot G. Continuum damage theory – application to concrete. *ASCE Journal of Engineering Mechanics* 1989, **115**: 345-365.
7. Faria R, Oliver J, Cervera M. A strain-based plastic viscous-damage model for massive concrete structures. *Elsevier International Journal of Solids and Structures* 1998; **35**: 1533-1558.
8. Lee J, Fenves GL. Plastic-damage model for cyclic loading of concrete structures. *ASCE Journal of Engineering Mechanics* 1998, **124**: 892-900.
9. Saetta A, Scotta R, Vitaliani R. Mechanical behavior of concrete under physical-chemical attacks. *ASCE Journal of Engineering Mechanics* 1998, (124) **10**: 1100-1109.
10. Saetta A, Scotta R, Vitaliani R. Coupled Environmental-Mechanical Damage Model of R.C. Structures. *ASCE Journal of Engineering Mechanics* 1999, (125) **8**: 930-940.
11. Scotta R, Vitaliani R, Saetta A, Oñate E, Hanganu A., A scalar damage model with a shear retention factor for the analysis of reinforced concrete structures: theory and validation. *Computers & Structures* 2001, **79**: 735-755.
12. Hanganu AD, Oñate E, Barbat AH. A finite element methodology for local/global damage evaluation in civil engineering structures. *Computers & Structures* 2002, **80**: 1667-1687.
13. Légeron F, Paultre P, Mazars J. Damage Mechanics Modeling of Nonlinear Seismic Behavior of Concrete Structures. *ASCE Journal of Structural Engineering* 2005, **131**: 946-955.

14. FEMA 356. *Prestandards and commentary for the seismic rehabilitation of buildings.* Federal Emergency Management Agency: Washington D.C., 2000.

15. DiPasquale E, Çakmak AS. Detection of seismic structural damage using parameter-based global indices. *Probabilistic Engineering Mechanics* 1990, **51**: 60–65.

16. Saetta A, Scotta R, Tesser L, Vitaliani R. Nonlinear analysis of reinforced concrete structures with a fiber two-parameters damage model. *2nd fib International Congress:* Naples, June 5-8 2006.

17. Dhakal RP, Maekawa K. Reinforcement stability and fracture of cover concrete in reinforced concrete members. *ASCE Journal of Structural Engineering* 2002, **128**: 1253-1262.

18. Bresler B, Gilbert H. Tie requirements for reinforced concrete columns. *ACI Journal* 1961; **58**: 555-570.

19. Papia M, Russo G, Zingone. Instability of longitudinal bars in R.C. columns. *ASCE Journal of Structural Engineering* 1998, **92**: 605-616.

20. Monti G, Nuti C. Nonlinear cyclic behavior of reinforcing bars including buckling. *ASCE Journal of Structural Engineering* 1992, **118**: 3268-3284.

21. Pantazopoulou SJ. Detailing for reinforcement stability in R.C. members. *ASCE Journal of Structural Engineering* 1998, **124**: 623-632.

22. CEN. *Eurocode 8: Design of structures for earthquake resistance Part 1: General rules, seismic actions and rules for buildings.* Comité Européen de Normalisation: Bruxelles, 2004.

23. Kent DC, Park R. Flexural members with confined concrete. *ASCE Journal of Structural Division* 1971, **97**: 1969-1990.

24. Mander JB, Priestley MJN, Park R. Observed stress-strain behavior of confined concrete. *ASCE Journal of Structural Engineering* 1988, **114**: 1827-1849.

25. Paulay T, Priestley MJN. *Seismic design of reinforced concrete and masonry buildings*. John Wiley & Sons: New York, 1992.

26. Bayrak O, Sheikh S. Plastic hinge analysis. *ASCE Journal of Structural Engineering* 2001; **127**: 1092-1100.

27. Berry M, Parrish M, Eberhard M. *PEER Structural Performance Database. User's Manual.* Pacific Earthquake Engineering Research Centre: University of California Berkeley, 2004.

28. Taylor RL, Filippou FC, Saritas A, Auricchio F. A mixed finite element method for beam and frame problems. *Springer Computational Mechanics* 2003, **31**: 192–203.

29. Marini A, Spacone E. Analysis of reinforced concrete elements including shear effects. *ACI Structural Journal*, 2006, **103**: 645-655.

30. Monti G, Spacone E. Reinforced concrete fiber beam element with bond-slip. *ASCE Journal of Structural Engineering* 2000, **126**: 654-661.

31. Salari MR, Spacone E. Finite element formulations of one-dimensional elements with bond-slip. *Elsevier Engineering Structures* 2001, **23**: 815-826.

32. Trogrlic B, Mihanovic A. The comparative body model in material and geometric nonlinear analysis of space R/C frames. *Emerald Engineering Computations* 2008, **25**: 155-171.

33. Gill WD, Park R, Priestley MJN. *Ductility of rectangular reinforced concrete columns with axial load*. Department of Civil Engineering, University of Canterbury, Christchurch: New Zealand, 1979; Report **1**.

34. Saatcioglu M, Grira M. Confinement of reinforced concrete columns with welded reinforcement grids. *ACI Structural Journal* 1999, **96**: 29-39.

35. Tanaka H, Park R. *Effect of lateral confining reinforcement on the ductile behavior of reinforced concrete columns*. Department of Civil Engineering, University of Canterbury, Christchurch: New Zealand, 1990; Report **2**.

36. CEN. *Eurocode 2: Design of concrete structures Part 1-1: General rules and rules for buildings*. Comité Européen de Normalisation: Bruxelles, 2003.

37. Scotta R, Tesser L, Vitaliani R, Saetta A. Global damage indexes for the seismic performance assessment of R.C. structures. *Wiley Intersciences Earthquake Engineering and Structural Dynamics*, 2009. doi: 10.1002/eqe.

Chapter 3

Composite Steel Truss and Concrete beam mechanics

3.1 Introduction

In order to evaluate the composite steel truss and concrete beam-column joint behaviour it's necessary to fully understand the resistant mechanisms of the beams. The original calculation method of S. Leone [1] is deposited at the Italian Superior Council of Public Works as prescribed by the previous and the actual Italian Code [2]. Starting from that study, the CSTC mechanics have been analyzed. Particular attention has been paid to the flexural and the shear strength, the ductile and the fragile possible failure, the influence of the concrete shrinkage, the influence of the stresses acting on the steel truss when the concrete becomes hard, the anchorage of the embedded element and their overlapping length, the welding influence in the steel truss elements, the cracking phenomena [3] ÷ [5]. All this research has been concluded with an improved assessment method both for the CSTC truss beams with the steel plate base and for the concrete base. The presented method respects not only the Italian but also the European Code for what concerns the reinforced concrete, the composite steel and concrete and the structural steel constructions [6] ÷ [8]. Focusing on the beam mechanics, the requirements of the Ultimate and Serviceability Limit States are expressed in terms of structural performances and the methodology to assess them has been developed. Particular issues, like the concrete confinement, has been taken into account in order to assess the avoidance of brittle failure mechanisms. The proposed method has been used in the next chapter to predict and evaluate the experimental test results.

3.2 General principles on the CSTC mechanics

The purpose is to establish a reliable method able to assess the CSTC beams behaviour in terms of resistance, stability, functional efficiency and durability. The CSTC beam has to possess adequate performances before and after the hardening of the in place concrete cast. This moment distinguishes two phases (or stages) in the life of the beam that are characterized by distinct resistant sections and different mechanics. During the first phase the beam behaves as a prefabricated steel truss. The bottom chord can be made by one more steel elements (that are flat or formed plates, round or square bars, profiles, etc.), that can be embedded in a concrete base if necessary. The steel truss usually works in a simple supported static scheme. The loads are usually its own weight, the weight of the slab and the weight of the concrete cast. During the second phase the previous truss collaborates with the hardened concrete. The base of the truss is usually the cast scaffold and the finial structure is a particular composite steel and concrete one with solid web. Its static scheme can be different from the first phase if additional reinforcements yield more continuous beams. In the simplest case the beam still has a simple supported static scheme. The incremental loads are usually all the permanent and the variable loads that burden on the slab. Therefore the mechanics of the CSTC beam should be studied for the first and second phases. More specifically the first phase truss is supposed to have only positive bending moments, whereas the second phase composite section can be submitted to positive and negative bending moments that should be studied separately.

For what concerns the ultimate limit states, the composite beams shall be checked for: resistance of critical cross-sections (maximum bending moment, maximum vertical shear, supports, etc.), resistance of lateral-torsional buckling, resistance to longitudinal shear.

The serviceability limit states shall be verified in terms of stresses, deformations and concrete cracking.

3.2.1 Simplified analysis of creep effects

The structural analysis has to obey the prescriptions for the composite steel and concrete structure that are contained or in the Italian Code [2] or in the Eurocode 4 [7]. In order to study and to verify the behaviour of the beams, it has been assumed that an elastic global analysis is applicable. As suggested by the Codes, the effects of concrete creep may be taken into account by using modular ratios n_L for the concrete. According to the Eurocode 4 the modular ratios depends on the loading type:

$$n_L = n_0\left(1+\psi_L\varphi_t\right) \tag{1}$$

where n_0 is the modular ratio E_a / E_{cm} for short term loading, E_{cm} is the secant Young

modulus of the concrete for short term loading, φ_t is the creep coefficient depending on the age of concrete at the considered moment and on the age at loading, ψ_L is the creep multiplier depending on the type of loading (permanent, primary and secondary effects of shrinkage).

3.2.2 Effective width of flanges for shear lag

Considering a final composite section, both the bottom steel plate and the top concrete cast widths should be verified to be effective. For what concerns the base steel plate it has to be considered that it can be subjected to compressive forces only in the second phase. During this phase the concrete is hard and, being connected by the web diagonal bars to the bottom plate, it is capable of preventing buckling of any of the compression flange towards the web. According to Eurocode 4 [7] the composite section can be classified as follows:

Class	Limit
1	$c/t \le 9\varepsilon$
2	$c/t \le 14\varepsilon$
3	$c/t \le 20\varepsilon$

where c is the transversal length of the outstand flange, t is the corresponding thickness and $\varepsilon = \sqrt{235MPa/f_y}$. The same Code also reports that a steel web in Class 3 encased in concrete may be represented by an effective web of the same cross section in Class 2.

For what concerns the in place concrete cast, since the typical composite web width is equal to about the width of the bottom base, it results as the effective one by means of the typical connection by the truss web bars. Whereas the effective width of the upper flange constituted by the concrete cast over the slab can be calculated according to the Eurocode 2 [6] as follows:

$$b_{eff} = \sum b_{eff,i} + b_w \tag{2}$$

$$b_{eff,i} = 0.2 \cdot b_1 + 0.1 \cdot L_0 \le 0.2 \cdot L_0 \tag{3}$$

where b_w is the concrete section web width, b_1 is half of the distance between two beams and L_0 is the distance between points of zero bending moment along the beam longitudinal axis.

3.3 First phase ultimate and serviceability limit states

The first phase steel truss supports the global bending and shear solicitations by means of internal forces acting along its constitutive bars. Depending on the element assembly (i.e. bend curvature of the diagonal bars) and on the load, this structure can more or less approach an ideal truss. It means that the lower are the nodal eccentricities, the lower are the bending solicitations in the bars. In any case the solicitation on each longitudinal and diagonal member can be found by means of a linear or geometrically non-linear elastic analysis. Referring to the steel truss the compressed member is usually composed by two or more steel bars that can be round or square. Therefore the typical cross section belongs to the Class 1 according to the Eurocode 3 [8]. If the structure can be considered a perfect truss all the bars are subjected to tension or to compression. The design tensile strength of the bottom chords can be computed as:

$$N_{pl,Rd} = A \cdot f_y / \gamma_{M0} \tag{4}$$

where A is the area of its gross-section, f_y is the steel yield strength and γ_M is the material partial factor (for resistance of cross section) that can be evaluated according to the code in force. The design resistance of the cross section for uniform compression may be determined as:

$$N_{c,Rd} = A \cdot f_y / \gamma_{M0} \tag{5}$$

The same compression member shall be verified against buckling and its design buckling resistance may be taken as the sum of each compressed member strength:

$$N_{b,Rd} = \chi \cdot A \cdot f_y / \gamma_{M1} \tag{6}$$

where χ is the reduction factor for the relevant buckling mode and γ_{M1} is the material partial factor for resistance of members to instability. The value of χ for the non-dimensional slenderness $\overline{\lambda}$ may be determined according to Eurocode 3 [8]:

$$\chi = \left(\Phi + \sqrt{\Phi^2 - \overline{\lambda}^2}\right)^{-1} \tag{7}$$

with 1.0 as a limiting value, where:

$$\Phi = 0.5 \cdot \left(1 + \alpha \cdot \left(\overline{\lambda} - 0.2\right) + \overline{\lambda}^2\right) \tag{8}$$

$$\overline{\lambda} = \sqrt{\left(A \cdot f_y\right) / N_{cr}} \tag{9}$$

and $\alpha = 0.49$ is an imperfection factor and N_{cr} is the elastic critical force for the relevant buckling mode based on the gross sectional properties. The evaluation of the

buckling wave length should take account for the particular welding condition at every intersection between the top chord with the web diagonal bars. The least favourable condition is represented by assuming a rotational hinge at every truss joints. In reality the welds have a finite longitudinal dimension that give each chord a bigger degree of fixity.

If the joints cannot be considered as a point because of the steel truss eccentricities every member is in general submitted to bending and axial force actions. In this case the design bending resistance of each compressed member can be determined as:

$$M_{pl,Rd} = W_{pl} \cdot f_y / \gamma_{M0} \tag{10}$$

where W_{pl} is the plastic section modulus. The interaction between the axial force (tensile or compressive) and the bending moment may be verified as:

$$M_{Ed} / M_{pl,Rd} + \left(N_{Ed} / N_{pl,Rd}\right)^2 \leq 1 \tag{11}$$

where M_{Ed} and N_{Ed} are respectively the bending moment and axial force design actions. If the member is compressed, it shall be verified against buckling. The verification may be in the elastic range or in the plastic one according to Eurocode 3 [8]:

$$N_{Ed} \cdot \gamma_{M1} / \left(\chi \cdot N_{pl,Rd}\right) + k \cdot M_{Ed} \cdot \gamma_{M1} / \left(M_{pl,Rd}\right) \leq 1 \tag{12}$$

where k is an interaction factor that can be evaluated according to the Annex A or Annex B of the same Code.

When a typical truss is loaded by the slab in some provisional stages, it has to support torsion solicitations. If the truss is made only by one web, the resulting section has a very low torsion stiffness. That's why the most common trusses are made at least by two webs. These can be inclined in the transverse direction in such a way to have an overall triangular shape section. On the contrary if the two trusses lay in vertical planes, the top chord should be connected by transverse elements. To obtain the highest efficiency, these connection should form triangular fields. Therefore, in general the torsion induced an increment on the axial (and bending) solicitation on each truss members, that can be determined by a linear elastic analysis. From the global point of view, the truss shall be verified from flexural-torsional buckling. It can be made by means of a linear buckling analysis. Savoia et al. [9] proposed the following formula to evaluate if the stiffness of the steel truss K can assure the truss nodes to be fixed:

$$K \geq K_{min} = \frac{\pi^2 \cdot N_{crit}}{4 \cdot \beta^2 \cdot L} \tag{13}$$

where N_{crit} is the critic Euler buckling load for the top chord member, L is the distance between two consecutive upper truss nodes, β, that is the ratio between the critical buckling length and L, can be assumed equal 1.2 increasing the buckling length because of

the flexibility of the truss.

It can result that this kind of buckling is avoided because of the dimensions and the assembly of the top chord, especially in those trusses in which the sections has triangular shape. Transversal bending and shear verifications shall be interest the bottom steel plate depending on the loads applied by the slab at the tip of the inferior flange. As a final consideration it's important to notice that the first phase is a provisional phase and the yielding of any of the steel truss member should be avoided. Hence it is reasonable that the ultimate limit states verifications are replaced by the stress ones considering the first phase as a serviceability limit state. In this case, all the previous equations can replace by similar ones in the elastic field. However some of the verifications can be critical in the design of the truss, especially the ones referring to the top chord.

For what concerns other serviceability limit states, since the first phase is a provisional phase, the deformations should be computed. Then the first phase truss deflections should be summed to the second phase composite beam ones and compared to the code's limits. If the steel truss has an inferior steel plate, it is possible to shape the steel truss with an initial counter deflection. In general the truss deflections can be computed with a linear or geometrically non-linear elastic analysis. The model should take into account the nodal eccentricities, depending on their influence in the global behaviour.

3.4 Second phase bending Ultimate Limit State

3.4.1 Positive bending Ultimate Limit Sate

Referring to the final composite section made by the steel truss and the concrete cast, the positive bending ultimate limit state is now considered. According to Eurocode 4 [7], the design bending strength shall be determined by rigid-plastic theory only if the composite cross-section is in Class 1 or in Class 2 and where pre-stressing by tendons is not used. Whereas elastic analysis and non-linear theory may be applied to cross sections in any case. Furthermore for elastic analysis and non-linear theory it may assumed that the composite cross-section remains plane if the shear connection is designed in accordance to the same Eurocode's provisions. This is discussed in the connection ULS paragraph. A CSTS beam, subjected to positive bending, is usually of Class 1 since the compressed steel section belongs to the Class 1. Still according to the Eurocode 4 [8] the tensile strength of concrete shall be neglected. The plastic resistance moment of the composite cross section can be made assuming the following hypotheses: full interaction between steel truss and concrete; the steel truss chord area is stressed to its design yield strength in tension or in compression; the effective area of concrete in compression resists a stress of 85% of its design cylinder

compressive strength f_{cd} constant over the whole depth between the neutral axis and the most compressed fibre of concrete (see Fig. 3.1).

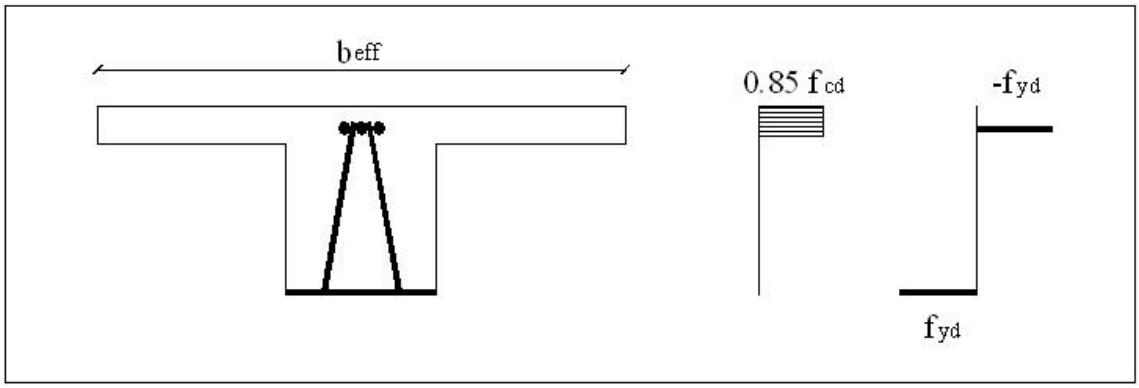

Fig. 3.1: Plastic resistant positive bending moment

As a consideration of general validity for this section, both the stresses of concrete and of steel material shall be subtracted from the stresses deriving from the first phase if necessary. For simplicity, the following formulas report only the total stresses, that is the sum of the first and second phase contributions. The plastic resistant positive bending moment can be determined as follows:

$$M_{pl,Rd} = f_{yk} \cdot As \cdot d \cdot (1 - \xi) \tag{14}$$

and by imposing the equilibrium of the section normal solicitation

$$\xi = f_{yk} \cdot (A_s - A_s') / (0.85 \cdot f_{cd} \cdot b_{eff} \cdot d) \tag{15}$$

where b_{eff} is the effective compressive concrete width, d is the effective depth, $\xi = x/d$ is the non-dimensional neutral axis depth, A_s and A_s' are respectively the tensile and compressive structural steel areas.

When the positive bending resistance of the composite cross section is determined by non-linear theory it can be assumed that the composite cross section remains plane. The stress-strain constitutive law of the materials shall be taken into account according to the code in force. In particular a parabola-rectangle stress-strain relation can be assumed for the concrete where the maximum strength is equal to the 85% of the cylinder compressive strength f_{cd}. A bi-linear relation, elastic-perfectly plastic, can be used as a constitutive law for the structural steel f_{yk} in which the maximum tensile stress is equal to the characteristic yield strength. A similar diagram can be used for reinforcing steel, if present, with the only difference in the maximum stress equal to the design yield strength f_{yd}. The ultimate limit state is defined in terms of maximum and minimum strains, i.e. it is equal to -3.5‰ for the compressive concrete and to +10‰ for the tensile steel. The bending resistance can be computed as the minimum value of the following two expressions depending on the first

crisis respectively of the compressive concrete or of the tensile steel:

$$M_{nl,Rd} = 0.85 \cdot f_{cd} \cdot b_{eff} \cdot d^2 \cdot \xi \cdot \alpha \cdot (1 - k_a \cdot \xi) - f_{yk} \cdot k' \cdot A_s' \cdot d \cdot (1 - \delta') \quad (16)$$

$$M_{nl,Rd} = f_{yk} \cdot k \cdot A_s \cdot d \cdot (1 - \xi) \quad (17)$$

where $k_a = a/d$ is the non-dimensional depth of the concrete compression centre, $k = \sigma_s / f_{yk}$ and $k' = \sigma_s' / f_{yk}$ are respectively the tensile and compressive non-dimensional steel stresses, δ' is the compressive steel depth, α is a coefficient given as

$$\alpha = -\frac{\int_0^x \sigma_c(y) \cdot b_{eff} \cdot dy}{0.85 \cdot f_{cd} \cdot b_{eff} \cdot x} \quad (18)$$

with $\sigma_c(y)$ the concrete stress.

The hypothesis of the plane section conservation is still valid for the calculation of the elastic resistance to bending and the extension of the previous formulas to the elastic case is very simple.

3.4.2 Negative bending Ultimate Limit State

If a certain degree of fixity is recover at the beam-column joint by means of additional steel reinforcement, the composite beam can be submitted to negative bending moment. Possible ways to create the fixity between the CSTC beam and the column are studied in the following chapter in detail. With no reference to this particular issue, the study of negative bending resistance of the typical CSTC beam section is discussed herein. In this case the beam needs another classification of the composite section since the typical CSTC beam has non symmetric structural steel. The compressive steel is usually a steel plate partially encased by the concrete cast or two or more bars embedded in the concrete base. In the first case the section usually belongs to lower classes, for example Class 3. In order to be able to calculate the negative bending resistance with the same formulas seen for the positive one, the evaluation of the effective compressive steel area is necessary and can be determined as shown in the previous paragraphs. For what concerns the tensile steel, it is usually constituted by two or more bars, round or square. Every other reinforcement can be considered if its solidarity with the section is assured by means or of welds to the original steel truss or of an adequate anchorage length. The case in which the beam presents an additional truss which doesn't provide confinement for the entire concrete section (for example a simple vertical truss), adequate connection with the original CSTC truss should be predisposed in order to avoid brittle failure due to local high shear stresses acting on concrete longitudinal vertical sections.

3.5 Second phase shear Ultimate Limit State

The determination of the second phase shear resistance of the CSTC beam has to take account of many structural differences compared with a classical composite steel and concrete section. The Eurocode 4 [7] writes that the plastic shear resistance should be taken equal to the structural steel section one unless the value for the contribution from the reinforced concrete part of the beam has been established. In the case of the CSTC some preliminary considerations can be drawn. The first important aspect is that, being the structural steel part a truss without solid web, its shear stiffness is lower than a typical composite beam's one. In addiction, the shear stiffness of a solid web concrete section of the same depth is higher before the cracking occurs. Therefore it can be expected that the first shear resistant mechanism of the CSTC beam deals mainly with the concrete that acts as a typical beam following the elastic theory of De Saint Venant. After the tensile concrete strength is reached the steel truss can provide resistance for the tensile stresses. The fact that the truss diagonal bars are not homogeneously distributed, but rather disposed with a certain step, suggests that a Ritter-Mörsch shear mechanism can be established after the concrete cracking. Referring to this static scheme a new composite truss can be considered in which: the truss bottom chord can maintain its role, the top chord is composed by the concrete section and the steel top bars, the diagonal members are alternated in tension and in compression and are respectively constituted by only steel bars or by composite steel bars and concrete. Hence it's important to notice that the diagonal bars that can absorb the tensile stresses are only the ones orthogonal to the cracks and not both of the truss diagonal bars (see Fig. 3.2).

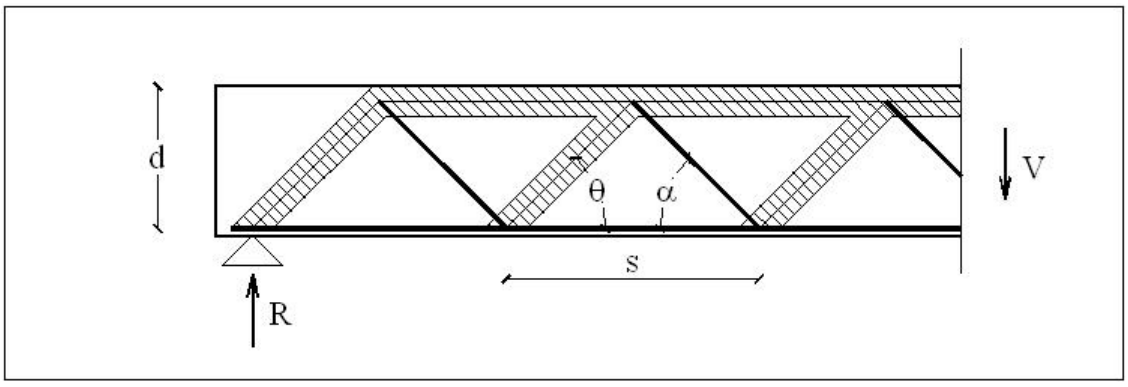

Fig. 3.2: Shear composite truss mechanisms of a typical CSTC beam

From this arguments it is clear that the CSTC beam has shear mechanisms quite different to the typical composite beam and more similar to a reinforced concrete beam with inclined web bars.

Therefore the shear resistance of the CSTC section can be evaluated with the following

formula similar to the one contained in the previous version of the Eurocode 2 [11]:

$$V_{Rd,3} = V_{cd} + V_{wd} \tag{19}$$

where V_{cd} is the concrete contribute, V_{wd} is the steel contribute. The first one is limited by the achievement of the shear stress before the cracking of the section. This condition can be expressed by the well known Jourawsky formula. For a generic concrete section, it can be approximated as follows:

$$V_{cd,1} = \tau_{cd} \cdot J \cdot b_w / S' \cong 0.6 \cdot f_{ctd} \cdot b_w \cdot d \tag{20}$$

$$V_{wd} = A_{sw} \cdot f_{yk} \cdot 0.9d \cdot (\cot\theta + \cot\alpha) \cdot \sin\alpha \cdot \cos\beta / s \tag{21}$$

in which J is the moment of inertia of the concrete section, S' is the static moment of the compressed part of the section respect to the principal axis, f_{ctd} and τ_{cd} are respectively the concrete design tensile strength and the design shear strength, b_w is the minimum concrete width along the effective depth d, s is the offset between two parallel diagonal bars of the steel truss, θ is the angle between the concrete compression strut and the beam axis perpendicular to the shear force, $\cos\alpha$ and $\cos\beta$ are the director cosine of the shear reinforcement respect to a couple of axis parallel respectively to a longitudinal beam axis and the vertical shear force axis. In fact the second one take account of the transverse inclination of the truss diagonal bars. It can be noted that the two contribute are not simultaneous but sequential. It means that two main trends of the stiffness are expected as the shear force increases. After the concrete cracks only the secondary concrete shear resistant mechanisms can be effective, like the arch-tie one, the compressive chord one, the dowel action of the longitudinal steel. When the CTSC beam with inferior steel plate or profile are considered the first two cited are the most effective. In fact the dowel action of the inferior steel is absent because it's external and it's connected only in correspondence to the shear connectors. In this case, to evaluate the secondary shear resistance near the collapse, the following Fig. 3.3 is considered, in which it has been assumed that the crack propagates up to the concrete web. Because of the lower compressive stresses the crack diminishes its slope approaching the top chord, that is the neutral axis, and it becomes almost parallel to the longitudinal beam axis. In this ultimate limit state the concrete shear contribution can be computed as follows:

$$V_{cd} \le V_{cd,2} = 0.1 \cdot f_{cd} \cdot b_w \cdot x \tag{22}$$

where x is the neutral axis depth.

To complete the verification of the composite truss, the strength of the concrete strut shall be assessed. In the least favourable case, the contribution of the compressed steel diagonal bar can be neglected. The resistant shear strength may be written as:

$$V_{Rd,2} = 0.85 \cdot f_{cd} \cdot b_w \cdot 0.9d \cdot (\cot\theta + \cot\alpha)/(1 + \cot^2\theta) \quad (23)$$

where all the symbol meanings are already explained. The design shear strength of a generic CSTC beam section is the minimum of $V_{Rd,2}$ and $V_{Rd,3}$. The last consideration can be drawn about the value of θ. The angle of the concrete strut cannot be unambiguously predicted since it depends on many factors. A reasonable assumption is that the concrete strut is conditioned by the shear cracks that appear before the Mörsch mechanism, according to the developed theory. Hence it can be assumed that the shear cracks follow the directions of the compression principal stresses. Near the external supports they may be assumed at 45° respect to the longitudinal beam axis [12] and [13].

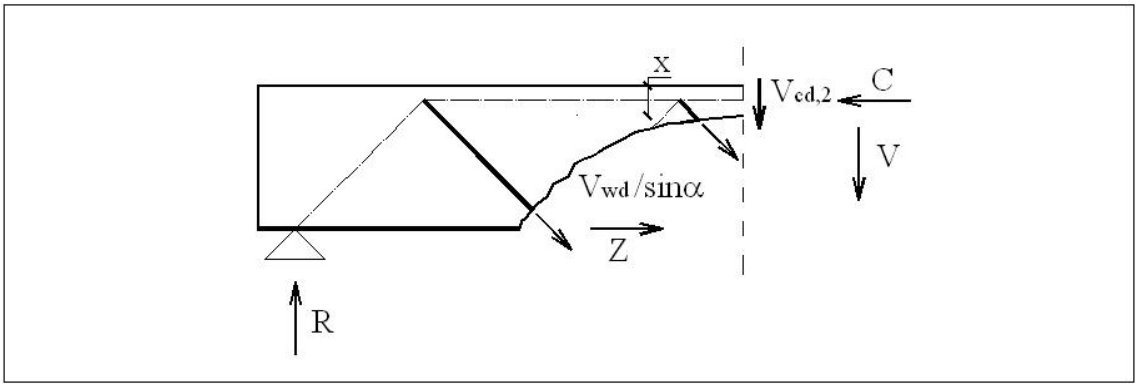

Fig. 3.3: Ultimate resistant mechanisms for the concrete shear contribution

3.6 Second phase connection Ultimate Limit State

Looking at the CSTC beam the bottom steel plate, if present, is connected to the concrete section by the steel truss diagonal bars. They can be considered particular shear connectors.

According to the Eurocode 4 [7], shear connection shall be provided to transmit the longitudinal shear force between the concrete and the structural steel element, ignoring the effect of natural bond between the two. Shear connectors shall have sufficient deformation capacity to justify any inelastic redistribution of shear assumed in design. Ductile connectors are those with sufficient deformation capacity to justify the assumption of ideal plastic behaviour of the shear connection in the structure considered. A connector may be taken as ductile if the characteristic slip capacity is at least 6 mm. Furthermore shear connectors shall be capable of preventing separation of the concrete element from the steel element, except where separation is prevented by other means. The total design longitudinal shear shall be determined in a manner consistent with the design resistance, taking account of the

difference in the normal force in concrete or steel over a critical length. The number of connectors should be at least equal to the total design shear force for the ultimate limit state, determined according to the elastic or plastic bending resistance, divided by the design resistance of a single connector. That number is called the number of connectors for full shear connection n_f.

In the case of the CSTC beams the diagonal bars are the connectors between the steel bottom plate and the concrete web. They should be welded with the plate in such a way to restore the entire axial and shear strength of the diagonal bars. The throat thickness of the welds shall be dimensioned according to the code in force. The minimum depth of the steel plate should prevent its rip due to the concentrated stresses coming from the diagonal bars. A minimum plate thickness shall be defined at least equal to the weld fillet all around the bar. The cut of the diagonal bar should leave a section parallel to the plate plane in order to avoid anomalous stress concentration. Since the diagonal bars are not singular element but they are part of the steel truss, they can perform very high ductile displacements when they are subjected to longitudinal shear. Puhali and Smotlak [10] were the first study on the longitudinal shear behaviour of the REP® beams with two sets of experimental push out tests. The test results showed the high stiffness and resistance capacity against the shear force. Only in a case, that is a very light diagonal bar connection, the cause of the failure was the fracture of the diagonal bars after 10 mm of ductile slip. In all the other tests the steel truss demonstrated to have a satisfactory ductility and the failure was caused by the concrete crushing due to the particular test method adopted.

3.7 Second phase Serviceability Limit States

3.7.1 Simplified analysis of shrinkage effects

The concrete shrinkage deformations produce reciprocal stresses between the concrete and the steel truss. In fact the steel truss constitutes an obstacle to the free shrinkage of concrete. The evaluation of the internal stresses due to the shrinkage the following simplified procedure can be adopted. Once the concrete shrinkage strain ε_{sh} in computed, the tensile axial force acting on the concrete section can be evaluated as:

$$N_{sh} = \varepsilon_{sh} \cdot E_c \cdot A_c \tag{24}$$

where E_c and A_c are the Young modulus and the section area of concrete. This imaginary force is applied to the centre of the concrete section. In addition, an opposite imaginary force should be applied to the total composite section for its equilibrium. Since, in general, the centre of the composite section and the centre of the concrete one are not

coincident, the following ideal solicitations can be written:

$$N_i = -N_{sh} \quad \text{and} \quad M_i = N_{sh} \cdot e_c \tag{25}$$

in which e_c is the eccentricity between the two mentioned centres. All these solicitations shall be applied to the corresponding sections thought as totally reacting and using the superposition principle. The modular ratio of concrete can be assumed according to the previous paragraphs to account the effects of the concrete creep. Particular attention shall be paid if the composite beam has a hyperstatic scheme, since secondary solicitations can arise.

3.7.2 Stress Serviceability Limit State

According to the Eurocode 4 [7] the calculation of stresses for beams at the serviceability limit state shall take into account the shear lag, the creep and shrinkage of concrete, the cracking and tension stiffening of concrete and the sequence of construction. In this case the creep and shrinkage of concrete may be taken into account by using modular ratios. The stress analysis, can be made by linear or non-linear theory with the conservation of plane section hypothesis. If required, the stress limitations for concrete, structural steel and reinforcement can be assess by the corresponding limitations given in the code in force.

3.7.3 Deformation Serviceability Limit State

The beam axis curvature can be evaluated from the following formula:

$$\kappa = M / EJ = (\varepsilon_s - \varepsilon_c)/d \tag{26}$$

where EJ is the flexural stiffness of the beam, ε_s is the tensile steel strain and ε_c is the lower compressive concrete strain and d is the effective depth of the section. Theoretically, if the curvature is known all along the beam axis, the rotation angle and the deflection of every section can be calculated by two subsequent integration processes with the integration constant determined by the boundary conditions. The difficulty to follow this method is that the flexural stiffness of the beam results to be very variable because of the materials' non-linearity. A simplified method [11] defines an equivalent curvature that can be used with the classical elasticity theory to calculate the beam deformations, as follows:

$$EJ_{eq} = \zeta \cdot EJ_{II} + (1-\zeta) \cdot EJ_I \tag{27}$$

where EJ_I and EJ_{II} are the flexural stiffness computed respectively with hypothesis of non cracked and cracked section and

$$\zeta = 1 - \beta_1 \cdot \beta_2 \cdot (M_{cr} / M)^2 \tag{28}$$

where β_1 is a coefficient that accounts for the bond properties of the steel and it can be

assumed equal to 1.0 for the ribbed bars and to 0.5 for the plain ones, β_2 is a coefficient that accounts for the duration of the applied load or for repeated loads and is equal to 1.0 for single short term load and to 0.5 for permanent load or repeated ones, M_{cr} is the cracking bending moment of the section and M is the acting bending moment. The structural steel can be treated as plain steel in first approximation. It is important to notice that the shear deformations are neglected by this method.

3.7.4 Concrete cracking Serviceability Limit State

In this section the concrete cracking phenomena are analyzed both for the positive and negative bending moment applied to a CSTC beam section. Within the cracking SLS it can be distinguished three levels: the decompression limit state, the cracking limit state and the crack width limit state. The last one consists in the verification that the crack width remain under adequate limits when the structure is subjected to specific load combinations. The limiting values of the crack opening can be determined according to the in force code. The decompression limit state is the more restricting. It must be verified that the section continues to operate in state I and so totally reacting. In the case of partial pre-compression every sections shall remain totally compressed for the quasi-permanent load combination. For what concerns the cracking limit state it shall be assess that, in the more tensile fibre of the section, the stress is below the concrete tensile characteristic strength. Even in this case the section is totally reacting. Only in the crack width limit state the crack opening is admitted and shall be limited. Even for the classical reinforced concrete structure the crack width is usually affected by many phenomena and it has a wide dispersion. This is the cause of the high coefficient used to obtain the characteristic crack width from the medium one adopted in many international codes:

$$w_k = 1.7 \cdot w_m \tag{29}$$

According to the Italian Code [15] the medium crack width can be evaluated starting from:

$$w_m = \varepsilon_{sm} \cdot s_{rm} \tag{30}$$

where ε_{sm} is the steel medium strain between two adjacent cracks and s_{rm} is the medium distance between two adjacent cracks. The last one depends on many factors as the stress distribution in the section, the quality of the materials, the bond between them, the shape and the dimension of the section, the quantity and the position of the reinforcement. In fact between two adjacent cracks, a part of the concrete section collaborates with the tensile reinforcement thanks to the bond effects. The definition of that area is based on the experimental results. The same Italian Code proposes the following relation for this size, originally presented by the CEB-FIP Model Code in 1978 [16]:

$$s_{rm} = 2 \cdot (c + s/10) + k_2 \cdot k_3 \cdot \phi / \rho_r \tag{31}$$

where c is the reinforcement cover, s is the transverse distance between two bars, ϕ is the bar diameter, k_2 is a coefficient that characterizes the bond and is equal to 0.4 for ribbed bars and to 0.8 for plain ones, k_3 is a coefficient that accounts for the section solicitation and is equal to 0.125 for combined bending and axial force and 0.250 for pure tensile axial force, ρ_r is the ratio between the steel area and the collaborating effective concrete area. For what concerns the medium steel strain between two adjacent sections, a formula similar to the Eq. 28 is proposed:

$$\varepsilon_{sm} = \frac{\sigma_s^{II}}{E_s} \cdot \left[1 - \beta_1 \cdot \beta_2 \cdot \left(\sigma_{sr} / \sigma_s^{II}\right)^2\right] \tag{32}$$

where σ_s^{II} is the steel tensile stress in a cracked section computed for the acting solicitation, σ_{sr} is the steel tensile stress in a cracked section for a solicitation equal to the one that causes the cracking, E_s is the steel Young modulus, the other coefficients maintain the same meaning than the ones presented in the deformation SLS paragraph. If the concrete section is partially pre-compressed the parameters are those of the reinforcing steel and not of the pre-stressing steel.

All the presented formulation deals with the cracking phenomena in ordinary reinforced concrete beams. The CSTC beams have very different characteristics and the previous method, even with accurate parameter choice, doesn't give adequate results. It has been focused on the concrete base CSTC as a first purpose. These beams have a concrete base that usually contains both structural steel as the bottom chord of the truss and ordinary reinforcements, at least as a minimum confinement net for the concrete. A bibliography study has been made in order to compare the results of a wide range of formulations that start from many different assumptions. The results of all the formulations, herein presented, have been compared with the experimental ones in order to evaluate which one is more efficient for the studied construction type.

Leonhardt [17] developed the following formula for the calculation of the cracks distance:

$$s_{rm} = 2 \cdot (c + s/10) + k_1(c,s) + k_2 \cdot k_3 \cdot \phi / \rho_r \tag{33}$$

where $k_1 = 1.5 \cdot (c + s/8)$ only if the cover is less than 3 cm and the bar step is less than 14 times their diameter, k_2 is equal to 0.40 for ribbed bars and 0.74 for plain ones and the other symbols has the same meaning already explained. The medium crack width is computed with the same Eq. 30 and the medium steel strain is equal to:

$$\varepsilon_{sm} = \frac{\sigma_s^{II}}{E_s} \cdot \left[1 - k_5 \cdot \left(\sigma_{sr} / \sigma_s^{II}\right)^2\right] \tag{34}$$

where k_5 is a coefficient that varies between 0.4 and 0.8 depending on the load cycles, intensity and duration. The characteristic value of the crack width is calculated as:

$$w_k = 1.5 \cdot w_m \tag{35}$$

The CEB-FIP Model Code 1990 [18] contains the following formula for the maximum crack distance, of which the medium distance would be a rate:

$$s_{r,max} = \frac{\phi}{36 \cdot \rho_r} \cdot (\varepsilon_{sm} - \varepsilon_{cm}) \text{ and } s_{rm} = s_{r,max} \cdot 2/3 \tag{36}$$

where ε_{cm} is the medium value of the concrete stresses between two cracks. In this formula the effective concrete contributing area is determined as it is in the Eurocode 2 [11]. The medium crack width is computed as follows:

$$w_m = s_{rm} \cdot (\varepsilon_{sm} - \varepsilon_{cm}) \tag{37}$$

where

$$\varepsilon_{sm} - \varepsilon_{cm} = \varepsilon_{s2} - \beta \cdot \varepsilon_{sr2} \text{ with } \varepsilon_s = \frac{\sigma_s^{II}}{E_s} \text{ and } \varepsilon_{sr2} = \frac{f_{ctm}}{E_c} \tag{38}$$

and β is a coefficient that varies between 0.38 and 0.60 depending on the load cycles and duration and on the cracking type.

The new edition of Eurocode 2 [6] modifies the previous text formula taking account of pre-compression if necessary:

$$s_{r,max} = k_3 \cdot c + k_1 \cdot k_2 \cdot k_4 \cdot \phi / \rho_{p,eff} \tag{39}$$

where k_1 is equal to 0.8 for ribbed bars and 1.6 for plain one, k_2 is equal to 0.5 for bending and 1.0 for tensile axial force, k_3 and k_4 are evaluated in the Italian National Annex as 3.4 and 0.425,

$$\rho_{p,eff} = \frac{(A_s + \xi_1^2 \cdot A_p)}{A_{c,eff}} \tag{40}$$

in which A_p is the pre-stressing steel area and

$$\xi_1 = \sqrt{\xi \cdot \phi_s / \phi_p} \tag{41}$$

again with ϕ_s, ϕ_p the diameters of respectively ordinary and pre-stressing steel and ξ the ratio between the bond characteristics of those types of steel that can vary between 0.6 for wire strands and 0.8 for ribbed bars. The crack width follows the formula:

$$w_k = s_{r,max} \cdot (\varepsilon_{sm} - \varepsilon_{cm}) \tag{42}$$

where

$$\varepsilon_{sm} - \varepsilon_{cm} = \frac{\sigma_s^{II} - k_t \cdot \frac{f_{ctm}}{\rho_{p,eff}} \cdot \left(1 + \alpha_e \cdot \rho_{p,eff}\right)}{E_s} \tag{43}$$

with k_t is equal to 0.6 for short duration load and to 0.4 for long duration one, α_e is the ratio between the Young modulus of the reinforcing steel and concrete, $\rho_{p,eff}$ is the ratio between the steel area and the effective concrete one based on the section shape and the strain distribution.

Broms [19] studied a simplified calculation method which doesn't take account of the concrete medium strain between two cracks. The medium distance is determined with the formula:

$$s_{rm} = 2 \cdot \left(c + \phi / 2\right) \tag{44}$$

with clear meaning of the symbols. Whereas the characteristic crack width is calculated as follows:

$$w_k = 4 \cdot \left(c + \phi / 2\right) \cdot \varepsilon_{sm} \tag{45}$$

the medium width is assumed to be half of the maximum one. In the present work the medium steel strain is calculated according to Eq. 32.

According to Beeby [20] the medium distance between adjacent cracks can be evaluated as:

$$s_{rm} = k_1 \cdot c + k_2 \cdot \phi / \rho_r \tag{46}$$

in which the coefficient are defined as function of the probability of exceeding that value, k_1 varies between 1.33 for the medium value and 1.94 for the 2% of exceeding probability, k_2 is equal to 0.01 for the medium value and 0.06 for the 2% of exceeding probability if the crack depth is expected to be more than three times than the cover. The crack width can be evaluated with the Eqs. 29 and 30. In the present work the medium steel strain is calculated according to Eq. 32.

Park and Paulay [21] evaluated the medium distance between cracks with the following formula:

$$s_{rm} = 1.33 \cdot \frac{f_{ctm} \cdot \phi}{4 \cdot \tau_{bm} \cdot \rho_r} \tag{47}$$

where τ_{bm} is the medium bond shear stress. They also proposed a simple estimation of the effective concrete area, whereas the maximum crack width is:

$$w_{max} = \frac{\sigma_s^{II} \cdot \phi}{k_1 \cdot \rho_r} \tag{48}$$

in which $k_1 = 2 \cdot \tau_{bm} \cdot E_s / f_{ctm}$ with clear meaning of the symbols.

For what concerns the CSTC beam with the steel base plate, all the previous formulations are based on very different geometrical configuration. In particular it is very difficult to characterize the interaction between the steel plate and the upper concrete cast. The efficiency of this bond is very low because the bond surface is only in the upper plane of the steel plate and it is little if compared to the plate sectional area. It can be assumed that the connection between the steel plate and the concrete is entirely entrusted to the truss diagonal bars that offer preferential support to the concrete struts. Hence it can be assumed that there in no transmission of stresses between the steel plate and the concrete web in the middle of two adjacent connectors. This produce that there can be only one crack between two connectors, that is, the crack distance is equal to the distance of the truss inferior nodes. Therefore, referring to the flexural cracks that have a mainly vertical development, the maximum crack width shall be equal to the stretching of the steel plate between two connectors. This condition can be expressed with the following formula:

$$w_{max} = \frac{M \cdot H_{tr}}{d \cdot E_s \cdot A_{pl}} \tag{49}$$

where M is the acting bending moment, d is the effective depth of the composite beam, H_{tr} is the truss depth, A_{pl} is the inferior steel plate area. For what concerns the crack due to the shear force, the main role is played by the tensile diagonal bar across the crack. In this case the bond between the external surface of the bar and the surrounding concrete can be moderately more efficient. The diagonal bar are usually plain and they have a relatively big diameter compared to ordinary reinforced concrete stirrups since, in the case of CSTC beams, the spacing is determined by the first phase steel truss. The failure of the bond between the diagonal bar and the concrete leads to the worst case in determining the crack width that can be expressed by the following formula:

$$w_{max} = \frac{V \cdot H_{tr}}{\sin^2 \alpha \cdot E_s \cdot A_d} \tag{50}$$

where V is the acting shear force, A_d is the total area of the diagonal bars across a crack and α is the angle between the diagonal bar and the longitudinal beam axis. The most likely shear crack width can be a percentage of the maximum one depending on many factors, like the position of the crack, the geometrical disposition of the bars and the section shape.

3.8 Complete analysis of stresses, shrinkage and creep effects

For what concerns the partially pre-compressed CSTC a more sophisticated analysis shall be done to evaluate the stresses, accounting for the external loads, for the concrete creep and shrinkage and for the pre-stressed steel relaxation. In fact in this case the typical process of fabrication is: steel truss assembly, pre-stressing strand positioning and stretching, base concrete cast, strand cut, first phase load application, completion concrete cast, second phase load application. The resisting section changes during the first and the second phase and every material develops its own elastic and non-elastic deformations during the structure lifetime. In order to study accurately the behaviour of a partially pre-compressed CSTC section constructed in two distinct phases, an adequate model has been developed. On this purpose, the strain and stress states of a beam section are evaluated for the entire life of the structure and for each fibres in which the section is subdivided. The life of the section is subdivided by the following events: stretching of the pre-stressing strands, considered time 0; cut of the strands and compression of the section made by the concrete base and the steel truss, at about 3 days; first phase permanent load application, at about 30 days; second phase permanent load application, at about 60 days; second phase variable load application, at about 1,000 days. For what concerns the concrete, the creep and the shrinkage phenomena have been taken into account according to the CEB-FIP Model Code 1990 proposals [18], whereas the pre-stressing steel relaxation has been modelled according to Gutiérrez et al. [22]. The concrete creep strain, due to a increment of applied stress, is considered as an additional contribute:

$$\varepsilon_{c,tot}(t,t_0) = \sigma_{c,0} \cdot \left(\frac{1}{E_c(t_0)} + \frac{\varphi(t,t_0)}{E_{c,28}} \right) \tag{51}$$

where $\varepsilon_{c,tot}(t,t_0)$ is the concrete total strain at time t under constant stress $\sigma_{c,0}$ acting from t_0 time, $E_c(t_0)$ and $E_{c,28}$ are the concrete Young modulus evaluated respectively at time t_0 and at 28 days, $\varphi(t,t_0)$ is the creep coefficient. In its general form the last coefficient can be calculated as follows:

$$\varphi(t,t_0) = \beta_a(t_0) + \varphi_d \cdot \beta_a(t-t_0) + \varphi_f \cdot (\beta_f(t) - \beta_f(t_0)) \tag{52}$$

in which $\beta_a(t_0)$ accounts for the concrete strength variation as a function of its age, φ_d is the coefficient of the delayed elasticity assumed equal to 0.4, β_d accounts for the development of the delayed elasticity as a time function the time, φ_f is the plastic strain coefficient, β_f accounts for the development of the plastic strain as a time function. The precise description and evaluation of all these factors is contained in the CEB-FIP Model

Code 1990 [18]. In general the creep coefficients depend on the environment relative humidity, on the structural element dimensions, on the concrete mix design, on the environment temperature and on the speed of the concrete hardening process.

The concrete shrinkage at time t has been evaluated as:

$$\varepsilon_{sh}(t,t_0)=\varepsilon_{sh,0}\cdot(\beta_{sh}(t)-\beta_{sh}(t_0)) \tag{53}$$

where $\varepsilon_{sh,0}$ is the shrinkage coefficient, β_{sh} accounts for the development of the shrinkage as a time function, t_0 is the time from which the influence of the shrinkage is considered to start. The adequate calculation of each factor can be made as proposed by the recalled CEB-FIP Model Code 1990 [18]. In general the concrete shrinkage depends on the age, on the environment relative humidity, on the concrete mix design and on the environment temperature.

The pre-stressing steel relaxation is based on the determination of its stress loss $\Delta\sigma_{pR}$ during the time. This value is a function of the initial stress value $\sigma_{p,0}$ after the strand stretching while the strain is kept constant. In a pre-compressed section, the initial strand tensile stress diminishes by the combined effects of delayed and non-elastic strain and of the external loads. Hence the value computed in the constant strain condition shall be reduced; Gutiérrez et al. [22] proposed the following formula:

$$\overline{\Delta\sigma_{pR}}(t)=\Omega_R(t)\cdot\Delta\sigma_{pR}(t) \tag{54}$$

in which $\overline{\Delta\sigma_{pR}}(t)$ is the reduced stress loss at time t, $\Omega_R(t)$ is a reductive coefficient of relaxation effect. The same authors furnish the evaluation method for the recalled parameters. To account for the steel relaxation due to accelerated concrete maturation process the following formula is adopted:

$$\Delta\sigma_{pR,32h}=0.049\cdot\sigma_{p,0} \tag{55}$$

A numerical time integration is used, subdividing the time domain in steps, with the assumption that the section stress state in constant between two adjacent steps. The numerical procedure has been implemented in MATLAB to analyze the stress state of a section subjected to axial force and bending moment. The section can be composed by materials with distinct properties. Every material can be added to the resistant section at an arbitrary time. The section is subdivided into fibres each of those has a different stress and strain history. The hypotheses assumed for the calculation of the strain and stress states of the composite section at each time step are: the plane section conservation, the perfect bond between steel and concrete, concrete tensile strength negligible after its cracking. The results of the presented method are compared with the experimental showing the accuracy and the effectiveness of the presented method.

3.9 Conclusions

Because of the lack of Italian or International Standards, the calculation methodology of the CSTC beams has to be deposited at the Italian Superior Council of Public Works by each patent owner and producer. The original calculation method of S. Leone had been developed under the Admissible Stress assessment method in the 60's. Starting from it, the CSTC beam mechanics have been analyzed and a new calculation method has been proposed as an improvement and an extension of the original one for what concerns the more wide applicability and the Limit State assessment method. Particular attention has been paid to define and correlate every Ultimate and Serviceability Limit Sates to the beam performances.

The hardening of the completion concrete cast distinguishes two phases in the life of the CSTC beam that are characterized by distinct resistant sections and different mechanics. During the first phase the beam behaves as a prefabricated steel truss. In the second phase the steel truss collaborates with the hardened concrete. The mechanics of the CSTC beam have been studied for the first and second phases. More specifically the first phase truss has only positive bending moments, whereas the second phase composite section is submitted to positive and negative bending moments that have been studied separately.

For what concerns the ultimate limit states of a CSTC beam, it has been proposed an assessment method for: resistance of critical cross-sections (maximum bending moment, maximum vertical shear, supports, etc.), resistance of lateral-torsional buckling, resistance to longitudinal shear. In terms of the serviceability limit states other verifications have been suggested to check the stresses, the deformations and the concrete cracking.

The developed method has been used in the next chapter to predict and analyze the experimental tests leaded to three distinct type of CSTC beams.

References

1. Leone S. REP® beam calculation methods. Deposited at the *Italian Superior Council of Public Works*, 1967.
2. D M LL PP 14 Jan 2008. Norme Tecniche per le Costruzioni (Construction Technical Codes). *Gazzetta Ufficiale* 04 Feb 2008.
3. Scotta R, Tesser L. Preliminary experiences and basic concepts on the structural performance of hybrid trussed beams. *4th Spec. Conference on The Conceptual Approach to Structural Design*, Venice, 2007.
4. Scotta R, Tesser L. Sperimentazione su travi tralicciate miste REP® – NOR (Experimental tests on composite truss beams REP® – NOR). *VII Italian Workshop on Composite Structures*, Benevento, 2008.
5. Scotta R, Tesser L. Sperimentazione su travi tralicciate miste con fondello in laterizio (Experimental tests on composite truss beams with bottom clay tile). *XVII CTE Congress,* Rome, 2008, **2**: 811-816.
6. CEN. *Eurocode 2: Design of concrete structures Part 1-1: General rules and rules for buildings*. Comité Européen de Normalisation: Bruxelles, 2003.
7. CEN. *Eurocode 4: Design of composite steel and concrete structures Part 1-1: General rules and rules for buildings*. Comité Européen de Normalisation: Bruxelles, 2004.
8. CEN. *Eurocode 3: Design of steel structures Part 1-1: General rules and rules for buildings*. Comité Européen de Normalisation: Bruxelles, 2003.
9. Vincenzi L, Mazzotti C, Savoia M. Stabilità in fase I del traliccio metallico delle travi reticolari miste (Stability in the first phase of the steel truss of composite steel truss and concrete beams). *XVII CTE Congress*, Rome, 2008, **2**: 741-750.
10. Puhali R, Smotlack I. Relazione sulle prove di push-out atte a determinare le leggi di carico-scorrimento delle travi in sistema composto REP (Report on the push-out tests fit for the determination of load-slip laws of REP composite truss beams). *Science of Constructions Institute Acts*, University of Trieste, 1980.
11. CEN. *Eurocode 2: Design of concrete structures Part 1-1: General rules and rules for buildings*. Comité Européen de Normalisation: Bruxelles, 1993.
12. Leonhardt F, Walther R. *Schubversuche an einfeldringen stahlbetonbalken mit und ohne schebbewehrung zur ermittlung der schubtragfähigkeit und der oberen schubspannungsgrenze*. W. Ernst & Sohn Deutcher Aussschuss für Stahlbeton, Berlin, 1962.

13. Leonhardt F, Walther R. *Schubversuche an plattebalken mit unterschiedlicher Schubbewehrung*. W. Ernst & Sohn Deutcher Aussschuss für Stahlbeton, Berlin, 1963.

14. Vitaliani R, Scotta R, Saetta A. *Il calcolo agli stati limite delle strutture in calcestruzzo armato*. Edizioni Libreria Progetto, Padova, 2002.

15. D M LL PP 09 Jan 1996. Norme Tecniche per il calcolo, l'esecuzione, ed il collaudo delle strutture in cemento armato, normale e precompresso e per le strutture metalliche. *Gazzetta Ufficiale* 05 Feb 1996.

16. CEB-FIP. CEB-FIP Model Code for concrete structures. *CEB Bulletin d'Information* 1978, **124**.

17. Leonhardt F. *Crack control in concrete structures*. International Association for Bridge and Structural Engineering Surveys, Zurich, 1977, S-4/77.

18. CEB-FIP. CEB-FIP Model Code for concrete structures. *CEB International Recommendation* 1990.

19. Broms BB. Crack width and crack spacing in reinforced concrete members. *ACI Journal* 1965, **62** (10): 1237-1255.

20. Beeby AW. The prediction of crack widths in hardened concrete. *The structural Engineers* 1979, **57A** (1): 9-17.

21. Park R, Paulay T. *Reinforced Concrete structures*. John Wiley & Sons Inc., 1975.

22. Gutierrez SE, Cudmani RO, Danesi RF. Time-dependent of reinforced and prestressed concrete members. *ACI Structural Journal* 1996, **94** (4): 420-427.

Chapter 4

Composite Steel Truss and Concrete beam experimental tests

4.1 Introduction

The analysis of the composite truss structures revealed the need of new experimental tests to fully understand and verify their mechanics and their resistant mechanisms [1], [2]. Toward this aim three sets of lab tests were designed. To find the best solution from both the mechanical and the economical points of view, some general issues were considered for the tests, such as the material choice for the steel, the test load schemes, the measure instruments to be used and their dispositions to record all the interesting values.

The first set deals with eight CSTC beams: four of them designed only with the bare steel truss and the other four with the completion concrete cast. The particularity of the beams is that the bottom chord of the truss is a longitudinal steel plate, with a rectangular section to support the slab and the concrete cast. This beam is the original one invented by S. Leone in the 60s. The beams have been submitted to six and four tests respectively. The beam sections, the static scheme, and the load positions were designed in order to investigate both the bending and shear failure modes [3], [4].

Another set of similar tests have been designed for a different type of truss whose bottom chord is formed by two cold rolled steel plates, having a sort of "S" shaped section specifically profiled to support a clay tile which constitutes the bottom end of the completed beam. This beam type is particularly suitable for using in conjunction with floors in concrete and hollow clay bricks. Two beams have been designed as bare steel truss in order to

characterise the behaviour in the first phase, while the other six were tested as complete hybrid structures [5].

The third set has been created with the pre-stressed concrete base beams. This particular type of beam have been designed only with the steel truss and the concrete base without the completion concrete cast. The aim is to investigate the behaviour of these beams with particular attention to the cracking phenomena.

The results of the three sets of experimental tests are presented. The tests were carried out in the Construction Material Experimentation Lab at the Department of Construction and Transportation of the University of Padua. All the experiments were preceded by the characterization of the concrete and steel materials by means of standard tests. In particular it has been verified that the welding points didn't affect the mechanical properties of the truss steel elements.

All the tests were carried out by displacement control and they made provision for successions of increasing amplitude displacements with loading and unloading cycles. All the tested beams had the four point load scheme. The responses were characterized by different type of failure, as expected. The measure instruments permitted to fully understand and characterize the behaviour of each of the beam tested.

All the three tests data are analysed by a critical and detailed review. Since the tests were designed to be redundant, the comparison with the results obtained from distinct specimens can prove the reliability of the structural typology and the goodness of the test measurements.

The results of the plate steel base beams [3], [4], "S" shape cold formed base beams [5], and pre-stressed concrete base beams are presented in terms of load-deflection curves, load-steel chord strain curves, load-steel diagonal member strain curves, load-crack width curves, distance between cracks. The first goal is to verify if the calculation method proposed can account for all the beam mechanisms and predict the results with accuracy. Secondly it's very important to find the reason of possible anomalous behaviours. They can be determined by intrinsic typology details or defects happened during the construction.

4.2 Lab equipment and measure instruments

In order to carry out the experimental tests, the equipment of the Construction Material Experimentation Lab at the Department of Construction and Transportation of the University of Padua was used. The general static scheme for all the tests is a simple supported beam with two symmetric point loads. The load had been applied by an hydraulic

jack set up on a steel contrast frame (see Fig. 4.1a). The last one had been firmly anchored to the lab floor. The jack had been commanded by an hydraulic control unit. It controlled the displacements during the tests. The jack applied the load to distributor beams. Between them a load cell was been placed that controlled the load value during all the test executions. The supports of tested beam were constituted by a couple of strengthened steel pedestals and particular steel elements, shaped as a low rail. These elements furnished the adequate degrees of liberty to the tested beam, leaving them free to have end rotations or longitudinal displacements. During the tests, global and local displacements had been measured. For the local one, strain transducers have been used. These instruments have a 100 mm base with two little knifes at the end that can be put in contact with the material. They can remain united with the material thanks to a system formed by a little stick glued to the material at one end and with an adjustable spring at the other. The little knifes can be placed in contact with the external surface of the steel or concrete materials (see Fig. 4.1b).

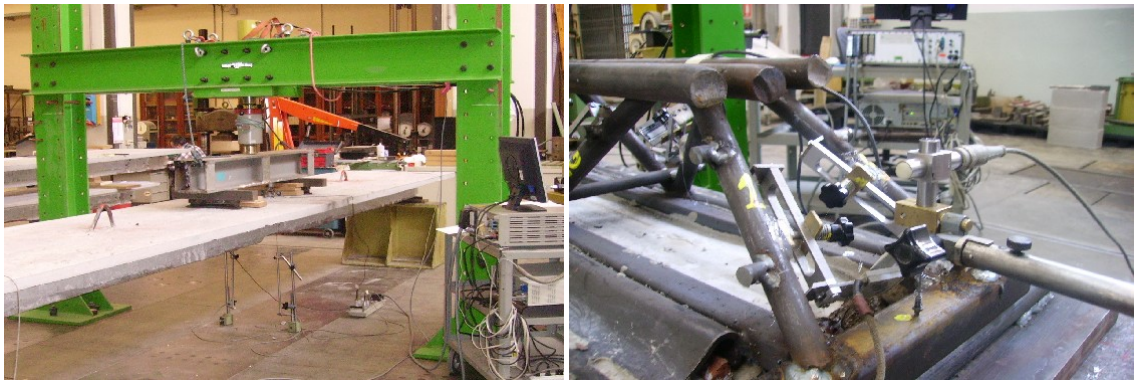

Fig. 4.1: Load frame with hydraulic jack, load cell and distributor beam (a) and example of strain transducers applied to the nude truss (b)

To measure the deformation of the steel truss embedded in the composite beams, some pieces of steel bar were welded perpendicularly to the truss and covered by rubber before the concrete casting. After the concrete hardening, the rubber was removed and the transducer's knifes were connected with them (see Fig. 4.2a). The accuracy of the transducers is 1/10,000 mm, that is a precision of 1 μstrain over the 100 mm. The nominal range is ± 2.5 mm that is ± 0.025 strain over the given base. To measure the displacement, for example of the mid-span displacement of the beams, inductive standard displacement transducer had been used (see Fig. 4.2b). Their nominal maximum range are 10 and 100 mm. In the experimental tests two of them had been placed in the mid-span under the beams and another two on the supports to control the support vertical stiffness. In the case of the beams with the lower tile, this last one were locally removed to make sure that the measurement weren't conditioned by local cracked or even collapsed tile. The electric signals from all the measurement instruments had converged in a data acquisition system controlled by a computer for the

instantaneous elaboration. The equipment let the immediate control of any transducer all during the test.

Fig. 4.2: Example of strain transducers applied to the embedded truss (a) and of inductive displacement transducers applied to the under the beam mid-span section (b)

4.3 REP®-NOR beams

4.3.1 Experimental test design

The CSTC beams called REP®-NOR are characterized by the truss bottom chord formed by a steel plate. This is the original truss invented by S. Leone for the CSTC beams. In this case the truss is actually constituted only by steel material and each part has a structural role. The theoretical and experimental studies are done with the purpose of verifying the behaviour of this beam both for shear and bending moment solicitations up to the failure. The design of these beams had been made to obtain different collapse mechanisms both for the 4 nude trusses and for the 4 composite beams, by mainly varying the length of the beams. Another considered criterion was to respect the REP® beam production rules in terms of diagonal bar bending diameter and welding method [1]. In particular the following beams had been tested:

- n. 2 nude trusses, called trusses 1, with clear span 280 cm;
- n. 2 nude trusses, called trusses 2, with clear span 150 cm;
- n. 2 composite beams, called beams 3, with clear span 280 cm;
- n. 2 composite beams, called beams 4, with clear span 280 cm.

The ratios between the span length and the distance of the load points were such that bending failure was expected in the trusses 1 and in the beams 3 and shear failure in the trusses 2 and in the beams 4, even if with different mechanisms between the composite beam and the nude truss. The four point load tests were conducted applying two concentrate loads under displacement control. The truss sections and the corresponding static schemes are

presented in the Fig. 4.3 - Fig. 4.5 for each tested beam. The design material properties are grade S355 for the steel truss and class C20/25 for the concrete [2]. It can be noted that the truss top chord is constituted by three round bars, welded together with the web diagonal bars. These lasts are composed by two sequences of bars that are bent in correspondence to the top chord and cut in correspondence to the lower one. The bottom chord is set up by a steel plate. The longitudinal distance between two truss nodes is about 374 mm (see Fig. 4.6).

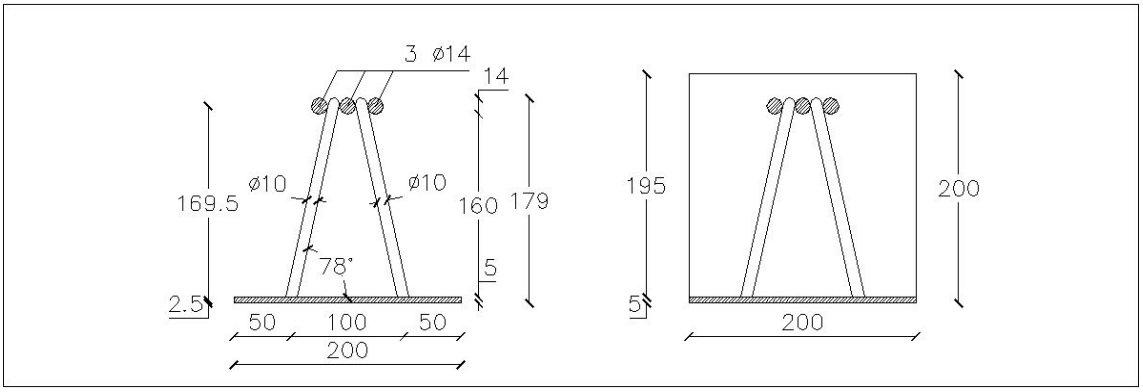

Fig. 4.3: REP®-NOR type sections for the trusses and the beams

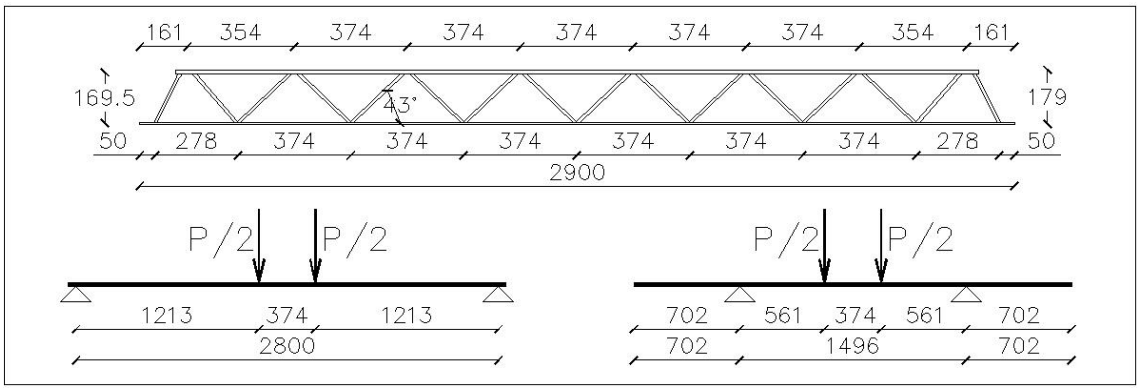

Fig. 4.4: REP®-NOR type profile and corresponding test static schemes for the trusses 1 and 2

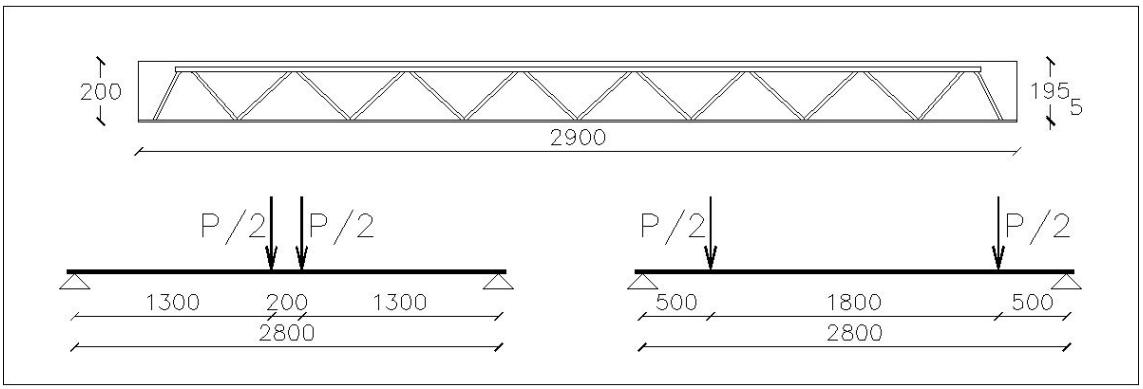

Fig. 4.5: REP®-NOR type profile and corresponding test static schemes for the beams 3 and 4

The steel trusses were similar and their dimensions are reported herein for each component:

- trusses
  - top chords n. 2 x 14 mm round bars;
  - web diagonal bars n. 2 x 10 mm round bars, 374 mm spacing;
  - bottom chord plate n. 1 x 200 mm x 5 mm plate.

The concrete completion cast produces a square shape section. There wasn't any additional reinforcement. Each beams has been submitted to cyclic load of increasing amplitude up to failure. The instrumentations collected the data of the mid-span deflections, the deformations of the upper and the steel truss bottom chords. In particular the following instruments were positioned:

- n. 6 strain transducers of 100 mm base in the truss diagonal bars (4 at a head and 2 at the other one);
- n. 1 strain transducer of 100 mm base in the steel truss top chord (at the mid-span);
- n. 1 strain transducer of 100 mm base in the steel truss bottom chord (at the mid-span);
- n. 2 displacement transducer of 10 mm range in the beam upper surface (in correspondence to the supports);
- n. 2 displacement transducer of 100 mm range in the beam lower surface (in correspondence to the mid-span);
- n. 1 load cell between the hydraulic jack and the load distributor beam.

The calculation method, presented in the previous chapter, has been applied to predict the experimental tests results of both the nude trusses and the composite beams. In order to have the possibility to compare the values, the medium mechanical properties of the material, determined by the adequate preliminary tests, has been used. The following Tab. 1 summarizes the theoretical expectations:

Tab. 1: theoretical resistance values of the beams

Beam	M_R [kNm]	a [m]	V_{c1} [kN]	V_{c2} [kN]	V_w [kN]	V_R [kN]	P [kN]
Trusses 1	18.6	1.30				22.1	28.6
Trusses 2	18.6	0.50				19.7	39.4
Beams 3	69.5	1.30	49.1	26.0	47.3	73.3	106.9
Beams 4	69.5	0.50	49.1	26.0	47.3	73.3	146.6

The study of the nude trusses required the use of a numerical model able to capture its effective geometry distinct from an ideal truss, as it has been underscored in the previous chapter. The geometric model, that considered for all the eccentricities of the truss, has been

defined taking into account all the production rules such as the bar bend minimum diameter and the weld minimum dimensions. The centreline model has been generated with a 3D draw program and then imported in a finite element method program (see Fig. 4.7). The following step was to assign to each element their mechanical properties and their appropriate connections. The welds were modelled with rigid links that connect the truss elements. A linear static analysis and a buckling analysis were carried out with the FEM program. The first one permitted the study of the global and the local stiffness of the truss whereas the second, while it confirmed the absence of the truss bending-torsional buckling, provided the local buckling load for the top chords. The load agrees with the Euler formula if the buckling critical length is assumed as 70% of the distance between two truss nodes. This is the consequence of the degrees of fixity that the welds give to the top chords in each node. The comparisons with the experimental results are presented below.

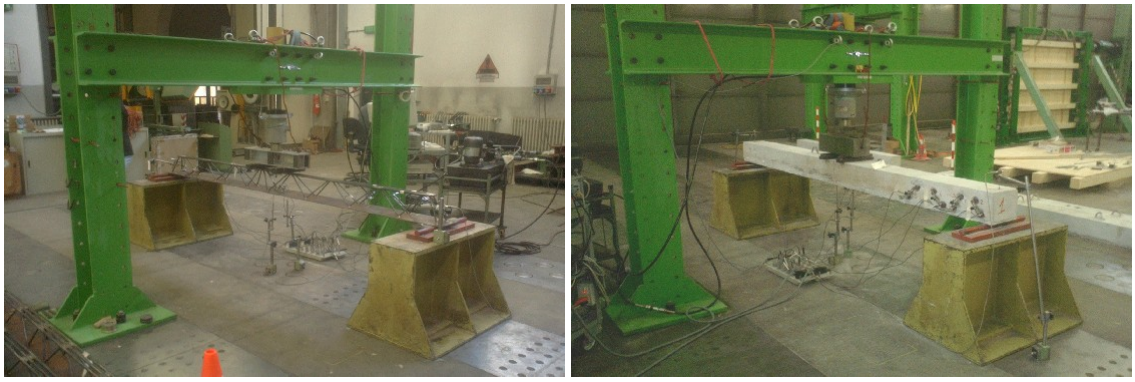

Fig. 4.6: Pictures of a REP*-NOR truss (a) and a REP®-NOR composite beam (b)

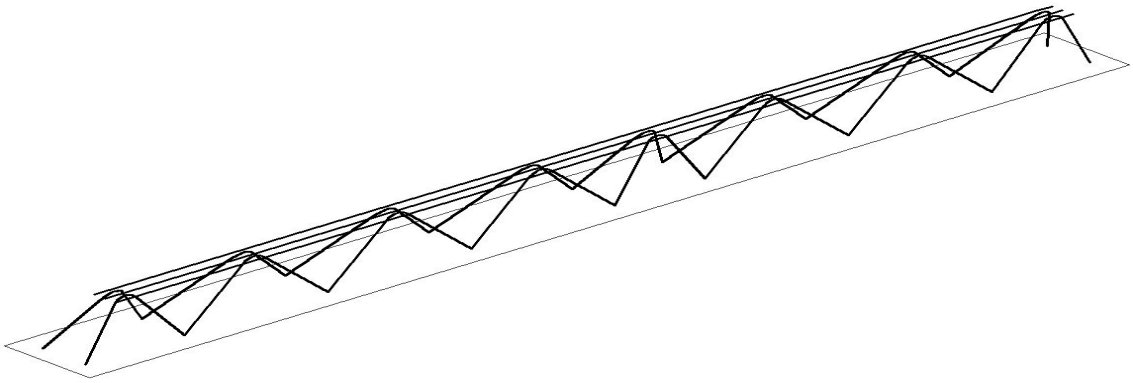

Fig. 4.7: Finite element model of the 3D truss

4.3.2 Material characterization tests

The material properties had been obtained by means of tests led in the Construction Material Experimentation Lab at the Department of Construction and Transportation of the University of Padua. In particular the following tests were carried out: standard compression test (UNI 12390-3/2002) on two concrete cube specimens (side equal to 15 cm) and

standard tensile test (UNI 10002/1) on eight steel bars (diameter 14 mm). For what concerns the steel bars, the last four specimens were taken from the top chord of the experimented trusses including welding points. The results are very homogeneous showing that the weld doesn't affect the behaviour of the steel. The results are summarized in the following Tab. 2 and Tab. 3.

Tab. 2: concrete cylinder test results

Specimen	base [mm^2]	height [mm]	R_c [MPa]
1	150x150	150	25.4
2	150x150	150	28.7
average			27.1

Tab. 3: steel bars tensile test results

Specimen	diameter [mm]	f_y [MPa]	f_u [MPa]
1	14	413	537
2	14	413	552
3	14	397	533
4	14	420	541
5	14	420	546
6	14	400	527
7	14	424	550
8	14	402	528
average		411	539

The average values for each material have been used to calculate the expected resistance of the beams.

4.3.3 Experimental test results and analyses

The results of the experimental tests on the 8 beams are presented herein with this order: the two tests on the nude trusses 102n; the two tests on the composite beams 101; the two tests on the composite beams 102; the two tests on the composite beams 103.

4.3.4 Nude trusses 1

The truss profile is depicted in Fig. 4.8 with the positions of the measure instruments. The expected failure was the yielding of the top chord due to bending solicitations. The test process was composed by three loading and unloading cycles before failure. The load cell values have been corrected adding the weight of the steel distribution beam (0.20 kN). Both the trusses reached the failure by rotation of an upper truss joint due to the buckling of the first compressed diagonal bars and the bending of the top chord in correspondence to a loads 28.6 kN and 30.1 kN (see Fig. 4.9).

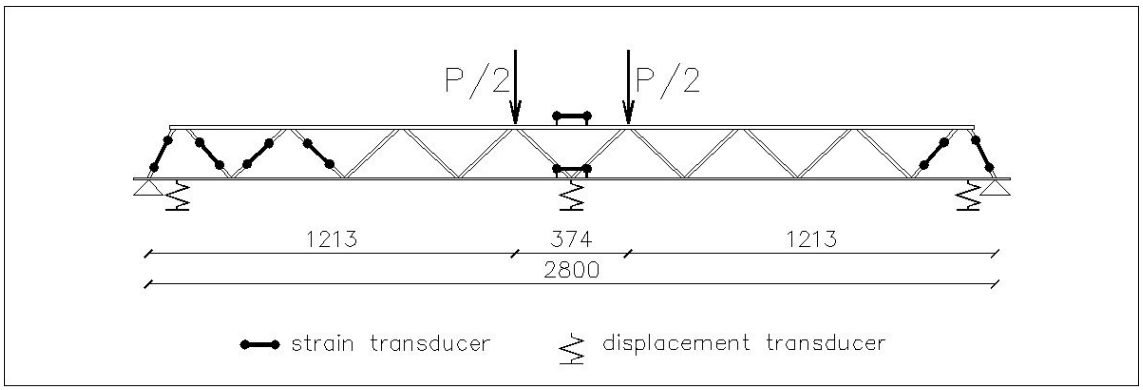

Fig. 4.8: Truss 1 profile with the instrument positions

Fig. 4.9: Pictures of the trusses 1 after the collapse

The failure mechanism is unrelated to the scheme of a perfect truss and the cause is the eccentricity at the nodes created by the bent bars. In fact, at the beginning of the loading process, the truss bars are subjected not only to axial force but also to bending moment. In particular the eccentricity between the two tensile-compressive diagonal bars creates the bending of the top chord (see Fig. 4.10). When the top chord yields, the rotational stiffness of the node decays and the critical length of the compressed bar increases leading to the bar buckling. In Fig. 4.11 the load vs. mid-span deflection curves for the last cycle are compared with the analytical results. The experimental curves have almost linear course until the yielding of the top chord occurs and brings to the compressed diagonal bars buckling. The

deflections at the first yielding were about 12 mm and the ultimate ones were about 24 mm and 26 mm. The geometry non-linear numerical model offers a good stiffness prediction and produces an higher strength because it cannot account for material non-linearity. In fact, even in the model, the bar stresses near the actual collapse load were very close to the steel yield strength. The strain transducers, placed on the lower steel plate and the top chord bars in the mid-span, showed a linear behaviour inside their elastic field. Also the strains collected from the first tensile diagonal bars reported an elastic behaviour. Both the strain measurements from the bottom chord and the tensile diagonal bars are well predicted by the linear elastic numerical model.

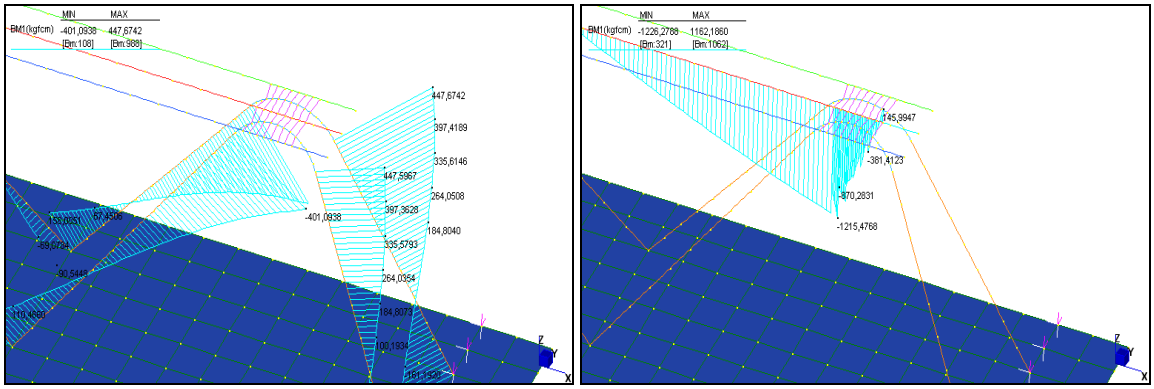

Fig. 4.10: Joint eccentricity in the trusses 1 and bar bending moment

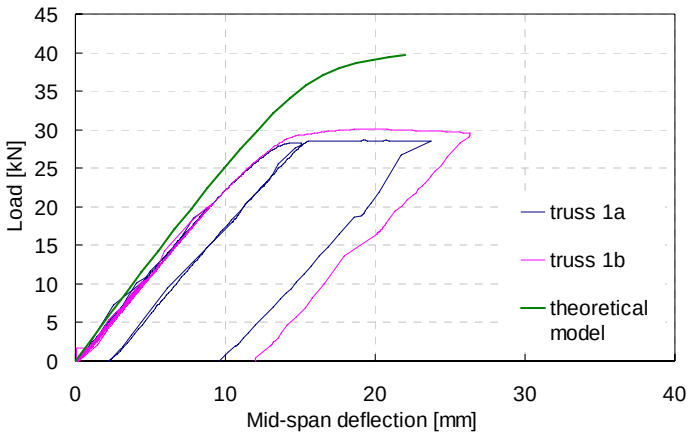

Fig. 4.11: Experimental and analytical load vs. deflection curves for the trusses 1

4.3.5 Nude trusses 2

The truss profile is depicted in Fig. 4.12 with the positions of the measure instruments. The expected failure was the buckling of the compressed diagonal bars. The test process was composed by three loading and unloading cycles before failure. The cell load values have been corrected adding the weight of the steel distribution beam (0.20 kN). Both the trusses

reached the failure for the buckling of the first compressed diagonal bars and the bending of the top chord for a load of 42.0 kN and 45.2 kN respectively(see Fig. 4.13). Hence the failure mechanism is the buckling of the first compressed bars as predicted. In Fig. 4.14 the load vs. mid-span deflection curves for the last cycle are compared with the analytical results. The experimental curves have mainly linear course until the buckling of the compressed diagonal bars occurs. After the buckling phenomena a softening behaviour takes place. The deflections in correspondence to the buckling were both about 6 mm.

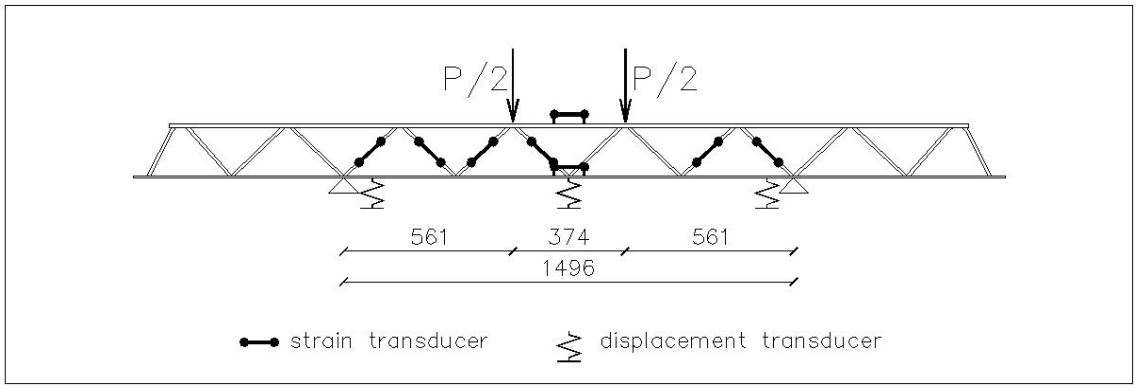

Fig. 4.12: Truss 2 profile with the instrument positions

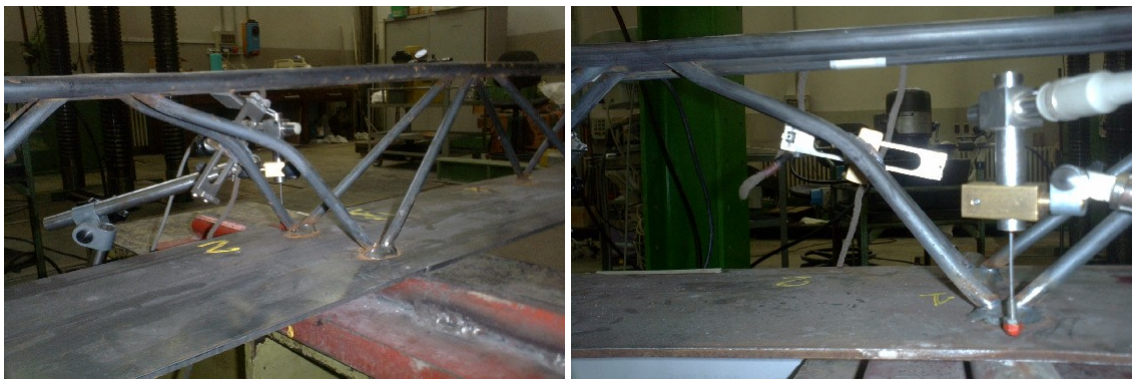

Fig. 4.13: Pictures of the trusses 2 after the collapse

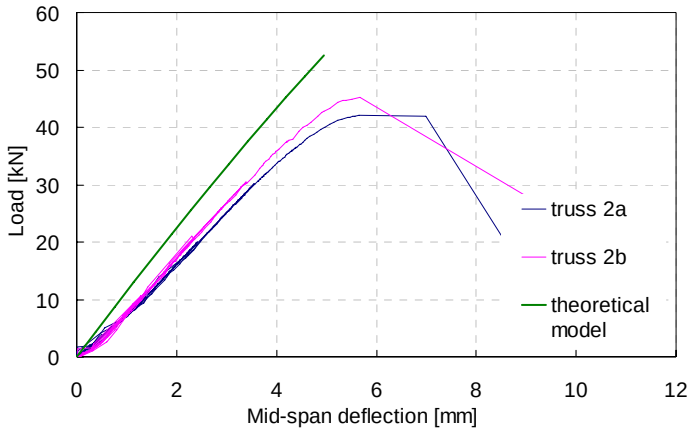

Fig. 4.14: Experimental and analytical load vs. deflection curves for the trusses 2

The geometry non-linear numerical model offers a good stiffness prediction and produces an higher strength. Only with a buckling assessment method that takes in account the possible imperfections the ultimate load can be accurately estimated. Even in this case the non-linear geometry analysis can evaluate the stiffness but not the buckling load because it doesn't account for the material non-linearity. All the other strain transducers showed a linear behaviour inside their elastic field until the buckling was reached and the values are well predicted by the non-linear elastic numerical model.

4.3.6 Composite beams 3

The truss profile is depicted in Fig. 4.15 with the positions of the measure instruments. The expected failure was the mid-span compressed concrete crushing. The test process was composed by three loading and unloading cycles before failure. The cell load values have been corrected adding the weight of the steel distribution beam (0.20 kN). The ultimate resisting loads were 120.0 kN and 119.3 kN. The failure mechanism is the compressed concrete crushing as predicted (see Fig. 4.16).

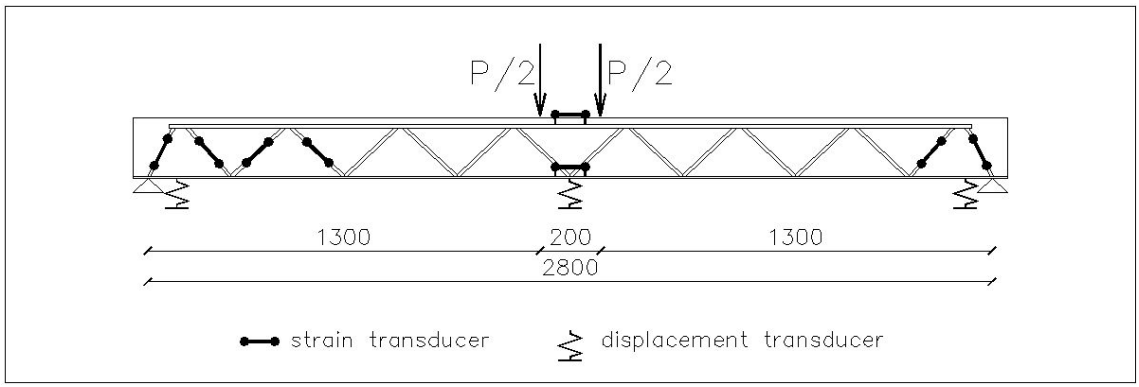

Fig. 4.15: Beam 3 profile with the instrument positions

Fig. 4.16: Pictures of the beams 3 after the collapse

In Fig. 4.17 the load vs. mid-span deflection curves for the last cycle are compared with the analytical results. The experimental curves have a first stiffness degradation in

correspondence to the tensile concrete cracking. After that the curves approach the cracked stiffness. The last cycle, when the sections are already cracked, have mainly a linear course until the yielding of the compressed steel bars. The deflections in correspondence to the yielding were both about 20 mm and the ultimate ones were both about 39 mm. The strain transducer at the bottom steel plate reveals that even the tensile steel yields after the compressive one, since its strain exceeds the elastic field at about 0.2% (see Fig. 4.18). All the other strain transducers, placed on the diagonal bars, remained inside their elastic field.

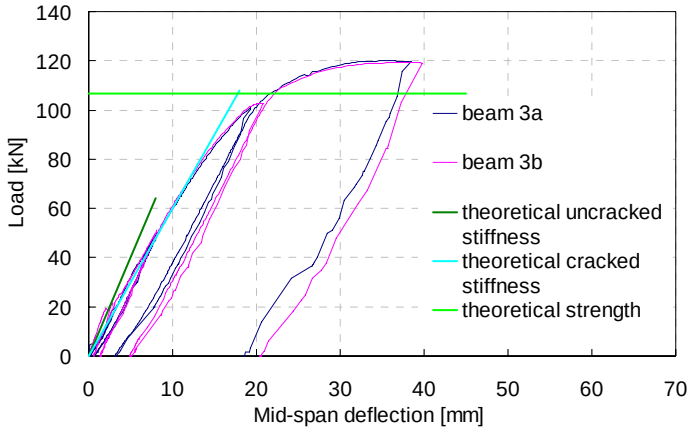

Fig. 4.17: Experimental and analytical load vs. deflection curves for the beams

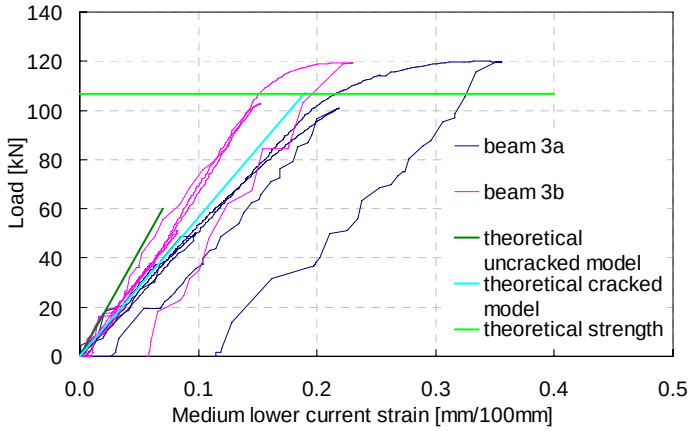

Fig. 4.18: Experimental and analytical load vs. bottom cord strain for the beams 3

4.3.7 Composite beams 4

The truss profile is depicted in Fig. 4.19 with the positions of the measure instruments. The expected failure was the tensile diagonal bars yielding. The test process was composed by three loading and unloading cycles before failure. The cell load values have been corrected adding the weight of the steel distribution beam (0.80 kN). The failure mechanism was the first diagonal bars yielding in correspondence to a loads 165.9 kN and 156.8 kN (see Fig. 4.20). The pictures highlight the inclined shear cracks and their slope reduction when they

approach the top compressed chord. Since the position of the diagonal bars can be noted by the welded transversal pieces of bar, the tests confirmed that the compressed concrete strut starts in correspondence to the lower truss node that offers preferential support. Even the separation of the inferior plate from the concrete section is clearly visible and corroborates the absence of dowel action as stated in the previous chapter.

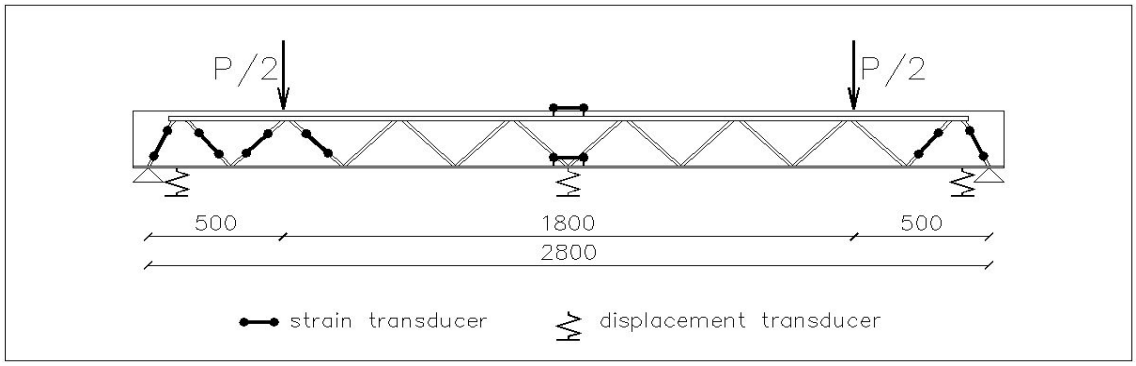

Fig. 4.19: Beam 4 profile with the instrument positions

Fig. 4.20: Pictures of the beams 4 after the collapse

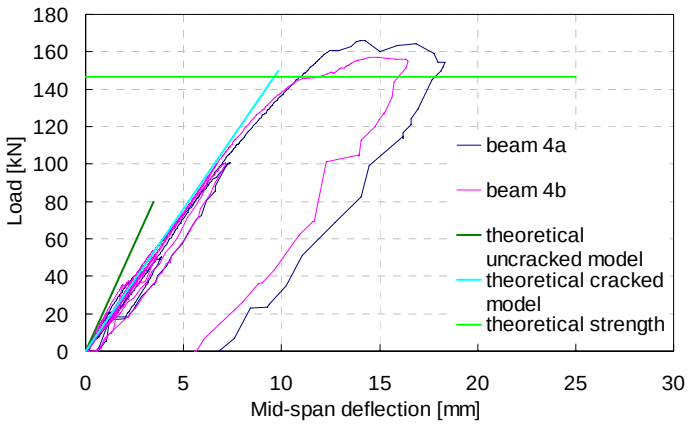

Fig. 4.21: Experimental and analytical load vs. deflection curves for the beams 4

In Fig. 4.21 the load vs. mid-span deflection curves for the last cycle are compared with the analytical results. The deflections in correspondence to the diagonal bars yielding were

about 12 mm and 13 mm and the ultimate ones were about 17 mm and 19 mm.

The strain transducers of the first tensile diagonal bars clearly show the two resistant mechanisms (see Fig. 4.22). The initial stiffness is due to the tensile strength of the concrete. In this phase the section in an elastic way and the stresses are below the tensile concrete strength. After the cracking the tensile diagonal bars have to support all the tensile stresses and the stiffness show a second slope.

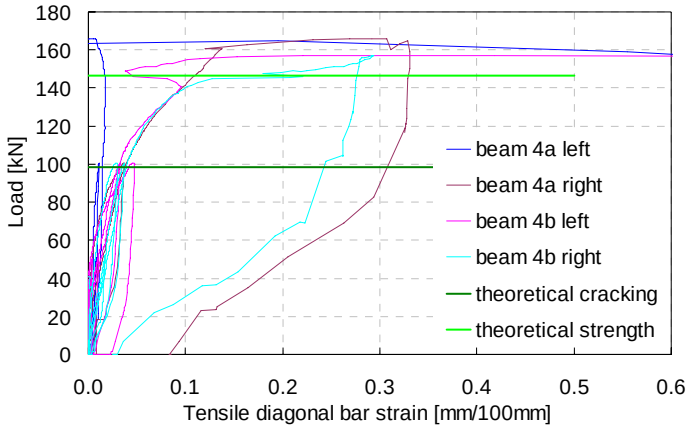

Fig. 4.22: Experimental and analytical load vs. tensile diagonal member strain for the beams 4

It's important to remark that the concrete tensile strength cannot always be available because of the concrete cracking due to the prevented shrinkage and the previous load history. After the cracking the contribute of the concrete, to sustain further shear solicitation, decays to a lower value due to the secondary shear resistant mechanisms like the arch-tie and the compressive chord ones. The tests confirmed the developed CSTC beam mechanics and the strength values were correctly predicted. The strain transducer of the first compressed diagonal bars is depicted in Fig. 4.23. The strain transducers of the upper and bottom chord in the mid-span reported an elastic behaviour.

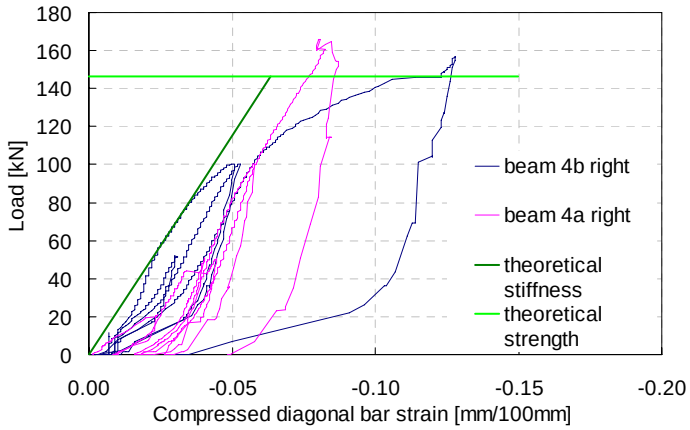

Fig. 4.23: Experimental and analytical load vs. compressed diagonal member strain for the beams 4

4.4 Ecotrave® Raftile® Beams

4.4.1 Experimental test design

The CSTC beams called ECOTRAVE® RAFTILE® are characterized by the truss bottom chord formed by two cold rolled steel plates, having a sort of "S" shaped section, specifically profiled to support a clay tile, and which constitutes the bottom finishing of the completed beam. This beam type is particularly suitable for using in conjunction with floors in concrete and hollow clay bricks, since the inferior plaster set up can be easier and can remain homogeneous in the time. The theoretical and experimental studies have for main aim to verify the behaviour of this beam both for shear and bending moment solicitations up to the failure. Furthermore it was important to verify that the connection between the steel bottom chord and the tile were enough to avoid separations. The design of these beams had been made on purpose to obtain different collapse mechanisms both for 2 nude trusses and for 4 composite beams, by mainly varying the length of the beams. The other criteria considered were to have spans representative of typical residential building slab and to respect the REP® beam production rules [1]. In particular the following beams had been tested:

- n. 2 nude trusses, called 102n, with clear span 420 cm;
- n. 2 composite beams, called 101, with clear span 594 cm;
- n. 2 composite beams, called 102, with clear span 420 cm;
- n. 2 composite beams, called 103, with clear span 240 cm.

The ratios between the span length and the distance of the load points were such that shear failure was expected in the short beams (103), bending failure in the long ones (101 and 102 and 102n) even if with different mechanisms for the nude truss. The four point load tests were conducted applying two concentrate loads in displacement control. The truss type sections and the corresponding static schemes are presented in the Fig. 4.24 - Fig. 4.30 for each tested beam.

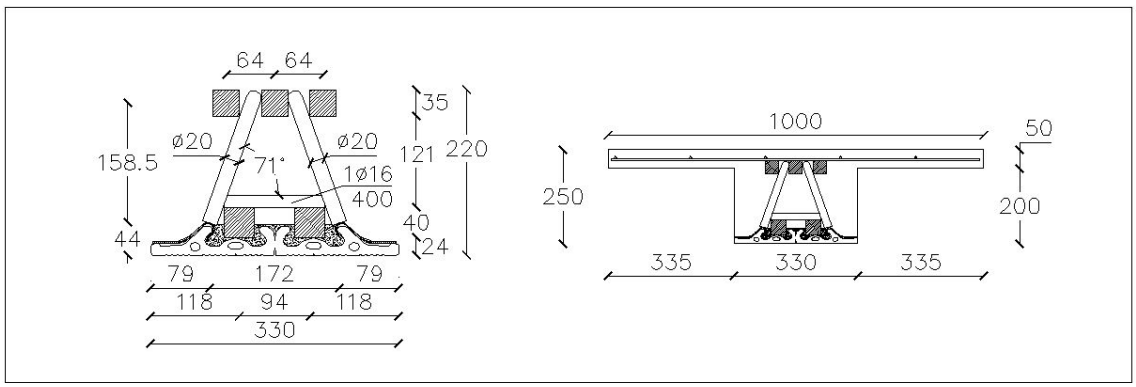

Fig. 4.24: ECOTRAVE® RAFTILE® truss and beam section of beam 101

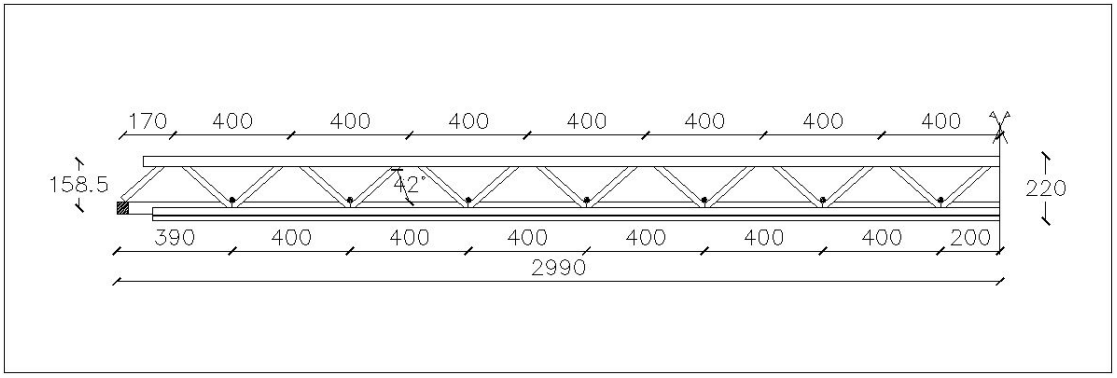

Fig. 4.25: ECOTRAVE® RAFTILE® truss profile of beams 101

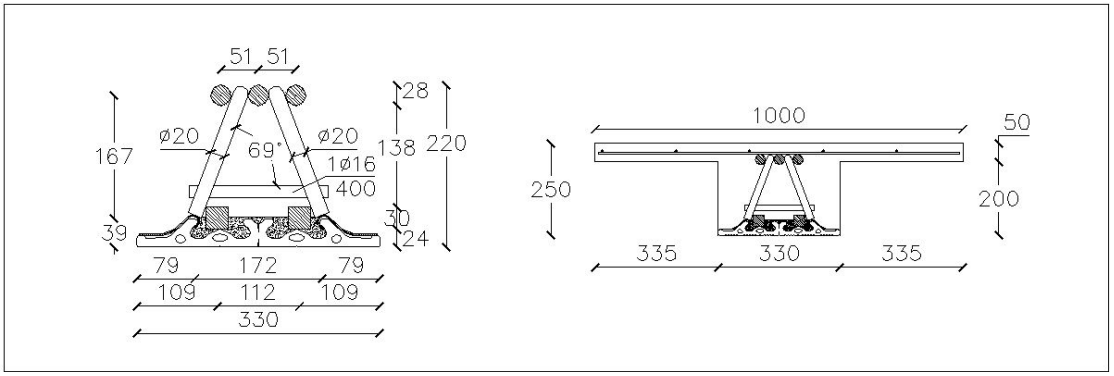

Fig. 4.26: ECOTRAVE® RAFTILE® truss section of beams 102n and 102

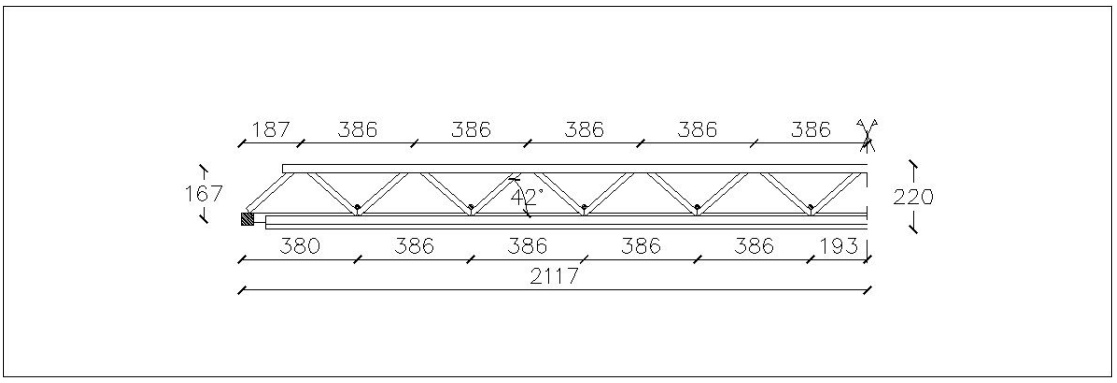

Fig. 4.27: ECOTRAVE® RAFTILE® truss profile of beams 102n and 102

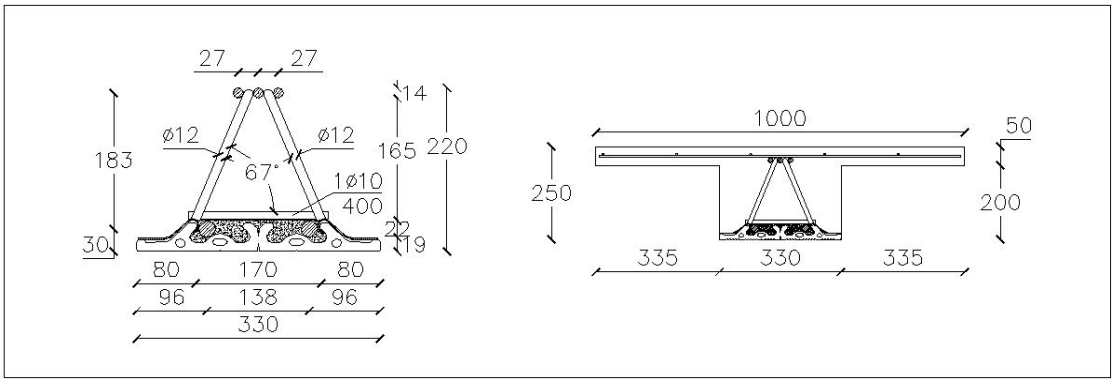

Fig. 4.28: ECOTRAVE® RAFTILE® truss section of beams 103

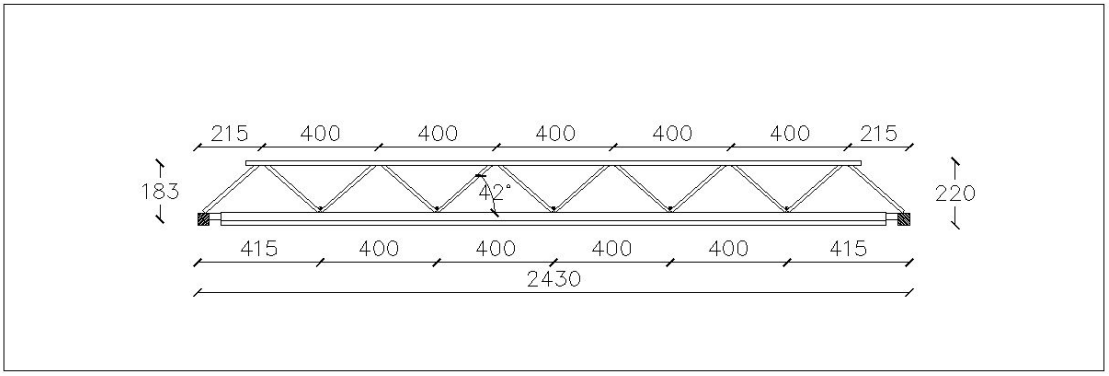

Fig. 4.29: ECOTRAVE® RAFTILE® truss profile of beams 103

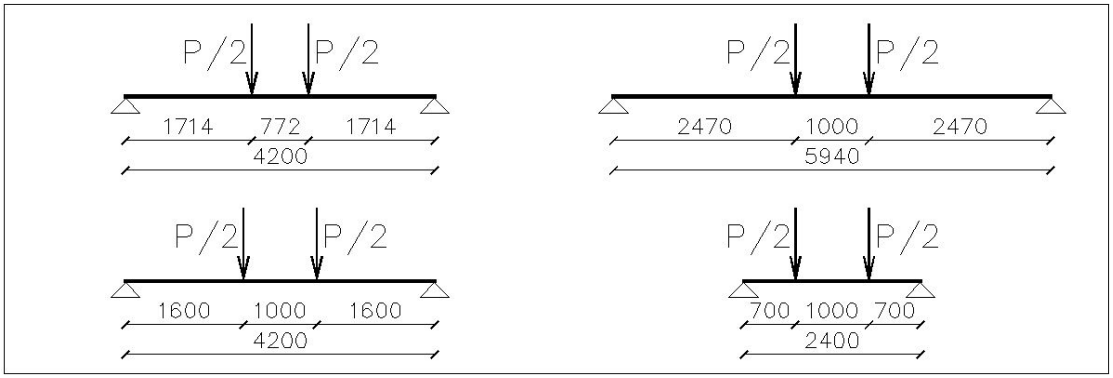

Fig. 4.30: ECOTRAVE® RAFTILE® static schemes of the beams 102n (upper left), 102 (lower left), 101 (upper right) and 103 (lower right)

The design material properties are grade S355 for the steel truss and class C40/50 for the concrete [2]. It can be noted that the truss top chord is constituted by three bars, round or square, welded between themselves and the web diagonal bars. These lasts are composed by two sequences of bars that are bent in correspondence to the top chord and cut in correspondence to the lower one. The bottom chord is set up by two longitudinal cold rolled steel profile and by two adjacent bars, round or square. The bars are welded to a transverse head hammer at both the beam heads. The longitudinal distance between two truss nodes is 200 mm. Short pieces of round bars are disposed in the transverse direction and welded to connect the adjacent lower nodes of the diagonal bars (see Fig. 4.31).

Fig. 4.31: particular view of a nude truss beam head

The dimensions of each elements of the steel trusses are reported herein:

- 101 beam truss
  - Top chords — n. 3 x 35 mm x 35 mm square bars;
  - web diagonal bars — n. 2 x 20 mm round bars, 200 mm spacing;
  - bottom chord bars — n. 2 x 40 mm x 40 mm square bars;
  - bottom cold rolled profiles — n. 2 x 395 mm^2 "S" shape profiles;
  - transverse bar pieces — n. 1 x 16 mm round bars, 400 mm spacing;
  - head hammers — n. 2 x 40 mm x 40 mm square bars;
- 102n and 102 beam truss
  - Top chords — n. 3 x 28 mm round bars;
  - web diagonal bars — n. 2 x 20 mm round bars, 200 mm spacing;
  - bottom chord bars — n. 2 x 30 mm x 30 mm square bars;
  - bottom cold rolled profiles — n. 2 x 395 mm^2 "S" shape profiles;
  - transverse bar pieces — n. 1 x 16 mm round bars, 400 mm spacing;
  - head hammers — n. 2 x 40 mm x 40 mm square bars;
- 103 beam truss
  - top chords — n. 3 x 14 mm round bars;
  - web diagonal bars — n. 2 x 12 mm round bars, 200 mm spacing;
  - bottom chord bars — n. 2 x 22 mm round bars;
  - bottom cold rolled profiles — n. 2 x 395 mm^2 "S" shape profiles;
  - transverse bar pieces — n. 1 x 10 mm round bars, 400 mm spacing;
  - head hammers — n. 2 x 40 mm x 40 mm square bars.

The concrete completion cast produce a T shape section. The only additional reinforcement was an upper 200 mm x 200 mm net of welded bars of 6 mm diameter. Each beams had been submitted to cyclic loading of increasing amplitude up to the failure. The instrumentations had collected the data of the mid-span deflections, the deformations of the upper and the lower steel truss chords. In particular the following instruments were positioned:

- n. 6 strain transducers of 100 mm base in the truss diagonal bars (4 at a head and 2 at the other one);
- n. 1 strain transducer of 100 mm base in the steel truss top chord (at the mid-span);
- n. 1 strain transducer of 100 mm base in the steel truss bottom chord (at the mid-span);
- n. 2 displacement transducer of 10 mm range in the beam upper surface (in correspondence to the supports);
- n. 2 displacement transducer of 100 mm range in the beam lower surface (in correspondence to the mid-span);
- n. 1 load cell between the hydraulic jack and the load distributor beam.

The calculation method, presented in the previous chapter, has been applied to predict the experimental tests results of both the nude trusses and the composite beams. In order to

compare the value, the medium mechanical properties of the material, determined by the adequate preliminary tests, has been used. The following Tab. 4 summarizes the theoretical predictions:

Tab. 4: theoretical resistance values of the beams

Beam	M_R [kNm]	a [m]	V_{c1} [kN]	V_{c2} [kN]	V_w [kN]	V_R [kN]	P [kN]
102n	116	1.71				103	136
101	258	2.47	157	77	166	243	206
102	175	1.60	161	75	168	243	213
103	113	0.70	168	74	62	136	272

The study of the nude truss required the use of a numerical model able to capture its effective geometry distinct from an ideal truss, as it has been underscored in the previous chapter. The geometric model, that considers all the eccentricities of the truss, has been defined taking into account all the production rules like the bar bend minimum diameter and the weld dimensions. The centreline model has been generated with a 3D draw program and then imported in a finite element method program (see Fig. 4.32).

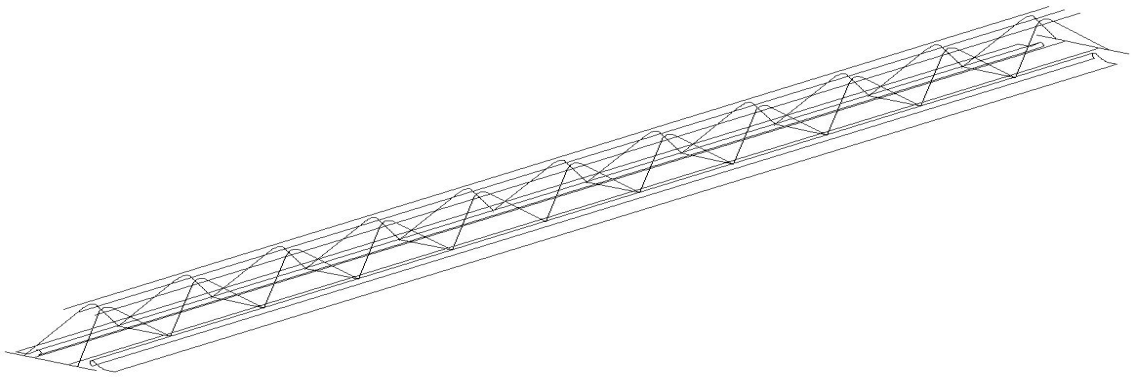

Fig. 4.32: centrelines of the 3D truss model

The following step was to assign to each element their mechanical properties and their appropriate connections. The welds were modelled with rigid links that connect the truss elements. A linear static analysis and a buckling analysis were carried out with the FEM program. The first one permitted the study of the global and the local stiffness of the truss whereas the second, while it confirmed the absence of the truss bending-torsional buckling, provided the local buckling load for the top chords. The load agrees with the Euler formula if the buckling critical length is assumed as 70% of the distance between two truss nodes. This is the consequence of the degrees of fixity that the welds give to the top chord in each node. The comparisons with the experimental results are presented below.

4.4.2 Material characterization tests

The material properties had been obtained by means of tests led in the Construction Material Experimentation Lab at the Department of Construction and Transportation of the University of Padua. In particular the following tests were carried out: standard compression test (UNI 61130/80) on three concrete cylinder specimens (diameter equal to 10 cm and height equal to 20 cm), standard tensile test (UNI 10002/1) on two steel bars (diameter 28 mm) and on three rectangular of the cold rolled steel. The results are summarized in the following Tab. 5, Tab. 6 and Tab. 7:

Tab. 5: concrete cylinder test results

Specimen	diameter [mm]	height [mm]	Mass [kg]	f_c [MPa]
1	98	191	3.48	46.2
2	98	192	3.50	45.5
3	98	184	3.34	42.9
average				44.9

Tab. 6: steel bars tensile test results

Specimen	diameter [mm]	f_y [MPa]	f_u [MPa]
1	28	390	492
2	28	363	483
average		377	488

Tab. 7: steel sheets tensile test results

Specimen	depth [mm]	base [mm]	f_y [MPa]	f_u [MPa]
1	6.2	22.0	363	520
2	6.2	22.1	351	507
3	6.2	22.3	355	508
average			356	512

The average values for each material have been used to the calculation of the expected resistance of the beams.

4.4.3 Experimental test results and analyses

The results of the experimental tests on the 8 beams are presented herein with this

order: the two tests on the nude trusses 102n; the two tests on the composite beams 101; the two tests on the composite beams 102; the two tests on the composite beams 103.

4.4.4 Nude trusses 102n

The truss profile is depicted in Fig. 4.33 with the positions of the measure instruments. The expected failure was the local buckling of the top chord. The test process was composed by three loading and unloading cycles before failure. During the load cycles it had been noted the formation of cracks on the lower clay tile but even in correspondence to the failure load no separation from the steel truss happened. The cell load values have been corrected adding the weight of the steel distribution beam (1.02 kN).

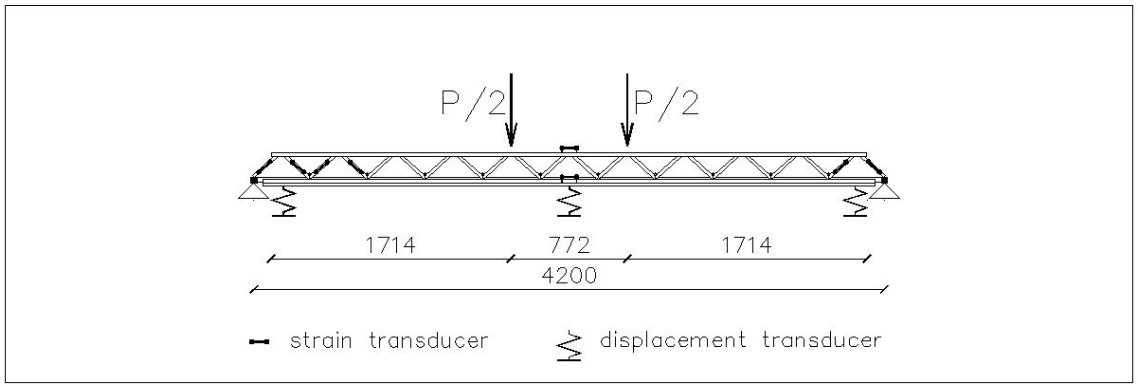

Fig. 4.33: Truss 102n profile with the instrument positions

Both the trusses reached the failure for the buckling of the top chord in correspondence to the loads 134 kN and 136 kN (see Fig. 4.34 and Fig. 4.35). The observed values agree perfectly with the predicted ones. Recalling that the top chord is composed by three round bars, it can be remarked that the central bar has a symmetric connection by means of the welds whereas the lateral ones have non-symmetric connections. This fact causes a further eccentricity for the external bars in the plane of the top chord itself.

In Fig. 4.36 the load vs. mid-span deflection curves for the last cycle are compared with the analytical results. The experimental curves have almost linear course until the buckling of the top chord bars where sensitive inflexions took place. The deflections in correspondence to the peak strength were about 37 mm. The linear numerical model offers a very good stiffness prediction at the beginning of the loading process and produces lower displacements than the experimental ones at the peak strength. This last is captured very well by the critical buckling load calculated with method specified at the previous chapter with the Euler buckling load confirmed by the finite element numerical model. The reason of the differences, between analytical results and predicted ones in the last part of the curve, is that the numerical model is linear and doesn't account for local plasticization due to imperfections and local phenomena.

Fig. 4.34: Pictures of the local buckling happened in the first truss 102n

Fig. 4.35: Pictures of the local buckling happened in the second truss 102n

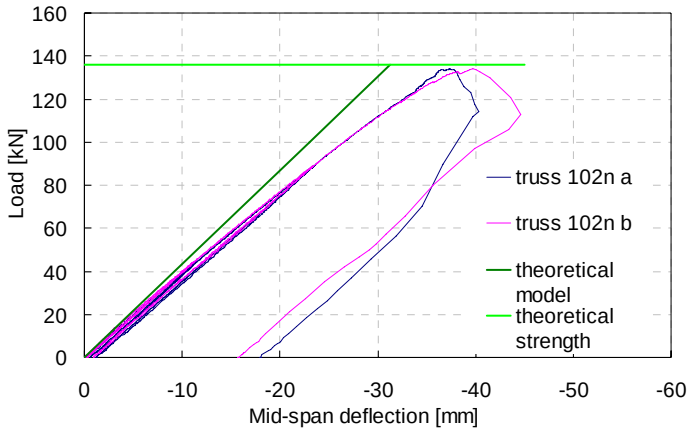

Fig. 4.36: Experimental and analytical load vs. deflection curves for the trusses 102n

The Fig. 4.37 shows the applied load vs. top chord strain curves of the tests compared with the analytical prediction. The bar strains are lower than the one at yielding, hence the collapse of the beams happened because of the bar buckling. Since the instruments were placed under the medium bar that buckled downward, the recorded strain should be considered higher than the bar average axial compressive strain. That can explain the apparently different course of the experimental curves with respect to the theoretical one. The strain transducers applied to the lower cold rolled profiles showed a linear behaviour

inside their elastic field. Also the strains collected from the first compressed and tensile diagonal bars reported a elastic behaviour. Both the strain measurement from the bottom chord and the diagonal bars are well predicted by the linear elastic numerical model.

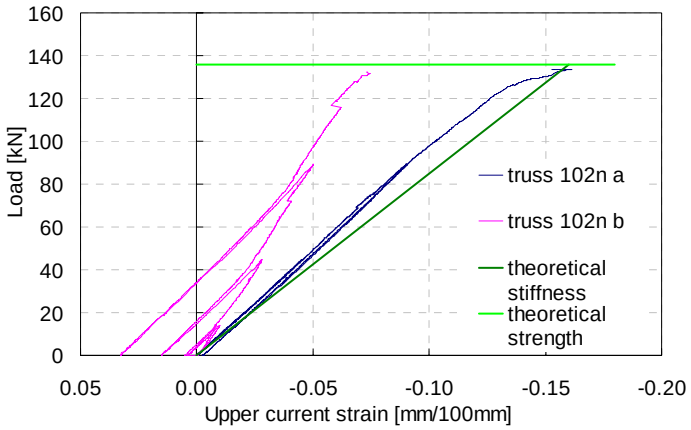

Fig. 4.37: Experimental and analytical load vs. top chord strain for the trusses 102n

4.4.5 Composite beams 101

The beam profile is depicted in Fig. 4.38 with the positions of the measure instruments. The expected failure was the yielding of the truss bottom chord. The test process was composed by three loading and unloading cycles before failure.

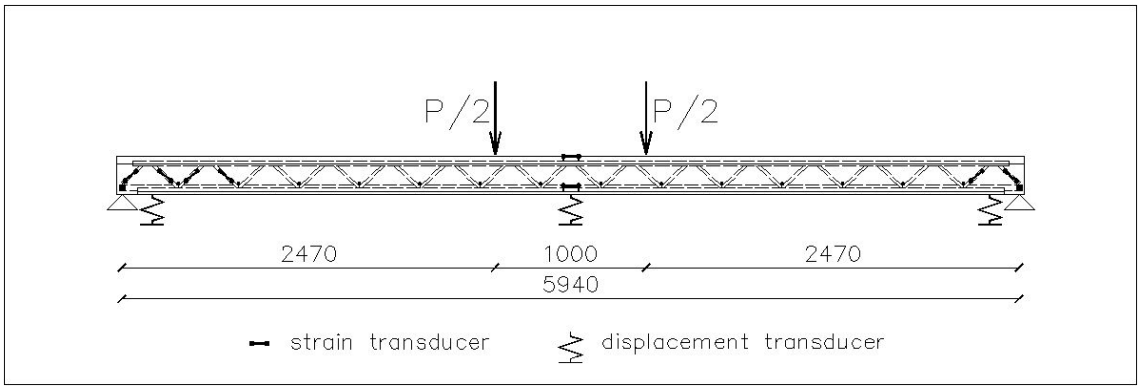

Fig. 4.38: Beam 101 profile with the instrument positions

During the load cycles it had been noted the formation of cracks on the lower clay tile but even in correspondence to the failure load no separation from the steel truss happened (see Fig. 4.39). The cell load values have been corrected adding the weight of the steel distribution beam (1.02 kN). Both the trusses reached their collapse for the yielding of the truss bottom chord in correspondence to the loads 199 kN and 196 kN. The predicted values are affected by an error of +0.05% more than the average of the observed values. The crack patterns of the two beams were very similar and the Fig. 4.40 shows one of them. It can be noted that some preliminary cracks formed and remained pretty small. Next to them

secondary cracks developed from the lower fibre up to the concrete web. The spacing between the larger ones is of the same order of the truss node distance, as predicted. Since no measurement instrument was placed across the crack it's not possible to have information about the crack width.

Fig. 4.39: Picture of the lower clay tile in the beam 101 mid-span close to the collapse

Fig. 4.40: Pictures of the crack pattern of the concrete web near the mid-span of the beam 101

In Fig. 4.41 the load vs. mid-span deflection curves for the last cycle are compared with the analytical results. During one test the mid-span displacement transducers became inefficient when the load reached a value of about 175 kN because of a sudden shake due to a crack opening. The experimental curves have almost linear course until the yielding of the bottom chord. After that point the deflection increased significantly under an almost constant load. The deflections in correspondence to the first yielding were about 42 mm and the ultimate deflection recorded was about 85 mm. The theoretical model offers a good stiffness and strength prediction and demonstrating its ability to reproduce the global beam behaviour. It can be noted that the presence of the concrete tends to eliminate the effects of the truss eccentricities and their influences on the global behaviour.

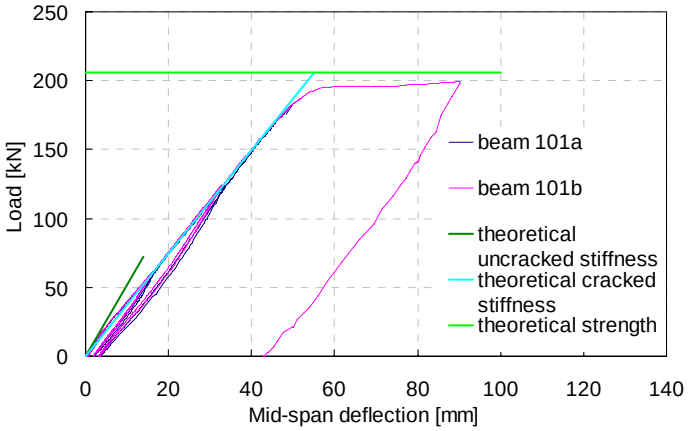

Fig. 4.41: Experimental and analytical load vs. deflection curves for the beams 101

The yielding of the bottom chord can be seen clearly from the applied load vs. top chord strain curves. The Fig. 4.42 compared the tests results with the theoretical ones. Whereas the Fig. 4.43 shows the applied load vs. top chord strain curves of the tests compared with the analytical prediction. From the comparison of the last two Figures, it can be remarked that the bottom chord yielded first and had a ductile plastic flow. In this phase even the top chord bars yielded, but they had a smaller plastic strain development since they acted in compression together with the concrete. The tensile strain of the web diagonal bars are depicted in Fig. 4.44. Their curves clearly denotes two slopes. The first one is characterized by an higher stiffness and corresponds to the shear mechanism before the beam shear cracking and the second represents the Mörsch mechanism in which the tensile stresses are absorbed only by the diagonal bars across the cracks and by the bottom chord. The analytical evaluations are in good agreement with the test results.

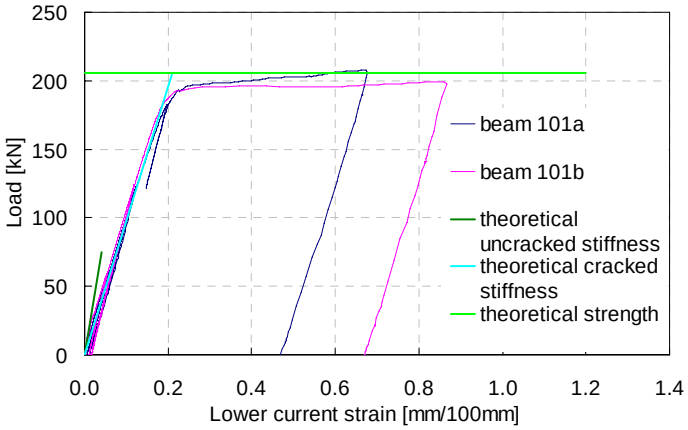

Fig. 4.42: Experimental and analytical load vs. bottom chord strain for the trusses 101

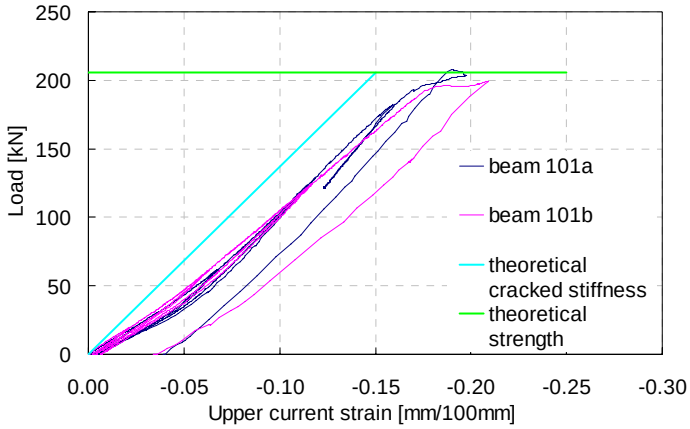

Fig. 4.43: Experimental and analytical load vs. top chord strain for the trusses 101

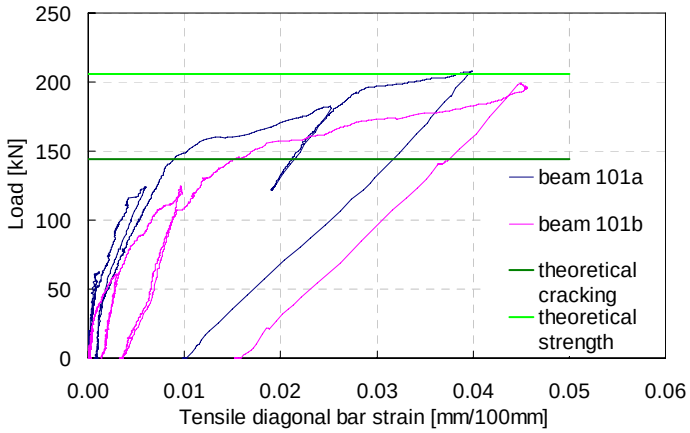

Fig. 4.44: Experimental and analytical load vs. diagonal bar strain for the trusses 101

4.4.6 Composite beams 102

The beam profile is depicted in Fig. 4.45 with the positions of the measure instruments. The expected failure was the yielding of the truss bottom chord. The test process was composed by three loading and unloading cycles before failure. During the load cycles it had been noted the formation of cracks on the lower clay tile but even in correspondence to the failure load no separation from the steel truss happened. The cell load values have been corrected adding the weight of the steel distribution beam (1.02 kN). Both the trusses reached their collapse for the yielding of the truss bottom chord in correspondence to the loads of 216 kN and 222 kN. The predicted values are affected by an error of -0.03% with respect to the average of the observed values. It can be noted that some preliminary cracks formed and remained pretty small and next to them secondary cracks developed from the lower fibre up to the concrete web. The spacing between the larger ones is of the same order of the truss node distance, as predicted. Since no instrument was placed across the crack it's not possible to have information about the crack width.

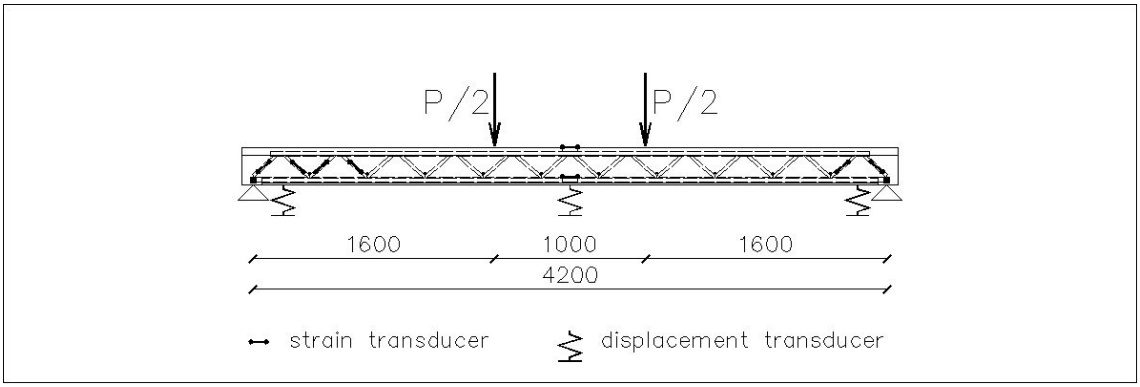

Fig. 4.45: Beam 102 profile with the instrument positions

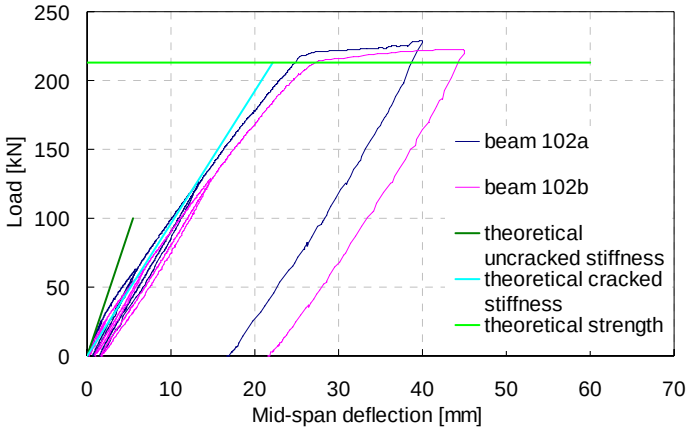

Fig. 4.46: Experimental and analytical load vs. deflection curves for the beams 102

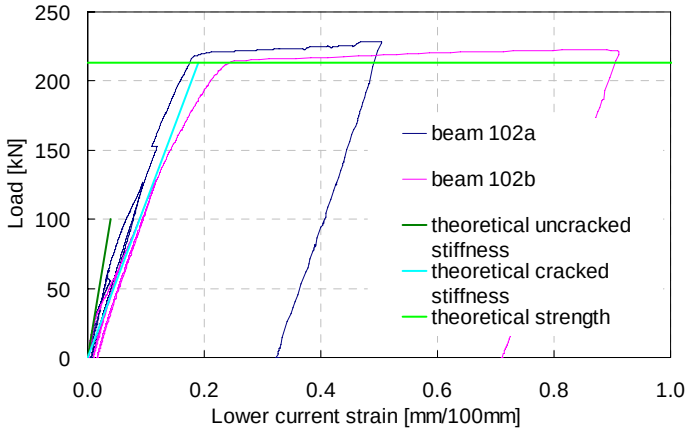

Fig. 4.47: Experimental and analytical load vs. bottom chord strain for the trusses 102

In Fig. 4.46 the load vs. mid-span deflection curves for the last cycle are compared with the analytical results. The experimental curves have almost linear course until the yielding of the bottom chord. After that point the deflection increase significantly under an about constant load. The deflections in correspondence to the first yielding were about 23 mm and the ultimate deflection recorded was about 42 mm. The theoretical model offers a good

stiffness and strength prediction and demonstrates its ability to reproduce the global beam behaviour. The yielding of the bottom chord can be seen clearly from the applied load vs. top chord strain curves. The Fig. 4.47 compared the tests results with the theoretical ones. Whereas the Fig. 4.48 shows the applied load vs. top chord strain curves of the tests compared with the analytical prediction. From the comparison of the last two Figures it can be remarked that the bottom chord yielded and had a ductile plastic flow. The top chord remains in its elastic range as it can be seen from its strain. The tensile strain of the web diagonal bars are depicted in Fig. 4.49. Even in this case the curves clearly denotes two slopes correctly predicted by the theoretical model.

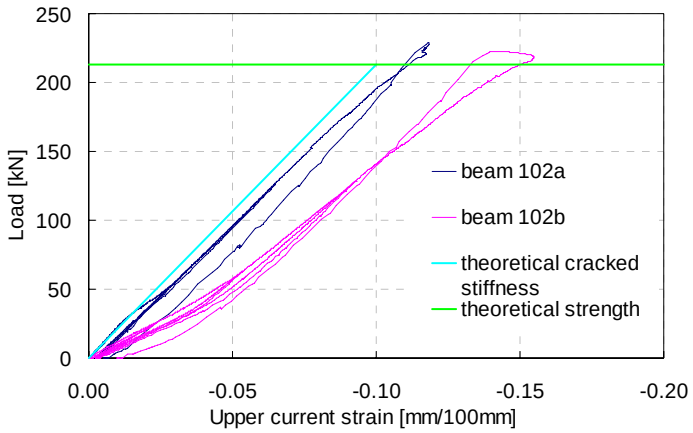

Fig. 4.48: Experimental and analytical load vs. top chord strain for the trusses 102

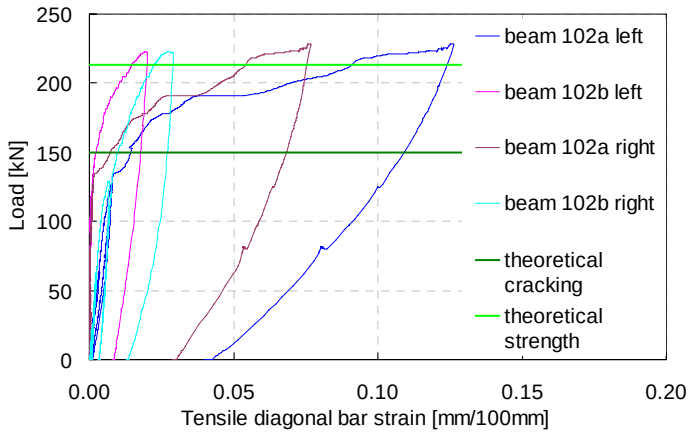

Fig. 4.49: Experimental and analytical load vs. diagonal bar strain for the trusses 102

4.4.7 Composite beams 103

The beam profile is depicted in Fig. 4.50 with the positions of the measure instruments. The expected failure was the yielding of the truss bottom chord. The test process was composed by three loading and unloading cycles before failure. During the load cycles it had been noted the formation of cracks on the lower clay tile but even in correspondence to the

failure load no separation from the steel truss happened (see Fig. 4.51).

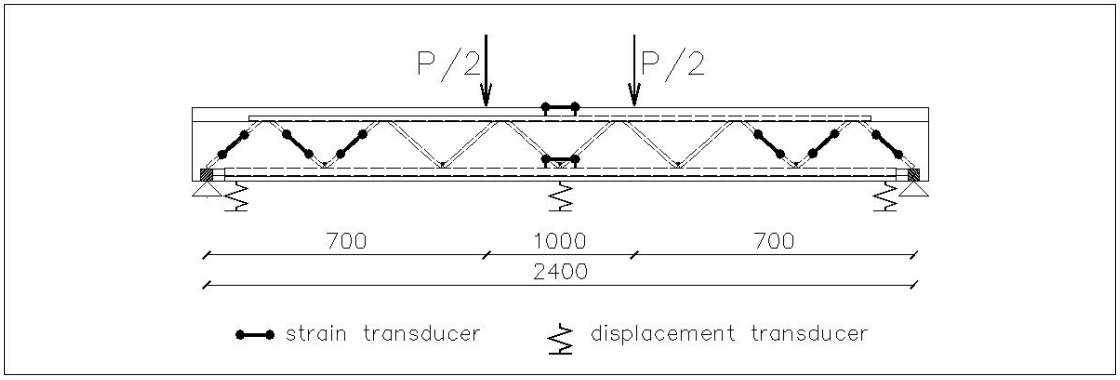

Fig. 4.50: Beam 103 profile with the instrument positions

Fig. 4.51: Pictures of the lower clay tile in the beam 103 close to the collapse

Fig. 4.52: Pictures of the composite beam 103 after their collapse

The cell load values have been corrected adding the weight of the steel distribution beam (1.02 kN). Both the trusses reached their collapse for the yielding of the truss bottom chord in correspondence to a loads 307 kN and 301 kN (see Fig. 4.52). The predicted values are affected by an error of -0.10% with respect to the average of the observed values. The crack patterns of the two beams were very similar. It can be noted that the cracks are concentrated at the head region of the beams and develop at about 45° degrees, which is typical of shear cracking. The spacing between the them is of the same order of the truss

node distance, as predicted. Since no instrument was placed across the crack it's not possible to have information about the crack width.

In Fig. 4.53 the load vs. mid-span deflection curves for the last cycle are compared with the analytical results. The experimental curves have an initial stiffness before the cracking occurs and then a second slope, in which the cracks develop starting from the bottom and going up to the flange. When the yielding of the tensile diagonal bar is reached the deflection increase significantly under an almost constant load. The deflections in correspondence to the diagonal bar yielding are about 9.5 mm and the ultimate deflection recorded was about 18 mm.

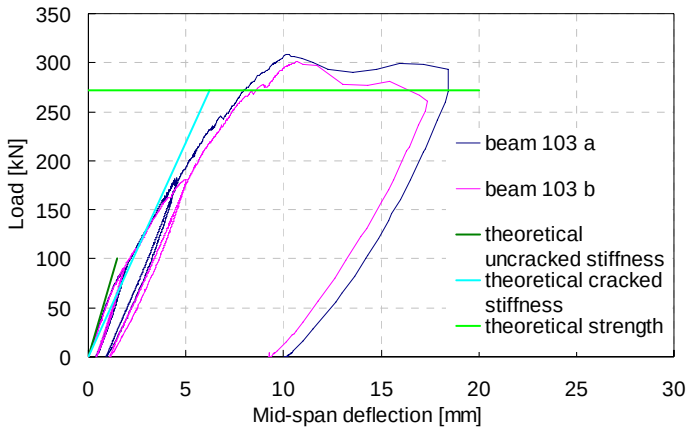

Fig. 4.53: Experimental and analytical load vs. deflection curves for the beams 103

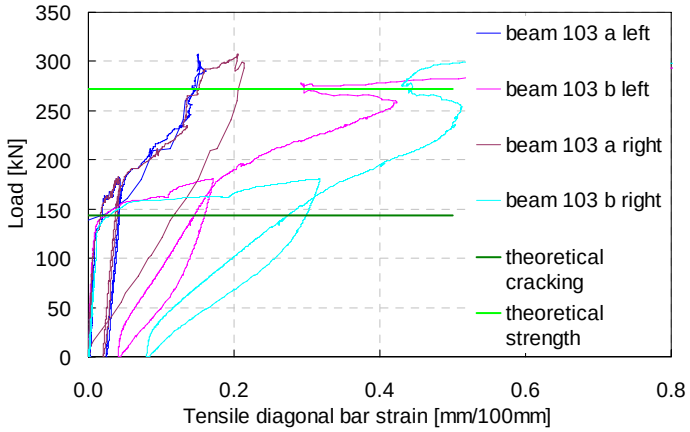

Fig. 4.54: Experimental and analytical load vs. first tensile diagonal bar strain for the trusses 103

The theoretical model offers a good stiffness and strength prediction and demonstrates its ability to capture the global beam behaviour. The upper and the lower mid-span strain of the steel truss remain elastic meaning that the maximum bending moment remain far lower than the resisting one. The tensile strain of the web diagonal bars are depicted in Fig. 4.54. Even in this case the curves clearly denote two slopes correctly predicted by the theoretical

model. After that, the strain becomes very high denoting the progressive yielding of the bar. It can be underscored how the collapse was reached by the yielding of the tensile diagonal bar while the compressive concrete struts remained far from their critical load. That fact let a certain ductility as can be seen from the global displacement reached.

4.5 PREREP® beams

4.5.1 Experimental test design

The CSTC beams called PREREP® beams are characterized by the pre-compressed concrete base that contains the steel truss bottom chord. The pre-compression of the base has the purpose to reduce the cracking of the concrete base in the CSTC beams and let this construction type be suitable for long span applications. In fact in the case of the lower concrete base, the shrinkage and the first phase loads can cause its preliminary cracking. The most applied technique is the mechanic pre-stressing of high strength strands, before the concrete cast and their cut after a concrete accelerated hardening. The theoretical and experimental studies have for main aim to verify the behaviour of this beam type both for what concerns the shear and bending behaviour of the first phase truss. Particular attention has been paid to the cracking and the decompression of the concrete base. With the experimental tests the proposed assessment method has been evaluated. Two similar trusses were designed as first phase structure of a partially pre-compressed CSTC beam. The steel truss design respected the REP® beam production rules [1]. In particular the following beams had been tested:

- n. 2 nude trusses, with clear span 534 cm.

The four point load tests were conducted applying two concentrate loads under displacement control. The truss type sections and the corresponding static schemes are presented in the Fig. 4.55 and Fig. 4.56 for tested beams. The design material properties are grade S355 for the steel truss, high strength steel f_{ptk} 1860 MPa for the strand, class C25/30 for the concrete, B450C steel for the reinforcement [2]. The truss top chord is constituted by six square bars welded together with the web diagonal bars. These lasts are composed by two sequences of round bars that are bent in correspondence to the top chord and cut in correspondence to the lower one. The bottom chord is set up by four longitudinal bars embedded in a reinforced concrete base with rectangular section. The longitudinal distance between two truss nodes is 460 mm. Longitudinal and transversal round bars are welded to connect adjacent diagonal bars at their mid-height (see Fig. 4.57) to stabilize them and prevent their local buckling. The dimensions of each elements of the beam are reported herein:

- PREREP® beam
  - Top chords — n. 3 x 30 mm x 30 mm square bars and
  - — n. 1 x 35 mm x 35 mm square bar
  - (and in one beam only) — n. 2 x 30 mm x 30 mm square bars;
  - web diagonal bars — n. 2 x 30 mm round bars, 460 mm spacing;
  - stabilizing bars — n. 8 x 10 mm round bars, 460 mm spacing;
  - bottom chord bars — n. 4 x 20 mm round bars;
  - concrete section base — n. 1 x 600 mm x 200 mm x 5500 mm;
  - strands — n. 6 x ½" round bars;
  - longitud. base reinforcement — n. 2 x 12 mm round bars at the bottom
  - — n. 4 x 12 mm round bars at the top
  - — n. 2 x 12 mm x 70 mm round bars at the top;
  - transv. base reinforcement — n. 1 x 8-12 mm round bar tie, spacing var.

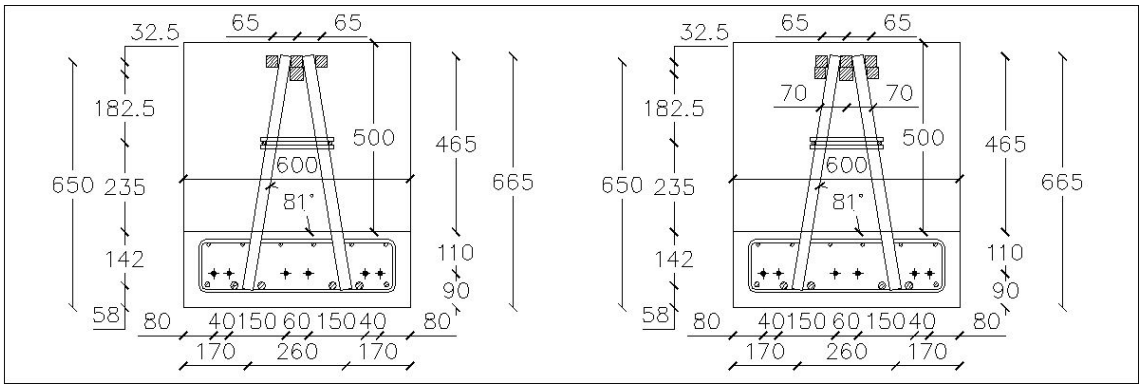

Fig. 4.55: PREREP® truss type sections

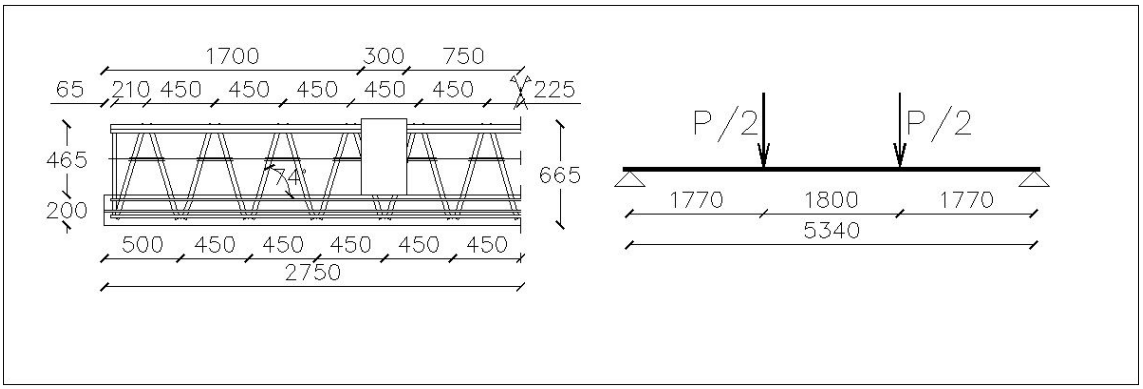

Fig. 4.56: PREREP® truss type profile and corresponding test static scheme

The experimented beams didn't get a completion concrete cast. But two little concrete columns (sides 600 mm x 300 mm and height 500 mm) were cast to create the base of the load application. The two loads had been applied by using two distribution beams (HEB 240, of weight 4.40 kN, and HEB 280, of weight 4.60 kN) and two neoprene little bases. Every PREREP® beam had been submitted to cyclic load of increasing amplitude up to the

failure. The instrumentations had collected the data of the mid-span deflections, the deformations of the steel truss top chords and the lower concrete base. In particular the following instruments were positioned:

- n. 6 strain transducers of 100 mm base in the truss diagonal bars (4 at a head and 2 at the other one);
- n. 1 strain transducer of 100 mm base in the steel truss top chord (at the mid-span);
- n. 1 strain transducer of 100 mm base in the steel truss bottom chord (at the mid-span);
- n. 2 displacement transducer of 10 mm range in the beam upper surface (in correspondence to the supports);
- n. 1 displacement transducer of 100 mm range in the beam lower surface (in correspondence to the mid-span);
- n. 1 load cell between the hydraulic jack and the load distributor beam.

The calculation method, presented in the previous chapter, has been applied to predict the experimental tests results of all the nude trusses with concrete base. In order to have the possibility to compare the values, the medium mechanical properties of the material, determined by the adequate preliminary tests, has been used. The following symbols are used to characterize geometrical properties of the beams:

- $L = 5.34$ m — clear span of the beam;
- $H_{tr} = 610$ mm — steel truss height;
- $s = 460$ mm — spacing of the truss web diagonal bars;
- $L_{tr} = 652$ mm — half of the truss diagonal bar length;
- $\alpha = 73°$ — diagonal bar angle respect to the beam longitudinal axis;
- $\beta = 12°$ — diagonal bar angle respect to the vertical;
- $A_s = 1797$ mm^2 — base structural and reinforcing longitudinal steel area;
- $A_{s1}' = 3925$ mm^2 — top chord total area for the beam 1;
- $A_{s2}' = 5725$ mm^2 — top chord total area for the beam 2;
- $A_p = 558$ mm^2 — pre-stressing strand total area;
- $A_{sw} = 1414$ mm^2 — truss diagonal bar area;
- $B = 550$ mm — distance between top chord centre and pre-stressing steel;
- $b = 600$ mm — concrete base width;
- $h = 200$ mm — concrete base depth;
- $d = 140$ mm — concrete base effective depth.

In order to compute the resisting moment, the maximum tensile strength of the lower steel has been considered neglecting the concrete base and has been compared to the top chord one. The resistant moments of the beams are conditioned by the compressed steel for the first one and by the tensile steel for the second. The following Tab. 8 summarizes the theoretical expectations:

Tab. 8: theoretical resistance values of the beams

Beam	M_R [kNm]	a [m]	V_R [kN]	V_c [kN]	V_{wb} [kN]	V_{wt} [kN]	P [kN]
1	769	1.77	808	154	172	270	540
2	797	1.77	808	154	172	350	700

where V_c is the concrete base shear resistance due to its tensile strength, V_{wb} is the shear resistance of the ties of the concrete base and V_{wt} is the shear resistance of the truss diagonal bars. In the case of the truss without the completion cast, the truss diagonal bars have higher stiffness and they can reach their failure before the development of the concrete base shear strength, but in this case the bending resistance is not available anymore and that justifies why only the shear resistance of the truss diagonal bar has been accounted for the global shear strength.

Fig. 4.57: particular view of a truss beam head

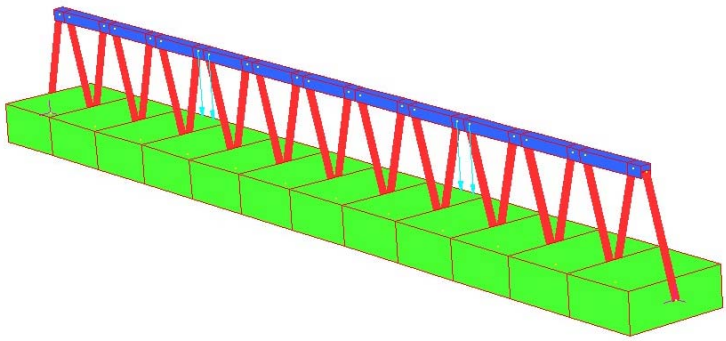

Fig. 4.58: 2D finite element model centrelines of the composite truss

The study of the nude truss required the use of a numerical model able to capture its effective geometry distinct from an ideal truss, as it has been underscored in the previous chapter. The model geometry accounted for all the eccentricities of the truss has been defined taking into account all the production rules like the bar bend minimum diameter and the weld dimensions. A simplified 2D model has been generated in which each truss

element has been simulated with an equivalent "beam" element (see Fig. 4.58).

This model cannot be used for local analysis but only for a global linear static analysis to evaluate the global bending stiffness. The eccentricities of the upper truss joint were modelled with joint offsets. For what concerns the serviceability limit state study, that can bring to the stress evaluation for the concrete base and to the estimation of the cracking and the decompression bending moment, the MATLAB code described in the previous chapter has been used. It can account for the effect of the non-elastic deformation component for each section of the composite truss in a precise way. The section of the two composite trusses are depicted in Fig. 4.56. In this section, the analysis of both tested beams in an hypothetical structural application, imagining also the completion concrete cast, has been completed to show the potentiality of the developed calculation method. In particular the theoretical study has been applied to the following practical case:

- composite beam web width equal to 400 mm;
- upper flange width equal to 1650 mm;
- hypothetical slab depth equal to 450 mm, completion cast included;
- first phase slab influence length for the calculation of its weight equal to 1.5 m;
- slab span equal to 12 m;

the loads applied being

- $g_{slab} = 5$ kN/m^2 weight of the slab, completion cast included;
- $g = 3$ kN/m^2 slab permanent load;
- $g = 3$ kN/m^2 slab variable load.

The static scheme of the beam is simply supported during the first phase with a clear span equal to 5.36 m and continuum beam with a span equal to 5.50 m in the hypothetical second phase. With the MATLAB algorithm, the strain-stress state of the beam has been computed for all its lifetime. The resulting diagrams are presented in Fig. 50. It can be remarked that the total pre-compression of the concrete base is assured until the quasi-permanent load condition, included. Furthermore the cracking of the concrete base is avoided until the application of the variable load. This is to respect the Italian and European Codes' prescriptions for the durability requirements. The behaviour of the composite truss without the completion cast is presented in Fig. 51, in which the decompression, the cracking and the ultimate bending moment are evaluated. As example and validation, the comparison with the variable modular ratio n_L is resumed in Fig. 52. From the graphs it can be seen that the main differences between the two methods start from the application of the permanent load in the second phase. From this step the variable modular ratio method furnishes higher stress in the inferior fibre of the completion cast while the concrete base is still entirely compressed. For what concerns the decompression and the cracking bending moment with this simplified method the results are lower of about 4 kNm, whereas the

ultimate bending moment is pretty higher and the failure is due to the high strength steel yielding, whereas the presented method foretells the compressed top chord crisis. A similar analysis with the proposed method have been made for the second designed beam and are presented in the Fig. 53 and Fig. 54. The comparisons with the experimental results are presented below.

Pre-compression t=3dd	Self weight a t=3dd	Permanent Load I phase t=30gg	Permanent Load II phase t=60dd	Variable Load (quasi-permanent load condition) II phase t=1000dd
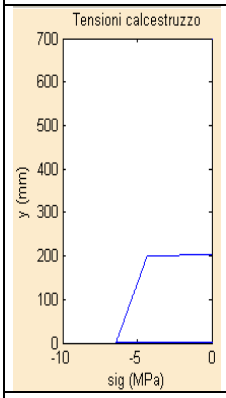	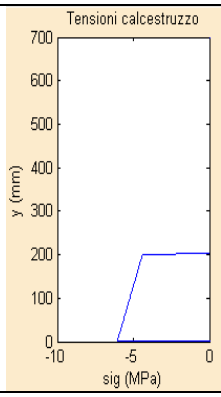	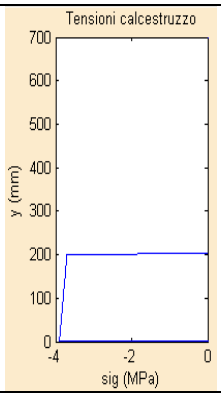	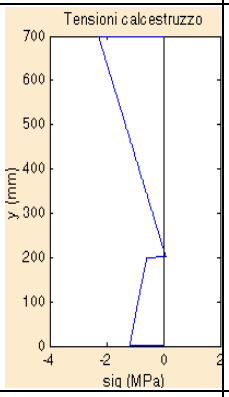	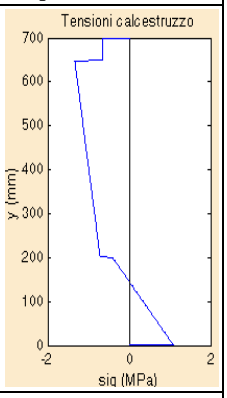
$\sigma_{c,low}$ = -6.42 MPa σ_s = -30.4 MPa σ_p = 1247.6 MPa no cracking	$\sigma_{c,low}$ = -6.05 MPa σ_s = -29.2 MPa σ_p = 1248.5 MPa no cracking	$\sigma_{c,low}$ = -3.90 MPa σ_s = -56.5 MPa σ_p = 1187.6 MPa no cracking	$\sigma_{c,up}$ = -2.29 MPa σ_s = -59.9 MPa σ_p = 1174.1MPa no cracking	$\sigma_{c,up}$ = -1.34 MPa σ_s = -86.8 MPa σ_p = 1088.4 MPa no cracking

Fig. 4.59: stress analysis for the composite beam 1 in the hypothetical application

Decompression limit state t=∞ M_{dec}= 147.1 kNm	Cracking limit state t=∞ M_{cr}= 266.1 kNm	Ultimate strength t=∞
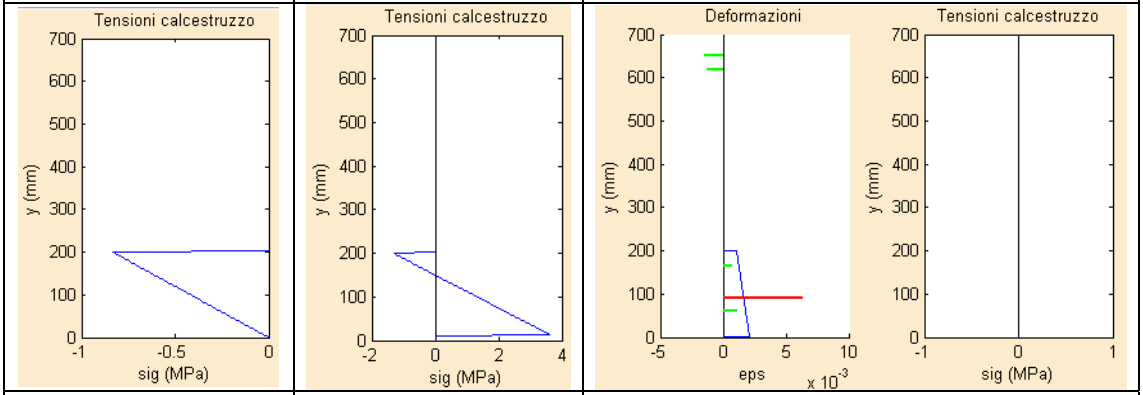		
$\sigma_{c,up}$ = -0.83 MPa σ_s = -126.1 MPa σ_p = 971.9 MPa no cracking	$\sigma_{c,up}$ = -1.30 MPa σ_s = -121.4 MPa σ_p = 982.0 MPa crack appearance	M_{Rd} = 769.2 kNm > M_{Sd} = 420.4 kNm M_{Ru} = 637.3 kNm concrete entirely cracked

Fig. 4.60: stress analysis for the incomplete composite beam 1 (the tensile values of the steel are the maximum ones)

Pre-compression t=3dd		Self weight t=3dd	
Proposed	Variable modular ratio	Proposed method	Variable modular ratio
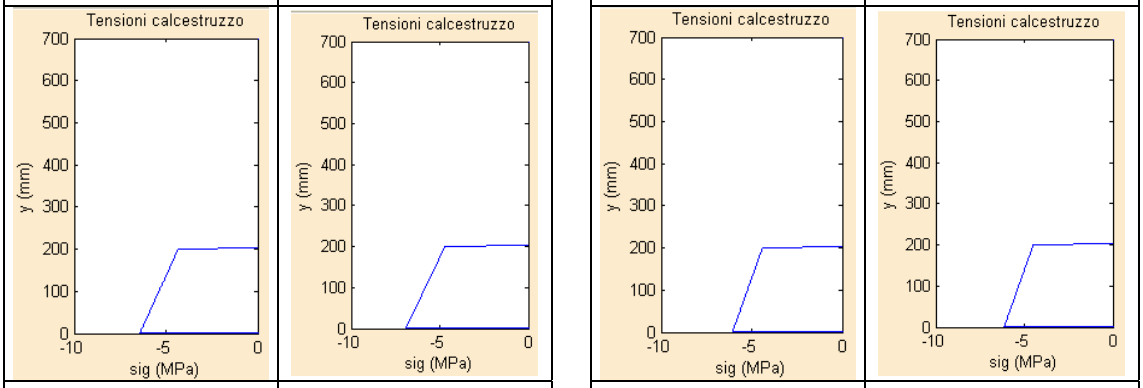			
$\sigma_{c,low}$ = -6.42 MPa σ_s = -30.4 MPa σ_p = 1247.6 MPa no cracking	$\sigma_{c,low}$ = -6.92 MPa σ_s = -32.0 MPa σ_p = 1346.1 MPa no cracking	$\sigma_{c,low}$ = -6.05 MPa σ_s = -29.2 MPa σ_p = 1248.5 MPa no cracking	$\sigma_{c,low}$ = -6.13 MPa σ_s = -28.9 MPa σ_p = 1266.2 MPa no cracking

Permanent load I phase t=30dd

Proposed	Variable modular ratio
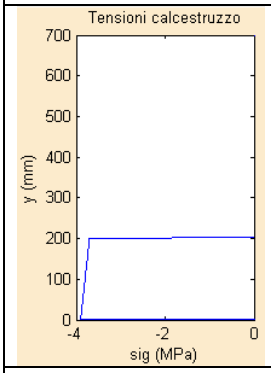	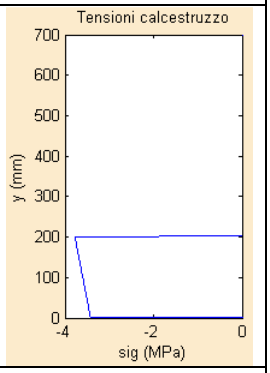
$\sigma_{c,low}$ = -3.90 MPa σ_s = -56.5 MPa σ_p = 1187.6 MPa no cracking	$\sigma_{c,up}$ = -3.78 MPa σ_s = -66.7 MPa σ_p = 1174.1 MPa no cracking

Permanent load II phase t=60dd

Proposed	Variable modular ratio
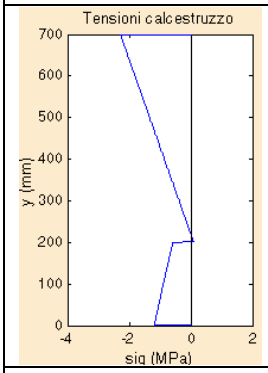	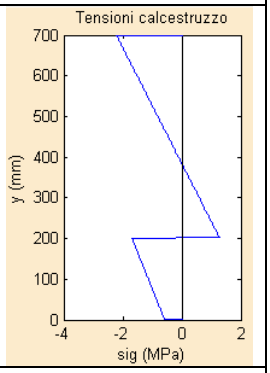
$\sigma_{c,up}$ = -2.29 MPa σ_s = -59.9 MPa σ_p = 1174.1MPa no cracking	$\sigma_{c,up}$ = -2.21 MPa σ_s = -44.1 MPa σ_p = 1057.3 MPa no cracking

Variable load II phase t=1000dd (quasi perm.)

Proposed	Variable modular ratio
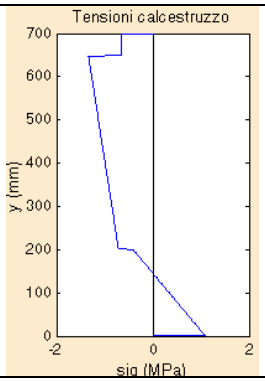	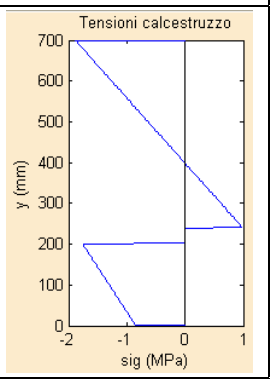
$\sigma_{c,up}$ = -1.34 MPa σ_s = -86.8 MPa σ_p = 1088.4 MPa no cracking	$\sigma_{c,up}$ = -1.89 MPa σ_s = -56.4 MPa σ_p = 1079.9 MPa no cracking

Permanent load I phase t=30dd

Proposed M_{dec}= 147.1 kNm	Variable modular ratio M_{dec}= 151.1 kNm
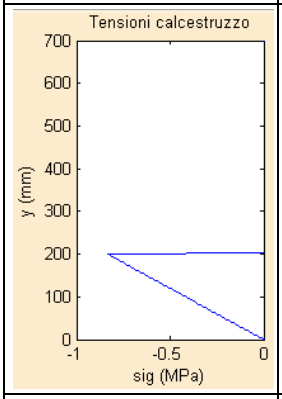	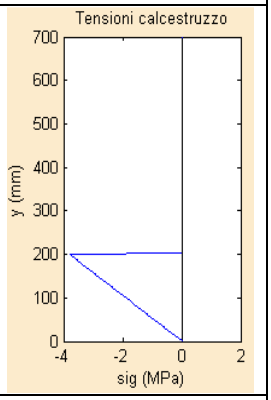
$\sigma_{c,up}$ = -0.83 MPa σ_s = -126.1 MPa σ_p = 971.9 MPa no cracking	$\sigma_{c,up}$ = -3.78 MPa σ_s = -66.1 MPa σ_p = 1046.1 MPa no cracking

Permanent load II phase t=60dd

Proposed M_{cr}= 266.1 kNm	Variable modular ratio M_{cr}= 270.1 kNm
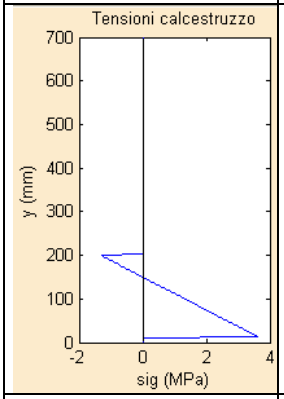	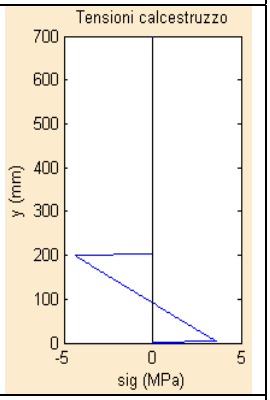
$\sigma_{c,up}$ = -1.30 MPa σ_s = -121.4 MPa σ_p = 982.0 MPa crack appearance	$\sigma_{c,up}$ = -4.38 MPa σ_s = -119.1 MPa σ_p = 1055.1 MPa crack appearance

Ultimate strength t=∞

Proposed	Variable modular ratio
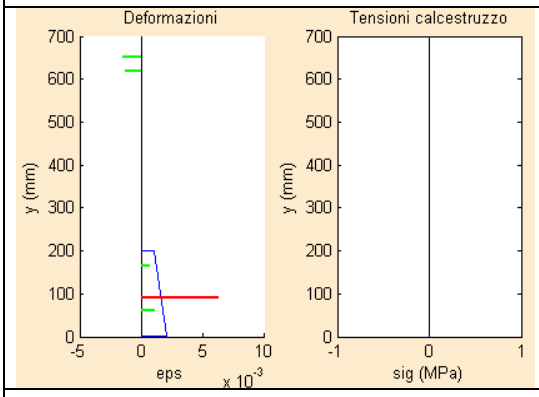	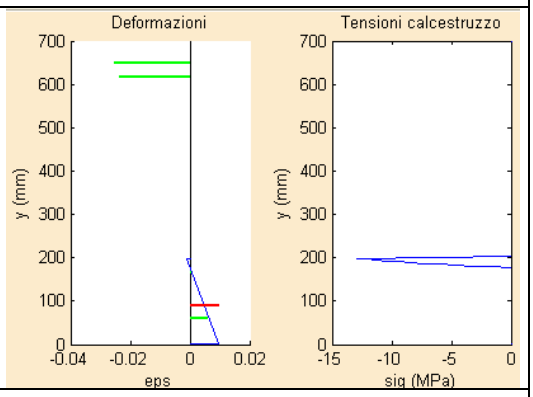
M_{Rd} = 769.2 kNm > M_{Sd} = 420.4 kNm M_{Ru} = 637.3 kNm concrete entirely cracked	M_{Rd} = 766.4 kNm > M_{Sd} = 420.4 kNm M_{Ru} = 779 kNm $\sigma_{c,up}$ = -12.92 MPa

Fig. 4.61: comparison between the proposed and the variable modular ratio methods (the tensile values of the steel are the maximum ones)

Pre-compression t=3dd	Self weight a t=3dd	Permanent Load I phase t=30gg	Permanent Load II phase t=60dd	Variable Load (quasi-permanent load condition) II phase t=1000dd
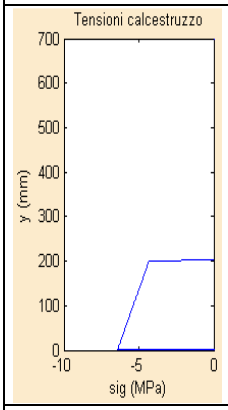	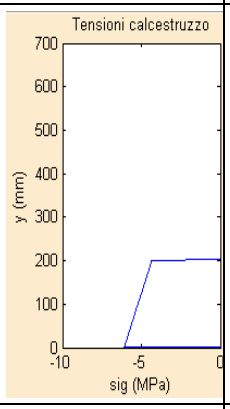	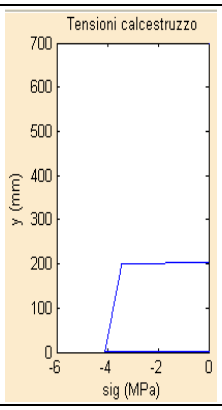	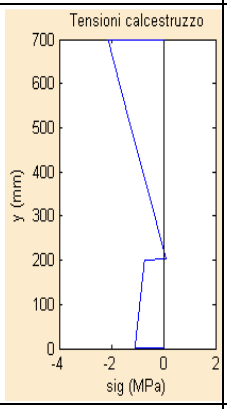	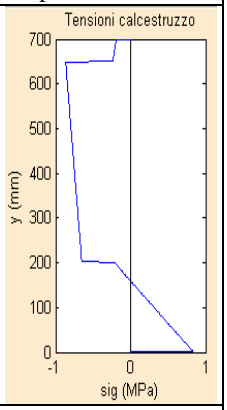
$\sigma_{c,low}$ = -6.43 MPa σ_s = -30.4 MPa σ_p = 1247.6 MPa no cracking	$\sigma_{c,low}$ = -6.09 MPa σ_s = -29.2 MPa σ_p = 1248.5 MPa no cracking	$\sigma_{c,low}$ = -4.10 MPa σ_s = -56.8 MPa σ_p = 1187.7 MPa no cracking	$\sigma_{c,up}$ = -2.13 MPa σ_s = -60.1 MPa σ_p = 1174.1 MPa no cracking	$\sigma_{c,up}$ = -0,87 MPa σ_s = -87,3 MPa σ_p = 1088,1 MPa no cracking

Fig. 4.62: stress analysis for the composite beam 2 in the hypothetical application (the tensile values of the steel are the maximum ones)

Decompression limit state t=∞ M_{dec}= 166.6 kNm	Cracking limit state t=∞ M_{cr}= 300.6 kNm	Ultimate strength t=∞
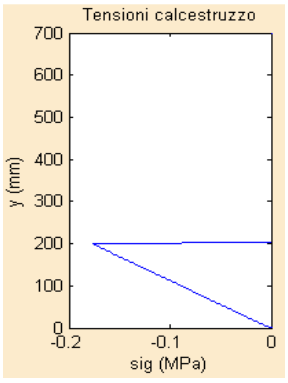	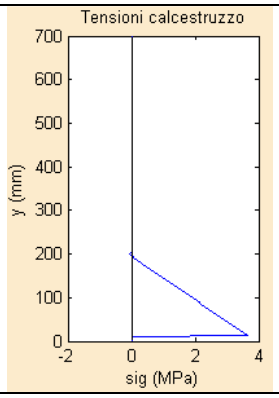	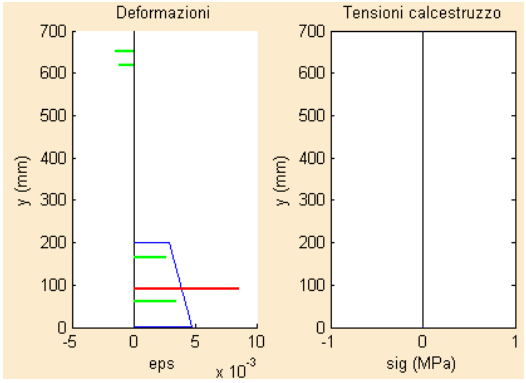
$\sigma_{c,up}$ = -0.18 MPa σ_s = -125.2 MPa σ_p = 973.6 MPa no cracking	$\sigma_{c,sup}$ = -0.08 MPa σ_s = -111.1 MPa σ_p = 984.7 MPa crack appearance	M_{Rd} = 795.9 kNm > M_{Sd} = 421.1 kNm M_{Ru} = 851.2 kNm concrete entirely cracked

Fig. 4.63: stress analysis for the incomplete composite beam 2 (the tensile values of the steel are the maximum ones)

4.5.2 Material characterization tests

The material properties had been obtained by means of tests led in the Construction Material Experimentation Lab at the Department of Construction and Transportation of the University of Padua. In particular the following tests were carried out: standard compression test (UNI 12390-3/2002) on two concrete cube specimens (side equal to 15 cm), standard tensile test (UNI 10002/1) on four steel square bars (side 30 mm and 35 mm). The results are summarized in the following Tab. 9 and Tab. 10:

Tab. 9: concrete cube test results

Specimen	base [mm^2]	height [mm]	mass [kg]	f_c [MPa]
1	150x148	150	7.85	36.5
2	150x148	150	7.88	34.0
average				34.7

Tab. 10: steel bars tensile test results

Specimen	base [mm^2]	f_y [MPa]	f_u [MPa]
1	30x30	423	537
2	30x30	419	521
3	35x35	425	552
4	35x35	413	532
average		420	536

The average values for each material have been used to the calculation of the expected resistance of the beams.

4.5.3 Experimental test results and analyses

The results of the experimental tests on the 2 pre-compressed truss beams are presented herein. The truss profile is depicted in Fig. 4.64 with the positions of the measure instruments. The test process was: a first loading and unloading cycle until an applied load equal to 100 kN to control the instruments to be in working order; a second cycle until 200 kN that is still in the elastic field, a third cycle until 500 kN that is after the concrete cracking and a fourth cycle up to the failure. The cell load values have been corrected adding the weight of the steel distribution beam (9.0 kN). The mid-span displacement transducer let evaluate the bending stiffness of the beams Fig. 4.66. It can be noted that the course of

the stiffness is very slowly decaying until the failure.

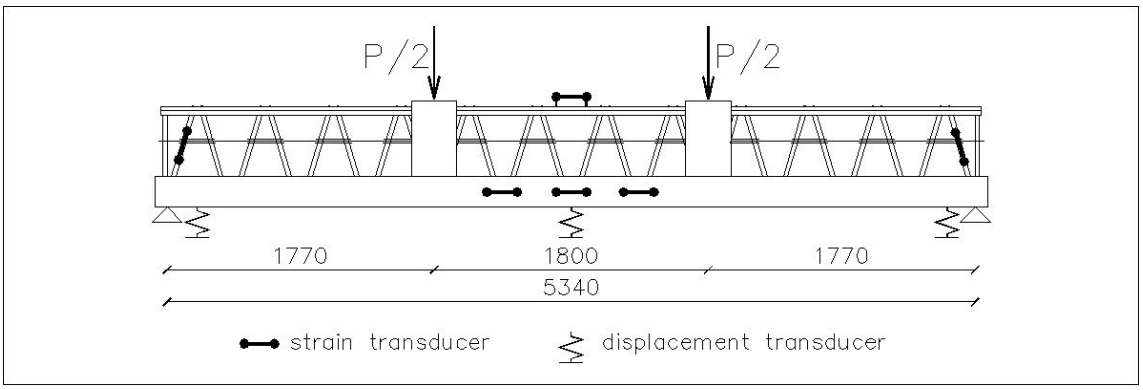

Fig. 4.64: Pre-compressed composite truss profile with the instrument positions

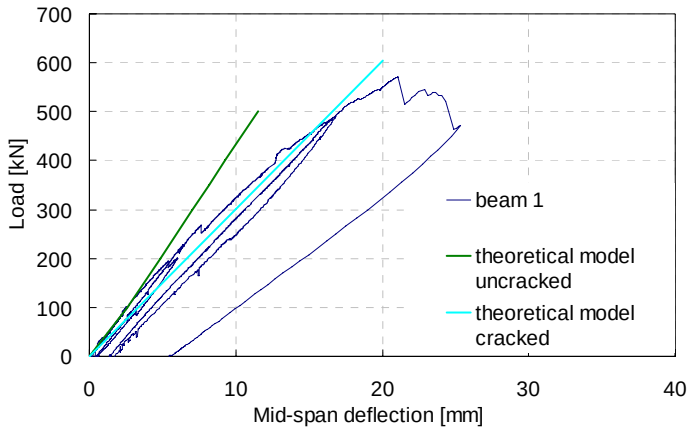

Fig. 4.65: Experimental and analytical load vs. deflection curve for the pre-compressed composite beam 1

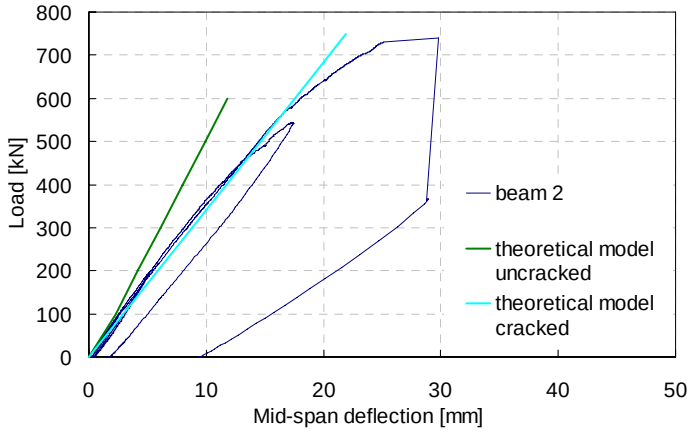

Fig. 4.66: Experimental and analytical load vs. deflection curve for the pre-compressed composite beam 2

The failure load were 571 kN and 739 kN respectively for the first and the second tested beam. The effect of the first three cycles was a low residual deflection of the order of 1 cm. The theoretical elastic behaviour has been obtained by the FE simplified model and its validity has been confirmed by the experimental results. The cracked behaviour has been

obtained reducing the bottom chord stiffness in the FE model, in particular to be compatible with the stiffness of the cracked section computed with the MATLAB program. For the evaluation of the cracking bending moment, the course of the strain transducer on the concrete base has been analyzed as a function of the applied load.

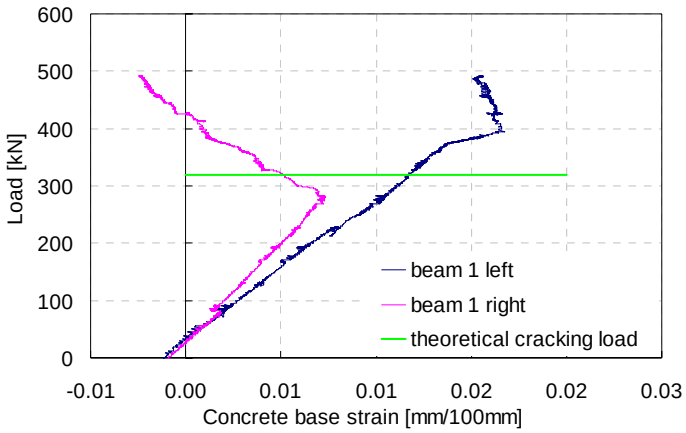

Fig. 4.67: Experimental load vs. concrete base strain for the pre-compressed composite beam 1 with cracking load valuation

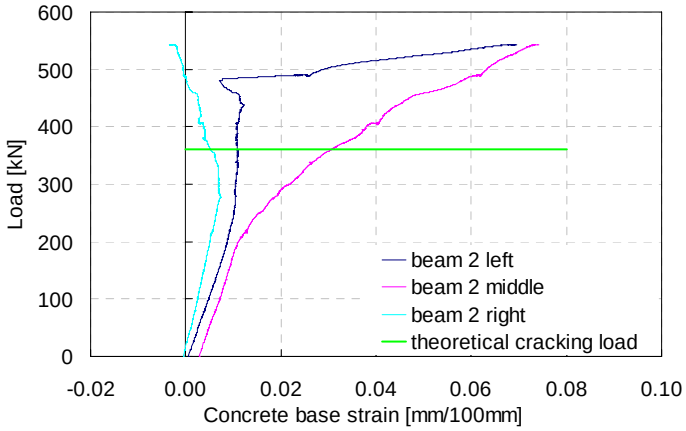

Fig. 4.68: Experimental load vs. concrete base strain for the pre-compressed composite beam 2 with cracking load valuation

Two graphs, one referring to each beam, are reported in Fig. 4.66 and Fig. 4.68, they deal with the third cycle effects. It should be remarked that the positioning of the strain transducers was made before the crack opening, hence some of them weren't placed across a future crack. But the change of the slope of the curves, due to the tension stiffening after the cracking, let valuate the cracking load. The predicted cracking loads 319 kN and 360 kN are in good agreement with the experimental average results considering that the crack opening depends on the tensile concrete strength that is a very delicate value since it's conditioned by the local discontinuities and non-homogeneities or even by occasional bump in the transportation stage. The crack medium distance was about 22 cm (see Fig. 4.69).

The theoretical distances are reported in the following Tab. 11 according to the model recalled in the previous chapter:

Tab. 11: crack distance according to the different theories

Crack Distance [mm]	CEB-FIP del 1978	Leonhardt	CEB-FIP del 1990	Eurocodice 2	Broms	Beeby	Park and Paulay
medium (s_{rm})	221,9	298,4	188,7	—	100,0	185,9	517,7
max ($s_{r,max}$)	—	—	283,1	487,1	—	—	—
min (s_{r0})	—	—	—	—	—	—	389,3

Fig. 4.69: Picture of the crack distance

This is a clear difference that distinguishes the CSTC with a concrete case. In fact in this case only the primary inferior cracks can be conditioned by the truss node presence whereas secondary cracks can develop in a way more similar to the ordinary reinforced concrete structure one. After the cracks localization, the third step had been concluded by the unloading. After that the strain transducers were re-placed across some cracks, they had the possibility to measure the crack width during the following load step. Before focusing on the experimental results it is opportune to resume the crack opening evaluations obtained by the theories recalled in the previous chapter. In particular the MATLAB program has been used, by imposing a zero tensile concrete strength, to calculate the input stress parameter needed in the models for the cracked condition. The Fig. 4.70 and Fig. 4.71 present the courses of the crack width according to the previous chapter formalities. From the graphs it

is clear how each theory considers a linear crack development.

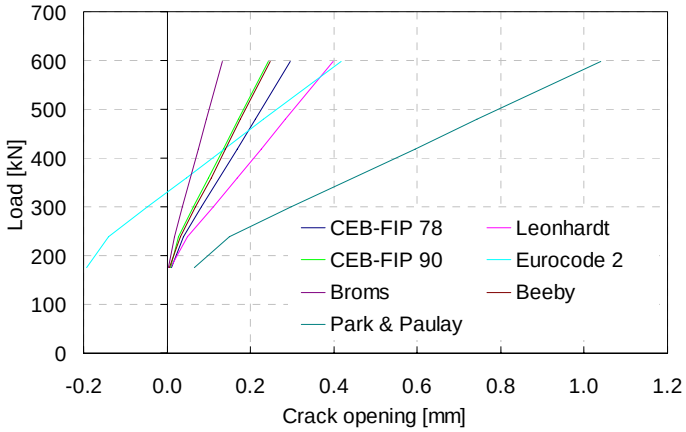

Fig. 4.70: Theoretical predictions for the load vs. crack width curves for the pre-compressed composite beam 1

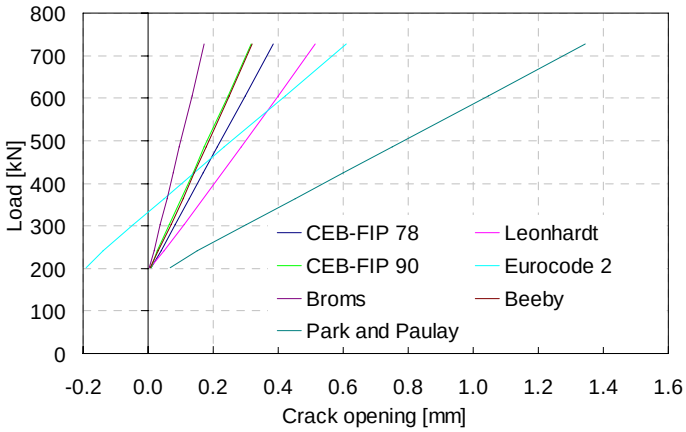

Fig. 4.71: Experimental and analytical load vs. crack width curves for the pre-compressed composite beam 2

The next Fig. 4.72 and Fig. 4.73 show the experimental curves compared only with the CEB-FIP Model Code 1990's and the Broms' theories. In the graphs are reported also the theoretical decompression load, as computed by the MATLAB program, respectively equal to 176 kN and 200 kN for the first and the second beam. It's important to remark that the Broms model gives a crack distance of about 10 cm, which is clearly in disagreement with the experimental evidence. On the contrary, the CEB-FIP Model Code predicts about 19 cm and guarantees a good evaluation of the experimental evidences.

The failure loads were 571 kN and 739 kN for the two beams. The failure mode was the fracture of the truss diagonal bars near their upper truss node (see Fig. 4.74). The cause was that the bending diameter of the bar (3-5 cm) was too short and almost equal to the bar diameter. As a consequence the resulting eccentricities can establish primary and secondary bending moments along the truss elements.

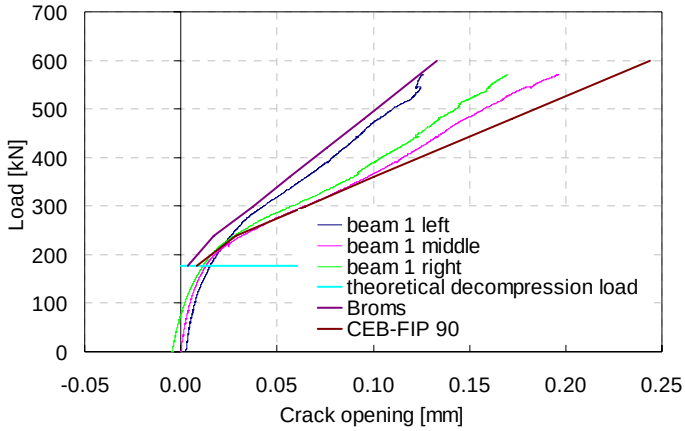

Fig. 4.72: Fracture location on the beam profile

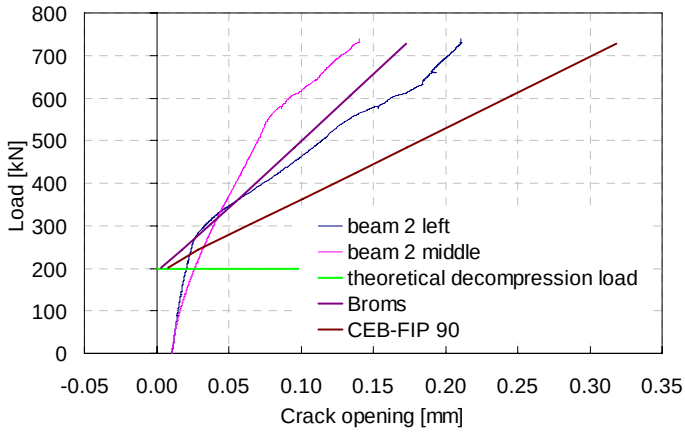

Fig. 4.73: Fracture location on the beam profile

Fig. 4.74: Pictures of the diagonal bar fractures: beam 1 (a), beam 2 (b)

4.6 Conclusions

In this chapter three sets of experimental tests, conduced on composite steel truss and concrete beams, have been presented and their results analyzed. In particular eight REP®-NOR beams, six ECOTRAVE® RAFTILE® and two PREREP® beams have been designed

and tested in the Construction Material Experimentation Lab at the Department of Construction and Transportation of the University of Padua. The global deformability, the bending and the shear resistant mechanisms, the global ductility, the cracking phenomena have been studied. The results have been compared to those obtained by means of the calculation method presented in the previous chapter. The beam mechanics have been confirmed and the method has demonstrated to be efficient and precise to assess the behaviour of the CSTC beams even with very different and innovative solutions.

After the test campaign some general considerations on the global behaviour of the CSTC beams are possible. The resistance of the nude truss demonstrated to be conditioned by local failure like buckling and bar fracture. If on one hand, this kind of mechanisms can be recognized only with a accurate model of the real beam, on the other hand the construction detail of the beam itself is very important. The welding detail, designed according to the S. Leone production rules demonstrated to be accurate since they behaved adequately in every test.

Particular attention should be paid to the assembly of the steel truss by limiting the eccentricities and the bending diameter for the diagonal bars. For what concerns the composite behaviour, a good ductile behaviour can be obtained by an adequate design of the steel truss and of the concrete resisting section. The shear behaviour showed particular characteristic since it can be heavily conditioned by the shear concrete and steel resistant mechanisms. In a CSTC with the bottom steel plate, the shear crack can open quite soon with respect to the maximum shear resistance. This drawback seems to be overcome in the CSTC with the pre-compressed concrete base.

References

1. Leone S. REP® beam calculation methods. Deposited at the *Italian Superior Council of Public Works*, 1967.
2. D M LL PP 14 Jan 2008. Norme Tecniche per le Costruzioni (Construction Technical Codes). *Gazzetta Ufficiale* 04 Feb 2008.
3. Scotta R, Tesser L. Preliminary experiences and basic concepts on the structural performance of hybrid trussed beams. *4th Spec. Conference on The Conceptual Approach to Structural Design*, Venice, 2007.
4. Scotta R, Tesser L. Sperimentazione su travi tralicciate miste REP® – NOR (Experimental tests on composite truss beams REP® – NOR). *VII Italian Workshop on Composite Structures*, Benevento, 2008.
5. Scotta R, Tesser L. Sperimentazione su travi tralicciate miste con fondello in laterizio (Experimental tests on composite truss beams with bottom clay tile). *XVII CTE Congress*, Rome, 2008, **2**: 811-816.
6. CEN. *Eurocode 2: Design of concrete structures Part 1-1: General rules and rules for buildings*. Comité Européen de Normalisation: Bruxelles, 2003.
7. CEN. *Eurocode 4: Design of composite steel and concrete structures Part 1-1: General rules and rules for buildings*. Comité Européen de Normalisation: Bruxelles, 2004.
8. CEN. *Eurocode 3: Design of steel structures Part 1-1: General rules and rules for buildings*. Comité Européen de Normalisation: Bruxelles, 2003.
9. Vincenzi L, Mazzotti C, Savoia M. Stabilità in fase I del traliccio metallico delle travi reticolari miste (Stability in the first phase of the steel truss of composite steel truss and concrete beams). *XVII CTE Congress*, Rome, 2008, **2**: 741-750.
10. Puhali R, Smotlack I. Relazione sulle prove di push-out atte a determinare le leggi di carico-scorrimento delle travi in sistema composto REP (Report on the push-out tests fit for the determination of load-slip laws of REP composite truss beams). *Science of Constructions Institute Acts*, University of Trieste, 1980.
11. CEN. *Eurocode 2: Design of concrete structures Part 1-1: General rules and rules for buildings*. Comité Européen de Normalisation: Bruxelles, 1993.
12. Leonhardt F, Walther R. *Schubversuche an einfeldringen stahlbetonbalken mit und ohne schebbewehrung zur ermittlung der schubtragfähigkeit und der oberen schubspannungsgrenze.* W. Ernst & Sohn Deutcher Aussschuss für Stahlbeton, Berlin, 1962.

13. Leonhardt F, Walther R. *Schubversuche an plattebalken mit unterschiedlicher Schubbewehrung*. W. Ernst & Sohn Deutcher Aussschuss für Stahlbeton, Berlin, 1963.

14. Vitaliani R, Scotta R, Saetta A. *Il calcolo agli stati limite delle strutture in calcestruzzo armato*. Edizioni Libreria Progetto, Padova, 2002.

15. D M LL PP 09 Jan 1996. Norme Tecniche per il calcolo, l'esecuzione, ed il collaudo delle strutture in cemento armato, normale e precompresso e per le strutture metalliche. *Gazzetta Ufficiale* 05 Feb 1996.

16. CEB-FIP. CEB-FIP Model Code for concrete structures. *CEB Bulletin d'Information* 1978, **124**.

17. Leonhardt F. *Crack control in concrete structures*. International Association for Bridge and Structural Engineering Surveys, Zurich, 1977, S-4/77.

18. CEB-FIP. CEB-FIP Model Code for concrete structures. *CEB International Recommendation* 1990.

19. Broms BB. Crack width and crack spacing in reinforced concrete members. *ACI Journal* 1965, **62** (10): 1237-1255.

20. Beeby AW. The prediction of crack widths in hardened concrete. *The structural Engineers* 1979, **57A** (1): 9-17.

21. Park R, Paulay T. *Reinforced Concrete structures.* John Wiley & Sons Inc., 1975.

22. Gutierrez SE, Cudmani RO, Danesi RF. Time-dependent of reinforced and prestressed concrete members. *ACI Structural Journal* 1996, **94** (4): 420-427.

Chapter 5

Reinforced Concrete beam-column joints

5.1 Introduction

Before 1980 the seismic design rules for RC frames all over the world were based on the wrong assumption that the joints, being bigger than the connected structural elements, were not a critical region [1]. This assumption was derived from the observations of earthquake damaged buildings, in which the RC frame joints damage was not the main cause of the collapse.

Subsequently it has been understood that the seismic behaviour of frames was conditioned by the constructive details of beams and columns, not adjusted to support horizontal cyclic load [2]. The results of a great number of analytical and experimental research works brought some improvements in the beam and column behaviour, subjected to seismic excitation, and in the formulation of the capacity design. As a consequence the resistance capacity of beams and columns for cyclic loads increases, raising the solicitations of the joints. These last ones could become new critical regions of RC frame [12].

During the early 90s a debate was raised on the interpretation of joint resistant mechanisms and on the main parameters influencing their strength [13], [20]. Filippou *et al.* [22] collected the results of many experimental tests and design provisions in 1994.

Even the more recent works seem to confirm that the two main mechanisms, underscored in the Paulay work [12], are actually the ones that permit the transmission of the solicitations across the joints to the RC frames. More precisely the mechanisms correspond to the concrete struts and the diagonal compressed fields. Both of them require a particular distribution of longitudinal and transversal reinforcements. Beside the assessment

of the mechanisms, the main goal is to assure a global plastic behaviour avoiding the brittle failure like premature crushing and shearing of concrete, fracturing of steel, loss of bond and anchorage under large cyclic load reversals. Now all these research achievements are taken in acccount by the modern building Codes.

The accurate description of the joint behaviour using numerical analyses is still a research issue [23], [36]. In the present chapter, two and three-dimensional numerical analyses have been proposed and have demonstrated to be able to describe efficiently and accurately the reinforced concrete joint behaviour.

5.2 Reinforced Concrete joints

5.2.1 General criteria

Concerning the reinforced concrete frames, the recent Italian and European Codes [38], [39], contain assessment methods and constructive details, in order to improve the joint's seismic behaviour. The prescriptions should let the frames, designed in high ductility class (HDC), achieve a global ductility level equal to about 5. This level should be assumed at the beginning of a design proces. It determines the design seismic action in terms of design acceleration spectra. Especially conerning the constructive details, since each critical mechanism is not always explained in those Codes, it is necessary to go back to the inherent theories if the design deals with anomalous or unusual configurations.

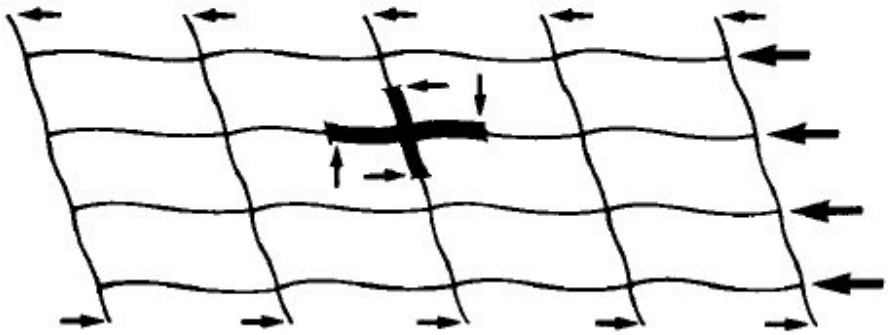

Fig. 5.1: Beam-column element highlighted in a typical laterally loaded frame (Paulay [12])

In general a typical beam-column joint (see Fig. 5.1) is subjected to high shear forces while the adjacent beams develop their maximum flexural strength. In fact the joint strength capacity should not be lower than the demand of the plastic hinges in the adjacent beams. In order to control the global displacements and to prevent any global or local collapse, the columns should remain elastic both above and below the joint. Then the attention can be focused on the shear transmission mechanisms and on the prevention of brittle failure.

Referring to this second point the confinement of the concrete is necessary in the joint and adjacent beam regions. In fact it let the concrete sustain higher compressive stresses and assure a better efficiency of the bond between concrete and steel reinforcements.

During a seismic action, the internal solicitations of a joint consist of a couple of bending moment transmitted by the columns which is counterbalanced by another couple of bending moment transmitted by the beams. The end faces of each element transmit shear forces that converge two at a time in the opposite corners of the joint. Moreover the columns have to sustain the respective longitudinal axial forces (see Fig. 5.2a).

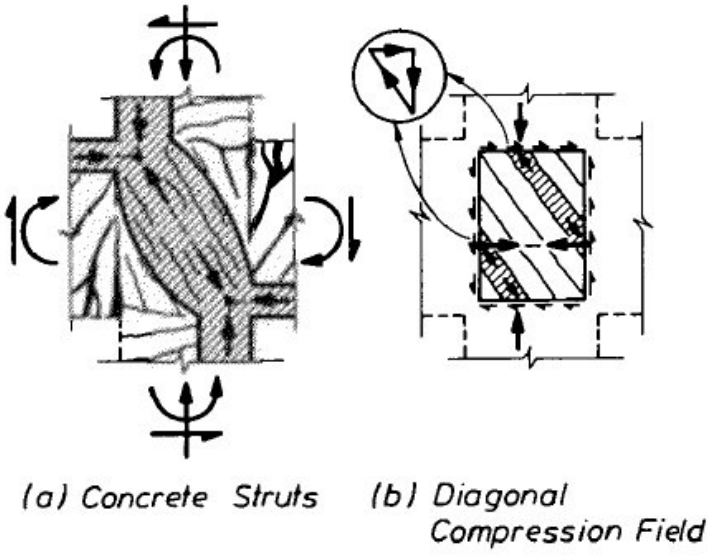

Fig. 5.2: Mechanisms of shear transfer in beam-column joints (Paulay [12])

The simultaneous bending moments, at the end sections of two opposite beams or columns, produce high stress gradient in the longitudinal reinforcements, through the joint. In fact they are compressed in correspondence to a joint face and tight in the opposite one. The possible failure of the bond leads to a drop of the resisting moment and of the stiffness.

The recent literature seems to confirm the effectiveness of the theory formulated by Paulay *et al.* [2], [12]. The joint behaviour has been characterized in terms of admissible mechanisms capable of transmitting shear forces starting from equilibrium criteria. The basic hypotheses are the presence of diagonal cracks in the concrete core and the contribution of concrete strut and reinforcement tie to sustain the shear solicitations. Then two principal mechanisms, resisting shear forces in beam-column joint depending on the geometry and the distribution of the reinforcing steel, have been located (see Fig. 5.2): the concrete strut and the diagonal compression field.

5.2.2 Column behaviour

A portion of an interior column, delimited by two points of contraflexure (approximately at half-story heights) can be isolated as a free body, as shown in Fig. 5.3a.

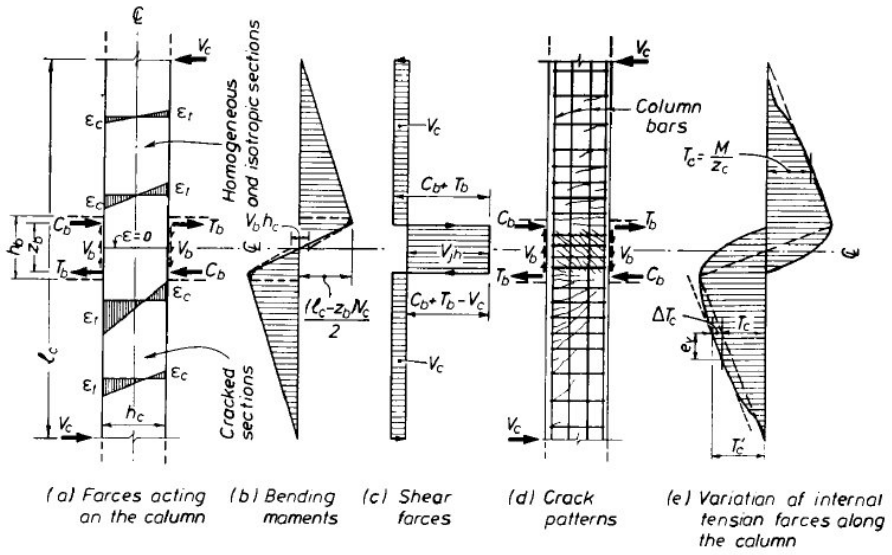

Fig. 5.3: Features of column behaviour (Paulay [12])

For simplicity it is assumed that both the column and the beams are symmetrically reinforced. The beam actions transmitted to the column are represented by the internal horizontal beam tension T_b, compression C_b and the vertical shear V_b forces. The equilibrium of the free body requires an horizontal column shear force of

$$V_c = \left(2 \cdot T_b \cdot z_b + V_b \cdot h_c\right) / l_c \tag{1}$$

where z_b is the internal beam lever arm, h_c is the column depth and l_c is the column length. In this example it is assumed that $T_b = C_b$ and that the column is not subjected to axial load. The corresponding moment and shear force diagrams for the column are shown in Fig. 5.3b and Fig. 5.3c. The horizontal shear force across the joint region is

$$V_{jh} = C_b + T_b - V_c = \left(l_c / z_b - 1\right) \cdot V_c - h_c / z_b \cdot V_b \tag{2}$$

Because the full line diagram in Fig. 5.3b does not show the moment decrement $h_c \cdot V_b$, its slope across the joint does not give the correct value of the horizontal joint shear force. The correct slope would be obtained if, for example, the moment decrement $h_c \cdot V_b$ was been introduced at the horizontal centreline of the joint. The upper part of Fig. 5.3a shows flexural strain distributions across sections of an assumed homogeneous isotropic column. In the lower part of the same figure, strain distributions corresponding to traditional assumptions of flexurally cracked reinforced concrete sections are shown. The symbols ε_c and ε_t denote compression and tension strains, respectively. In both cases, the strain gradients, i.e. curvatures, at sections are proportional to the bending moments at the

same levels. With either the assumption of uncracked or cracked sections, the strain at the horizontal centreline of the example joint is zero. The top half of the Fig. 5.3d shows a typical reinforced concrete column in which a number of approximately horizontal flexural cracks developed. The total internal steel tension force across column sections is proportional to the bending moments $T_c = M / z_c$, where z_c is the internal lever arm in the column. This condition corresponds to the strain distributions shown in the lower half of Fig. 5.3a. Where moments are small, the concrete may resist some flexural tension and hence the steel tensile force would be reduced accordingly. The variation of the magnitude of the steel tension force, consistent with these assumptions and traditionally used in design, is shown in the top half of Fig. 5.3e. The tension stiffening behaviour has been ignored. As a different example, the bottom half of Fig. 5.3d shows a column in which, because of a larger intensity shear force V_c, predominant diagonal cracks developed. Such cracks lead to an increase of the internal flexural tension forces. Thus at a section, the force $T'_c = T_c + \Delta T_c$ is no longer proportional to the moment at the same section. In the presence of web reinforcement, diagonal cracking mobilizes a diagonal compression field. This leads to an increase of the tension force by ΔT_c, as shown in the lower half of Fig. 5.3e. It may be shown that

$$\Delta T_c = V_c \cdot e_v / d \tag{3}$$

where the tension shift is

$$e_v = \left[\cot\alpha - 0.5 \cdot \eta \cdot (\cot\alpha + \cot\beta)\right] \cdot d \tag{4}$$

and where α is the inclination of the diagonal compression field of the truss mechanism with respect to the longitudinal axis of the member, β is the inclination of the web reinforcement, d is the effective depth of the flexural member, and $\eta = V_s / V_c$ is the ratio between the shear force assigned to the truss mechanism V_s and the total shear force to be resisted by the column V_c. The horizontal shear force across the beam-column joint V_{jh} usually leads to extensive diagonal cracking in the joint core as shown in Fig. 5.3d. As a consequence, the effect of tension shift in this region will be dominant. Therefore, contrary to what is implied by the bending moment shown in Fig. 5.3b or by the strain distribution across the sections of idealized flexural members such as shown in Fig. 5.3a, the internal tension forces of the column will not reduce to zero at the center of the joint. The magnitude of the vertical internal tension forces T_c at the horizontal centreline of the beam-column assembly will be significant at both faces of the column.

5.2.3 Joint shear forces

The upper half of the column, above the horizontal centreline of the beam-column assembly, is considered in Fig. 5.4a as a free body.

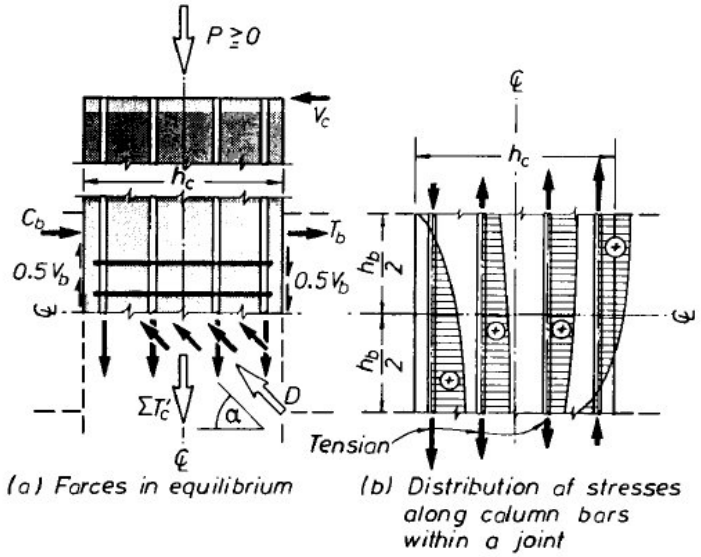

Fig. 5.4: Action on a column within a joint (Paulay [12])

Summation of the horizontal forces led to the horizontal joint shear force V_{jh}. The effect of tension shift, as a result of the assumed total loss of tension capacity of the diagonally cracked concrete of the joint, leads to the development of significant tensile forces in all vertical column bars. These vertical forces and their resultant $\sum T'_c$ are shown in Fig. 5.4a. Assumed that no axial load P is applied to this column, an equal and opposing compression force must exist at the bottom end of free body to balance the vertical tensile forces generated in the reinforcement. To supply both, the necessary horizontal resisting shear force V_{jh} and the vertical compression force $-\sum T'_c$, a diagonal compression force D must be generated in the concrete of the joint so that

$$D = V_{jh} / \cos\alpha \tag{5}$$

and

$$\sum T'_c = V_{jh} \cdot \tan\alpha \tag{6}$$

where α is the inclination of the diagonal compression force with respect to the horizontal centreline axis, as shown in Fig. 5.4a. Its magnitude will emerge from the consideration of beam forces.

The tensile forces in the column bars $\sum T'_c$ at a section, where no strain should exist according to the traditional concepts of flexure, must result in stress distributions along the vertical bars, qualitatively shown in Fig. 5.4b. At the center of the joint, the vertical stresses, shown positive in Fig. 5.4b, have been assumed to be approximately the same in all bars. The variation of stresses between the four sets of bars across either of the critical column sections at the top or bottom of the joint core suggests gross incompatibility with corresponding stresses, derived by a standard analysis for an elastic cracked column section

subjected to maximum moments at these two levels.

The equilibrium of another free body consisting of one half of the continuous beam is considered in Fig. 5.5a.

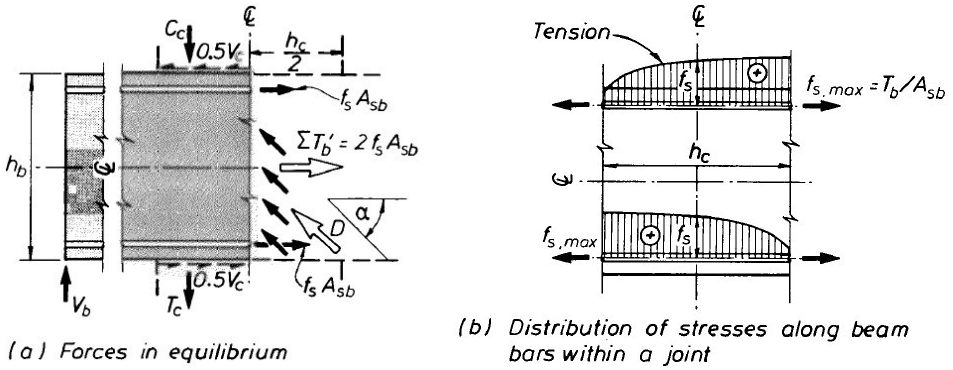

Fig. 5.5: Action on a beam within a joint (Paulay [12])

The symbols C_c and T_c are the maximum internal compression and tension forces, respectively, transmitted by the columns from above and below the beam. These forces transmit the column moments to the joint core. By considering the equilibrium of vertical forces acting on the shaded free body in Fig. 5.5a, the vertical joint shear force is

$$V_{jv} = C_c + T_c - V_b \tag{7}$$

The Beam bending moments are the effects of a tension shift of the internal tensile forces along the beam bars, not shown here, similar to this shown in Fig. 5.3e. As a result, significant equal tensile forces are to be expected in both the top and bottom beam bars at the vertical centreline of the joint. The sum of these two tensile forces in the beam $\sum T'_b$ must be balanced by an internal horizontal compression $D \cdot \cos\alpha$, as shown in Fig. 5.5a. It is then seen that

$$D = V_{jv} / \sin\alpha \tag{8}$$

and

$$\sum T'_b = V_{jv} \cdot \cot\alpha \tag{9}$$

In contrast to the column there are usually no intermediate horizontal bars passing through the joint. Therefore, the total horizontal steel force $\sum T'_b$ will generate tensile stresses f_s in the top and bottom beam bars at the vertical centreline. These will only be a little less than the maximum stress at the critical beam section. The distribution of the steel stresses along the elastic beam bars is qualitatively shown in Fig. 5.5b. As a consequence of this phenomenon, the beam bars may not function as flexural compression reinforcement at the boundaries of the joint. And only a small fraction of the intended steel forces can be

transmitted by bonding with the concrete core of the joint, irrespective of any deterioration in the bond mechanism.

If Eq. 5 and Eq. 8 are combined, it is found that

$$\tan\alpha = V_{jv} / V_{jh} \tag{10}$$

Using the known strength properties of the critical beam sections and the corresponding internal forces at the column cross sections, the vertical and horizontal joint shear forces V_{jv} and V_{jh} are obtained from Eq. 7 and Eq. 2. Also for the example case, without axial load on the column, it is found from Eq. 10, Eq. 6 and Eq.9 that the sums of the internal steel tension forces at the center of the joint core are

$$\sum T'_c = V_{jv} \tag{11}$$

and

$$\sum T'_b = V_{jh} \tag{12}$$

in the vertical and horizontal directions, respectively. For design purposes, the inclination of the diagonal compression force D may be approximated by

$$\tan\alpha \approx z_b / z_c = h_b / h_c \tag{13}$$

When a weak beam-strong column system is used in a ductile design for seismic actions, plastic hinges in the beams may be expected to develop their flexural overstrength at the column faces. Thus for the example structure, the maximum internal beam forces shown in Fig. 5.3a may increase to $T_b^o = C_b^o = \lambda_o \cdot f_y \cdot A_{sb}$, where A_{sb} is the area of flexural tension reinforcement in one face of the symmetrically reinforced beam, f_y is the specified yield strength of the steel and λ_o is the factor quantifying the probable overstrength of the steel developed at large curvature ductility demands. Hence from Eq. 11 and Eq. 2, it is found that at this extreme stage of seismic loading of the beam

$$\sum T'_b = V_{jh} = 2 \cdot T_b^o - V_c = 2 \cdot \lambda_o \cdot f_y \cdot A_{sb} - V_c \tag{14}$$

As Fig. 5.5a shows, $\sum T'_b = 2 \cdot A_{sb} \cdot f_s$. Hence the tensile stress in the beam bars at the center of the joint are expected to be

$$f_s = V_{jh} / 2 \cdot A_{sb} = \left(2 \cdot T_b^o - V_c\right) / \left(2 \cdot A_{sb}\right) \tag{15}$$

Thus the stress in the beam bars at the center of the joint may approach the probable yield strength of the steel. The consequences of this phenomenon, enumerated in the previous section for elastic conditions, are accentuated in this limit state.

Hence the aims in improving the performance of a joint can be: tensile stresses generated along beam bars within the joint should be reduced; beam bars should be able to

act as compression reinforcement within the beam plastic hinges on either side of the beam-column joint; anchorage for the beam bars should be provided within the joint core, rather than outside in the adjacent beams.

These aims can be achieved by providing significant amounts of horizontal reinforcement placed between the top and bottom beam bars without increasing the beams flexural strength. This requires the use of horizontal ties or stirrup, as shown in Fig. 5.6a.

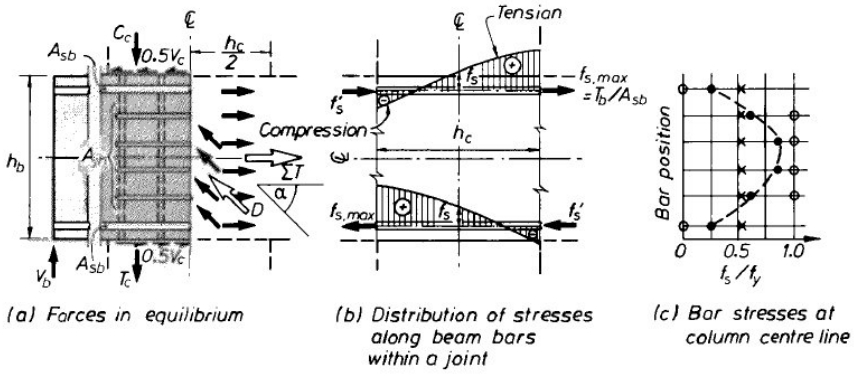

Fig. 5.6: Actions on beam within a joint containing horizontal joint shear reinforcement (Paulay [12])

The forces shown in this figure are similar to those given in Fig. 5.5b, as they correspond to the equilibrium criteria from which Eq. 7, Eq. 8 and Eq. 9 have been derived. If the total area of all effective tie legs is A_{jh}, then the average stress in all horizontal bars at center of the joint is by Eq. 15 of the order of

$$f_s = V_{jh} / \left(2 \cdot A_{sb} + A_{jh}\right) \tag{16}$$

The theoretical stress distribution along beam bars in such a reinforced joint is qualitatively shown in Fig. 5.6b. When this distribution is compared with the one shown in Fig. 5.5b, the improvements become evident. A possible uniform distribution of stresses over the depth of the joint in different horizontal bars is shown by cross markers in Fig. 5.6c. This derivation was based on the assumption that horizontal tensile strains and hence stresses along the vertical centreline of the joint are approximately the same. However, because of the extensive diagonal cracking in the joint core and the radically different anchorage conditions to develop stresses in beams or in tie bars, strains along these two types of bars need will not be compatible.

It has been recommended [38] that in joints of this type, intermediate joint shear reinforcements should be provided to resist the entire horizontal joint shear force V_{jh}. This recommendation is based on a different approach that considers the diagonal compressed field as a mechanism of shear resistance. If the horizontal ties provided can resist the entire horizontal force, then the beam bars do not need to resist horizontal forces at the vertical centreline of the joint core. Accordingly, at this section, the stress in the beam bar should be

$f_s = 0$. This hypothetical condition, shown by circle markers in Fig. 5.6c, implies that unless there is a bond deterioration, the beam bars could attain their maximum strength $\lambda_o \cdot f_y$ simultaneously in tension and in compression at opposite boundaries of the joint with zero stress at the joint centre. To enable beam plastic hinges to exhibit stable hysteretic response, the design should strive to approach these ideal conditions for the beam rebars within a joint. However, considerations of deformation compatibility of beam bars within the joint and adjacent tie legs will show that it is not possible to attain this state. The total elongation of beam bars with approximately equal tensile and compression stresses applied at each face and with zero stress at the centreline of the column should be negligable. On the other hand, as Fig. 5.6c shows, a tie leg adjacent to and parallel with a beam bar subjected to yield stress over its entire length would become significantly longer.

In a thoroughly cracked but well designed beam-column joint, particularly after a few cycles of reversed loading and because of inevitable bond failure, the stresses induced in the horizontal beam bars will be somewhere between the hypothetical limits. A typical distribution over the depth of the joint of tensile stress in bars at different levels, also observed in experiments, is shown in Fig. 5.6c by the curve (connecting full circles). The total tensile force sustained by the horizontal bars corresponding to the three cases of stress distribution is the same.

The principle governing the relationship between the horizontal joint shear force and the mobilized internal horizontal tensile forces are equally applicable to the column reinforcements. However, the combined flexural strength of the two critical column sections, will normally be considerably higher than the moment demands arising when nearby beam plastic hinges develop their flexural overstrength. The two column sections above and below a joint in typical multistory frames, proportioned accordly to capacity design principles, will usually have a combined flexural reserve strength. This means that, when suitably arranged, the column bars can readily accommodate the vertical tensile forces without approaching the yield stress.

5.2.4 Effects of column axial compression

If the axial compression of the columns is taken into account, the equilibrium of internal column forces at the critical column sections, such as the ones shown in Fig. 5.5a, will require that

$$C_c - T_c = P \tag{17}$$

where P is the axial compression load on the column. The internal lever arm z_c, at these sections across the column, will now be somewhat smaller than that in the previous cases. By considering now the equilibrium of horizontal and vertical forces acting on the free

body shown in Fig. 5.4a it is found as before that:

$$D = V_{jh} / \cos\alpha^* \tag{18}$$

and the requirement that

$$P + \sum T'_c - D \cdot \sin\alpha^* = 0 \tag{19}$$

leads to

$$\sum T'_c = V_{jh} \cdot \tan\alpha^* - P \tag{20}$$

When this equation is compared with Eq. 6, it is seen that the internal vertical tensile forces at the horizontal centreline of the joint are reduced by the axial load P, as expected. Because of the reduced internal lever arm in the column sections z_c, the inclination α^* of the diagonal compressed force D will, however, be larger than that in the case without axial compression load. When the axial compression load exceeds the intensity of the horizontal shear force V_{jh}, it can be expected that no vertical tensile forces will be generated in the joint core. This would not be uncommon in interior joints at the lower floors of multistory frames.

5.2.5 Evaluation of the two resistant mechanisms

The two postulated mechanisms, the concrete strut and the diagonal compression field, have to provide the joint with the necessary strength. Each of the horizontal and vertical soliciting shears, being sustained by the concrete and the reinforcing steel, can be splitted in two parts, as follows

$$V_{jh} = V_{ch} + V_{sh} \quad \text{and} \quad V_{jv} = V_{cv} + V_{sv} \tag{21}$$

with self-explanatory symbols. The value of concrete horizontal shear force is equal to

$$V_{ch} = C'_c + \Delta T'_c - V_{col} \tag{22}$$

where C'_c is an upper beam concrete compressive resultant acting on a joint face near a corner, $\Delta T'_c = T + C'_s$ is the contribution of the steel as an addition to the tensile force at the opposite face and a compressive force at the same face of the concrete one. The contribution of the reinforcing steel depends on the distribution of the bond stresses along the bars. The maximum value can be estimated as 1.25 times the medium bond stress u_0. Assuming that the bond can develop over a length equal to $0.8 \cdot c$, where c is the compression depth of the column member in elastic field. This last can be calculated as

$$c = 0.25 + 0.85 \cdot P_u / \left(f'_c \cdot A_g\right) \tag{23}$$

where P_u is the maximum compressive load acting on the column. Hence the contribution of the steel can be computed as if the maximum bond stress acts on the

assumed bond length

$$\Delta T'_c = 1.25 \cdot u_0 \cdot 0.8 \cdot c = u_0 \cdot c = c \cdot (C'_s + T)/h_c \tag{24}$$

According to Paulay [12], the equilibrium of the joint and the deterioration of the bar bond cause the decrease of steel compressive stresses f'_s. Hence the compressive stress contribution can be a fraction of the tensile one, that is

$$C'_s = \gamma \cdot f_y \cdot A_b = T \cdot \gamma / \lambda_0 \tag{25}$$

remembering that $T = \lambda_0 \cdot f_y \cdot A_b$ and with γ / λ_0 less than 1.

From the absence of beam axial load, the compressive concrete resultant can be expressed as

$$C'_c = T' - C'_s = \beta \cdot T - T \cdot \gamma / \lambda_0 \tag{26}$$

being β the ratio between the upper and the lower reinforcement area of the beam. With the previous formulas the estimation of the concrete contribution to support the horizontal shear force is

$$V_{ch} = \left[(1 + \gamma / \lambda_0) \cdot c / h_c + \beta - \gamma / \lambda_0 \right] \cdot T - V_{col} \tag{27}$$

This force can be sustained by the concrete strut mechanism of the joint.

Subtracting the obtained value of the V_{ch} from the total horizontal shear force, the shear sustained by the reinforcing steel can be found

$$V_{ch} = (1 + \gamma / \lambda_0) \cdot (1 - c / h_c) \cdot T \tag{28}$$

This contribution can be sustained by the truss mechanism of the joint.

In a similar way the division of the vertical shear leads to a concrete and a reinforcement parts. From the above developed theory, the vertical shear can be computed starting from the horizontal one

$$V_{cv} = V_{ch} \cdot \tan \alpha = V_{ch} \cdot h_b / h_c \tag{29}$$

and the same can be written for the reinforcing steel part.

5.2.6 Observations

In a reinforced concrete joint the maximum shear strength is determined by two mechanisms, the concrete strut and the diagonal compression field.

The shear soliciting force within the joint leads to high stresses in the concrete core. The tensile ones produce the core cracking in both diagonal directions and the tensile stresses should be carried by adequate reinforcing bars. The core concrete should be verified for the compressive stresses and the concrete tangential stresses should be limited.

5.3 RC joint Code prescription comparison

5.3.1 General criteria

This section presents a review of the design and detailing requirements of interior joints of special moment resisting reinforced concrete frames, with reference to two codes of practice: American Concrete Institute (ACI 318M-02 [40]) and Eurocode 8 (EN 1998-1:2003 [39]). The discussions with respect to Eurocode are pertaining to High Ductility Class defined by that code.

One of the objectives of detailing is to ensure that the full strength of the reinforcing bars, serving either as principal flexural or transverse reinforcement, can be developed under the most adverse conditions that an earthquake may impose. Detailing features relevant to beam-column joints are concerned with some aspects such as transverse reinforcement for shear strength and confinement, spacing of column longitudinal reinforcement and development length for embedded bars. In a global sense, the design procedure of beam-column joints consists of the following steps:

- Design the preliminary size for members based on anchorage requirements for the chosen longitudinal bars.
- Ensure adequate flexural strength of columns to get the desired beam yielding mechanism.
- Arrive at the design shear force for the joint by evaluating the flexural overstrength of the adjacent beams and corresponding internal forces. The simultaneous forces in the column that maintain joint equilibrium must also be determined. From these, the joint shear force demand can be calculated.
- Obtain effective joint shear area from the adjoining member dimensions.
- Ensure that the induced shear stress is less than the allowable stress limit. The allowable shear stress limit is expressed as a function of the compressive strength or diagonal tensile strength of concrete. If not satisfied, alter the associated member dimensions, i.e. width of the beam or depth of the column.
- Provide transverse reinforcements both as confining reinforcement and as shear reinforcement.
- Provide sufficient anchorage for the reinforcement passing through or terminating in the joint.

The above listed points are elaborated in sequence with respect to code provisions. The variables involved in the code provisions are expressed with the help of commonly adopted notations and symbols.

5.3.2 Depth of member in interior joint

In seismic conditions involving reversed cyclic loading, anchorage requirements assume great importance in deciding the sizes of the members. This is because the limiting bond stress around the longitudinal bar has to be satisfied by the development length available within the member. In an interior joint, the force in a bar passing continuously through the joint changes from compression to tension. This causes push-pull effect with distribution of bond stress as shown in Fig. 5.7. The severe demand on bond strength necessitates that adequate development length for the bar be made available within the depth of the member. For the longitudinal bar of the beam the development length should be provided by the column depth and vice versa. In recognition of this, the codes limit the ratio between the bar diameter and the member depth. By adopting smaller diameter bars which require reduced development length, the sizes of the members can be controlled.

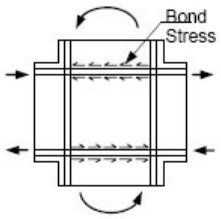

Fig. 5.7: Bond condition in an interior joint

ACI 318M-02 suggests that where longitudinal beam reinforcement extends through an interior joint, the column depth, h_c shall not be less than 20 times the diameter of the largest longitudinal bar.

$$h_c \geq 20 \cdot d_b \tag{30}$$

where d_b is the diameter of the longitudinal beam bar to be anchored and h_c is the width of the column parallel to the beam. The purpose of the recommended value for h_c / d_b is to provide reasonable control on the amount of potential slip of the beam longitudinal bars through the joint. However, bar slippage may occur even with column depth of 20 d_b. Slippage of bars considerably reduces the stiffness and energy dissipation capacity of the connection region.

EN 1998-1: 2003 considers the effects of axial load, of material strength and of tension-compression reinforcement ratio. Anchorage of longitudinal bars for interior beam column joints high ductility class (DCH) must satisfy the following expression:

$$\frac{d_b}{h_c} \leq \frac{7.5 \cdot f_{ctm}}{\gamma_{Rd} \cdot f_{yd}} \cdot \frac{1 + 0.8 \cdot \upsilon_d}{1 + 0.75 \cdot k_D \cdot \rho' / \rho_{max}} \tag{31}$$

where f_{ctm} is the mean value of tensile strength of concrete given as, f_{yd} is the design

value of yield strength of steel; ρ'/ρ_{max} is the ratio of compression reinforcement to maximum tension reinforcement of the beam framing in the joint; k_D is a coefficient equal to 1 for HDC structure; γ_{Rd} is the uncertainty model factor for the design value of resistances due to overstrength at strain hardening of longitudinal steel in the beam and υ_d is the normalised design axial force in column taken with its minimum value for seismic load combination.

Comparing the two Codes, the EN 1998-1:2003 shows larger column depth. The ACI provision is less conservative as compared to EN code except when the grade of concrete is considerably higher.

5.3.3 Flexural strength of column

The codes recommend expressions to preclude formation of plastic hinges in columns which essentially aim at providing stronger columns with capacity more than the flexural strength of beams, obtained considering over strength factors.

ACI 318M-02 recommends that the sum of the nominal flexural strengths of the column sections above and below the joint should not be less than 1.2 times the nominal flexural strength of the beam sections at the joint faces.

$$\sum M_c \geq 1.2 \cdot \sum M_b \tag{32}$$

where M_c and M_b represent the nominal flexural strength of column and beam, respectively. In T-beam construction, where the slab is in tension under moments at the face of the joint, slab reinforcement within an effective slab width suggested by the code should be assumed to contribute to the flexural strength of the beams, if the slab reinforcement is developed at the joint face for flexure.

EN1998-1:2003 suggests the following condition to be satisfied at all joints

$$\sum M_{Rc} \geq 1.3 \cdot \sum M_{Rb} \tag{33}$$

where M_{Rc} is the sum of the design values of the minimum moments of resistance of the columns within the range of column axial forces produced by the seismic design situation and M_{Rb} is the sum of the design values of the moment of resistance of the beams framing into the joint.

5.3.4 Shear force acting on the joint

With the assumption that the beams are designed for plastic hinge formations, the flexural overstrength of beams on either side of the joint is evaluated corresponding to positive and negative moment capacities. The contribution of floor slab is considered in the

form of the effective flange width for the beam. The flexural strength in positive and negative bending is arrived at and is referred to as M_{1o} and M_{2o}. The column shear can be calculated as

$$V_{col} = 2 \cdot \frac{M_{1o} + M_{2o}}{l'_c + l_c} \tag{34}$$

where l'_c and l_c are the heights of the columns above and below the joint.

The shear force demand, V_{jh}, in the horizontal direction, can be obtained as the net force acting on a horizontal plane across the joint so as to include the forces from the beam and the shear force in the column.

$$V_{jh} = (A_{s1} + A_{s2}) \cdot \lambda_0 \cdot f_y - V_{col} \tag{35}$$

where A_{s1} is top reinforcement in the beam including reinforcement in effective flange width and A_{s2} is bottom reinforcement in the beam.

Similarly, consideration of equilibrium of vertical forces at the joint should lead to expressions for the vertical joint shear force, V_{jv}. However, because of the multilayered arrangement of the column reinforcement, the derivation of vertical stress resultant is more cumbersome. For common design situations, it is generally considered sufficiently accurate to estimate vertical joint shear force in proportion to horizontal shear force. This can be expressed as

$$V_{jv} = (h_b / h_c) \cdot V_{jh} \tag{36}$$

where h_b and h_c are the depth of the beam and the column respectively.

5.3.5 Shear strength of joint

The shear forces in the joint region in vertical and horizontal directions develop diagonal compressive and tensile forces within the joint core. The shear transfer mechanisms are very complex since interplay of shear, bond and confinement takes place within the joint. Hence, conflicting views exist between researchers with regard to the design parameters of the joint. The model proposed by Paulay, Park and Priestley (1978) [1] considers that the total shear within the joint core is carried partly by a diagonal concrete strut (see Fig. 5.8a) and partly by an idealized truss consisting of horizontal hoops, intermediate column bars and inclined concrete bars between diagonal cracks (see Fig. 5.8b).

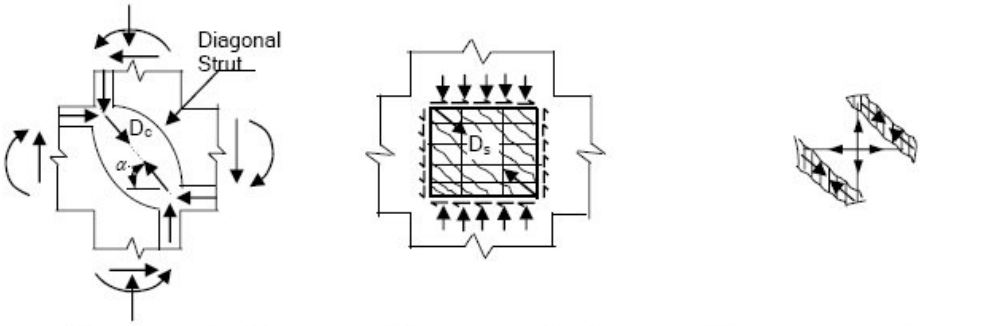

Fig. 5.8: Shear resisting mechanisms: (a) concrete strut mechanism; (b) truss mechanism; (c) truss components

The strut mechanism is associated with a diagonal force, D_c within the concrete strut, developed by major diagonal concrete compression forces formed at the corners of the joint. A substantial portion of the total joint shear, horizontal and vertical, can be resisted by this mechanism. However, the strength of the strut mechanism is reduced by tensile strains perpendicular to the direction of the strut. In such situations, confinement of the joint core would help improving the strength of the strut. The steel forces transferred through bonding are introduced into concrete at the four boundaries of the joint core, forming a compression field with diagonal cracks in the joint as shown in Fig. 5.8b. These forces being in equilibrium generate a total diagonal compression force D_s coming from all the concrete bars between the diagonal cracks. The mechanism associated is called truss mechanism and is supported by well distributed transverse reinforcement within the joint. The diagonal forces D_c and D_s are acting at an angle α with respect to the horizontal axis of the joint. The sum of the horizontal components of these forces from both mechanisms gives an estimate of the shear resistance in horizontal direction. Similarly, the sum of the vertical components gives the shear resistance in vertical direction.

When the compression stress within concrete strut is not excessive, the strut mechanism is efficient in resisting the shear, and the truss mechanism is hardly mobilized. Nevertheless, the transverse reinforcement provides confinement to improve the efficiency of the concrete in the strut mechanism. However, when the core concrete is thoroughly cracked and no more diagonal tensile stresses can be transferred by concrete, the transverse reinforcements resist shear as shown in Fig. 5.8c. In such situations the contribution of truss mechanism becomes significant, provided good bond conditions are granted.

In essence, the design of joint to resist the shear force demand is associated with the adoption of adequate joint dimensions to support the strut mechanism and with the provision of adequate transverse reinforcement to take care of truss mechanism. On the other hand, the truss mechanism tends to diminish in case of bond deterioration and the transverse reinforcements can no longer be utilized to sustain the joint shear. Hence, for

design considerations, the compressive strength of the diagonal concrete strut is considered as the reliable source of strength, based on hopw the Codes define nominal shear capacity of the joint. The nominal shear capacity is expressed in terms of allowable stress in concrete and effective joint area. As a first design step, it is verified that the shear force demand in the joint is less than the nominal shear capacity, if not the dimensions of the joint are to be revised irrespective of the amount of reinforcement available within the joint. Increasing the joint dimensions improve the strength of strut by increasing the effective joint area and also by reducing the nominal shear stress acting on the joint. In addition towards the truss mechanism, the joint is provided with necessary shear reinforcement.

5.3.6 Effective joint area

The effective joint area A_j is the area resisting the shear within the joint and it is constituted by the framing members in the considered direction of loading. The width b_j and the depth h_j of the joint are calculated from the member dimensions. The joint depth h_j is assumed equal to the column depth h_c. The joint width b_j involves the beam width b_b, the column width b_c, and the column depth h_c.

ACI code uses the distance of the column edge beyond the beam edge denoted as x

$$b_j = \min\{b_b + h_c; b_b + 2 \cdot x\} \quad \text{if} \quad b_c > b_b \tag{37}$$

$$b_j = b_c \quad \text{if} \quad b_b > b_c \tag{38}$$

Eurocode 8 adopts the following values

$$b_j = \min\{b_c; b_b + 0.5 \cdot h_c\} \quad \text{if} \quad b_c > b_b \tag{39}$$

$$b_j = \min\{b_b; b_c + 0.5 \cdot h_c\} \quad \text{if} \quad b_b > b_c \tag{40}$$

It is to be noted that in no case the joint effective area is greater than the column cross sectional area.

5.3.7 Nominal shear stress of the joint

The level of shear stress, as expressed by nominal shear stress, is an important factor affecting both strength and stiffness of the joint. The codes restrict the nominal shear stress to be less than a fraction of compressive strength of concrete. Both Codes evaluate the nominal shear capacity based on strut mechanism and express it as a function of concrete strength irrespective of the amount of shear reinforcement. The nominal shear capacity is influenced by the confinement provided by the adjoining members. A beam member that frames into face is considered to provide confinement to the joint if the framing member covers at least three-quarter of the joint face.

ACI 318M-02 sets the nominal shear strength of the joint as a function of only concrete strength, which in turn depends upon the degree of confinement, offered by the members and is given as $1.7 \cdot \sqrt{f'_c} \cdot A_j$ if confined on four faces, $1.25 \cdot \sqrt{f'_c} \cdot A_j$ if confined on three faces and $1.0 \cdot \sqrt{f'_c} \cdot A_j$ for the other cases. Apart from this fact, the code requires a minimum amount of transverse reinforcement in the joint as shear reinforcement to provide for confinement of the core concrete.

EN 1998-1:2003 has limited the nominal shear stress υ_{jh} within interior beam column joint to be less than the stress value given by the expression

$$\upsilon_{jh} = \eta \cdot f_{cd} \cdot \sqrt{1 - \frac{\upsilon_d}{\eta}} \tag{41}$$

where $\eta = 0.6 \cdot \left(1 - \frac{f'_c}{250}\right)$ denotes the reduction factor on concrete compressive strength due to tensile strains in transverse direction.

ACI 318M-02 Code gives an higher estimation of nominal joint shear capacity compared to the other code for interior joint at lower value of concrete strength.

5.3.8 Design of shear reinforcement

Shear reinforcements in horizontal and vertical directions are designed to support the truss mechanism. Usually, the horizontal shear is supported by stirrups and hoops placed in the horizontal direction while the vertical shear is taken care adequately by intermediate column bars. Since the intermediate column bars are expected to be in compression, the bars will have adequate strength to sustain tensile stresses developed during shear resisting mechanism. The horizontal shear supported by the truss mechanism is resisted by transverse steel in the joint. Codes suggest expressions for design of shear reinforcement based on the assumption that plastic hinges develop only in the beams.

5.3.9 Horizontal shear reinforcement

The transverse reinforcement in the joint contributes to the core confinement and to the shear resistance. ACI 318M-02 does not require an explicit calculation for shear reinforcement but it recommends a minimum reinforcement area to confine the joint. The provided confinement is expected to be sufficient for the force transfer within the joint. In members with circular cross section, when spiral reinforcement or circular hoop is used, the volumetric ratio ρ_s, nor should not be less than

$$\rho_s = 0.12 \cdot f'_c / f_{yh} \tag{42}$$

neither than

$$\rho_s = 0.45 \cdot \left(A_g / A_c - 1\right) \cdot f'_c / f_{yh} \tag{43}$$

where f_{yh} is the specified yield strength of the spiral reinforcement but not greater than 420 MPa, A_g is the gross sectional area and A_c is the area of core concrete within the spirally reinforced compression member measured outside the spiral diameter.

In rectangular sections, rectangular hoops and crossties are used as horizontal transverse reinforcement. The efficiency of the confinement provided by these hoops is considered to be 0.75 times the one provided by circular hoops. Thus, the total cross-sectional area of stirrups A_{sh}, in each direction of a single hoop, over lapping hoops, or hoops with crossties of the same size in a layer, should be at least equal to

$$A_{sh} = 0.3 \cdot \left(s \cdot h''_c \cdot f'_c / f_{yh}\right) \cdot \left(A_g / A_{ch} - 1\right) \tag{44}$$

but it should not be less than

$$A_{sh} = 0.09 \cdot s \cdot h''_c \cdot f'_c / f_{yh} \tag{45}$$

where s is spacing of transverse reinforcement within the joint, h''_c is cross-sectional dimension of column core measured center-to-center of the transverse reinforcement, A_{ch} represents cross-sectional area of rectangular member measured out-to-out of the transverse reinforcement.

EN 1998-1:2003 gives expressions for adequate confinement to be provided to limit the maximum diagonal tensile stress in the concrete core. The minimum amount of reinforcement required for adequate confinement and for limitation of diagonal tensile concrete stresses is given as

$$\frac{A_{jh} \cdot f_{yhd}}{b_j \cdot h_{jw}} \geq \frac{\left[V_{jh} / \left(b_j \cdot h_{jc}\right)\right]^2}{f_{ctd} + \upsilon_d \cdot f_{cd}} - f_{ctd} \tag{46}$$

where V_{jh} is the horizontal shear force demand, h_{jw} is the distance between top and bottom beam bars, h_{jc} is the distance between extreme column corner bars, f_{ctd} is the design value of tensile strength of concrete, f_{yhd} is the design value of yield strength of transverse reinforcement. EN code imposes also a requirement to maintan the integrity of the joint after diagonal cracking and hence the necessary reinforcement to be provided to the interior joint is given as

$$A_{jh} \cdot f_{yhd} \geq \gamma_{Rd} \cdot \left(A_{s1} + A_{s2}\right) \cdot f_{yd} \cdot \left(1 - 0.8 \cdot \upsilon_d\right) \tag{47}$$

where the parameters have already been defined and A_{jh} represents the total area of horizontal hoops to be provided within the joint.

Comparing the previous expressions it can be seen that the amount of reinforcement

increases proportionately to the grade of concrete using the ACI code. For what concerns the Eurocode, if the Eq. 38 governs, its expression does not vary with the concrete strength when the axial load ratio is assumed constant.

5.3.10 Vertical shear reinforcement

Vertical shear reinforcements sustain basically the truss mechanism. Besides, the vertical reinforcements resist vertical shear V_{jv}, and are provided in the form of intermediate column bars placed in the plane of bending between corner bars or vertical stirrup ties or special vertical bars, placed in the column adequately anchored to transmit required tensile force within the joint. In seismic design principles, column hinging is generally precluded and hence the stresses in column reinforcements are expected to remain within an elastic range. Therefore, the vertical joint shear is not expected to be critical compared to horizontal joint shear. On this basis, codes estimate the vertical shear reinforcement in proportion to the required horizontal shear reinforcement. Usually, since the intermediate column bars experience compressive stresses lower than their yield stress, those bars are expected to have higher reserve strength to take tension due to vertical joint shear. Hence, it is acceptable to rely on column longitudinal distributed bars to take vertical shear along with flexural and axial load. ACI 318M-02 does not provide expressions for vertical shear reinforcement. However, the code insists on placing intermediate column bars with restrictions on spacing on each face of the column. EN 1998-1:2003 gives specific recommendations to arrive at the necessary shear reinforcement in the vertical direction. The vertical joint shear V_{jv} is expressed proportionately to the horizontal joint shear, and the vertical reinforcement is recommended to be a percentage of the horizontal shear reinforcement. The ENV 1998-1:2003 suggests the following expression

$$A_{sv,i} = \frac{2}{3} \cdot A_{sh} \cdot \frac{h_{jc}}{h_{jw}} \tag{48}$$

where $A_{sv,i}$ denotes the total area of the intermediate bars located in the column faces between the corner bars. The code assumes that the intermediate column bars are subjected to compression approximately equal to 50% of their yield strength, thus offering a tensile stress margin of $A_{sv,i} = 1.5 \cdot A_{sh} \cdot f_{yd}$ to take vertical shear.

5.3.11 Detailing for shear reinforcement

The shear reinforcement within the joint is provided in the form of closed stirrups, cross ties or hoops. The detailing requirements concerned the spacing and the arrangement of the hoops within the joint.

The ACI 318M-02 code imposes the following limit to the vertical spacing of

horizontal stirrups

$$\min\{h_c / 4; 6 \cdot d_b; s_x\} \tag{49}$$

and the following one to the horizontal spacing of vertical reinforcement

$$\min\{350\} \tag{50}$$

where

$$s_x = 100 + \left(\frac{350 - h_x}{3}\right) \text{ with } 100 < s_x < 150 \tag{51}$$

and h_x is the maximum horizontal spacing of hoop or crosstie legs on all column faces.

The ENV 1998-1:2003 code suggests the following values for the same parameters

$$\min\{b_0 / 2; 8 \cdot d_b; 175\} \tag{52}$$

$$\min\{150\} \tag{53}$$

where b_0 is the minimum core dimension of the column.

In principle, the restrictions on the vertical spacing of transverse reinforcement are given with respect to the least member dimension to obtain adequate concrete confinement and in terms of the diameter of the longitudinal column bar to restrain buckling of bar after spalling of concrete. The spacing found by the above two criteria should be less than a prescribed numerical value. The spacing of the horizontal lateral reinforcement is relaxed with respect to the confinement offered by the adjoining members and also based on the distribution of the column longitudinal reinforcements. It can be noticed that the spacing of lateral reinforcement is more or less the same for the two codes of practice.

The preferred shape of a single leg cross-tie should have a 135-degree bend at both ends. Since installation with such a configuration is difficult, ACI 318M-02 allows standard 90-degree hook at one end of the cross tie with an extension not less than 6 times the diameter of the stirrup. But a 90-degree hook does not provide effective anchorage since it is not embedded in the confined column core. Hence, ACI 318M-02 recommends alternate placement of a 90-degree hook on opposite faces along the columns. However, EN 1998-1:2003 prefers 135-degree bend at both ends. This code suggests an extension of 8 and 10 times the stirrup diameter respectively.

5.3.12 Observations

The principles adopted in the design of joints by the two codes attach high importance to the provision for adequate anchorage of longitudinal bars and confinement of core concrete in resisting shear. The important observations from the comparison studies are enumerated below.

- ACI 318M-02 requires smaller column depth, as compared to the other two codes, to satisfy the anchorage conditions for joints. The effect of higher concrete grade in reducing the column depth has been included in EN 1998-1:2003. The EN 1998-1:2003 also accounts for column axial load in deciding the minimum column depth from beam bar anchorage point of view.
- The shear reinforcement required to ensure truss mechanism and to confine the core concrete varies considerably between the two codes. ACI 318M-02 requires transverse reinforcement in proportion to the strength of the concrete whereas EN 1998-1:2003 provides shear reinforcement to confine the joint and to reduce the maximum tensile stress to a design value. Also, the last code gives a bound on the estimate of shear reinforcement to maintain the integrity of joint after diagonal cracking.
- Both the codes accept the intermediate column bars as a part of vertical shear reinforcement.
- The detailing requirements ensure adequate confinement of core concrete and preclude the buckling of longitudinal bar. The horizontal and vertical transverse reinforcements are to be distributed within the joint to resist the diagonal shear cracking and to contain the transverse tensile strain in core concrete. EN code emphasizes on the provision of a 135-degree hook on both ends of the cross-ties. Whereas ACI code accepts a 135-degree hook at one end and a 90-degree one at the other end and insists on the proper placement of stirrups to provide effective confinement.

5.4 Joint test structural design

5.4.1 Test joint static scheme

The test joints refer to a four-story frame, with an interstory height of 3.5 m. The columns constitute a net of 6 m by 4 m and the slab beams present the resisting direction along the higher span. The loads are assumed to be equal to $7\,kN/m^2$ for the total permanent load and to $2\,kN/m^2$ for the total variable load. From this hypothetical frame an internal joint of the first floor is considered between the four contraflexure points of columns and beams. The joint is supposed to be a reference joint to compare the design and the analysis behaviour of different structural type. The test static scheme used to simulate the cyclic behaviour of the joint under seismic actions is shown in Fig. 5.9.

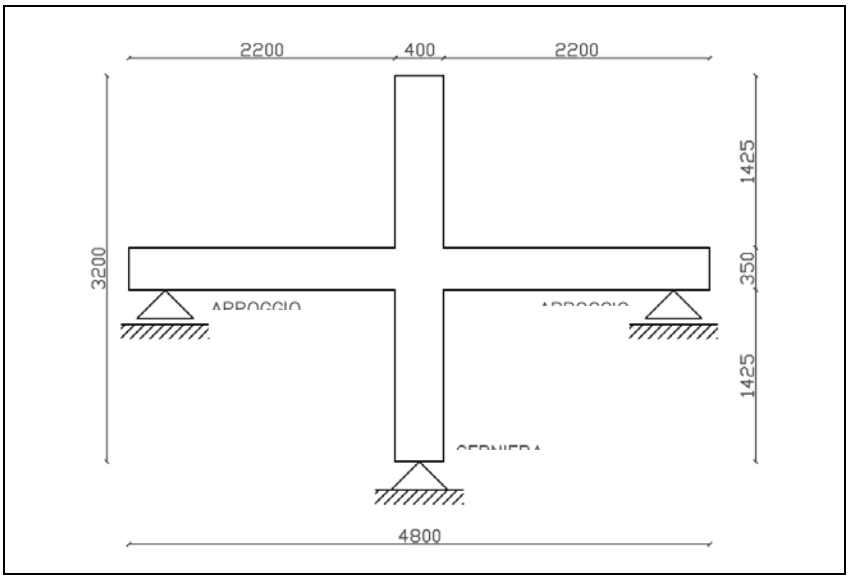

Fig. 5.9: Static scheme of the test joint

The axial load of the column is assumed equal to -700 kN to take in account the vertical loads sustained by the structural member.

5.4.2 Design of the RC joint

The test joint is constituted by a column with square section of 40 cm and by a beam 35 cm depth and 40 cm width. The design materials, typical of RC frames, consist of concrete C25/30 and reinforcing steel B450C according to the Italian [38] and European [39] Codes.

The joint has been designed according to the seismic provisions of both Codes in High Ductility Class for a site of 0.35g peak ground acceleration. For simplicity, and in view of possible experimental verifications, the upper and lower reinforcements of the beam have been thought symmetric, neglecting the effects of the vertical load. This simplification does not affect the validity of the test since the cyclic properties of the joint will be investigated. The Fig. 5.10 and Fig. 5.11 show the results of the design process. In particular the confinement effect on the beam, by the missing slab, have been simulated by the presence of continuous reinforcement crossing the sections of the beam. In an hypothetical experimental test the axial load of the column can be imposed by means of a post tensioned wire stretch between the two end faces of the column itself.

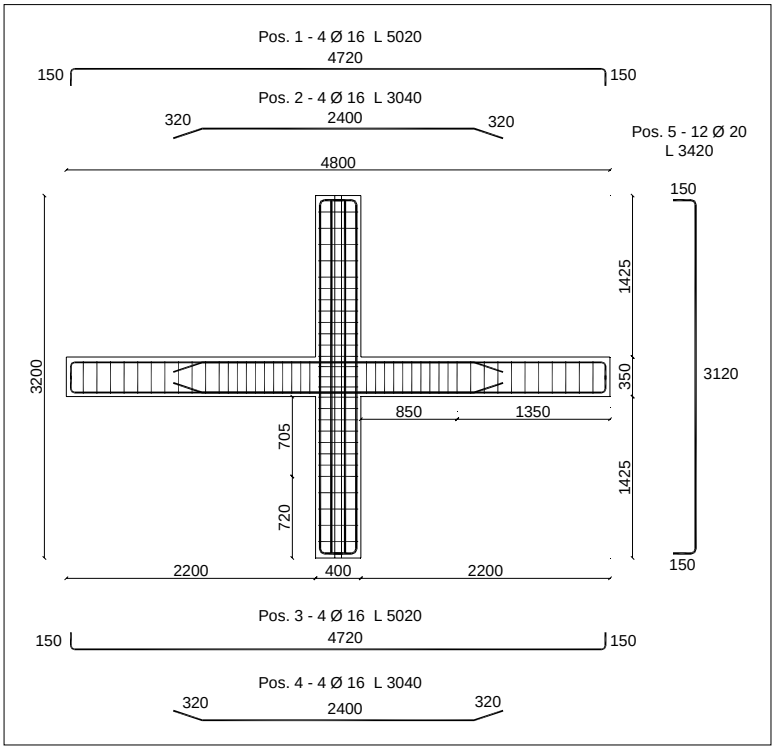

Fig. 5.10: Profile of the designed .reinforced concrete joint

For what concerns the beam, the flexural bending moments are coming out of a linear dynamic analysis with appropriate load combinations. The calcul hypotheses are standard : plain section remain plain, failure of compressive concrete at –3.5‰ of strain and failure of reinforcing steel at +10‰ of strain. The beam shear resisting strength is calculated neglecting the contribution of tensile concrete. In order to avoid shear brittle failure, the soliciting design shear forces have been calculated starting from the resisting bending moment of the previously designed beam sections amplified with a factor γ_{Rd} equal to 1.20 or 1.30 depending on the Code. The maximum concrete shear strength is computed as

$$V_{R1} = 10 \cdot \tau_{Rd} \cdot b_{wd} \cdot d \tag{54}$$

where d is the beam effective depth, b_{wd} is the beam web width and the design resisting shear stress

$$\tau_{Rd} = \sqrt[3]{R_{ck}} / 28 \tag{55}$$

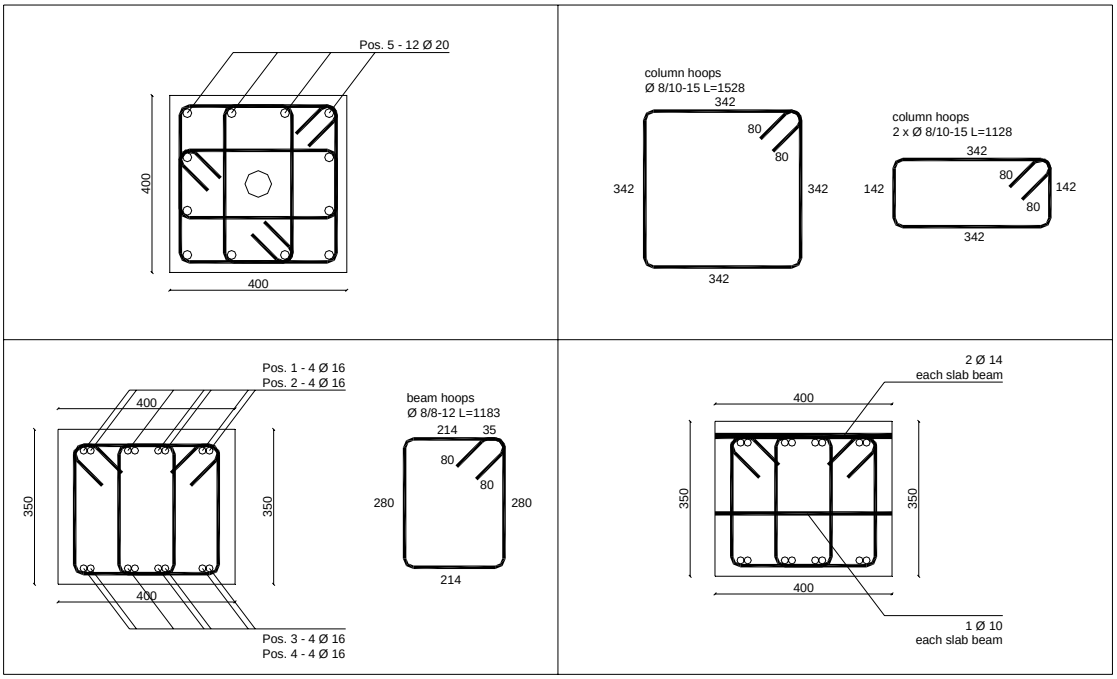

Fig. 5.11: Reinforcement bar detail on the column and beam sections

The column was then verified under flexion-compression and shear solicitations. For the HDC structure the soliciting bending moments are obtained from a linear dynamic analysis amplified for the following factor

$$\alpha = \gamma_{Rd} \cdot \frac{\left|\sum M_{Rb}\right|}{\left|\sum M_{Sc}\right|} \tag{56}$$

where γ_{Rd} has been already defined, $\sum M_{Rb}$ is the sum of the converging beam resisting bending moments of equal sign and $\sum M_{Sc}$ is the sum of the converging column analysis bending moments of equal sign. The computation has been conducted by applying the compressive axial load of $N_{Sd} = -700\text{kN}$. The column shear soliciting forces can be obtained from equilibrium considerations with the resisting bending moments of the upper M_{Rc}^{u} and lower M_{Rc}^{l} end sections

$$V_{Sd} = \gamma_{Rd} \cdot \frac{M_{Rc}^{u} + M_{Rc}^{l}}{l_c} \tag{57}$$

where the only new symbol l_c represents the column interstory length. The section shear resisting strength can be computed as for non seismic cases by checking of the compressive concrete strut and the tensile transverse reinforcement. The minimum size of 30 cm for the column is respected and the longitudinal reinforcement percentage is within the limits, that is

$$1\% \le A_s / A_c \le 4\% \tag{58}$$

The designed joint is expected to sustain the characteristic seismic solicitations by showing a ductile behaviour and by preventing any local or global brittle failure.

5.5 Numerical models

5.5.1 Mesh properties

The numerical analysis were carried out by means of different research and commercial programs as OPENSEES [University of California at Berkeley, California, USA], ATENA [Cervenka Consulting, Czech Republic] and MIDAS FEA [Advanced Nonlinear and Detail Analysis Program, Midas Information Technology Co., Ltd], comparing and validating their results.

Two and three dimensional models have been created. The 2D models use four node MITC elements or nine node isoparametric shell elements in alternative whereas the 3D ones use tetraedric four node elements, while discrete bars model the reinforcement with truss element behaviour.

For the beam and the column 2D models, a coarser mesh turned out to be satisfactory. Full bond between the reinforcement and the concrete was assumed. Thus, the actual bond behaviour can only be represented by the deformations of the elements surrounding the reinforcing bars. Therefore, it was necessary to use a finer mesh within the joint. Because of the expected stress concentrations, the intersections of the beam and column compression zones were also modelled using a finer mesh. In some connections, the beam tensile reinforcement was anchored by anchor plates at their ends. These anchor plates were modelled using shell elements having the material properties of the steel.

5.5.2 Material properties

For the reinforcing bars, an elastic-plastic stress-strain relationship was used, with a combination of isotropic and kinematic hardening. The yield stress was obtained from the experimental data or some typical medium values of the material were assumed.

For the concrete material, different models were adopted in each of the three programs used. The two parameter plastic damage model of Faria and Oliver [41] were implemented in the Opensees program, the fracture-plastic model Cervenka [42] was used in the Atena program whereas the smeared fixed crack model (SFCM) [43] was used in the Midas FEA program. The first one is based on the definition of effective stress correlated to the Cauchy stress by means of distinct positive and negative damage parameters. The second one combines models for tensile fracturing and compressive plastic behaviour using the

constitutiove concrete law defined by van Mier [44]. In the third one the compressive and the tensile concrete constitutive laws have been assumed according respectively to the Thorenfeldt [44] and Hordijk [46] models. All the material models have demonstrated to be able to effectively reproduce the reinforced concrete behaviour. Each concrete model assumed distinct constitutive law both for the tensile and for the compressive behaviour. But after the calibration with the test data, they assume slightly different envelope curves.

5.5.3 Solution algorithm

The total column normal force was applied in the first step of the analysis and then kept constant during the following steps. In this step, the Newton-Raphson method is applied to solve the nonlinear equation system. In the steps to follow, the beam loading was gradually increased. The arch length method combined with the line search method was used to solve the nonlinear equation system. The arc length method makes it possible to reflect the descending branch in the post-peak behaviour of the connection. By applying the line search method, the number of lead steps, required to minimize the work done by the unbalanced forces, was determined.

5.5.4 Verification of finite element model

To verify the finite element model, the analytical results are compared with the some experimental results. Six interior beam column joints, tested by Hegger et al. [23], were modelled. The static scheme was the same as the one defined as the test scheme. The column has a total height of 1.66 m, its section has a width of 150 mm and its depth varies from 240 to 300 mm. Each beam span is 0.85 m and the section of the beam has the same width of the column and 300 mm of depth.

The test parameters are summarized in the following Table 1. In general, the theoretical and experimental load-deflection curves are in good agreement as shown in Fig. 5.12. The failure mechanism obtained from the FE analysis, using the program ATENA [42], agreed well with the one observed in the experiments. The concrete damage started always in the beam compression zone and moved with increasing deformations along the concrete compressive strut inside the joint.

Table 1 experimental test parameters (Hegger et al. [23])

ID	h_b/h_c	f'c	beam reinforcement	column reinforcement	F [kN]
RA1	1.25	53.1	4 N14 + N20 diagonal	2x4 N20	82.7
RA2	1.25	66.1	4 N14	2 x4 N20	95.8
RA3	1.25	43.6	4 N14 + 1 N12	2 x4 N20	77.9
RA4	1.50	66.1	2 N20 + 2 N16	2x2 N20 + 2 x3 N16	114.4
RA5	1.50	56.2	4 N14 + 1 N12	2 x4 N20	80.8
RA6	1.00	56.2	4 N14	2 x4 N20	109.2
RA7	1.25	79.7	4 N16 + 1 N12	2 x4 N20	123.0

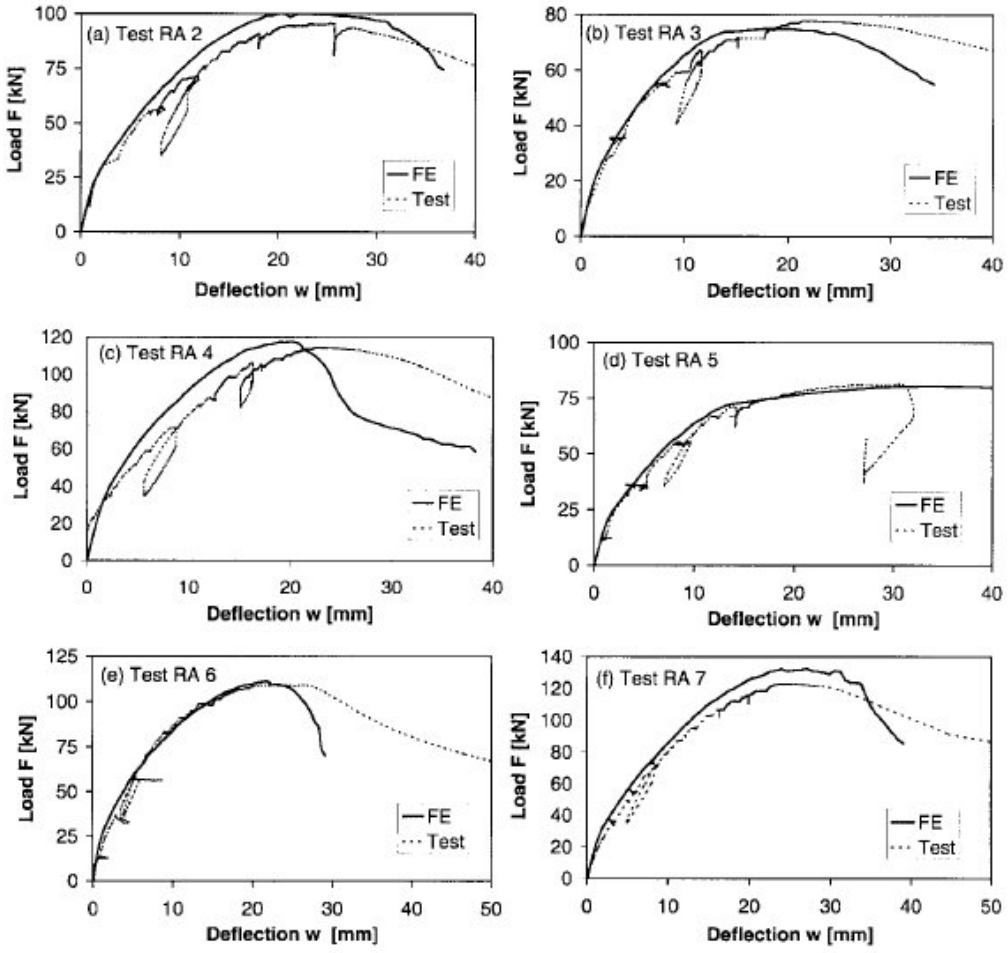

Fig. 5.12: Load-deflection curves of finite element and test results for interior beam column connections (Hegger et al. [23])

5.6 Numerical analysis

5.6.1 Two-dimension analyses

The 2D models, though being simplifications of the real structures, give effective results for stiffness and strength but not for peculiar effects, such as confinement, that are predictable only with 3D models. Since a strong computational effort is required to simulated all the tested structures, and since the nonlinear behaviour is expected only in the joint and in the regions close to it, the beam and column end parts are modelled by linear beam elements and they are connected in adequate sections to the bi-dimensional model, and then in the next chapter to the three-dimensional model, by means of opportune rigid links.

The reinforcing bars are modelled by using truss elements and their joints coincide with those of the shell element concrete material mesh (see Fig. 5.13 and Fig. 5.14).

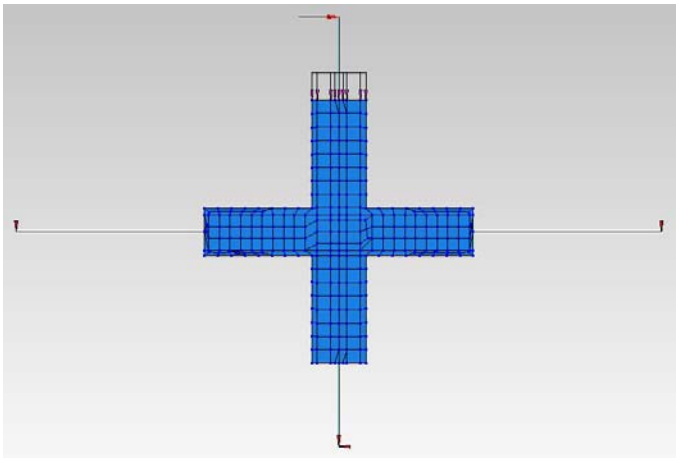

Fig. 5.13: Mesh for the concrete element model

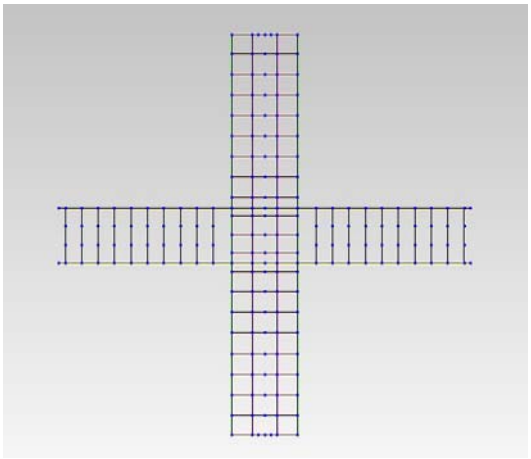

Fig. 5.14: Mesh for the reinforcing bar element model

In Fig. 5.14 the longitudinal and transversal reinforcing bars of the column pass through the joint according to the common detailing for seismic reinforced concrete frame. The aim is to confine the joint concrete core to avoid any brittle failure in the column, considering also its axial compression load.

The first loading phase is the application of the column axial load as a constant load applied to both the column end faces. The second loading phase corresponds to the application of the top imposed cyclic displacements. For all the analyses carried out, the applied displacement history is shown in Fig. 5.15.

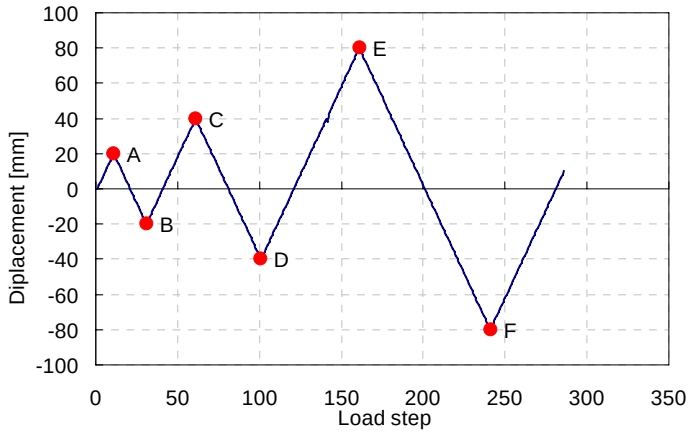

Fig. 5.15: Imposed displacement cycle history

The maximum top displacement obtained from the analysis is about 80 mm, which is about 2.9% of the column length. The top displacement in correspondence to the first bar yielding is about 15 mm (see Fig. 5.16).

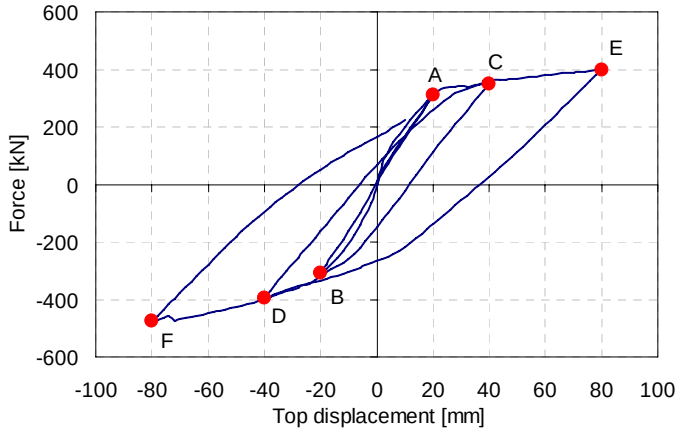

Fig. 5.16: Force-displacement diagram for the tested reinforced concrete joint

The diagram of the longitudinal reinforcing bar stresses is shown in Fig. 5.17. The location of the beam plastic hinges just outside the joint region can be identified. In one of those region a steel bar reaches the maximum imposed plastic strain of 0.04 mm/mm

corresponding to a tensile stress equal to about 540 MPa. All the longitudinal column bar in the joint region are submitted to a small stretching due to the two joint shear resisting mechanisms. In the ultimate conditions, all the reinforcing bars of the column remain in elastic condition, meaning that the column is slightly affected by the dissipative phenomenon as the capacity design prescribes.

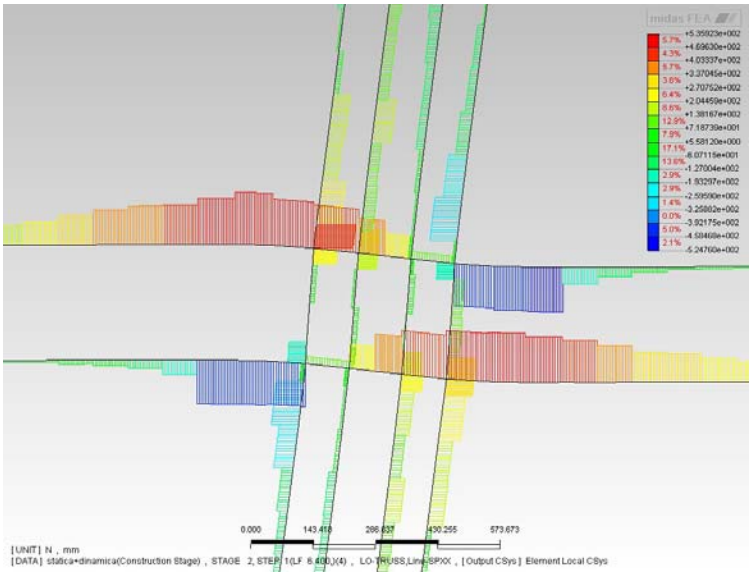

Fig. 5.17: Diagrams of the longitudinal reinforcing bar stresses in ultimate conditions

The image of the joint transverse reinforcement stresses (see Fig. 5.18) shows the high tensile stresses along every hoop in the joint region. These high stresses confirm the dilatation of the concrete core of the joint. They are the effect of the horizontal solicitations from the truss resisting mechanism of the joint.

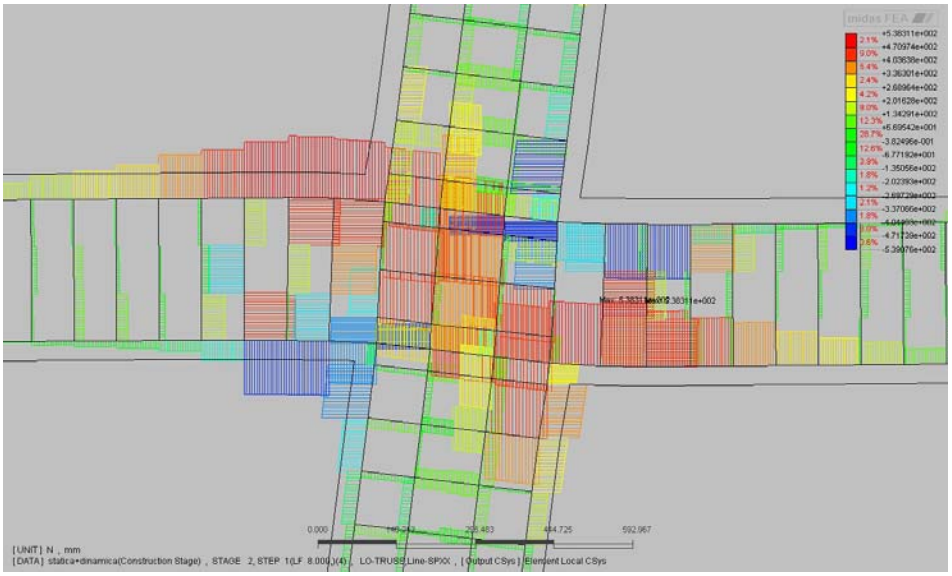

Fig. 5.18: Diagrams of the reinforcing bar stresses at the joint near in ultimate conditions

In Fig. 5.19, the contour map of the concrete negative principal stresses is depicted. The diagonal concrete strut is marked by the green colour that defines the region with stresses higher than approximately 20 MPa.

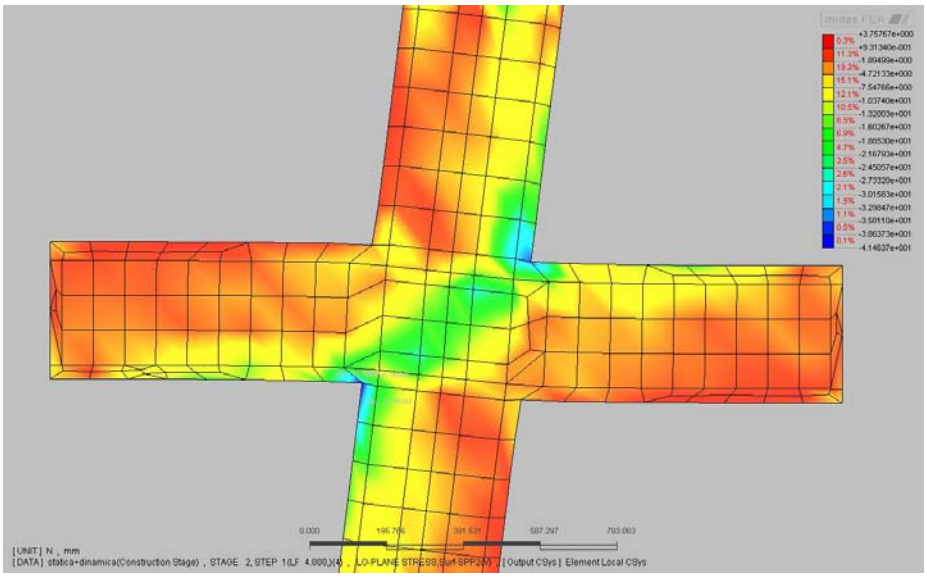

Fig. 5.19: Concrete minimum principal stresses

5.6.2 Three-dimension analyses

The aim of 3D model is to assess the reliability of the numerically lighter 2D model and to verify the influence of other parameters such as the concrete confinement effect and the accurate modelling of the reinforcement geometry. The mesh has been created by the Midas FEA automatic function after the three dimensional CAD had been imported. Even in this case, the reinforcing bars were simulated by truss elements linked to the concrete tetraedric elements in correspondence to each of their joints. The Fig. 5.20 shows the reinforcement net simulated by truss elements. This net is connected at each of its joints with the concrete model shown in Fig. 5.21.

The same displacement history presented for the 2D analysis is applied to this new model. The Fig. 5.22 shows the reinforcement bar stresses after the first cycle for a top displacement of 20 mm. The longitudinal beam bars have already yielded. The lower absolute value of the compressive stresses in the beam longitudinal bar is coherent with the theoretical development. Even the moderately high stresses on the joint column hoops demonstrate their necessary functions both in giving the equilibrium to the diagonal concrete struts and in confining the joint concrete core. A zoom of the transverse column reinforcement is presented in the Fig. 5.23. The subsequent Fig. 5.24 shows the reinforcement yielding areas for 40 mm of top displacement.

Two plastic hinges are located in correspondence to the two beam ends adjacent to the

joint. The yielding regions in correspondence to 78 mm of top displacement, which is the ultimate condition, are depicted in Fig. 5.25. The tensile yielding phenomena concerns a deeper region of the beam ends and the corresponding yield strain is close to the limit of 0.04 mm/mm. Some compressed beam bars are also yielded in small regions. In this ultimate state, even some of the transverse joint reinforcement are close to yielding, due to progressive crack openings that produce the dilatation of the joint core. This fact demonstrates the importance of the transverse reinforcement in confining the joint concrete core.

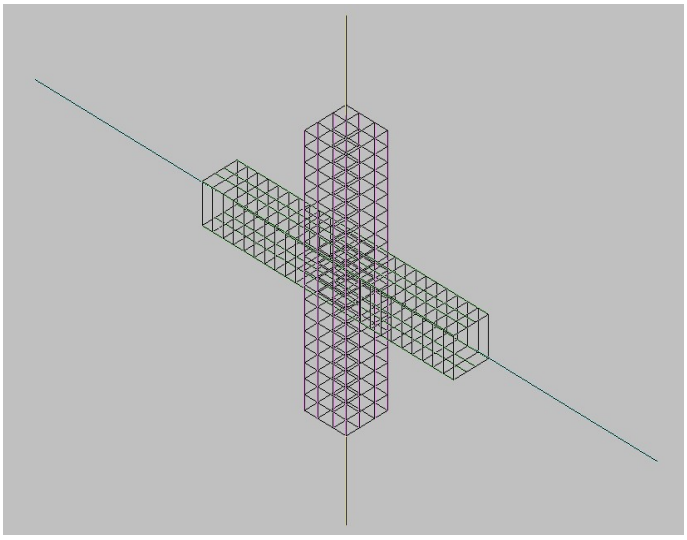

Fig. 5.20: Steel reinforcement net modelling

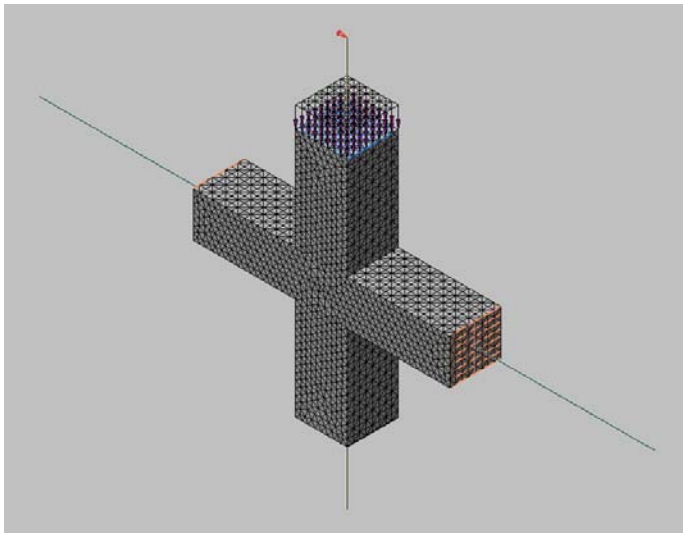

Fig. 5.21: Complete three dimensional joint model

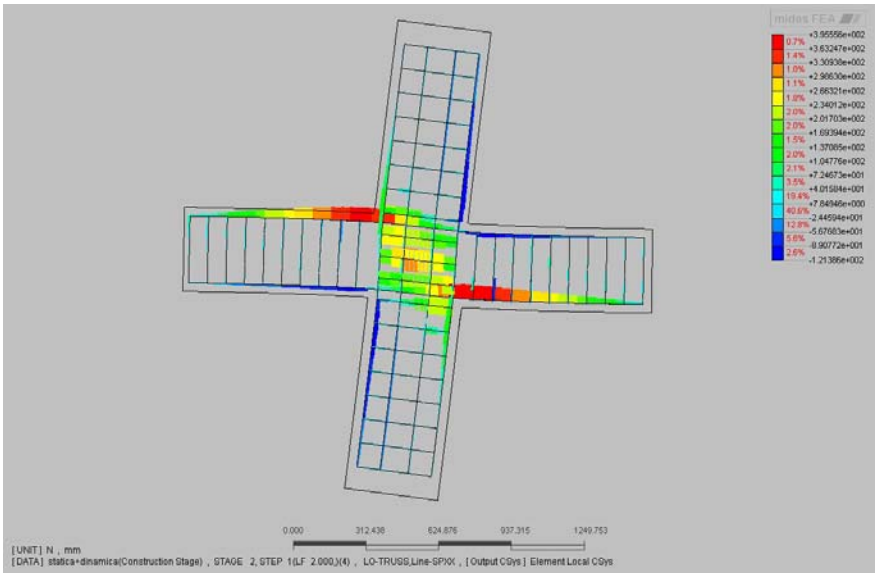

Fig. 5.22: Diagrams of the reinforcing bar stresses at 20 mm of top displacement

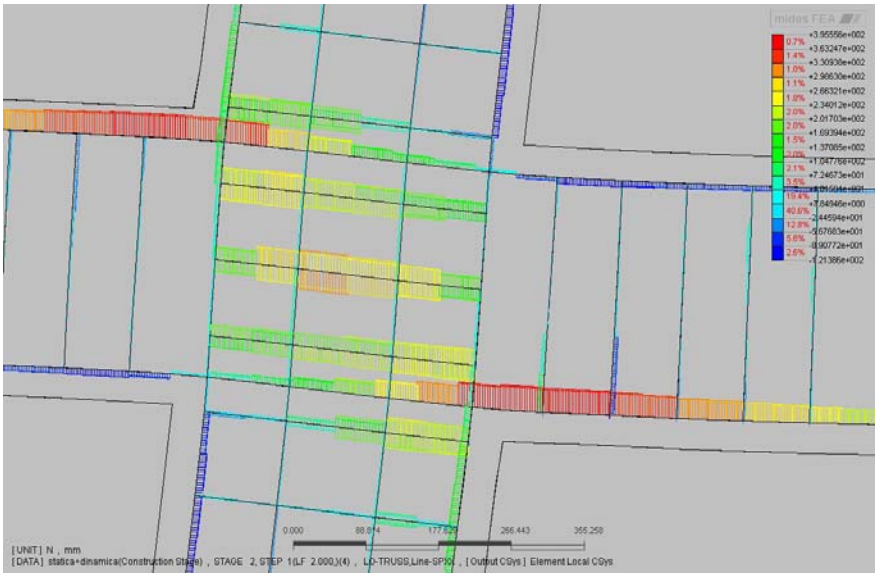

Fig. 5.23: Zoom of the previous figure in the joint region

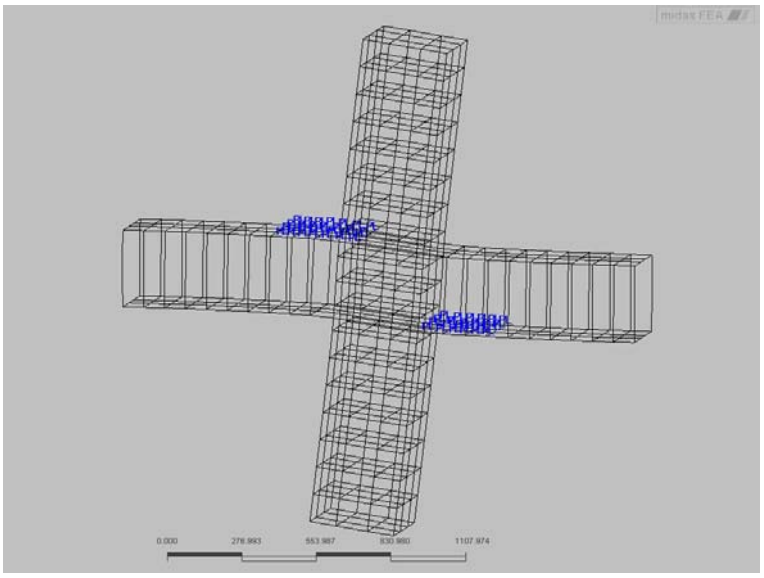

Fig. 5.24: Reinforcing bar yielding location at 40 mm of top displacement

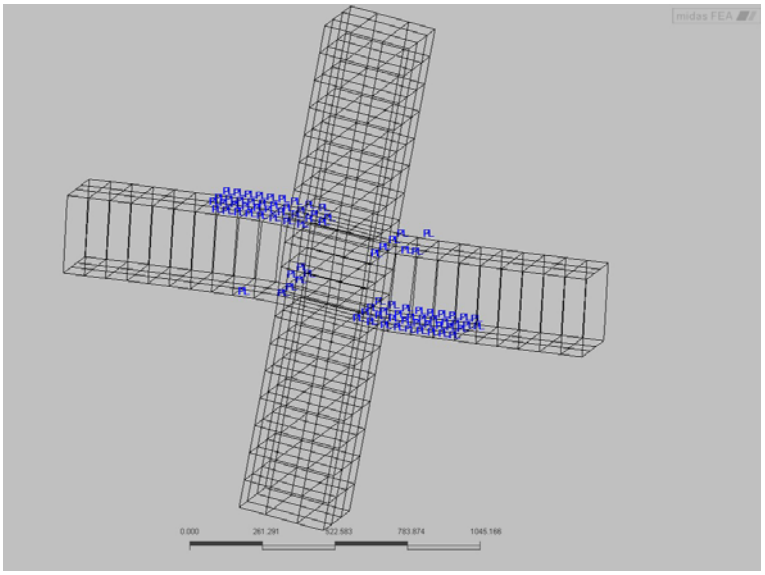

Fig. 5.25: Reinforcing bar yielding location at 78 mm of top displacement

From the picture representing the concrete principal compressive stresses (see Fig. 5.26), the diagonal strut is clearly visible. This represents the concrete contribution in the first mechanism in sustaining the joint shear forces.

The applied force vs. displacement diagram is reported in Fig. 5.27. During the first cycle, the node reach the first yielding. In the following cycles, the formation of the plastic hinges leads to a progressive reduction in the stiffness of the structure. In correspondence to the maximum imposed displacement of 80 mm, the structure shows a strength equal to about 390 kN. The finite element program cannot find convergent solutions applying higher displacement because of the widespread structural damage. The difference between the 2D and 3D analyses are the effects of the simplifications adopted in the first model. In fact the

2D mesh has to project in a plane all the members loosing their original dispositions. Furthermore the condition of stress plane state, in the 2D analyses, cannot capture the confinement effect produced bu the reinforcement net. From the numerical point of view, the softening behaviour of the concrete material decreases the convergence speed. For instance, it can be less than linear in three dimensional cyclic analyses.

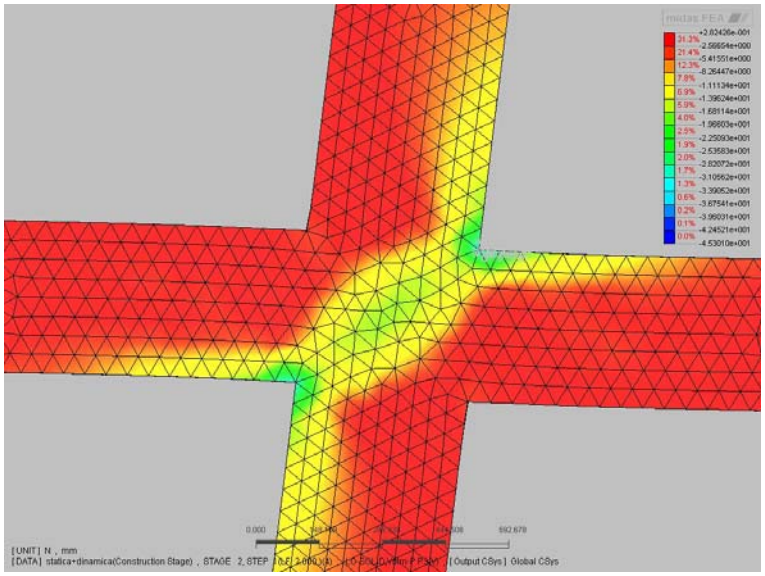

Fig. 5.26: Zoom of the previous figure in the joint region

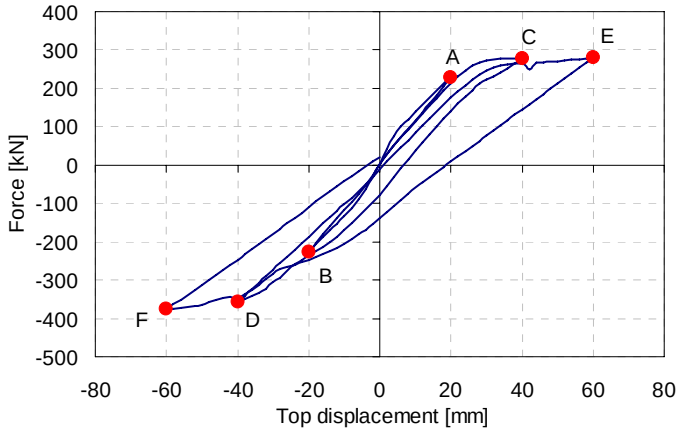

Fig. 5.27: Force-displacement diagram for the tested reinforced concrete joint

By means of the integration of the applied load vs. displacement curve it is possible to estimate the external work produced on the structure. It should be underscored that the resulting work can supply only a coarse valuation of the actual spent work, since the concrete model doesn't take into account the plastic strain. Nevertheless the resulting esteem can be useful in sight of a comparison between other analyses carried out by the same model. The Fig. 5.28 shows the the external work spent by the applied force at the top of the column. The minimum point of each parabola is reached when a load semicycle is completed and it

represents the cumulative energy dissipated by all the nonlinear phenomena in the concrete and in the reinforcing steel materials. During the first two cycles the structure remain almost in the elastic field and the external work is stored as elastic energy. During the last cycle the structure is able to dissipate an high percentage of the maximum spent work by means of inelastic deformations and structural damage.

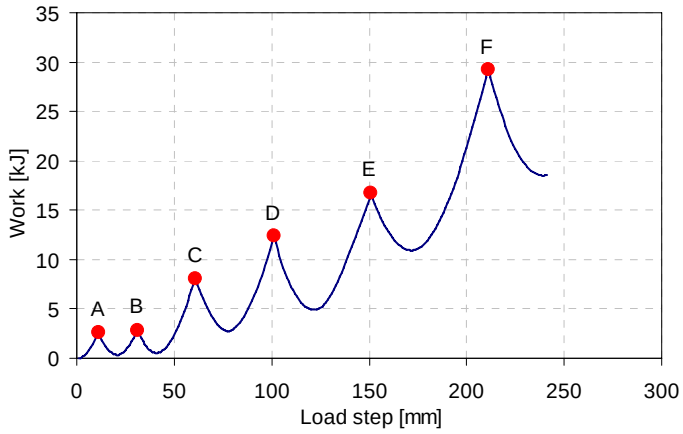

Fig. 5.28: External work during the applied displacement history

5.7 Conclusions

The reinforced concrete joint mechanics have been exposed, recalling the main theory and their recent development. Two resistant mechanisms has been evaluated, the concrete strut mechanism and the diagonal compressed field or truss mechanism. Their contribution to the total joint shear strength has been investigated. The recalled theory can explain all the Code prescriptions and can be applied to generalized joint problem.

The Eurocode, similar to the Italian code, and ACI 318M code provisions have been compared and the main points have been underlined. A test structural joint element has been defined and designed according to the Italian and European actual Code for seismic zone of 0.35g peak ground accelerations.

By means of an improved academic program and another two commercial ones the accurate numerical analysis of the frame joint has been faced. Some preliminaries validation examples have been carried out comparing the numerical results with the experimental ones. Using two dimensional and three dimensional models, it has been possible to evaluate with efficiency and accuracy the behaviour of the designed reinforced concrete test joint. The numerical analyses have shown all the features and the issues underlined by the theory. The numerical results have been compared qualitatively and quantitatively with the ones obtained by theoretical simplified schemes showing a good agreement.

References

1. Park R, Paulay T. *Reinforced concrete structures*, J. Wiley & Sons, New York, 1975.
2. Paulay T, Priestley MJN. *Seismic design of reinforcement concrete and masonry buildings*. J. Wiley & Sons, New York, 1992.
3. Paulay T. Lapped splices in earthquake-resisting columns. *ACI Journal* 1982, **79**: 458-469.
4. Filippou FC, Popov EP, Bertero VV. Modeling of R/C joints under cyclic excitations. *ASCE Journal of Structural Engineering* 1983, **109**: 2666-2684.
5. ACI-ASCE Committee 352. Recommendations for design of beam-column joints in monolithic reinforced concrete structures. *ACI Journal* 1985, **82**: 266-283.
6. Abrams DP. Scale relations for reinforced concrete beam-column joints. *ACI Structural Journal* 1987, **84**: 502-512.
7. Fattah BA, Wight JK. Study of moving beam plastic hinging zones for earthquake resistant design of reinforced concrete buildings. *ACI Structural Journal* **84**: 1987, 31-39.
8. Durrani AJ, Wight JK. Earthquake resistance of reinforced concrete interior connections including a floor slab. *ACI Structural Journal* 1987, **84**: 400-406.
9. Soroushian P, Obaseki K, Nagi M, Rojas MC. Pullout behavior of hooked bars in exterior beam-column connections. *ACI Structural Journal* 1988, **85**: 269-276.
10. El Metwally SE, Chen WF. Moment-rotation modelling of reinforced concrete beam-column connections. *ACI Structural Journal* 1988, **85**: 384-394.
11. Chung L, Shah SP. Effect of loading rate on anchorage bond and beam-column joints. *ACI Structural Journal* 1989, **86**: 132-142.
12. Paulay T. Equilibrium Criteria for reinforced concrete beam column joints. *ACI Structural Journal* 1989, **86**: 635-643.
13. Leon RT. Shear strength and hysteretic behavior of interior beam-column joints. *ACI Structural Journal* 1990, **87**: 3-11.
14. Seckin M. Fu HC. Beam-column connections in precast reinforced concrete construction. *ACI Structural Journal* 1990, **87**: 252-261.
15. Zerbe HE. Durrani AJ. Seismic response of connections in two-bay reinforced concrete frame subassemblies with a floor slab. *ACI Structural Journal* 1990, **87**: 406-415.
16. Wong PK, Priestley MJN, Park R. Seismic resistance of frames with vertically distributed longitudinal reinforcement in beams. *ACI Structural Journal* 1990, **87**: 488-498.

17. Stevens NJ, Uzumeri SM, Collins MP. Reinforced concrete subjected to reversed cyclic shear-experiments and constitutive model. *ACI Structural Journal* 1991, **88**: 135-146.

18. Soroushian P, Choi KB, Analytical evaluation of straight bar anchorage design in exterior joints. *ACI Structural Journal* 1991, **88**: 161-168.

19. Tsonos AG, Tegos IA, Penelis GG. Seismic resistance of type 2 exterior beam-column joints reinforced with inclined bars. *ACI Structural Journal* 1992, **89**: 3-12.

20. Pantazopoulou S, Bonacci J. Consideration of questions about beam-column joints. *ACI Structural Journal* 1992, **89**: 27-36.

21. Popov EP, Cohen JM, Thomas KK, Kazuhiko K. Behavior of interior narrow and wide beams. *ACI Structural Journal* 1992, **89**: 607-616.

22. Filippou FC, Pantazopoulou V, Bonacci J. State of the art report on beam-column joints. *CEB Bulletin d'Information* 1993, **222** (3).

23. Hegger J, Sherif A, Roeser W. Nonlinear finite element analysis of reinforced concrete beam-column connections. *ACI Structural Journal* 2004, **101**: 604-614.

24. Hwang SJ, Lee HJ, Liao TF, Wang KC, Tsai HH. Role of hoops on shear strength of reinforced concrete beam-column joints. *ACI Structural Journal* 2005, **102**: 445-453.

25. Brooke NJ, Megget LM, Ingham JM. Bond performance of interior beam-column joints with high-strength reinforcement. *ACI Structural Journal* 2006, **103**: 596-603.

26. Guimaraes GN, Kreger ME, Jirsa JO. Evaluation of joint-shear provisions for interior beam-column-slab connections using high-strength materials. *ACI Structural Journal* 1992, **89**: 89-98.

27. Bonacci J, Pantazopoulou S. Parametric investigation of joint mechanics. *ACI Structural Journal* 1993, **90**: 61-71.

28. Hwang SJ, Lee HJ. Analytical model for predicting shear strengths of exterior reinforced concrete beam-column joints for seismic resistance. *ACI Structural Journal* 1999, **96**: 846-858.

29. Hakuto S, Park R, Tanaka H. Effect of deterioration of bond of beam bars passing through interior beam-column joints on flexural strength and ductility. *ACI Structural Journal* 1999, **96**: 859-864.

30. Paul S. Baglin and Richard H. Scott. Finite element modeling of reinforced concrete beam-column connections. *ACI Structural Journal* 2000, **97**: 886-894.

31. Hwang SJ, Lee HJ. Analytical model for predicting shear strengths of interior reinforced concrete beam-column joints for seismic resistance. *ACI Structural Journal* 2000, **97**: 35-44.

32. Quintero-Febres CG, Wight JK. Experimental study of reinforced concrete interior wide beam-column connections subjected to lateral loading. *ACI Structural Journal* 2001, **98**: 572-582.

33. Anderson M, Lehman D, Stanton J. A cyclic shear stress-strain model for joints without transverse reinforcement. *Elsevier Engineering Structures* 2008, **30**: 941-954.

34. Murty CVR, Rai DC, Bajpai KK, Jain SK. Effectiveness of reinforcement details in exterior reinforced concrete beam-column joints for earthquake resistance. *ACI Structural Journal* 2003, **100**: 149-156.

35. Khaloo AR, Parastesh H. Cyclic loading of ductile precast concrete beam-column connection. *ACI Structural Journal* 2003, **100**: 291-296.

36. Mitra N, Lowes LN. Evaluation, calibration, and verification of a reinforced concrete beam-column joint model. *ASCE Journal of Structural Engineering* 2007, **133**: 105-120.

37. Hwang SJ, Lee HJ, Liao TF, Wang KC, Tsai HH. Role of hoops on shear strength of reinforced concrete beam-column joints. *ACI Structural Journal* 2005, **102**: 445-453.

38. D M LL PP 14 Jan 2008. Norme Tecniche per le Costruzioni (Construction Technical Codes). *Gazzetta Ufficiale* 04 Feb 2008.

39. CEN. *Eurocode 8: Design of structures for earthquake resistance Part 1: General rules, seismic actions and rules for buildings*. Comité Européen de Normalisation: Bruxelles, 2003.

40. ACI 318M-02. *Metric Building Code Requirements for Structural Concrete Commentary*. ACI Committee 318 American Concrete Institute, 2002.

41. Faria R, Oliver J, Cervera M. A strain-based plastic viscous-damage model for massive concrete structures. *Elsevier International Journal of Solids and Structures* 1998, **35**: 1533-1558.

42. Cervenka Consulting, ATENA. *Program Documentation - Part 1: Theory*. Cervenka Consulting, Czech Republic, 2000.

43. MIDAS FEA, Advances Nonlinear and Detail analysis program. *Analysis reference*, 2008.

44. Van Mier JGM. *Strain-softening of concrete under multiaxial loading conditions*. PhD thesis, Eindhoven University of Technology, The Netherlands, 1984, 244 pp.

45. Thorenfeldt E., Tomaszewicz A., and Jenen JJ. Mechanical properties of high strength concrete and application in design. Proceeding Symposium, *Utilization of High Strength Concrete*, Tavanger, Norway, 1987.

46. Hordijk DA. *Local approach to fatigue of concrete*. PhD Thesis, University of Delft, 1991.

Chapter 6

Composite Steel Truss and Concrete beam-column joints

6.1 Introduction

The composite steel truss and concrete beam was born as an isostatic beam since the prefabrication of the steel truss and its easiest position in place didn't match with hyperstatic schemes. In fact the original steel truss doesn't cross the joint region, because of the superposition with both the column reinforcement and the symmetric truss coming from the adjacent beam. The prefabrication of multiple bay steel truss is not feasible since the transportation issue limits the longitudinal dimensions and the superposition problem still remains.

Dealing with the use of typical reinforced concrete column, three solution categories have tried to recover the continuity of the beams. The simplest one concerns the introduction of steel reinforcement bars crossing the joint ion correspondence of the top and the bottom of the beam section, they should be long enough to have their anchorage lengths within the beam regions. Another modification is the production of steel trusses longer than a single bay but non symmetrically disposed in such a way that they can cross the joint without encountering each other [1]. The third solution is the adoption of an integrative steel truss, of different shape respect to the beam ones, that can be placed across the joint [2].

The first category has the problems of the transmission of the stresses between the steel trusses and the integrative bars and of the confinement of both the bars and the concrete. Because of that, the efficiency of these additional rebars is low. Further problems can arise if

the steel truss has a reinforced concrete base instead of the steel plate. In this case the bottom rebars can be put only over this base reducing their effective depth. Moreover the bottom concrete base cannot be efficient in transmitting compressive stresses to the joint since it is made by a prefabricated cast and the column concrete shrinkage can make it separated.

A realization of the second solution category were tested by Di Marco [3] and showed a brittle failure. The cause was the cracking of the upper concrete beam region and its expulsion by the extended steel trusses that acted as knifes. In fact the lack of any transversal retention to make them collaborating with the original beams trusses was verified.

The third idea is the more promising one, even if there isn't any application that can solve satisfactorily both the superposition with the column reinforcement and the confinement of the joint region. Besides the integrative trusses should permit to extend the benefits of a fast in place assembly.

For the application in a seismic resistant frame new joint proposals are designed and evaluated in terms of strength underscoring the main characteristics that have more influence on the ductility [4], [5]. The design of the CSTC beam-column joints have been based on the calculation and assessment methods proposed in the third chapter, with the support of the experimental beam tests presented in the fourth chapter. The resistant mechanisms and their contributions to the global behaviour have been underscored.

Two-dimensional and three-dimensional numerical analyses have been performed to test a designed joint. The results have permitted the verification of the theoretical assumption and the assessment of the joint in terms of stiffness, strength, ductility and energy dissipation capacity. It has been presented a critical resume of the simplifications adopted during the numerical analysis that can influence the final result.

6.2 CSTC beam-column joint theory and design

6.2.1 General criteria

The CSTC beams were invented to be applied in simple supported static schemes. In fact those conditions can be easily realized with partially prefabricated beams. On the other hand the application of the CSTC beams to hyperstatic schemes can be convenient both for gravity and seismic loads. Different solutions were proposed to overcome the issue that can be subdivided in three main groups.

The introduction of pieces of reinforcing bars across the joints restores the beam continuity changing the structural type within the joint region (see Fig. 6.1). In fact the joint becomes kind of reinforced concrete structure while the beams remain kind of composite

structure. The drawback of this proposal is to introduce structural members that increase the bending moment strength of the beams across the joint but they don't assure the confinement of the compressed materials.

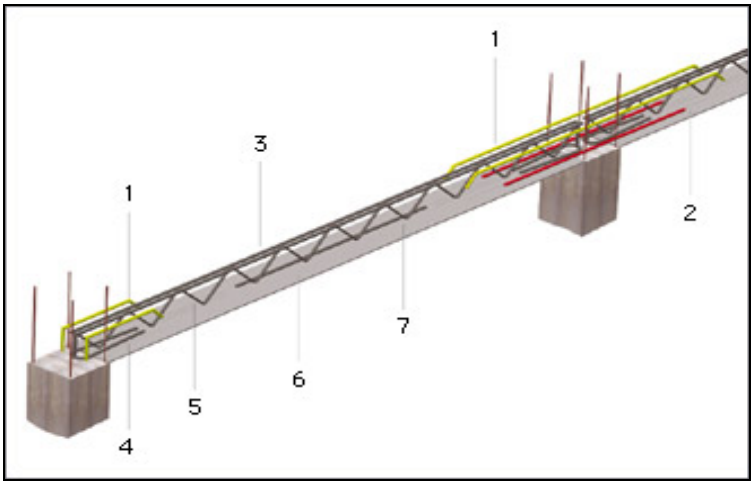

Fig. 6.1: Solution by means of reinforcing bar pieces: (1) reinforcing bar pieces; (2) e (6) steel plate as truss bottom chord; (3) steel bars as truss top chord; (4) additional bars nears the support; (5) diagonal curved bars as vertical truss web; (7) additional bars across the middle span

Extending the beam trusses across the joint needs non symmetric trusses or adjacent trusses with shifted longitudinal axes (see Fig. 6.2). In this case the joint type is the same as the beam one and the continuation of the trusses within the joint increases both the bending moment and the shear strength. The problem of the confinement of the compressed concrete still arises. Moreover the transmission of the stresses between the extensions of the beam trusses can be critical. In fact the two extensions act as two knifes next to each other, having high stiffness in their plane and no transversal connection a part from the surrounding concrete (Di Marco [3]).

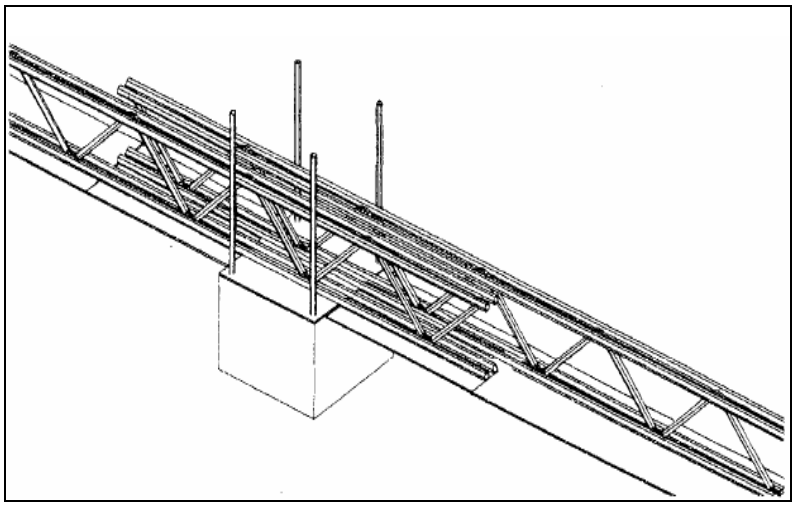

Fig. 6.2: Solution by means of truss extensions

The third solution is the overlapping of an additional truss across the joint (see Fig. 6.3). It consists in a new prefabricated steel truss that can be placed over the common beam trusses across the joint. Its shape must take into account the beam truss presence and the longitudinal column bar obstacle. The most important benefit is that the integrative truss, if accurately designed, can also create confinement to the concrete core and it can provide give the joint with transversal connection. This solution perhaps cannot avoid completely the problem of the fragile failure of concrete transferring the force between the beam and the integrative trusses.

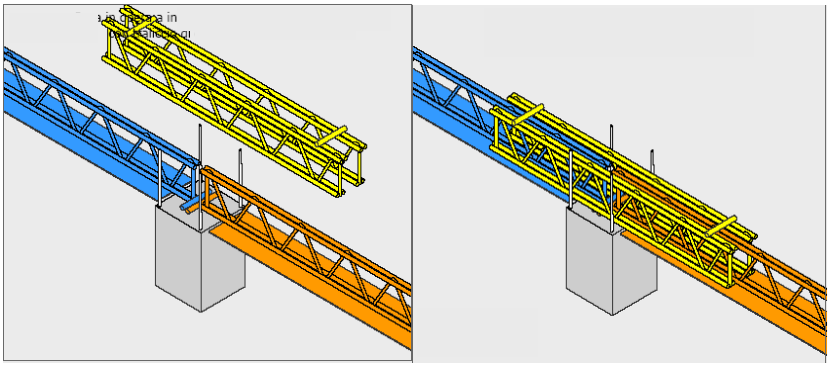

Fig. 6.3: Solution by means of joint additional trusses

Some improvements of the most promising third proposal has been proposed. The main purpose of the design of an efficient CSTC beam-column joint is to extend the high performance criteria of the reinforced concrete joint. If it is possible to find correlations between the RC and the CSTC joint mechanics, then it's also possible to go back over the reinforced concrete provisions and to try to confer the same characteristics on the CSTC joint dealing with distinct geometry and mechanic.

6.2.2 Joint resistant mechanisms

The considerations on the shear force distribution within a RC joint is recalled here with the applications to a different geometry. Starting from equilibrium criteria, the admissible stress distributions have been individuated neglecting the concrete tensile strength. These schemes ensure the equilibrium even if the consistency is not respected.

The design solution has been found as an improvement of the third category of CSTC joint, that is using an integrative steel truss across the joint. The truss should be prefabricated as the common beam truss and should be placed easily. Its shape should be adequate not to interfere with the usual beam truss and the column reinforcement. Because of that its geometry depends on the particular composite steel truss used to construct the beams. The integrative joint truss can lean on the beam composite trusses but it doesn't have any physical connection with them before the second phase concrete cast. It means that the

integrative truss cannot sustain any load and cannot play any structural role before the cast in place concrete becomes hard. Its function is then completely developed in the second phase collaborating with the concrete. The concrete constitutes also the link and the bond between the beam composite trusses and the joint integrative one. To be used together with usual reinforced concrete columns, the additional truss should not constitute an interruption of the column continuity. In fact the column longitudinal bars should overpass the joint and the column concrete should not have any break due to the presence of the steel truss. Because of these reasons the composite integrative truss cannot be stiff and strong enough to sustain by itself a large part of the joint shear solicitations. It means that the shear solicitations, that are usually supported by the steel in a common composite steel and concrete structure, should be assimilated both by the concrete and the truss acting together. Thus, as already seen with the CSTC beam, the proposed CSTC joint has a joint shear mechanic similar to the typical reinforced concrete one.

The first RC joint resistant mechanism called concrete strut remains the main one even in the CSTC joint since it continues to represent the stiffer mechanism. Though the second joint mechanism is still the diagonal compression field, the realization of the stress distribution deals with the deeply different geometry of the steel truss. Hence the first step has to be the recognition of the possible composite resistant configurations.

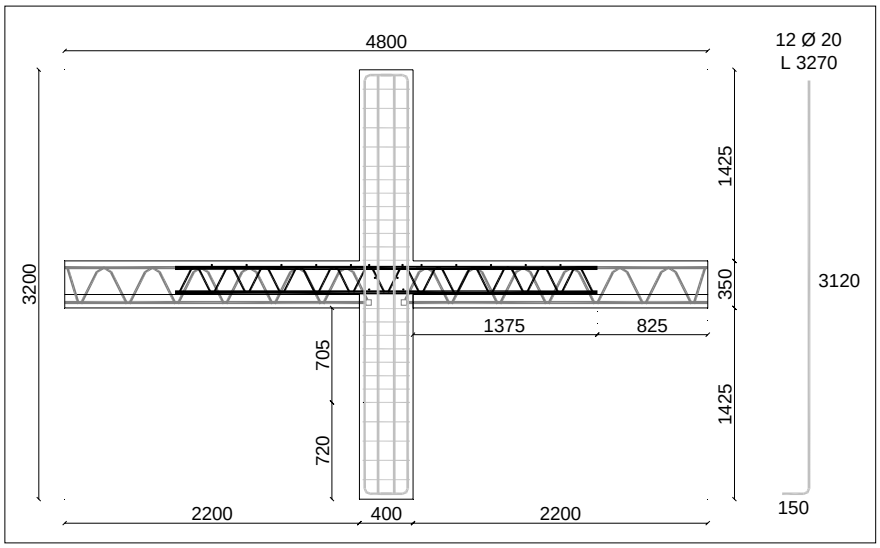

Fig. 6.4: Proposed CSTC beam-column joint profile

The Fig. 6.4 shows a proposed joint geometry when the beam are constituted by CSTC members with the concrete base. The design process will be after in detail. The following Fig. 6.5 and Fig. 6.6 depicts possible resistant schemes against the horizontal and the vertical joint shear forces respectively (the concrete strut are underscored by a bold zigzag line). It can be noted that the presence of the beam concrete bases reduces the beam effective depth

both in the joint region and in the adjacent ones. That constitutes one of the most evident, but inner, limit in the application of this typology to the hyperstatic frame joints. Another characteristic that distinguish the CSTC joint strength respect to the RC one is the absence of the column transverse reinforcement within the joint, in fact their presence is blocked by the joint integrative truss.

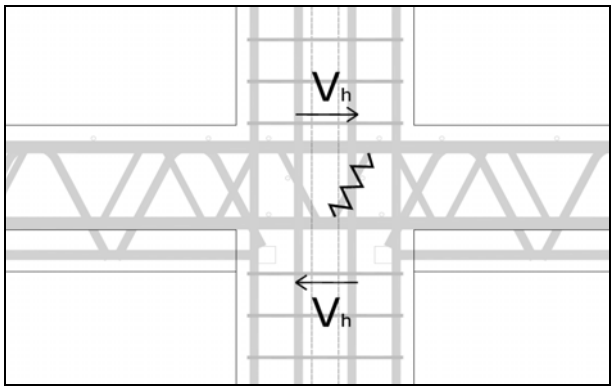

Fig. 6.5: Joint truss mechanism resisting the horizontal shear force

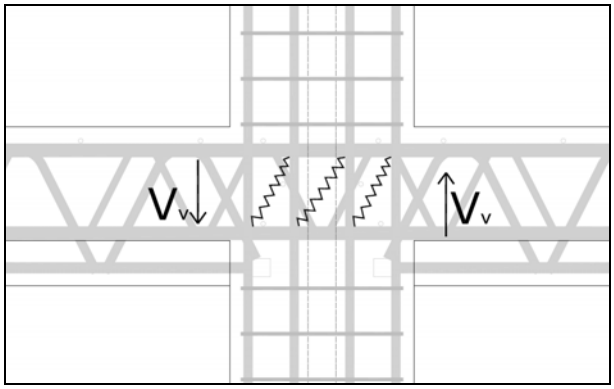

Fig. 6.6: Joint truss mechanism resisting the vertical shear force

After the evaluation of the possible internal static schemes, it is necessary to compute the shear forces to be sustained. Recalling the symbols of the previous chapter 5, the soliciting vertical joint shear force is V_{jh} and the horizontal one is V_{jv}. The integrative truss leads the CSTC joint to have similar distribution of joint shear forces as the RC joint one. In fact the proposed joint has corner bars both for the column and the beams crossing the joint. Thus the beam reinforcement tensile force is

$$T = \lambda_0 \cdot \left(A_{s1} + A_{s2}\right) \cdot f_{yd} \tag{1}$$

where A_{s1} and A_{s2} are the integrative truss bar areas, at the top and and the bottom respectively, λ_0 is the steel over strength coefficient and f_{yd} is the design yield strength for the steel material of the truss. In analogy to what already seen for the RC structure, the horizontal joint shear force is computed as

$$V_{jh} = T + C'_c + C'_s - V_{col} = T' + C_c + C_s - V_{col} \quad (2)$$

and its part, that can be sustained by the concrete strut mechanism, is

$$V_{ch} = \left[\left(1 + \gamma / \lambda_0\right) \cdot c / h_c + \beta - \gamma / \lambda_0\right] \cdot T - V_{col} \quad (3)$$

whereas the part of the shear force assimilated by the truss mechanism is

$$V_{sh} = \left(1 + \gamma / \lambda_0\right) \cdot \left(1 - c / h_c\right) \cdot T \quad (4)$$

with the symbol meaning already specified in the previous chapter. The following step is to verify the material strength. For what concerns the concrete strut the formula of Eurocode 8 [6] is used by which the compression of the diagonal strut should be lower than the concrete compressive strength in presence of tensile transverse stresses

$$V_{jhd} \le \eta \cdot f_{cd} \cdot \sqrt{1 - \upsilon_d / \eta} \cdot b_j \cdot h_c \quad (5)$$

where η is a coefficient reducing the concrete strength, υ_d is the column axial load normalized, b_j is the effective joint width and h_c is the joint depth. The reduction factor of the concrete compressive strength can be assumed as

$$\eta = 0.6 \cdot \left(1 - f_{ck} / 250\right) \quad (6)$$

The term within the square root in the Eq. 5 accounts for the presence of the column axial load that reduces the concrete available strength. The joint shear strength, after the diagonal cracking, can be verified with the following inequality

$$A_{sh} \ge \gamma_{Rd} \cdot \left(A_{s1} + A_{s2}\right) \cdot \left(1 - 0.8 \cdot \upsilon_d\right) \quad (7)$$

where γ_{Rd} is an amplification factor and can assume values that range from 1.20 to 1.30 depending on the considered Code. To verify the vertical shear strength the column longitudinal bars, passing through the joint, should satisfy

$$A_{sw,i} \ge \left(2/3\right) \cdot A_{sh} \cdot \left(h_{jc} / h_{jw}\right) \quad (8)$$

where A_{sh} is the horizontal steel bar area within the joint and $A_{sw,i}$ is the total area of the column longitudinal bars.

6.2.3 CSTC joint design

The test joint, as defined in the previous chapter, has been designed using the CSTC type beam in three configurations. The first two deals with additional trusses applied to CSTC beam with concrete base and bottom steel plate whereas the last one proposes a different solutions with a additional crossed truss.

The first proposed configuration has been developed for the concrete base beam trusses. The joint is composed by a typical reinforced concrete column with square section of 400

mm of size. The REP® beams are 400 mm wide, 350 mm deep and the concrete base is 100 mm deep. The beam trusses are made by S355 structural steel as the integrative truss is. The last one is constituted by a system of top and bottom longitudinal bars bound by web diagonal curved bars and top transversal pieces of bars both welded to the longitudinal ones. The integrative truss, so composed, leans on the beam concrete base. Within the joint other transversal pieces of 10 mm bar are welded to the web diagonal truss with the aim to confine the joint concrete core. The column longitudinal reinforcement is constituted by twelve 20 mm bars and the transversal reinforcement by 8 mm hoops with four legs interrupted in the joint region.

The resisting bending moment of the beams has been calculated as presented in the chapter 3. The material partial safety coefficients are the same as non seismic conditions. It has been verified that the soliciting bending moment, computed by a linear dynamic analysis, is lower than the resisting one. The section type of the beam is shown in Fig. 6.7.

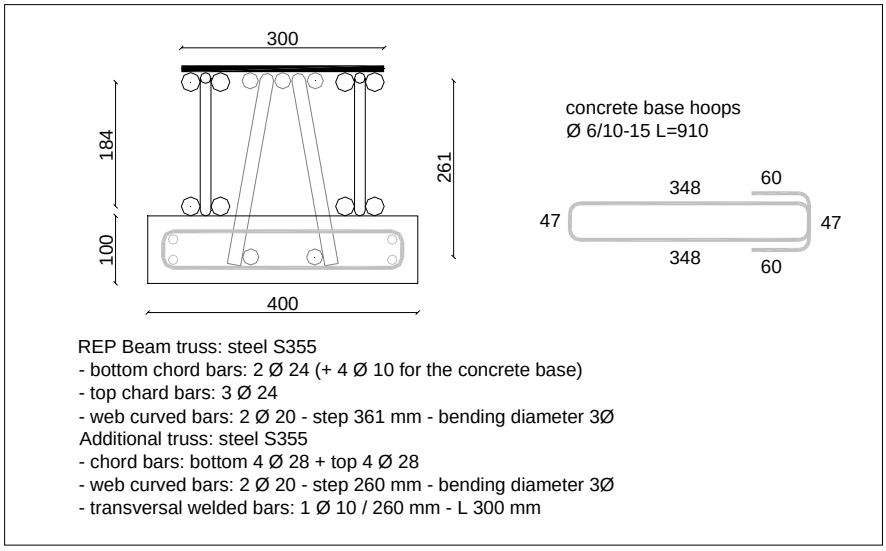

Fig. 6.7: CSTC beam section with concrete base and integrative truss

For the beam shear solicitations the capacity design has been applied as per the high ductility class of RC structures. Thus the soliciting shear force is calculated adding the gravitational load contributions to the shear solicitations due to the bending resisting moments at the beam ends. All the shear soliciting values are then amplified by the coefficient γ_{Rd} already seen. The shear strength is computed as proposed in the chapter 3 considering only the contributions of the steel diagonal bars for the tensile stresses.

For what concerns the column, the calculation is similar to the usual reinforced concrete member applying the capacity design. The method is already been presented in the previous chapter 5. The type section is shown in the following Fig. 6.8.

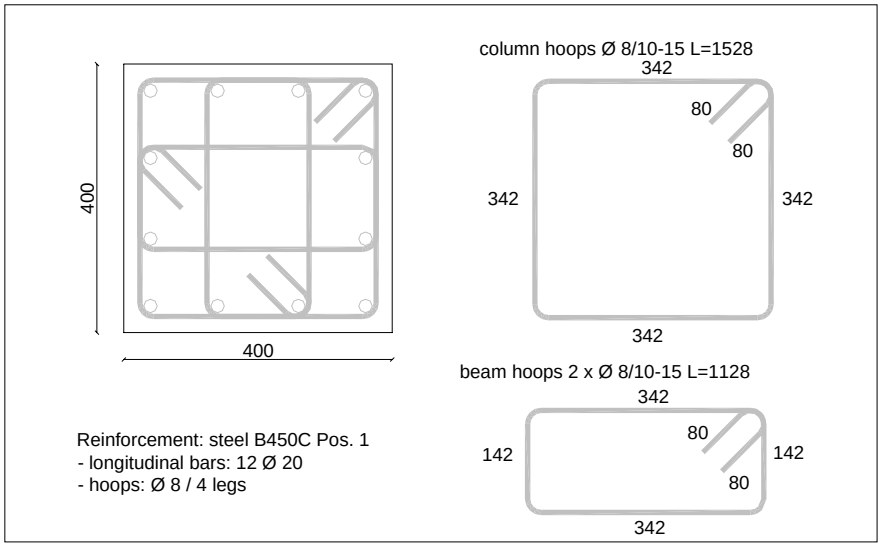

Fig. 6.8: RC column section

The given joint geometry has been thought out to maximize the construction speed with an easy assemblage. After the prefabrication of the beams' and the integrative trusses, the first steps are the reinforcement positioning and the concrete cast of the inferior column. Then the prefabricated beam trusses can be placed (see Fig. 6.9). The positioning of the slab and of the integrative truss constitutes the next step. The following floor concrete cast completes the beam sections geometry (see Fig. 6.10).

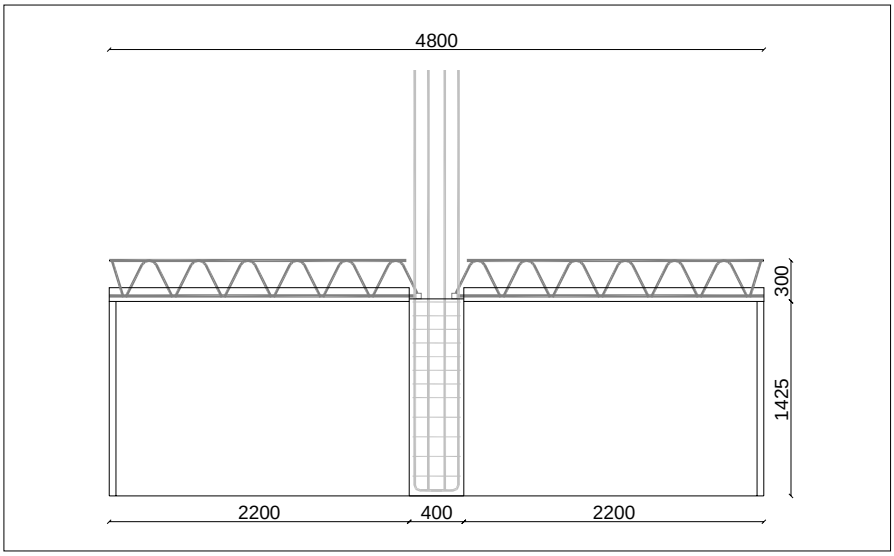

Fig. 6.9: CSTC beam trusses positioning after the lower column concrete cast

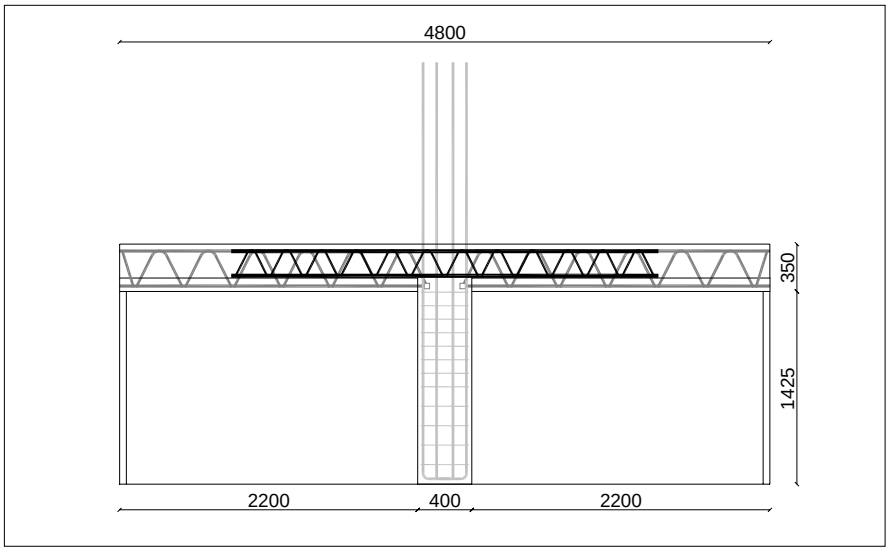

Fig. 6.10: Floor concrete cast after the integrative truss positioning

The process can continue with the concrete cast of the new storey column after the corresponding reinforcements are set (see Fig. 6.11).

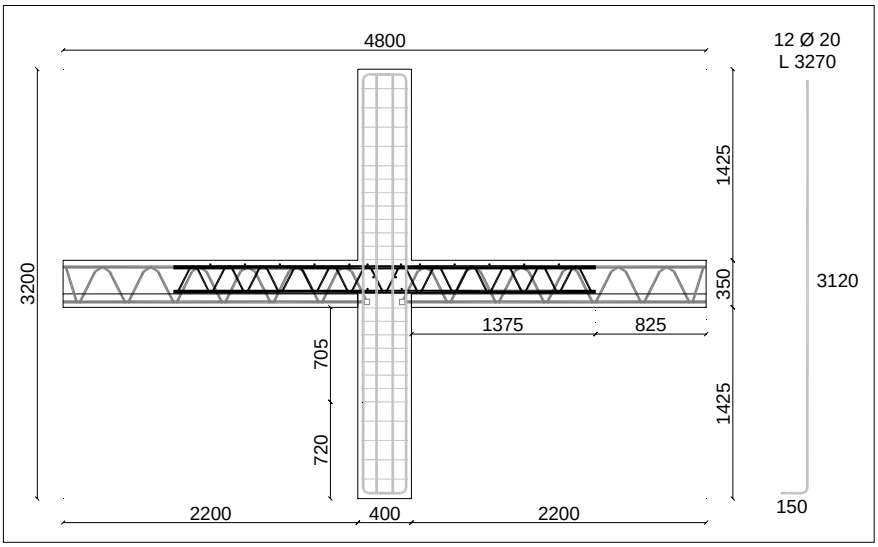

Fig. 6.11: New storey column concrete cast

Some of the calculation results are presented here to draw useful considerations. From the test joint the estimation for the column shear V_{col} is about 170 kN. With the assumed design compressive strength the reduction factor η of the joint compressive concrete strength is equal to about 0.54. The horizontal joint shear force V_{jh} is equal to about 2,016 kN. The concrete strut shear resistance V_{ch} can sustain about 1,150 kN while the truss mechanism resistance V_{sh} should absorb the difference, that is about 866 kN. Therefore, according to the assumed hypotheses, the first concrete mechanism can support the 57% of the soliciting force and the remaining 43% should be taken by the second truss mechanism.

The second proposed joint is similar to the previous one. The main difference is the application along with bottom steel plate trusses like the REP®–NOR beams. The section of the column remains the same as the previous example. The following Fig. 6.12 and Fig. 6.13 show two steps of the construction of the joint. The new section of the beam close to the joint region is presented in Fig. 6.14. The additional longitudinal bars can be smaller since the integrative truss can exploit the same depth of the beam truss.

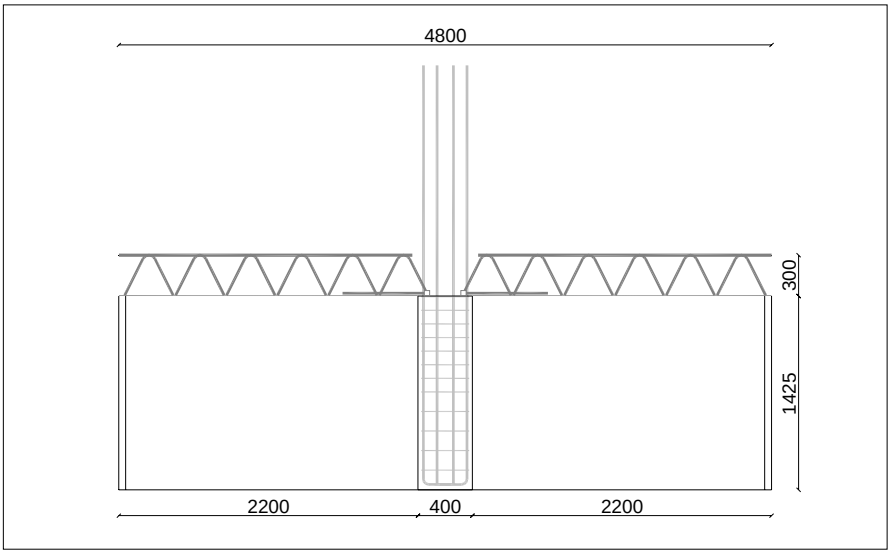

Fig. 6.12: CSTC beam trusses positioning after the lower column concrete cast

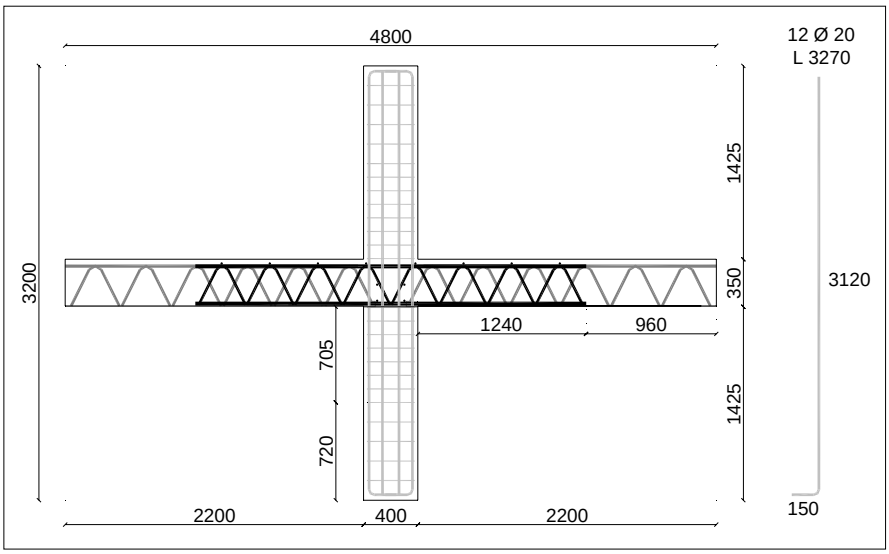

Fig. 6.13: CSTC joint profile with bottom steel plate beam trusses

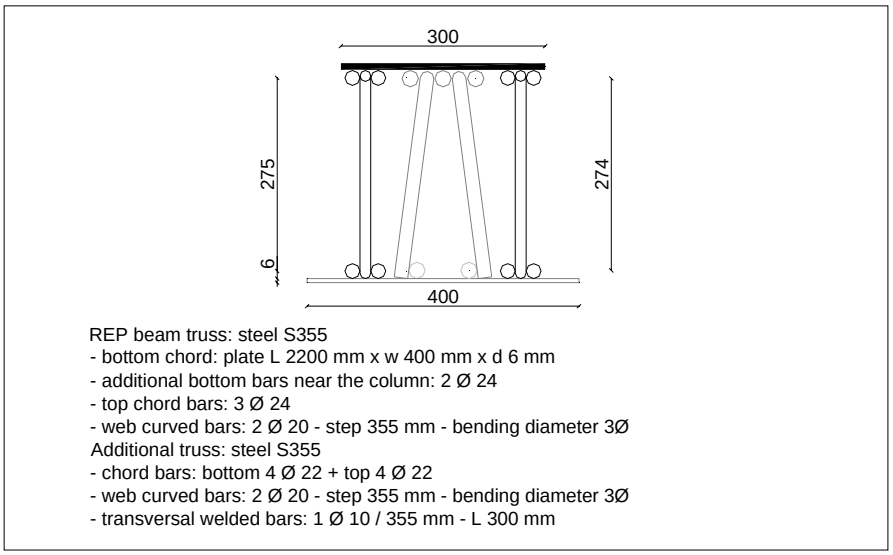

Fig. 6.14: CSTC beam section with bottom steel plate and integrative truss

Once determined the possible geometry of the joint resistant mechanisms, the horizontal and vertical shear forces can be computed and subdivided (see Fig. 6.31 and Fig. 6.16). The horizontal joint shear force V_{jh} is equal to about 1,180 kN. The concrete strut shear resistance V_{ch} can sustain about 645 kN while the truss mechanism resistance V_{sh} should absorb the difference, that is about 535 kN. Therefore, according to the assumed hypotheses, the first concrete mechanism can support the 55% of the soliciting force and the remaining 45% should be taken by the second truss mechanism. It can be noted that the joint shear soliciting force is quite different between the two presented cases. It mainly depends on the amount of longitudinal steel used in the additional joint truss that is lower in the second case, as already underscored.

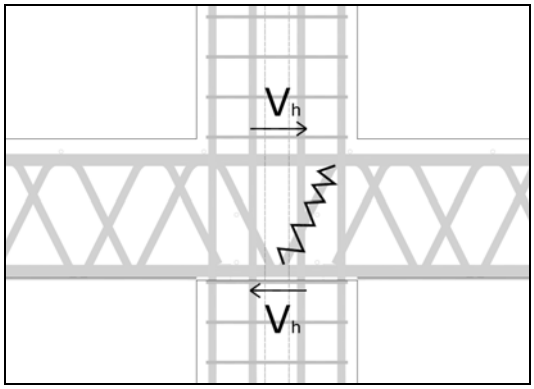

Fig. 6.15: Joint truss mechanism resisting the horizontal shear force

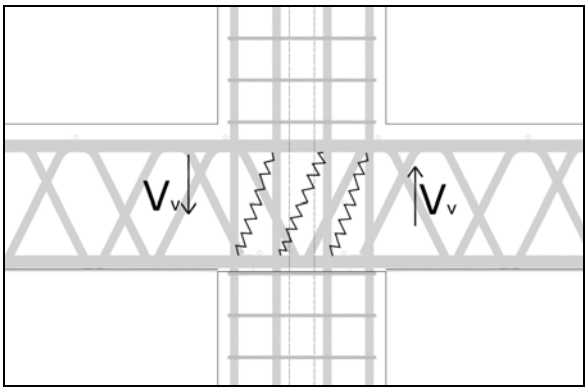

Fig. 6.16: Joint truss mechanism resisting the vertical shear force

The last CSTC joint solution derives from an idea by S. Leone [2] originally applied to concrete filled tubular columns and here extended for reinforced concrete column. It consists in a prefabricated steel trussed cross which penetrates into both the end of beams and columns (see Fig. 6.17). The horizontal truss is composed by a set of longitudinal bars at the top and at the bottom, four truss webs coupled two by two composed by four diagonal bar rows. The vertical part is constituted by corner longitudinal bars and welded transversal pieces of bar.

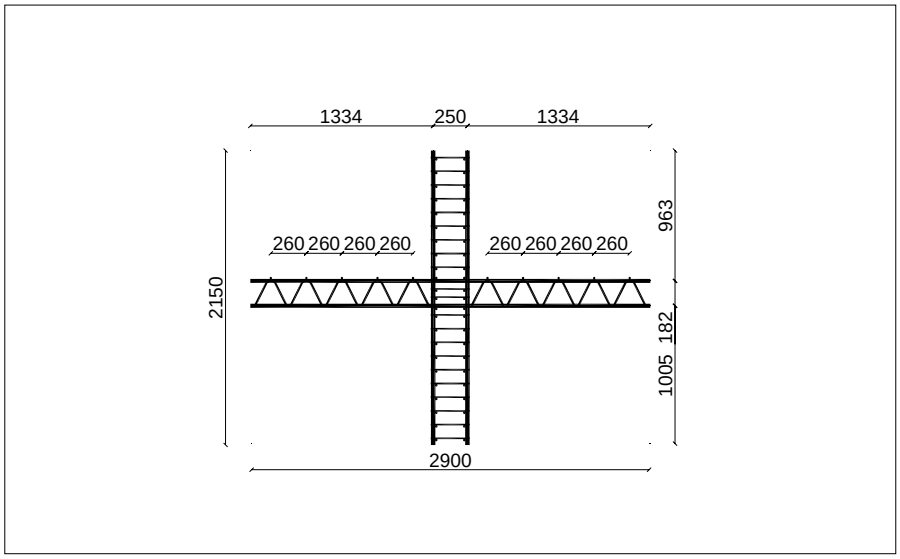

Fig. 6.17: CSTC integrative crossed truss profile

The construction process of this joint is resumed with the help of the phase assembling figures (see from Fig. 6.18 to Fig. 6.20). The formwork for the column concrete cast can be also the support of the beam. Then the additional crossed truss can be positioned overlapping both the column and the beam steel. Only after the concrete cast of the column and the floor becomes hard, the temporary supports can be removed. The last step is the concrete cast of the upper column.

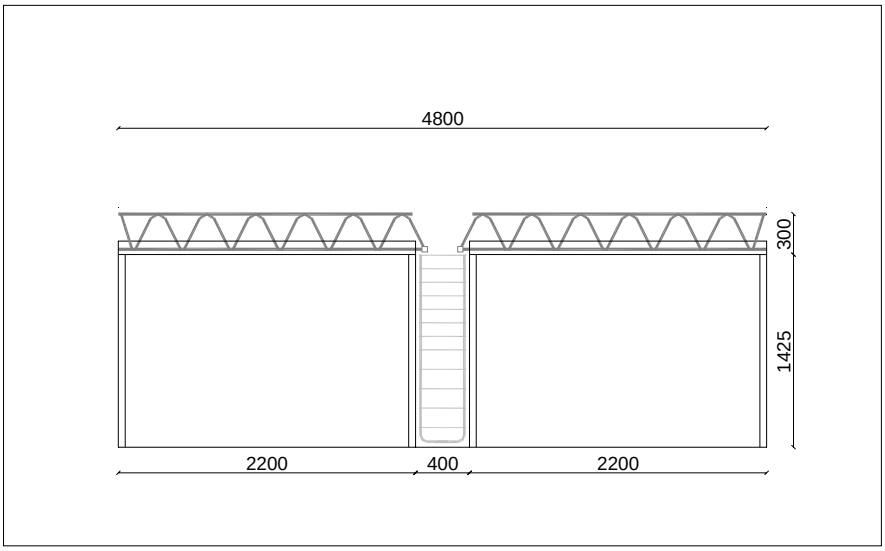

Fig. 6.18: CSTC beam trusses positioning before the lower column concrete cast

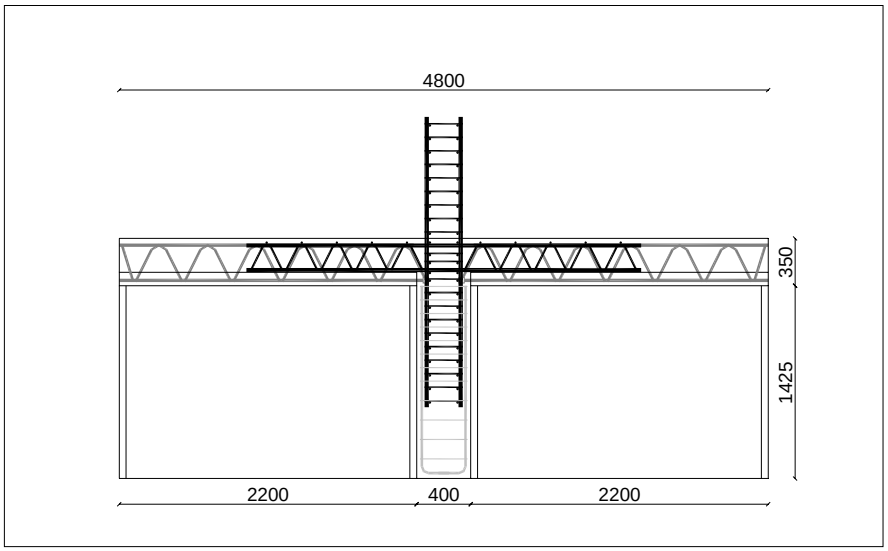

Fig. 6.19: Floor concrete cast after the integrative truss positioning

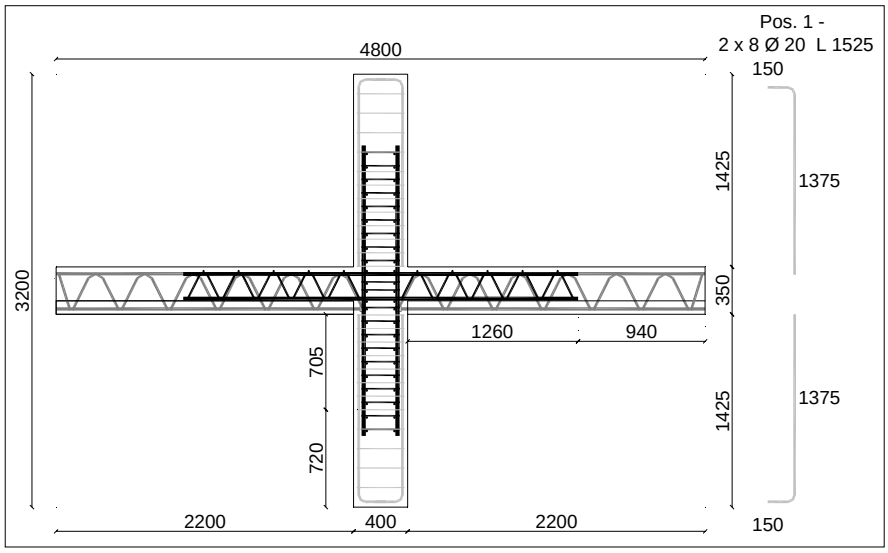

Fig. 6.20: Profile of CSTC joint with the integrative crossed truss

The resulting type sections for the beam and the column are presented in Fig. 6.21 and Fig. 6.22. Even this joint was designed to be applied along with concrete base truss beams. This fact forces the horizontal additional truss to have a reduced depth as already seen in the first proposed joint. The reinforcement of the column should be arranged in such a way not to generate intersections with the additional vertical truss. The simplest way is to concentrate the longitudinal column bars at each corner and to use 90-degree hooks in the column hoops instead of 135-degree ones. To obtain the same efficiency the hoops can be profitably welded.

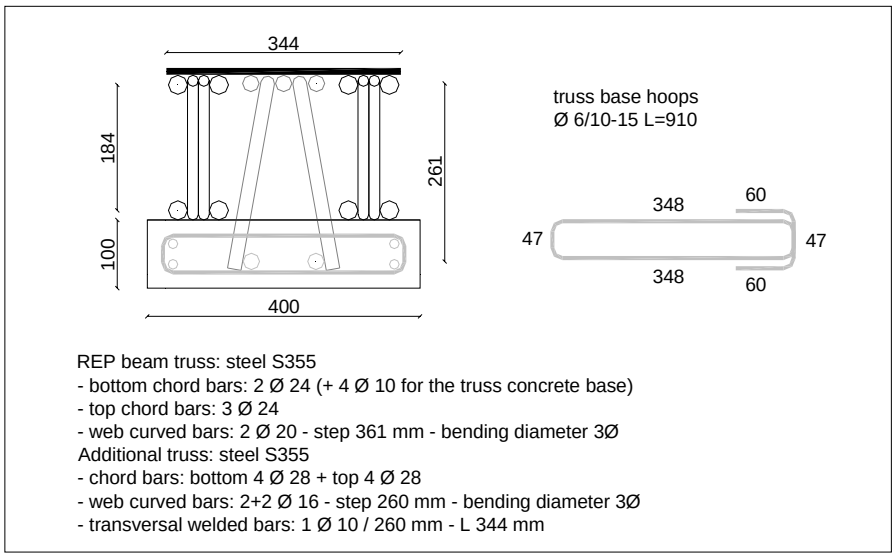

Fig. 6.21: CSTC beam section with the additional horizontal truss

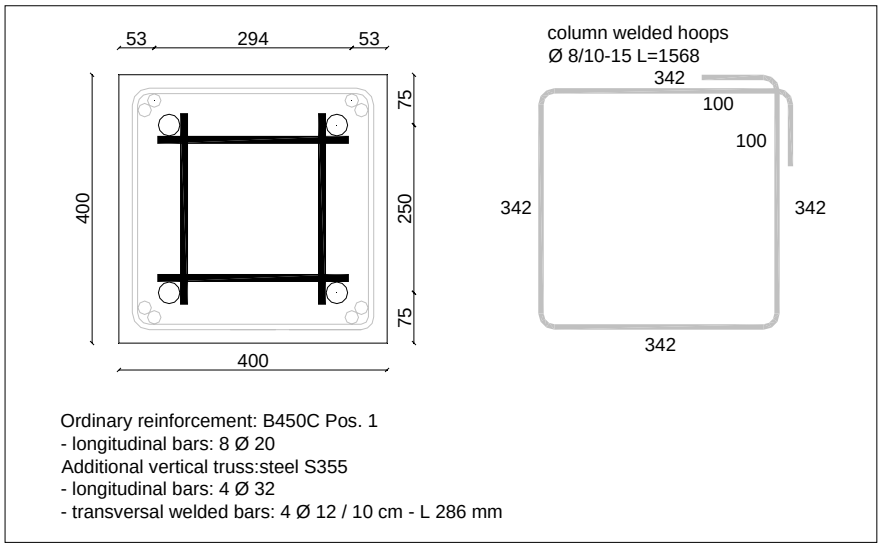

Fig. 6.22: RC column section with the additional vertical truss

After the characterization of the possible internal static schemes (see Fig. 6.23 and Fig. 6.24), the calculations for the soliciting and resisting joint shear forces can be drawn. The horizontal joint shear force V_{jh} is equal to about 2,016 kN. The concrete strut shear resistance V_{ch} can sustain about 1,150 kN while the truss mechanism resistance V_{sh} should absorb the difference, that is about 866 kN. Therefore, according to the assumed hypotheses, the first concrete mechanism can support the 57% of the soliciting force and the remaining 43% should be taken by the second truss mechanism. Again, the high joint shear force depends on the amount of longitudinal steel used in the additional joint truss.

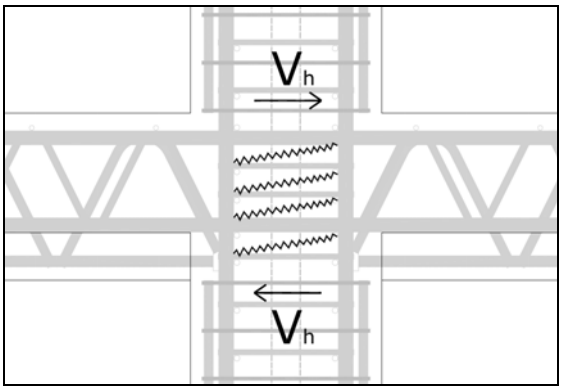

Fig. 6.23: Joint truss mechanism resisting the horizontal shear force

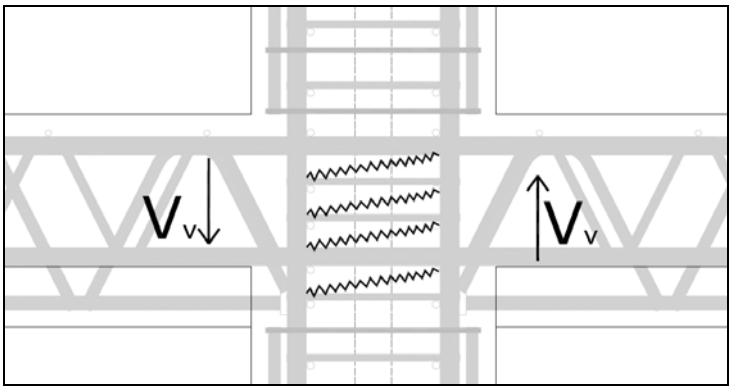

Fig. 6.24: Joint truss mechanism resisting the vertical shear force

6.3 Numerical analyses of CSTC beam-column joint

The composite joint with concrete base truss, has been verified by means of finite element numerical analyses using the code MIDAS FEA [16]. The joint has been chosen with the purpose to investigate the behaviour of the concrete base and bottom chord of the beam trusses under cyclic load conditions. In fact the contribution to the joint strength of the original beam truss members has been neglected during the design. Two- and three-dimensional analyses of the proposed joint have been performed.

The steel constitutive model uses the yield criterion of Von Mises which considers the deformation energy of the deviatoric part of the stress tensor. This criteria has a cylinder yield surface on the principal stress space and the cylinder has the directrixes parallel to the first octant trisetrix and an elliptic section. The yield surface can be defined by the value of the steel yield strength. For what concerns the concrete it has been used the smeared crack model with the fixed crack method. The compressive and the tensile constitutive laws have been assumed according respectively to the Thorenfeldt [17] and Hordijk [18] models.

6.3.1 Two-dimensional numerical model

In analogy to what already seen for the reinforced concrete test joint, the following analysis has been carried out by means of a stress plane state model. The image of the resulting mesh is presented in the Fig. 6.25. The used mesh is more refined than the RC model one because the truss steel has a more complex geometry (see Fig. 6.26) and their elemental nodes need the consistency with the concrete element ones. Thus the mesh has small size element and an huge number of nodes. The new medium element size is used to calculated the new fracture energy in defining the concrete tensile constitutive law.

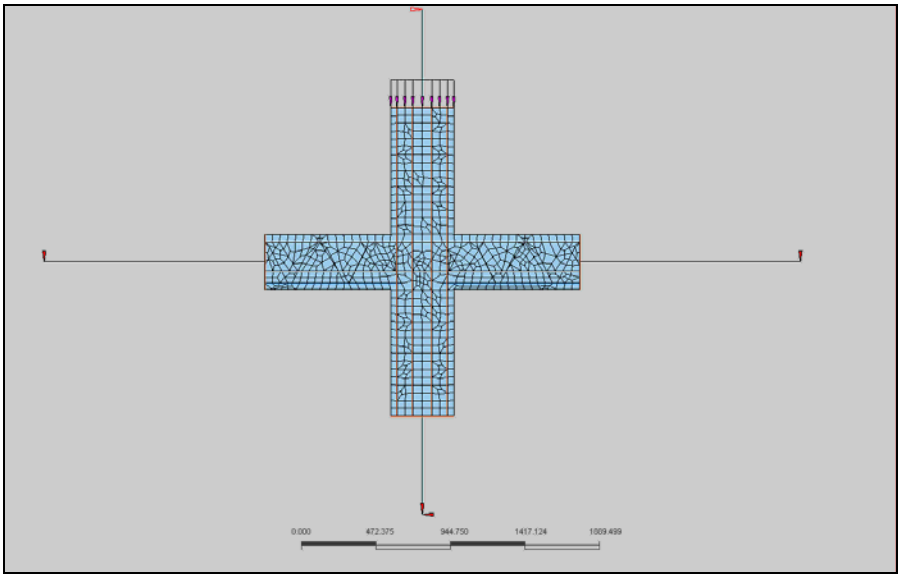

Fig. 6.25: Two-dimensional CSTC joint model

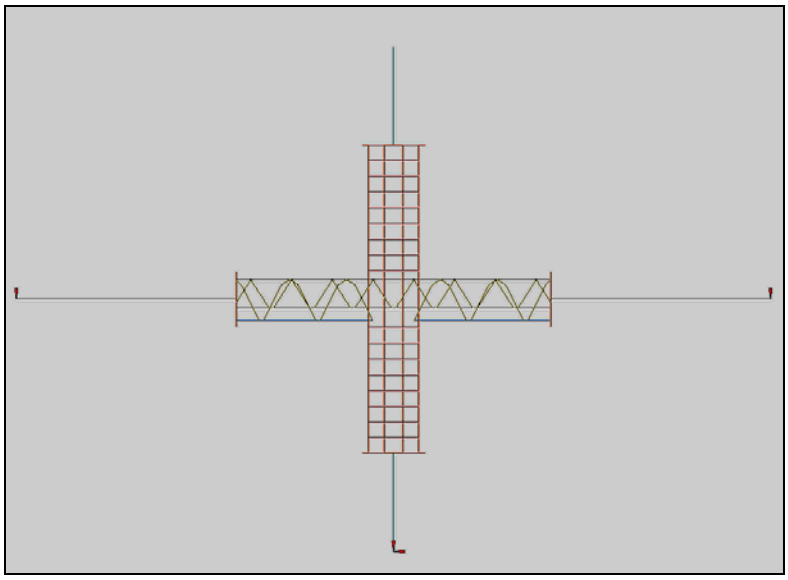

Fig. 6.26: Two-dimensional CSTC joint reinforcement model

The crucial point is to model the connection between the beam trusses and the column. In fact the beam truss concrete base is connected to the column concrete cast by the lower longitudinal chords of the beam truss. These chords enter in the column for few centimetres and, at their end, they are welded on a transversal bar called head hammer. The hammer is designed to be placed inside the joint core defined by the longitudinal column bars. This fact suggest the connection between the end nodes of the beam and the node of the concrete joint. The efficiency of those bars will be low since they don't pass through the joint. The three dimensional model will be more accurate in reproduce the behaviour of this connection.

The history of the imposed displacement at the column top remains the same of the RC

one. The Fig. 6.27 shows the steel stress diagram along both the trusses and the reinforcing bars. The picture corroborates the joint truss mechanism assumed in the design phase. The absence of horizontal hoops within the joint causes an initial weakness until the additional joint truss, that has lower effective depth, starts to work. The following Fig. 6.28 depicts the minimum principal stresses of concrete material. The main concrete strut resisting mechanism is clearly visible with some stress peaks in correspondence to the bottom part of the beam concrete base.

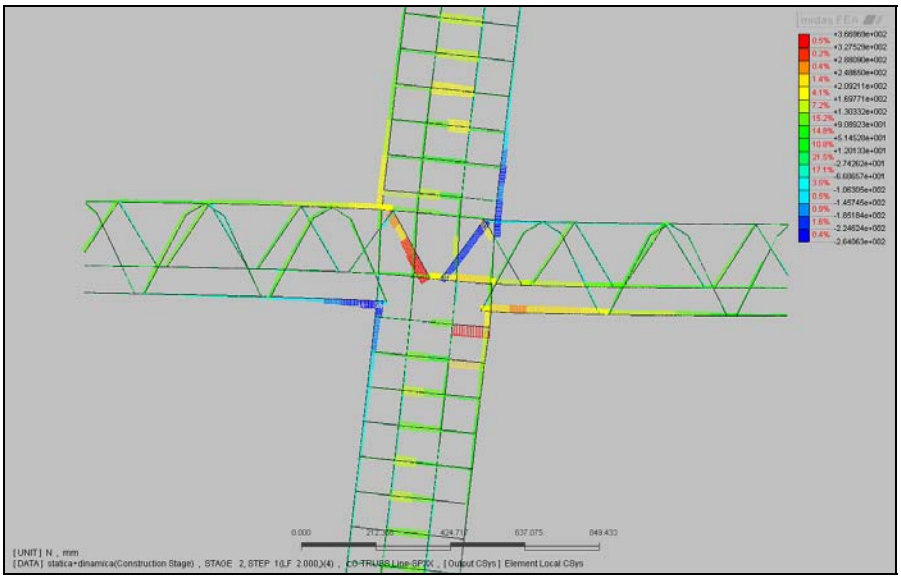

Fig. 6.27: Steel stress diagram at 20 mm of top displacement

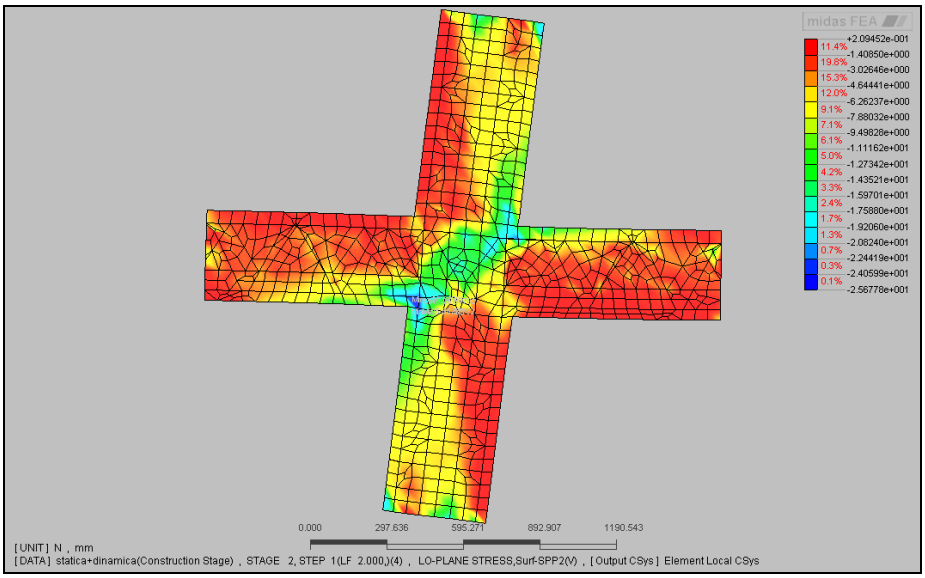

Fig. 6.28: Concrete minimum principal stress diagram at 20 mm of top displacement

The same images are then presented during the reverse deformation of -20 mm (see Fig. 6.29 and Fig. 6.30). The stresses are of the same magnitude of the first leading branch and they show the same characteristics. With the change of loading sign the cracks, opened in the

first quarter of cycle, close and other cracks open in transversal directions. The resume of the joint response is shown in Fig. 6.31 in terms of applied load vs. top displacement. The ultimate conditions are reached at about 64 mm of top displacement.

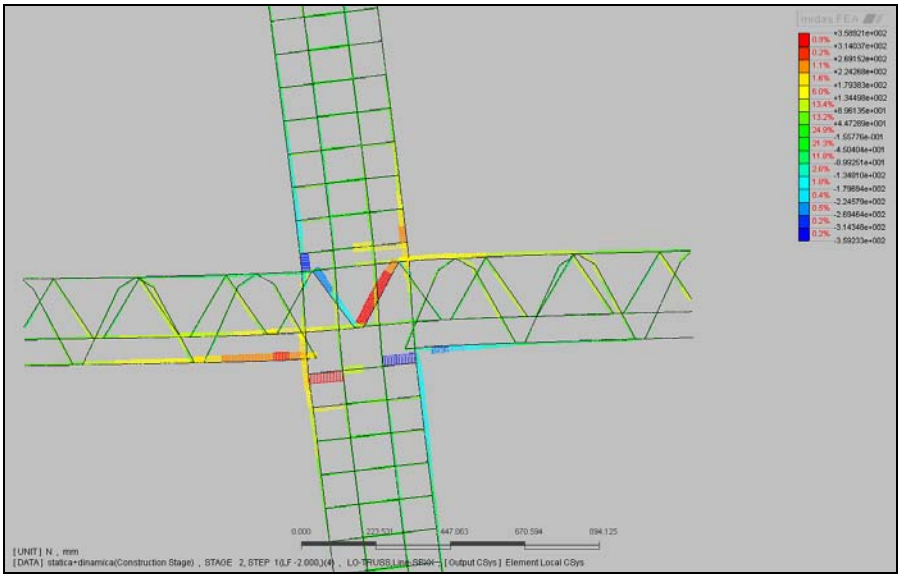

Fig. 6.29: Steel stress diagram at -20 mm of top displacement

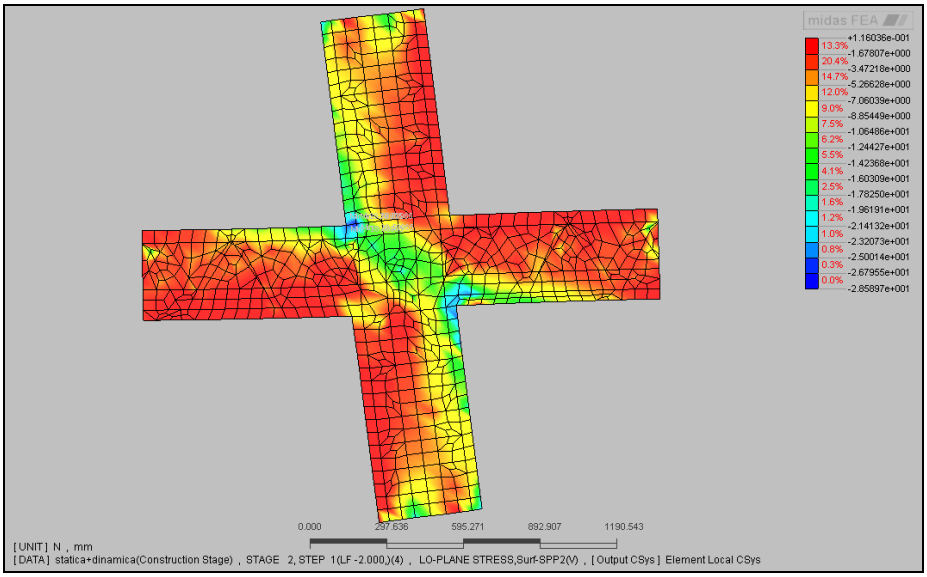

Fig. 6.30: Concrete minimum principal stress diagram at -20 mm of top displacement

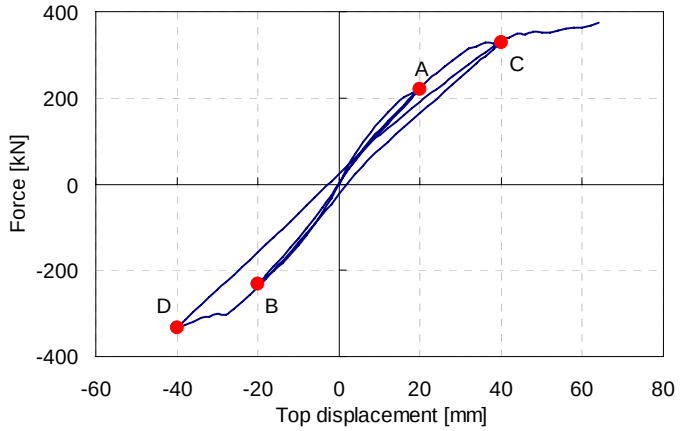

Fig. 6.31: Applied load-top displacement diagram of the CSTC joint

Thus it is possible to compare the applied load vs. top displacement curves for the RC joint and the CSTC one coming out from two-dimensional analyses (see Fig. 6.32). It's important to remark that both the joints were designed to resist the same solicitations. The initial stiffness of the RC joint seems to be higher because of the lower effective depth of the joint additional truss in the CSTC joint and the absence of the joint horizontal hoops. The transition between the elastic and the plastic fields is smoother in the CSTC joint. The reached ductility levels are different between the two joint type as also the energy dissipated whereas the peak strengths are similar. This result is influenced by the different computational effort to perform the two analyses. In fact in the CSTC case the solver founded some convergence problems for further top displacements. More accurate comparisons will be possible by means of the three-dimensional models.

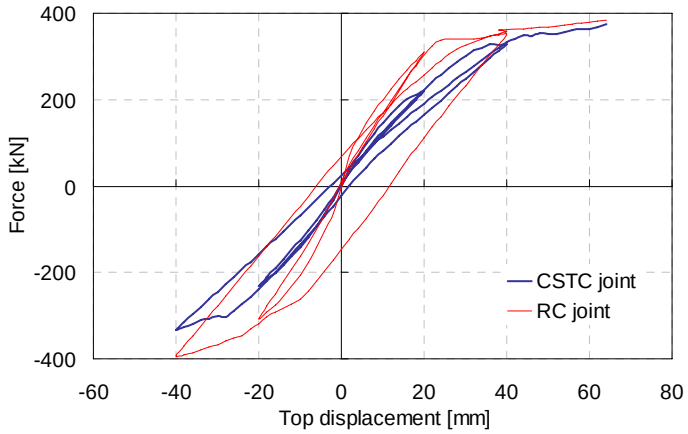

Fig. 6.32: Comparison between RC and CSTC joint by 2D models

6.3.2 Three-dimensional numerical model

The mesh of the three dimensional model for the proposed CSTC joint with the concrete base beams is more complex than the RC one. In fact the overall steel quantity is

higher and the truss geometry is more tangled. The following Figures in sequence show the progressive construction of the steel model (see from Fig. 6.33 to Fig. 6.37). The Fig. 6.36 shows the transversal bars of the integrative joint truss. Their function is to confine the concrete core, substituting the horizontal hoops of the typical RC joint.

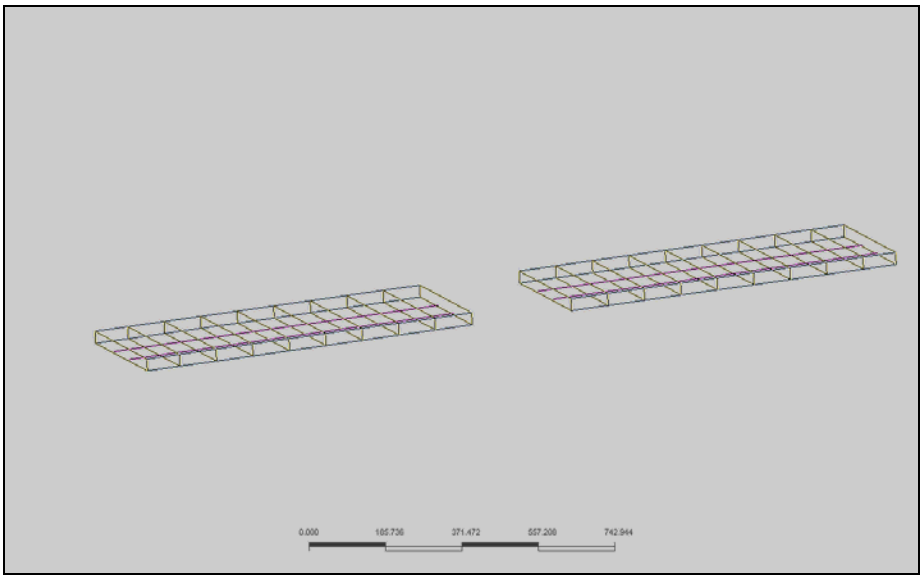

Fig. 6.33: Truss concrete base reinforcement

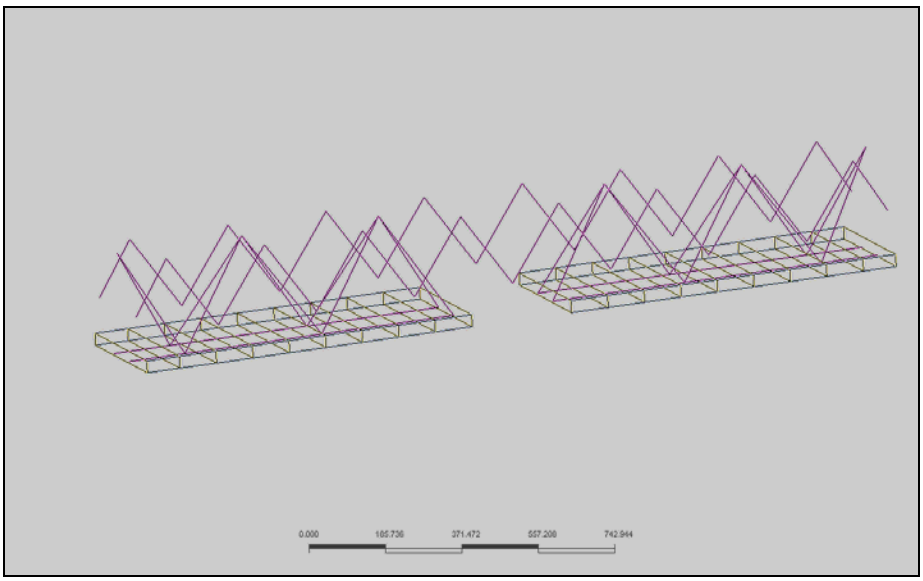

Fig. 6.34: Addition of the web diagonal bars of the beam and joint trusses

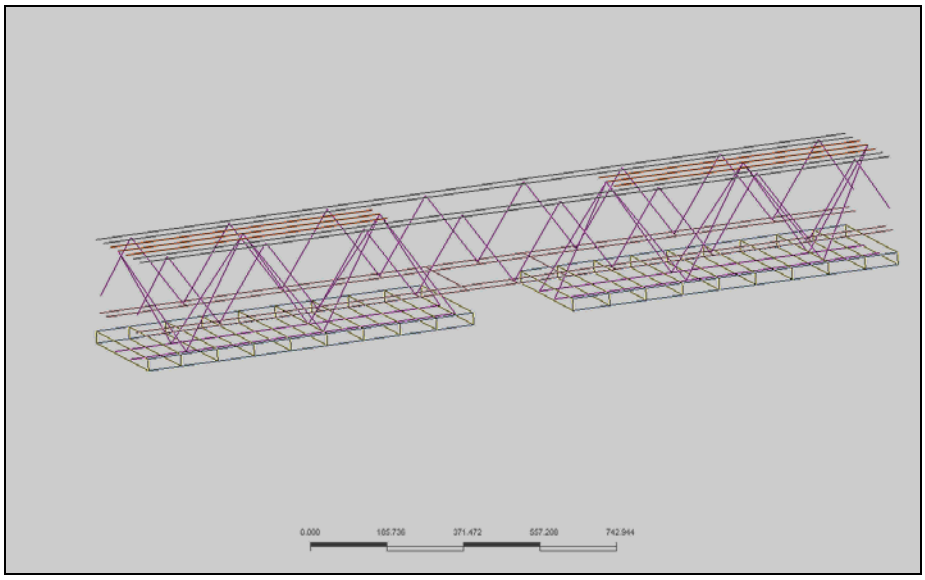

Fig. 6.35: Addition of the truss longitudinal chords

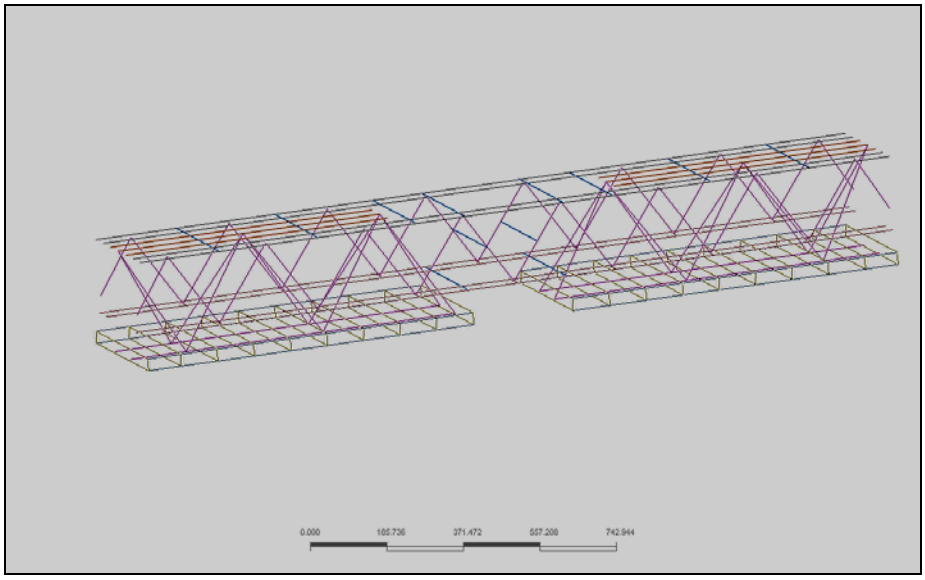

Fig. 6.36: Addition of the transversal truss bars

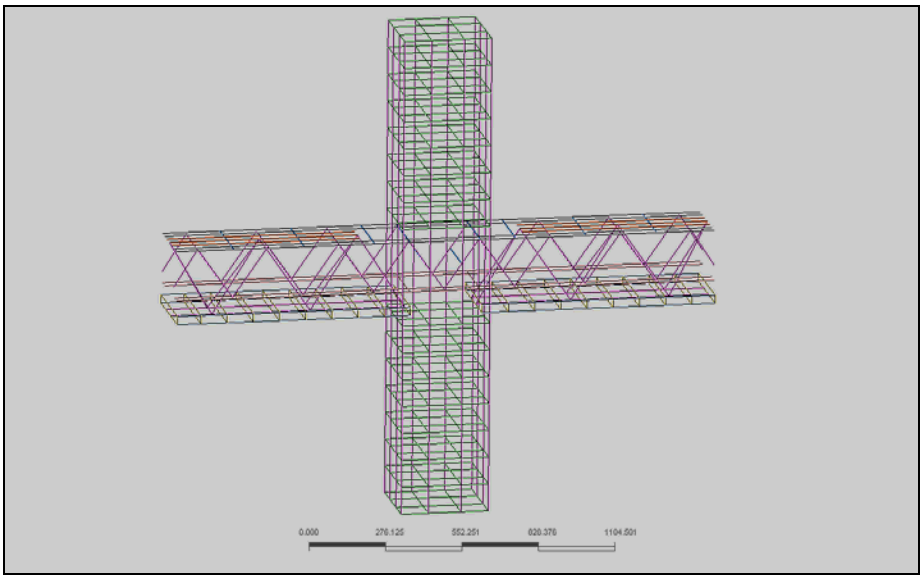

Fig. 6.37: Complete view of the CSTC joint steel work model

The test joint behaviour is now analyzed with the same load history described in the previous chapter 5. In correspondence to 20 mm of top displacement, the truss steel stresses underscored the joint truss mechanism within the joint involving the inclined truss bars (see Fig. 6.38). The concrete stresses indicates that the diagonal strut has a large contribution during the first cycle (see Fig. 6.39). In fact at 40 mm of top displacement the concrete stresses contour shows that the resisting strut has a reduced depth even if the corresponding stresses are 50% higher (see Fig. 6.40).

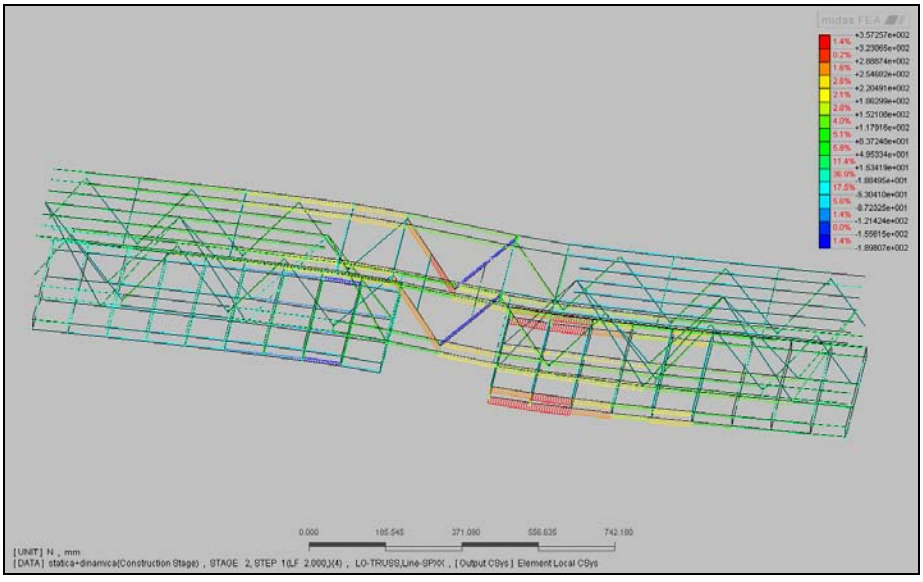

Fig. 6.38: Truss steel beam stresses at 20 mm of top displacement

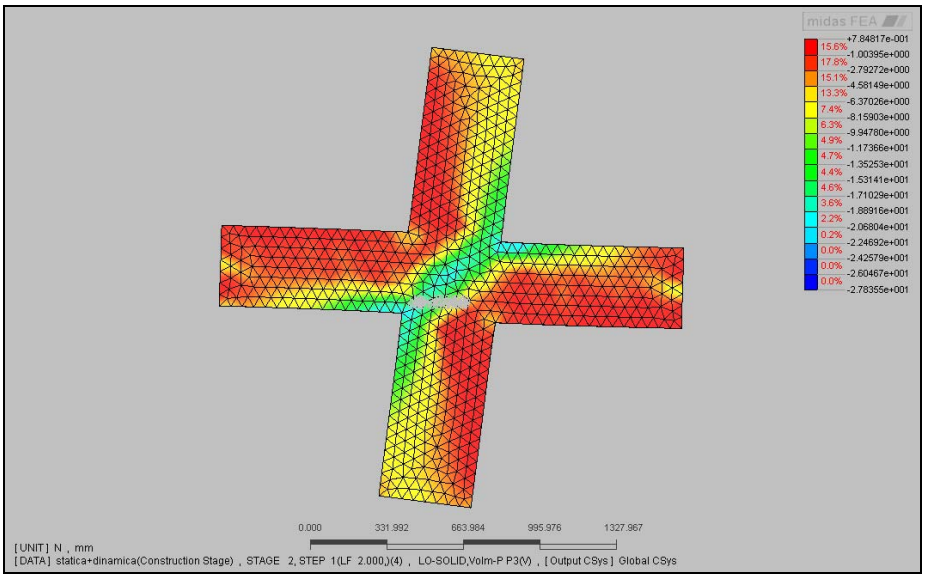

Fig. 6.39: Concrete stress contour at 20 mm of top displacement

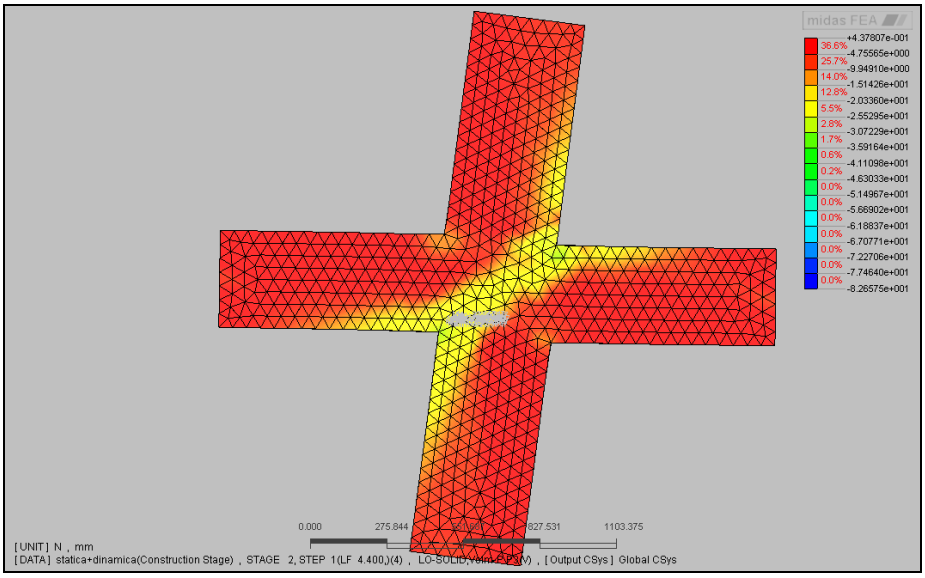

Fig. 6.40: Concrete stress contour at 40 mm of top displacement

The numerical solver cannot go forward in the analysis after a maximum top displacement equal to about 60 mm. The high nonlinearities of the damaged concrete condition the convergence. The applied load-top displacement diagram shows that the passage from the elastic field to the plastic field is progressive without a sudden change of slope (see Fig. 6.41). The peak joint strength is about 10% higher of the RC joint one. The higher stiffness is caused by the partially efficacy of the bottom chord bars of the beam trusses. The joint member shows an overall good ductility. Integrating the area contained in the diagram, it is possible to draw the total displacement energy as a function of the load step (see Fig. 6.42). The minimum points of that curve, again, represent the dissipated energy during the previous cycles. Comparing the curves of the CSTC joint to the RC one, it can

be noticed that the amount of dissipated energy is a little lower for the first one. In other word the CSTC joint stores more elastic energy being equal the external work spent.

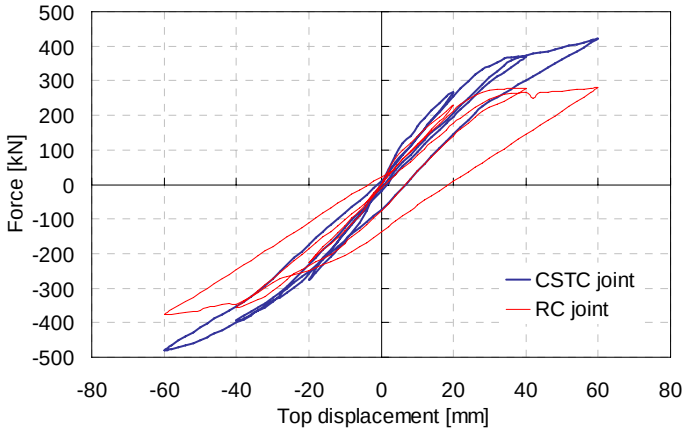

Fig. 6.41: Applied load-top displacement diagram: comparison between the CSTC and the RC joints

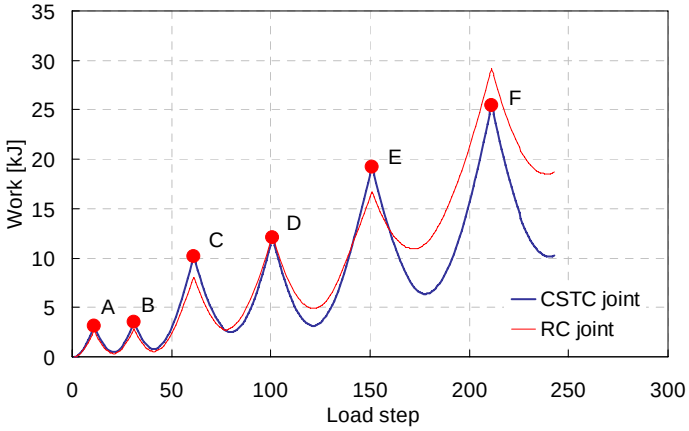

Fig. 6.42: Total displacement energy diagram: comparison between the CSTC and the RC joints

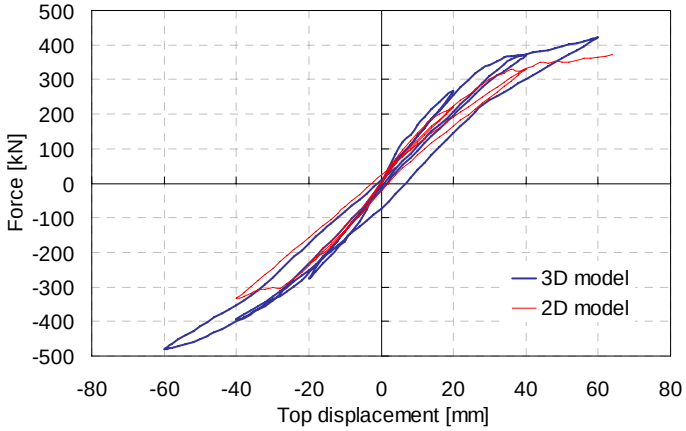

Fig. 6.43: Applied load-top displacement diagram: comparison between 2D and 3D models

Comparing the 2D and the 3D model results (see Fig. 6.43) the higher stiffness and

higher strength of the 3D model can be seen. This is due to the better evaluation of the confinement effect of the proposed joint integrative truss. The 2D model cannot represent the benefit of the confining transversal bars along the joint width.

6.4 Conclusions

Starting from theoretical considerations new CSTC joints has been proposed. The main purpose has been the achievement of an adequate stiffness, strength and ductility in sight of the application on seismic resistant frames. The similarity of the resisting mechanisms has permitted the extension of the RC joint theory to the CSTC structural type. The calculation of the proposed joint started with the investigation of admissible stress distributions within the joint and it followed with their quantitative evaluations. By means of numerical model, already evaluated in the previous chapter on the RC structures, the analyses of a designed joint have been carried out. Both two dimensional and three dimensional analysis results have been presented along with their comparison with the RC joint ones. The convergence of the numerical model is quite difficult increasing the number of cycles and the deformation amplitude, the convergence is less than linear, when the concrete damage is widespread. Nevertheless the numerical analyses showed the achievement of important targets as the joint stiffness, the joint strength and the joint ductility. From the comparison between the numerical analysis results it can be noted that, the dissipated energy being equal, the elastic energy stored in the CSTC joint is higher than the RC one. This fact turned out in a narrower hysteresis cycles of the CSTC joint as it can be seen from the applied load vs. top displacement diagrams. This behaviour is conditioned by the presence of the lower concrete base and by the lower chord bars of the beam trusses. The last ones are necessary to support the beam trusses during the first construction phase and though they increase the whole strength of the joint, their efficiency is low especially after cycle reversals. The local force, that the tight bottom chord bars exert on the joint, tends to dilate the joint core. Furthermore, since the stiffness of the bottom chord bars is not enough to sustain the tensile seismic solicitation, the crack between the concrete truss base and the joint face is quite large, thanks also to the distinct concrete casts. Because of that the compressive contribution of the concrete truss base, after the force sign reversal, is low. A part for these facts inherent to the CSTC structural type, the designed joint showed a good cyclic behaviour and its ductility is similar to the RC one, whereas its strength and stiffness are higher. The results confirm a good efficiency of the proposed CSTC joint. The proposed joint can be profitably proposed for future experimental tests in order to verify the numerical results and in sight of a possible application in seismic regions.

References

1. Leone S. *REP®-DIS and REP®-TR beams Patent*, Brevetto d'invenzione, Italy, 1990.
2. Leone S. *SISMIREP® Patent*, Brevetto d'invenzione, Italy, 2002.
3. Di Marco R. Sperimentazione su travi continue REP con traliccio tipo TR (Experimental tests on hyperstatic REP beams with TR truss type). *Internal Report University IUAV of Venice*, 2004.
4. Sassone M, Bigaran D, Massa S. Le travi composte nel nuovo quadro normativo (The composite beams in the new code framework). *XVI CTE Congress*, Parma, 2007, 715-723.
5. Petrovich F. *Un nuovo sistema strutturale per edifici multipiano in zona sismica realizzato mediante elementi tralicciati misti acciaio-calcestruzzo: analisi numerica e sperimentale* (A new structural system for multi-storey building in seismic zone made by composite steel truss and concrete elements: numerical and experimental analyses). Ph.D. Thesis, University of Trieste, 2008.
6. CEN. *Eurocode 8: Design of structures for earthquake resistance Part 1: General rules, seismic actions and rules for buildings*. Comité Européen de Normalisation: Bruxelles, 2003.
7. D M LL PP 14 Jan 2008. Norme Tecniche per le Costruzioni (Construction Technical Codes). *Gazzetta Ufficiale* 04 Feb 2008.
8. Paulay T. Equilibrium Criteria for reinforced concrete beam column joints. *ACI Structural Journal* 1989, **86**: 635-643.
9. Stevens NJ, Uzumeri SM, Collins MP. Reinforced concrete subjected to reversed cyclic shear-experiments and constitutive model. *ACI Structural Journal* 1991, **88**: 135-146.
10. Hegger J, Sherif A, Roeser W. Nonlinear finite element analysis of reinforced concrete beam-column connections. *ACI Structural Journal* 2004, **101**: 604-614.
11. Hwang SJ, Lee HJ. Analytical model for predicting shear strengths of exterior reinforced concrete beam-column joints for seismic resistance. *ACI Structural Journal* 1999, **96**: 846-858.
12. Hakuto S, Park R, Tanaka H. Effect of deterioration of bond of beam bars passing through interior beam-column joints on flexural strength and ductility. *ACI Structural Journal* 1999, **96**: 859-864.
13. Paul S. Baglin and Richard H. Scott. Finite element modeling of reinforced concrete beam-column connections. *ACI Structural Journal* 2000, **97**: 886-894.

14. Hwang SJ, Lee HJ. Analytical model for predicting shear strengths of interior reinforced concrete beam-column joints for seismic resistance. *ACI Structural Journal* 2000, **97**: 35-44.

15. Mitra N, Lowes LN. Evaluation, calibration, and verification of a reinforced concrete beam-column joint model. *ASCE Journal of Structural Engineering* 2007, **133**: 105-120.

16. MIDAS FEA, Advances Nonlinear and Detail analysis program. *Analysis reference*, 2008.

17. Thorenfeldt E., Tomaszewicz A., and Jenen JJ. Mechanical properties of high strength concrete and application in design. Proceeding Symposium, *Utilization of High Strength Concrete*, Tavanger, Norway, 1987.

18. Hordijk DA. *Local approach to fatigue of concrete*. PhD Thesis, University of Delft, 1991.

Chapter 7

A new joint between Composite Steel Truss and Concrete beams and CFT columns

7.1 Introduction

Steel tubes have been popular as compression members because of efficient cross-sectional use in compression and in torsion. Filling a tube with concrete increases the strength and the stiffness of the section by inhibiting its local buckling, and it also improves its fire resistance (Park *et al.* [1]). In fact the concrete core adds stiffness and compressive strength to the tubular column and reduces the possibility of inward local buckling. Conversely, the steel tube acts as longitudinal and lateral reinforcement for the concrete core helping it to resist tension, bending moment and shear and providing confinement for the concrete. Due to the benefit of composite action of the two materials, the CFT columns provide excellent seismic resistant properties such as high strength, high ductility and large energy absorption capacity.

Due to the complexity of connections between steel beams and circular hollow sections, their use in structural steelwork is limited. For a long while welded connections were the common solution. The numerous failures of fully welded moment connections during the 1994 Northridge and 1995 Kobe earthquakes indicated that conventional fully welded moment connections had several inherent drawbacks, whereas bolted and riveted connections had performed well in past earthquakes, particularly when encased in concrete

(Swanson and Leon, [2]). An innovative composite steel and concrete joint, that can be used along with typical CSTC beams and composite columns using blind bolts has been developed for loading conditions at regions of low to medium seismicity.

A 3D finite element model incorporating nonlinear material properties has been used to verify numerically the strength, the stiffness and the deformation of the proposed new joint assembly joint.

7.2 Composite joint theory and design

7.2.1 General criteria

The composite columns can be subdivided in three category: the fully encased columns, the partially encased columns and the concrete filled ones. The distinction relays on the position of the steel member respect to the composite section. Thus, in a fully encased column the steel member is completely covered by concrete, whereas in a partially encased column the steel member is partially covered by concrete and in the concrete filled column the steel member is hollow and is filled by the concrete cast (see Fig. 7.1).

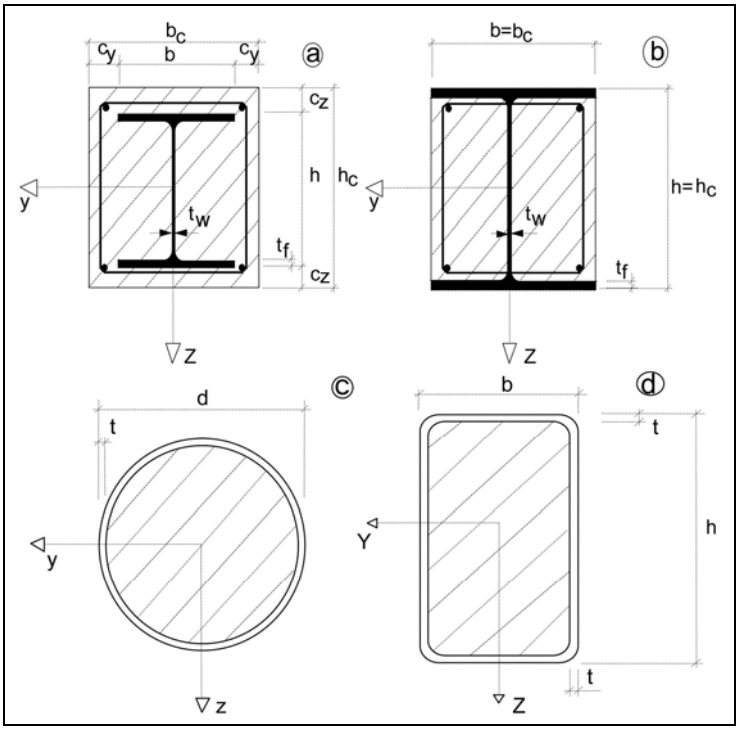

Fig. 7.1: Section types of composite steel and concrete columns

These composite sections have some benefits respect to those of RC one due to the collaborations of the two materials. For instance, many experimental studies demonstrated

that the presence of the concrete reduces the local buckling problems of the steel member, even if in different ways depending on the particular geometry. In fact the local buckling is usually avoided in the fully encased sections, is reduces in the partially encased and in the concrete filled; for the last one the most efficient case is the one of the circular tubes. Another benefit is the confinement effect exerted by the steel to the concrete. The concrete can show an higher compressive strength. Furthermore the concrete filled columns don't need any formwork for the concrete cast and the assembly of all the steel parts, of a generic building, can be independent from the concrete cast phases.

It's relevant to underscored that the quality of the concrete material plays an essential role. Since the concrete cast shall fill completely the steel hollow member, it should have:

- satisfactory workability to ensure an adequate compaction;
- satisfactory cohesion to reduce the possibility of bleeding and segregation;
- satisfactory mix design to control the maximum aggregate size;
- adequate distance between possibly additional reinforcing element.

An internal poker vibrator should be used to ensure the compaction of the cast in alternative to the cast from the bottom using pumps. The last technology have been applied in Australia, Japan and North America. It lets an high construction speed with the use of common pumps till about 25 meters tall buildings.

The evaluation of the improvement in the ductility of the composite columns is interesting as the increase in bearing capacity. Theoretical and experimental studies demonstrated that the concrete filled steel tube (CFT) has a larger ductility than the steel reinforced concrete column, that is a RC section with a steel member inside.

The efficacy of the composite column relies on the efficiency of the stress transfer between the two materials. The use of connectors is typical of encased steel elements and is possible for the CFT columns.

Even for what concerns the fire resistance, the improvement of the composite columns is evident both respect to the steel and to the RC columns. A research leaded by the Canadian Institute for Research in Construction (IRC) has demonstrated, by means of tests in furnace, that the CFT columns have higher load bearing capacity and higher fire resistance. In fact in standard conditions concrete and steel work together, with the same displacements and strains but with different stresses. At the beginning of a fire event, the steel tube dilates more than the concrete core, its elasticity modulus and yield strength decrease. Then the concrete core start to absorb a huge amount of heat transforming it into vapour. During this process the temperature of the core remain almost constant and so the concrete bearing capacity decrease relatively slowly. The resume in terms of axial

deformation vs. time is shown in Fig. 7.2.

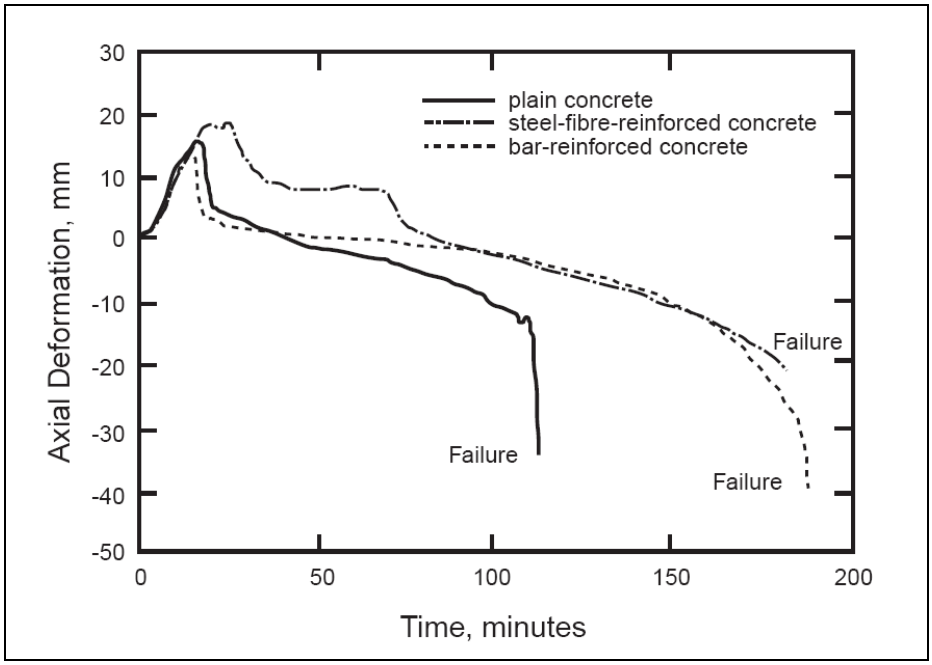

Fig. 7.2: Comparison of fire resistance properties between three structural types

7.2.2 CSTC beam-CFT column joint description

The purpose of the design of the beam-column connection is to realize the structural continuity between distinct members. In the proposed joint the steel tube of the column results continuous between subsequent storey by means of a particular connection. At the floor height two horizontal steel plate are welded to the column tube in the directions of the beams. Over the last ones and in correspondence of their axis, a vertical steel plate is placed across the column passing through a couple of hole on the tube surface. This plate will guarantee the transmission of the axial and shear force of the beam across the column. At the ends of the vertical plates, some holes constitute the predisposition for the connection to the beams by means of bolts. To restore the continuity of the upper longitudinal beam bars an new element composed by four bars is inserted. The four bars are welded at their end to a couple of steel plate as shown in the following Fig. 7.3. The steel plates, at their time, necessitate of holes for the connection to the beams.

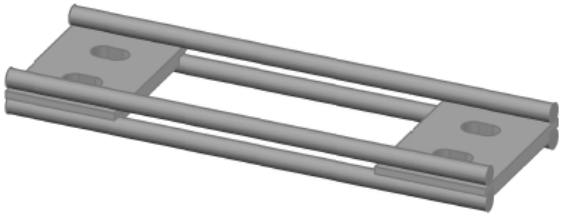

Fig. 7.3: Additional top bars within the joint

Then, each beam has an horizontal steel plate welded just under the longitudinal top chord as presented in the Fig. 7.4. The bolt connections between the plates are made by particular wedge (see Fig. 7.5) to ensure the continuity of the bars, to leave adequate tolerance and to guarantee a certain speed in the construction phase.

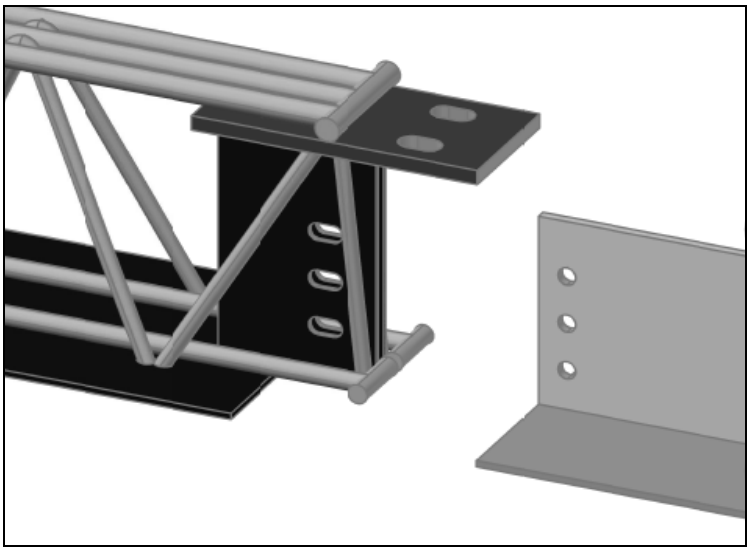

Fig. 7.4: Particular of the beam-column connection

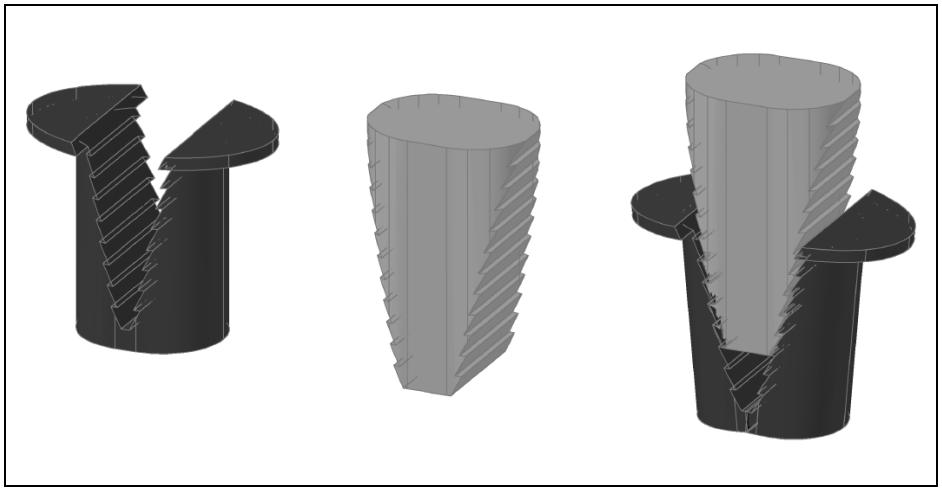

Fig. 7.5: Wedge for the connections of the top longitudinal beam bars

The connection of the beam bottom chord to the inferior horizontal joint plate is realized by Nelson connectors (see Fig. 7.6). In fact the aim is to weaken the column tube as less as possible.

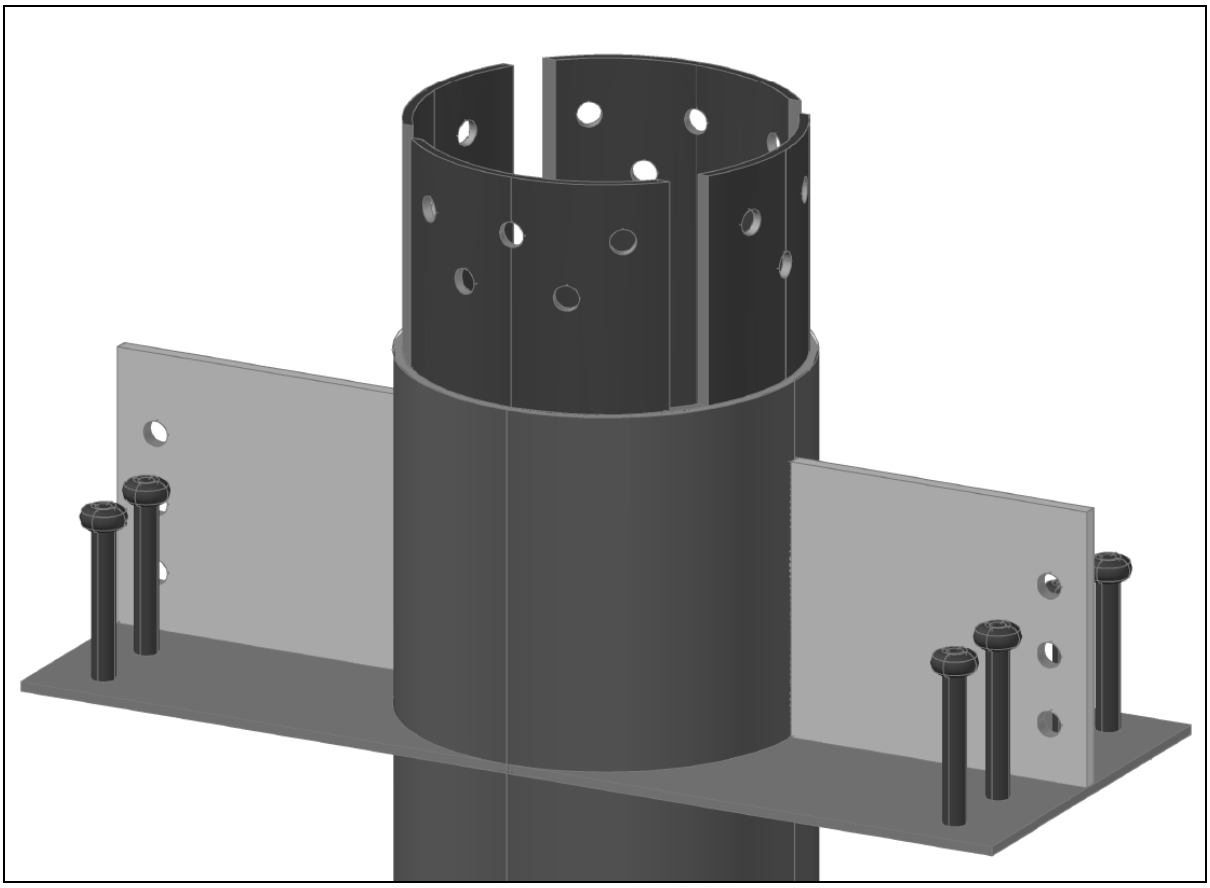

Fig. 7.6: Particular of the Nelson connectors

To connect the bottom and the top column tubes, blind bolts are used since it's impossible to fix the stock cube inside the tube. This kind of bolt increases its dimension during the fastening (see Fig. 7.7).

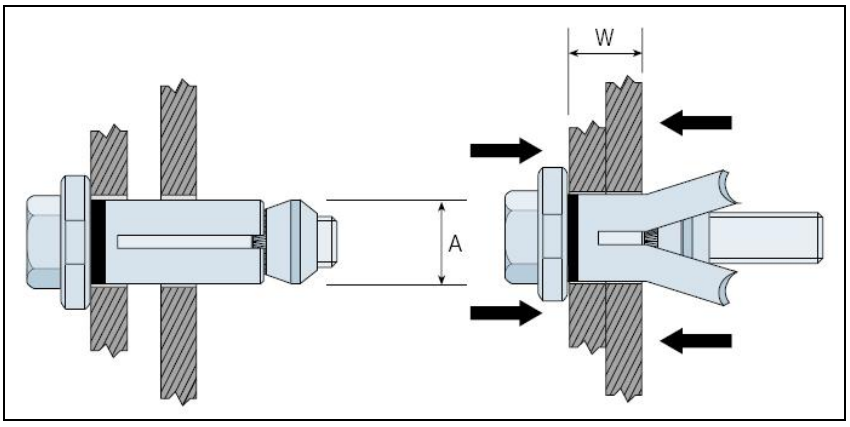

Fig. 7.7: Particular of the blind bolt

Another two construction steps before the concrete cast are shown in Fig. 7.8 and in Fig. 7.9. It can be noticed that the manpower operations needed in site are relatively limited and easy enough to ensure a good construction speed and accuracy.

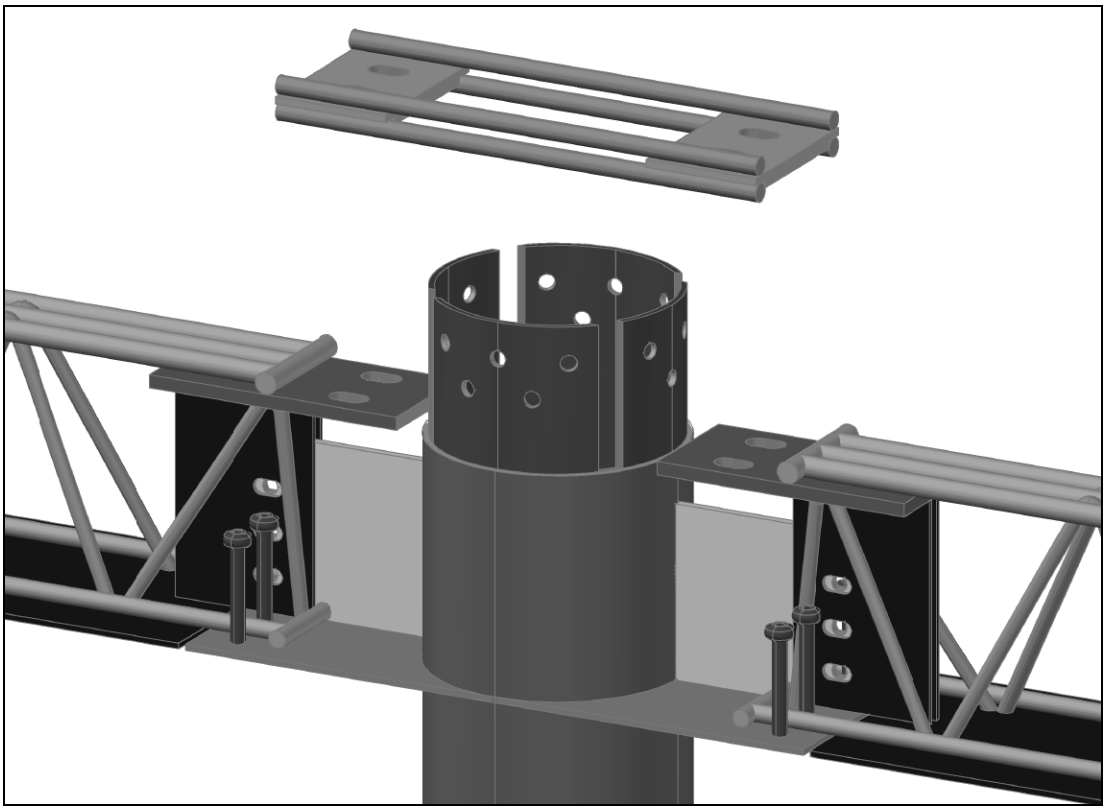

Fig. 7.8: Assembly of the top additional bars

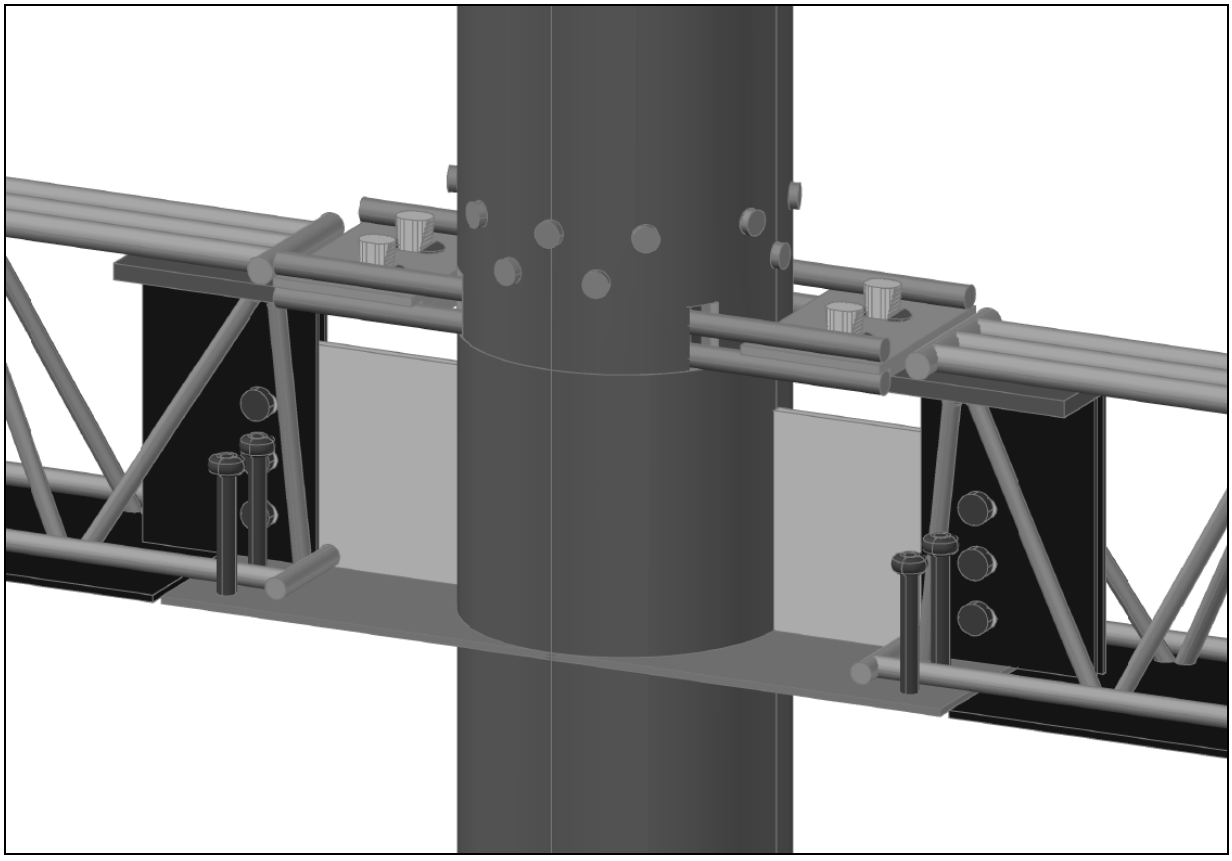

Fig. 7.9: Composite joint before the concrete cast

7.2.3 CSTC beam-CFT column joint design

The composite joint presented has been calculated for the test joint of the RC frame presented in the chapter 2. The frame has four storeys of 3.5 m height and four bays of 4.0 m width.

The first calculations concern the CSTC beams. They can be distinguished in two parts dealing with the first and the second phase. In the first phase, the static scheme is simple supported in correspondence of the connection bolts, while in the second phase the static scheme is that of a continuous beam. The loads are: self weight of the steel truss, concrete cast weight, share of the slab weight, further permanent and variable loads. The assessments are those described in the third chapter. The truss is constituted by:

- top chord of three round bars of 24 mm diameter;
- diagonal bars of two curved round bars of 20 mm with 355 mm step;
- bottom chord of a steel plate of 5 mm x 350 mm section dimension;
- additional bottom chord of two round bars of 24 mm diameter.

The designed sections, for what concerns the steel, are presented in the Fig. 7.10.

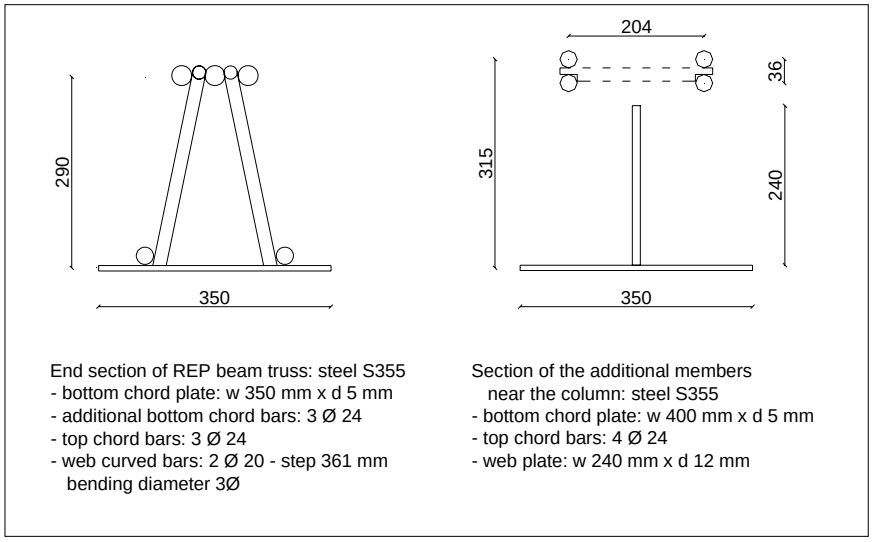

Fig. 7.10: Sections of the beam truss

For what concerns the section close to the column, where the beam truss is substituted by plates and bars, the vertical plate is designed to resist against the shear force. Its section in correspondence of the bolt holes, can be assess with the "shear block" mechanism (see Eurocode 3 [8]), that is characterized by two possible collapse procedures:

- tensile failure along an horizontal line passing through the lower hole and shear failure along a gross vertical line (see Fig. 7.11);

- shear failure along a net vertical line.

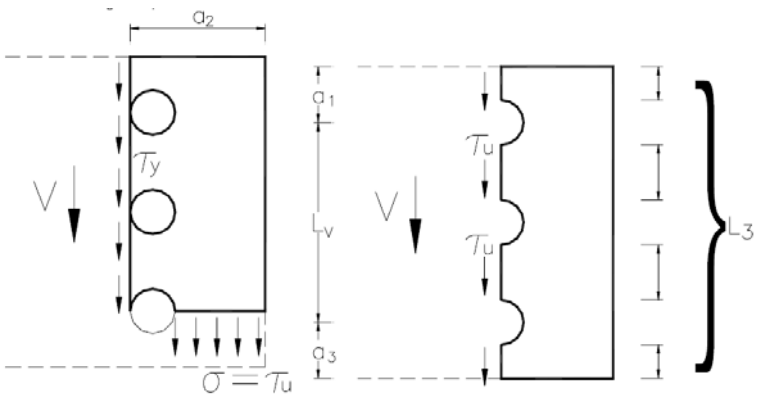

Fig. 7.11: Shear block mechanisms

The column has a steel hollow tube of 350 mm external diameter and of 8 mm thickness. The round tube is completely filled by concrete. To design the column it has been referred to the Eurocode 4 [9]. In the case of bending and compression the M-N resistant domain con be calculated and then reduced for the geometrical non linearity of the whole column (see Fig. 7.12). That domain has been computed according to the appendix C of the Eurocode 4 [9] that proposes a simplified procedure for composite sections with double symmetry. The same procedure has been applied to the section with the holes in correspondence of the connection between consecutive columns. The net area, without the holes, has been considered as an equivalent tube area of the same inner diameter and different thickness than the whole one (see Fig. 7.13).

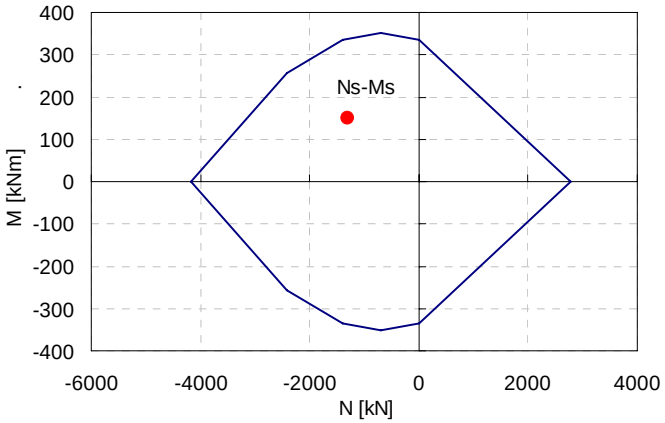

Fig. 7.12: Axial force (N) vs. bending moment (M) resisting domain of the column whole section

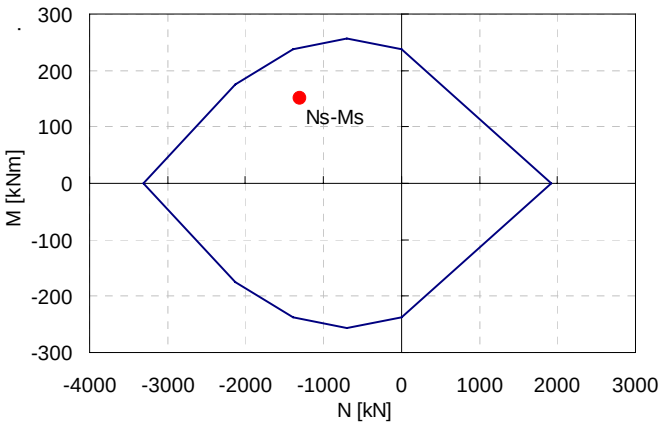

Fig. 7.13: Axial force (N) vs. bending moment (M) resisting domain of the column holed section

After the calculation of the main elements, the other connecting members have been evaluated. For each plate the net area has been considered to compute the resisting parameters. The wedge bolts have been designed as usual bolt. The design class of all the bolts are 10.9 having the following characteristic: the yield strength f_{yb} = 900 MPa and the ultimate strength f_{ub} = 1000 MPa.

The additional bars passing through the joint are aligned with the top chord bars of the beam trusses in order to avoid bending secondary solicitations (see Fig. 7.14). Even if the secondary moments are partially absorbed by the surrounding concrete during the second phase.

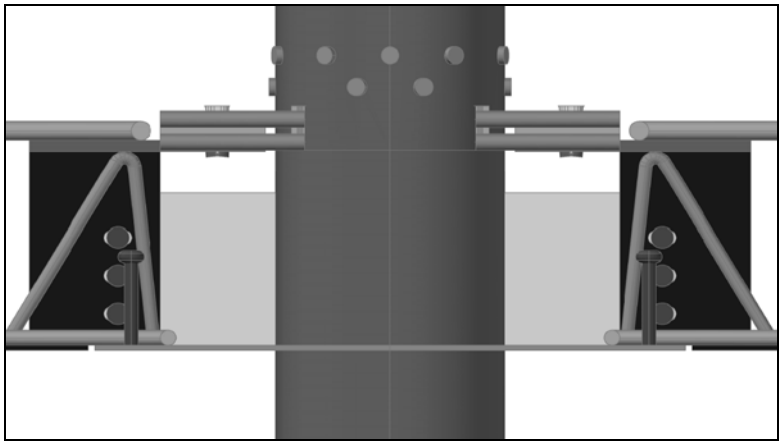

Fig. 7.14: Composite joint profile

For what concerns the Nelson pegs, their function is to let the formation of concrete struts between themselves and the beam supporting hammer. In general, these connectors can be designed by two distinct criteria:

- complete resistance restoration: even in the ultimate limit state the connection yield cannot be reached;

- partial resistance restoration: the connection can yield before the structure ultimate limit state and its ductility shall be verified.

The choice, for the case in exam, is the complete resistance restoration and four Nelson pegs are necessary (see Fig. 7.6).

7.3 Numerical analyses

7.3.1 Numerical model

After the design, the composite joint has been verified by means of a finite element numerical analysis using the code MIDAS FEA [10]. Truss, shell and brick elements have been used to define the model. The truss element has only two nodes and has only axial stiffness. The sectional area is considered constant along its length. The four node shell element can be submitted to in plane and out of plane solicitations. Every node has 5 degrees of freedom, three displacement and two rotations. The thickness of each element is considered as constant. The brick element used was esaedric with eight nodes and the shape functions are quadratic. The iteration scheme used is Newton-Raphson.

The yield criterion for the steel is the Von Mises one which considers the deformation energy of the deviatoric part of the stress tensor. This criteria has a cylinder yield surface on the principal stress space and the cylinder has the directrixes parallel to the first octant trisetrix and an elliptic section. The yield surface can be defined by the value of the steel yield strength.

For what concerns the concrete it has been used the smeared crack model with the fixed crack method. The compressive and the tensile constitutive laws have been assumed according respectively to the Thorenfeldt [11] and Hordijk [12] models.

The complexity of the geometry requires a three dimensional model. In fact some particulars, like the connection between the bottom plate and the circular column, are difficult to simplify in a two dimensional model. The truss finite elements have been used to create the steel truss (see Fig. 7.15). For the top chord, the actual bars have been schematized by one with equivalent diameter. In the figure it can be noticed that four truss elements have been used to model the Nelson pegs connection between the truss bottom steel plate and the joint bottom horizontal plate.

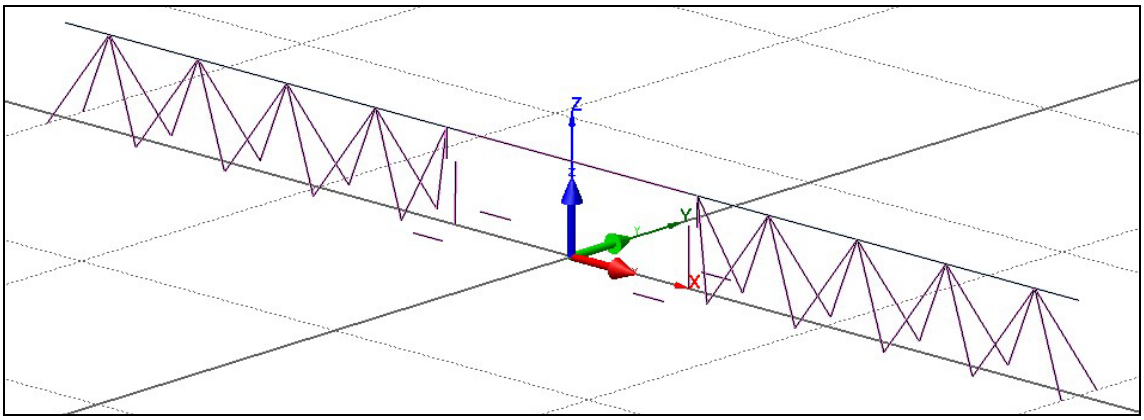

Fig. 7.15: Truss elements in the joint model

All the steel plates have been modelled by shell finite elements (see Fig. 7.16). Even in this case the mesh has been created after having imported a CAD draw in the FEM program.

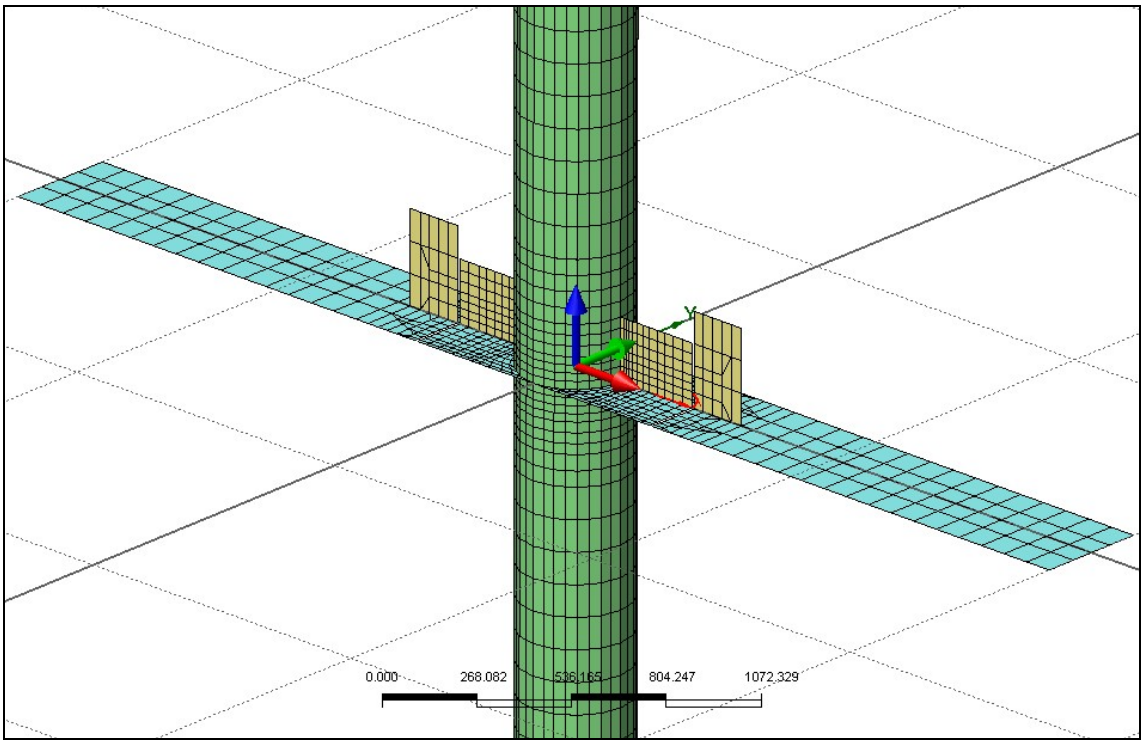

Fig. 7.16: Plate elements in the joint model

The eight node brick elements have been used for the concrete material both in the beams and in the columns (see Fig. 7.17). The consistency between the nodes of the truss, the shell and the brick elements is respected everywhere with the exception of the additional steel members passing through the column. The additional truss top bars are very close to each other and their sectional area is relatively large respect to their external surface within the joint. Because of these reason the bond between them and the surrounding concrete cannot be efficient especially after load cycle reversals. Thus it has been modelled the worst

case, that is the absence of that bond. Since a similar conclusion can be drawn for the vertical additional plate, even this element are modelled as detached from the column concrete.

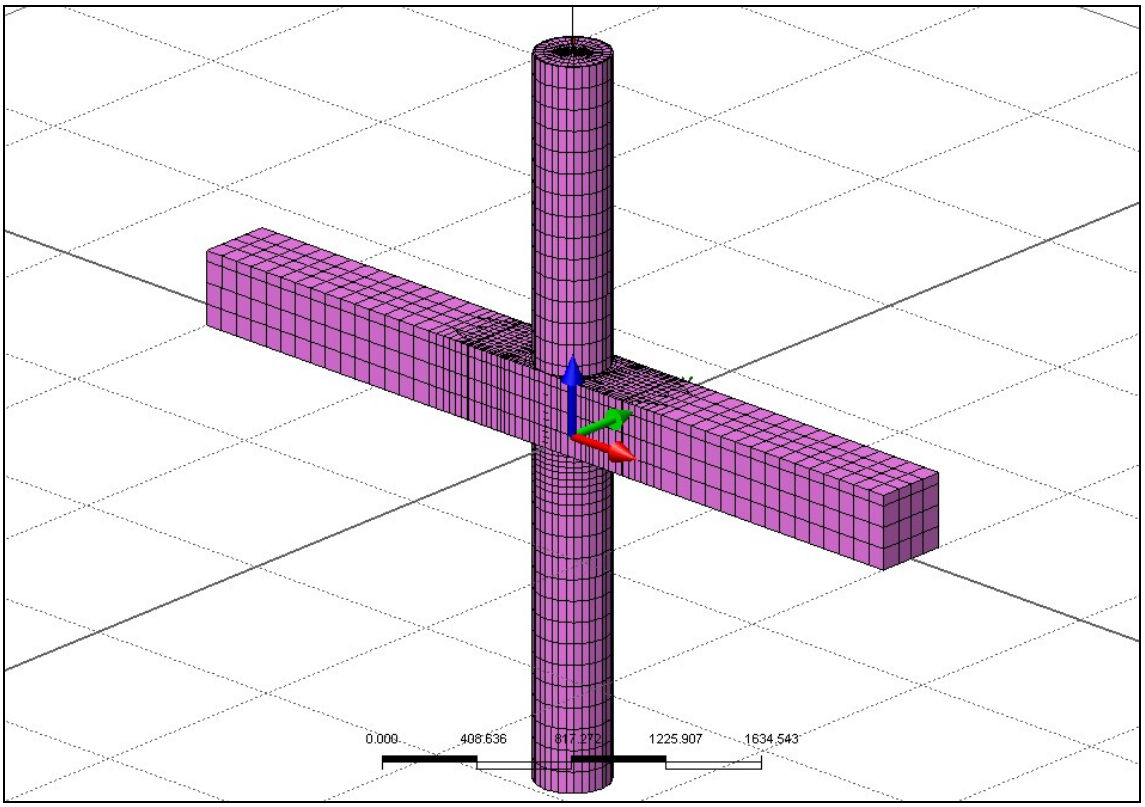

Fig. 7.17: Brick elements in the joint model

The extremity sections of beams and columns have been constrained to remain plane with the use of rigid link. To simulate the behaviour of the connection bolts, particular kind of link element has been applied in such a way they can exert only shear stiffness (see Fig. 7.18).

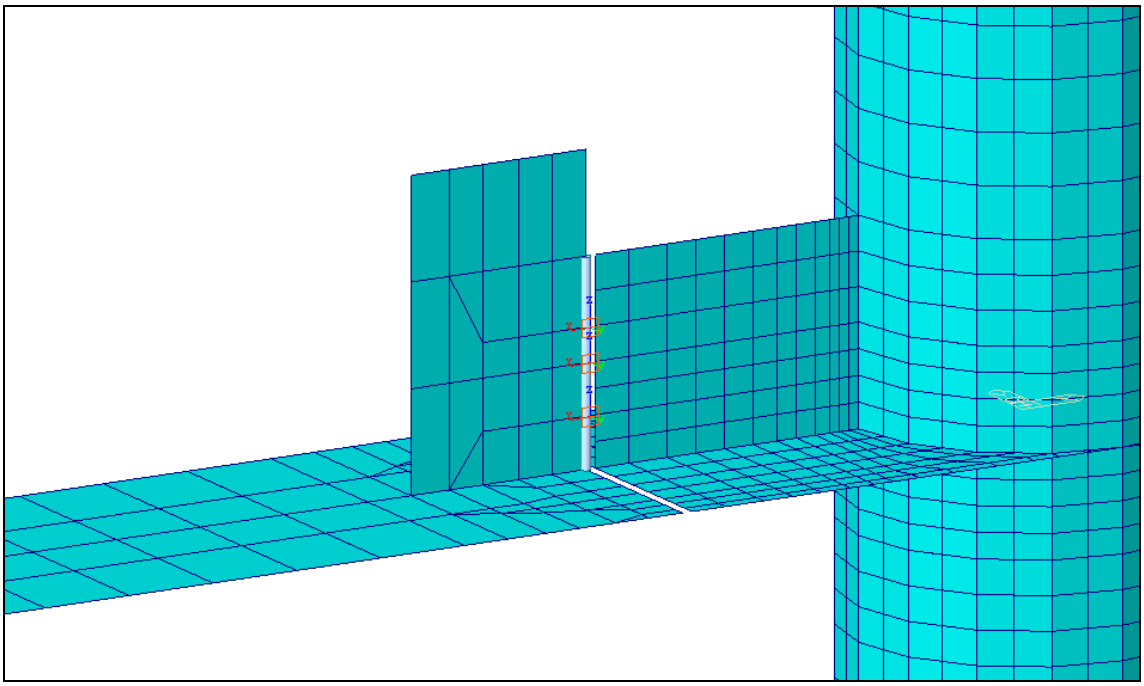

Fig. 7.18: Bolt simulation by means of link elements

The same test joint static scheme defined in chapter 5 is used here. The applied displacement at the column top section is composed by three reversed cycles up to the displacement of 100 mm that is the 3% of the interstorey height (see Fig. 7.19). The column is subjected to a constant axial compression load equal to -700 kN.

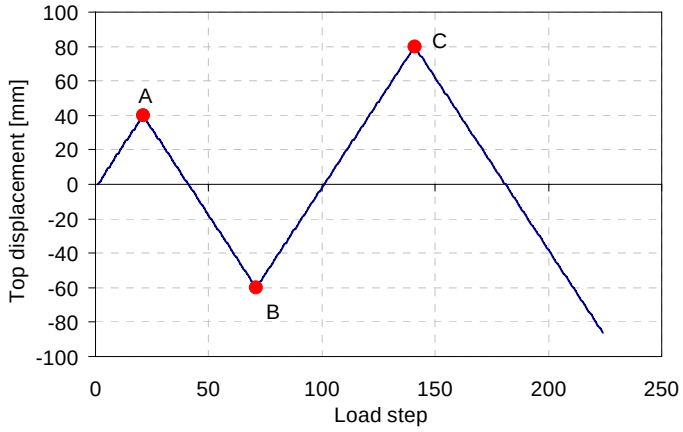

Fig. 7.19: Applied top displacement history

7.3.2 Analysis results

In this section the analysis results are presented. The top displacement has been applied as a quasi-static load by means of a non linear static analysis with the convergence criterion of the Euclid norm of the displacements.

After 40 mm of top displacement during the first cycle, the deformed shape shows that

the two beams are more bent than the column which remains more straight (see Fig. 7.20).

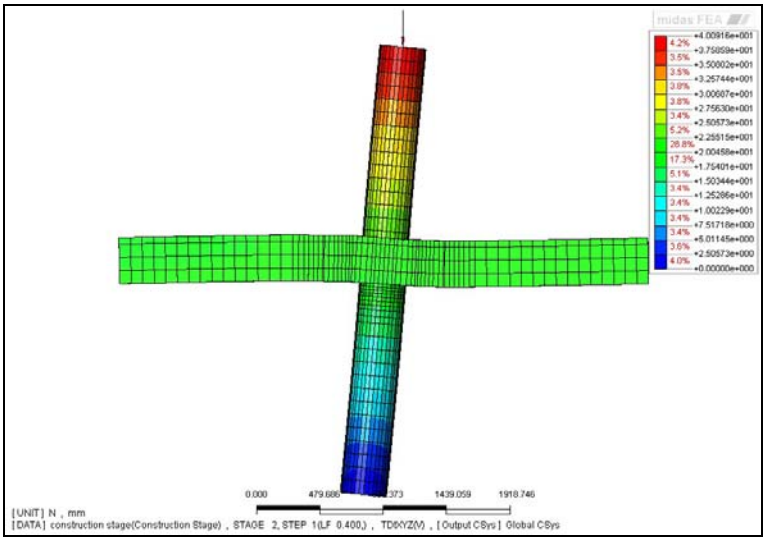

Fig. 7.20: Deformed shape at +40 mm of top displacement

From the truss element stress diagram, it can be noted that the bars remained elastic (see Fig. 7.21). The additional top bars maintained a nearly constant tensile stress crossing the joint, because of the bond absence. The same bars have a relatively high tensile stress, because of the concrete fractures after reaching its low tensile strength.

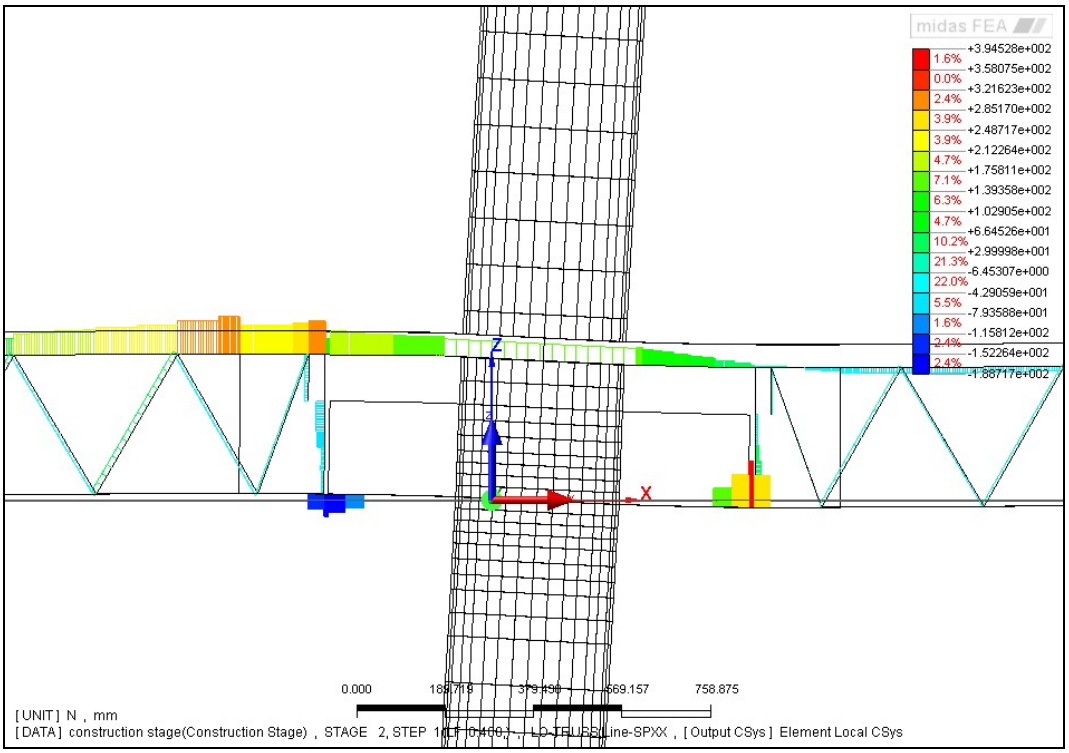

Fig. 7.21: Truss stress diagram

The bottom plates of the trusses show a local plasticization more noticeable in the

tensile parts (see Fig. 7.22). This is emphasized in the model by the truss elements that model the peg connection and induced high concentrated stresses. But even in the designed joint, the Nelson pegs can produce concentrated stresses in the bottom additional plates. Even the additional bottom bars of the steel truss, that constitute the support of the beam during the first phase, are subjected to high stresses since their section is quite smaller than the section of the bottom chord plate of the beam truss.

The stresses along the longitudinal beam axis of the truss bottom plate are depicted in Fig. 7.23. The tensile and compressive bottom plates are already yielded after this first quarter of cycle.

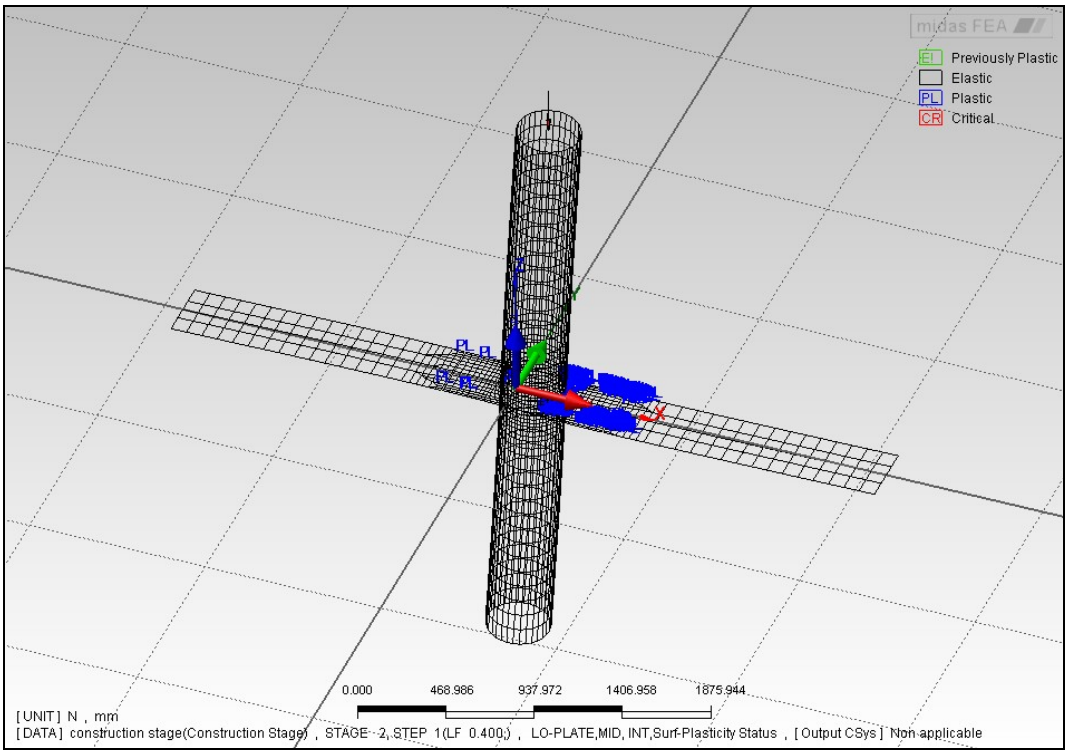

Fig. 7.22: Yielded points of the bottom plates

The horizontal normal stresses of the vertical additional plate are shown in Fig. 7.23. Even for that plate we assumed the absence of friction between the steel and the concrete within the joint. The part of the plate within the joint region has higher stresses because of the interruption of the bottom additional plate. The following Fig. 7.24 depicts the contour of the tangential stresses of the same vertical plate. Their values are considerably high because the plate sustains the joint shear force. This is a different resisting mechanism respect to the reinforced concrete joint in which the shear force is decomposed in compressive and tensile components sustained respectively by the concrete and the steel.

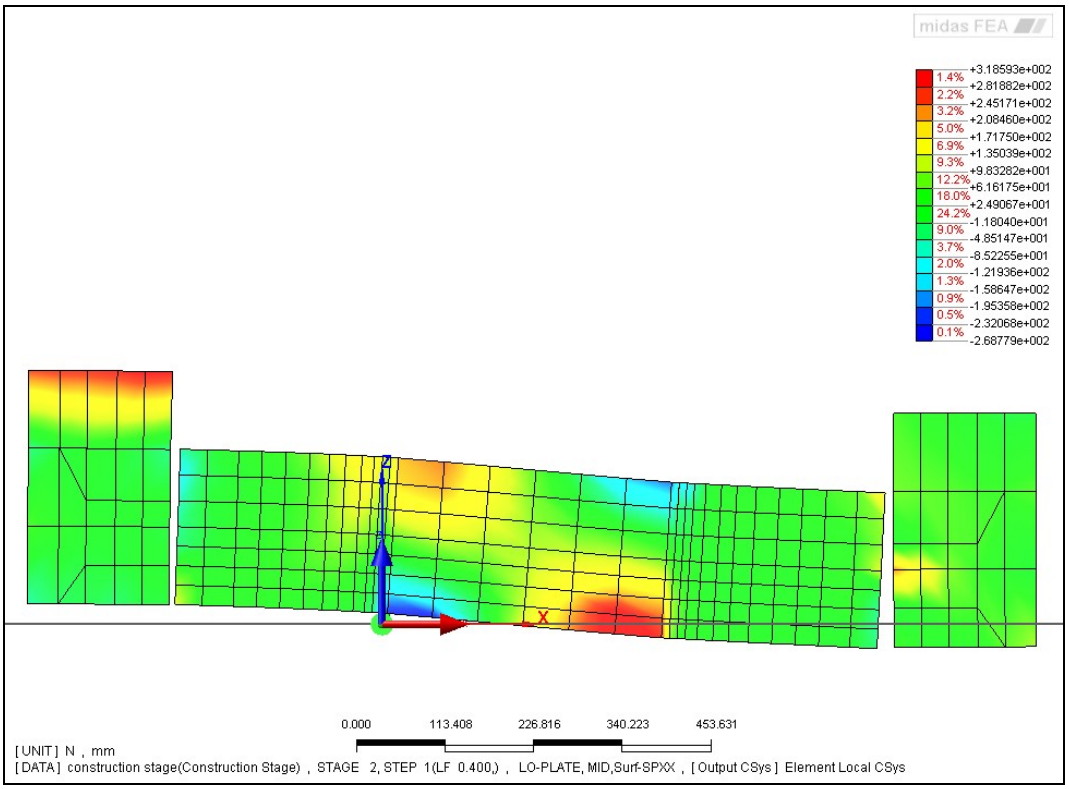

Fig. 7.23: Horizontal normal stress diagram of the vertical plate

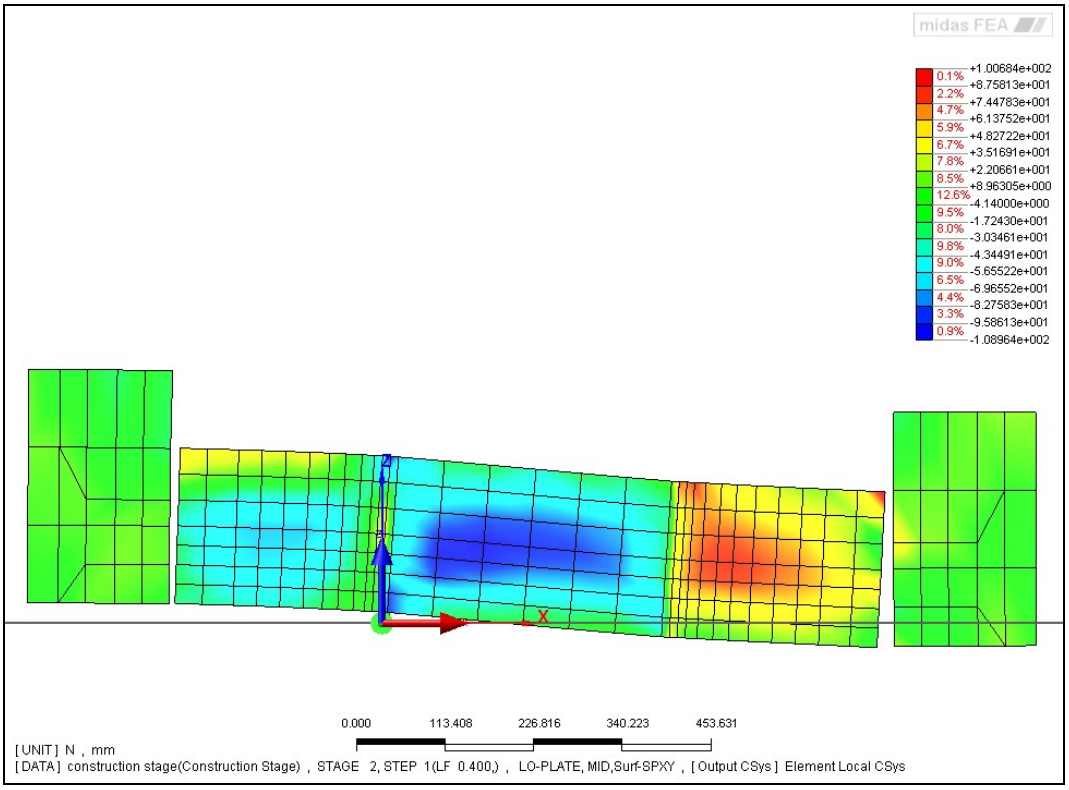

Fig. 7.24: Tangential stresses diagram of the vertical plate

Analyzing the stress state of the Gauss points of the concrete elements, it is possible to

know which ones reach the tensile strength and where cracks can be expected (see Fig. 7.26). The fully open cracks are concentrated in the tensile part of the beam faces near the joint. For instance, the beam subjected to the negative bending moment, that stretches the top section fibres, has a concentration of high tensile strain near the interface between the concrete element and the column steel tube.

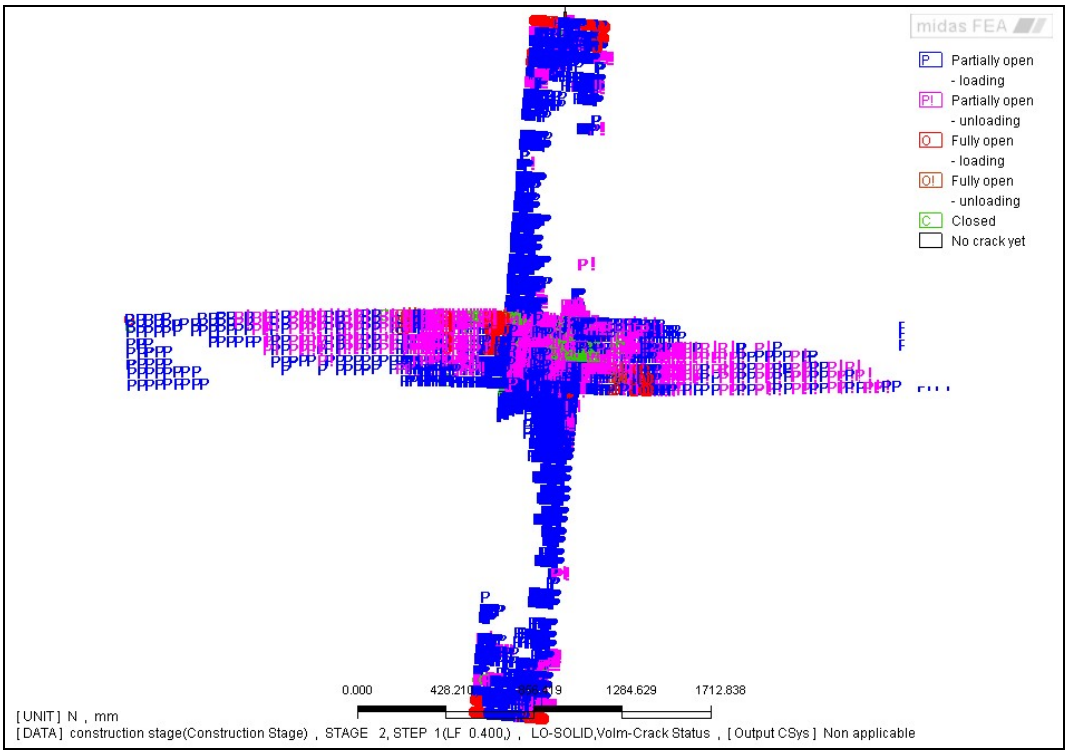

Fig. 7.25: Cracking state of the brick Gauss points

Following the load path, the column is unloaded and then loaded in the other direction until the top displacement reaches -60 mm. In this condition the deformed shape is shown in Fig. 7.26. Amplifying the displacement multipliers the higher stiffness of the column respect to the beam one can be clearly seen.

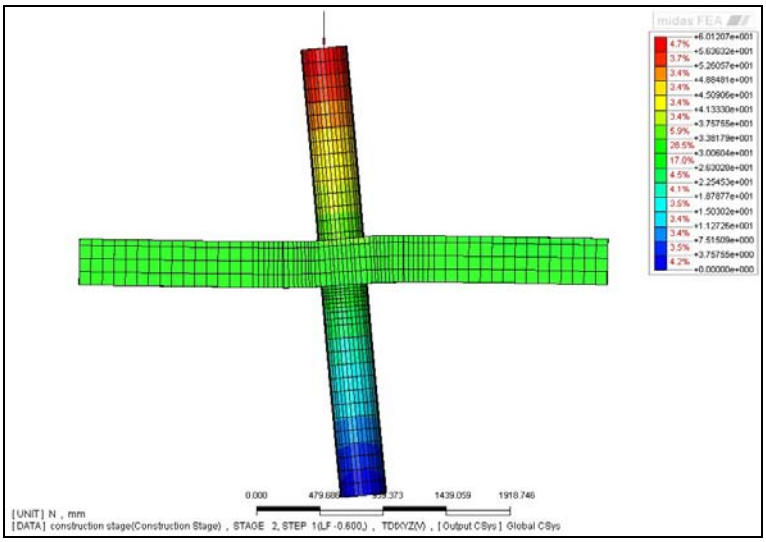

Fig. 7.26: Deformed shape at -60 mm of top displacement

After the reversion of the applied load the steel truss bars have the stresses shown in Fig. 7.27. The top bars within the joint are tight as expected since they cannot pass stresses on the column concrete. The tensile stresses of the same bars are a little lower than their elastic limit.

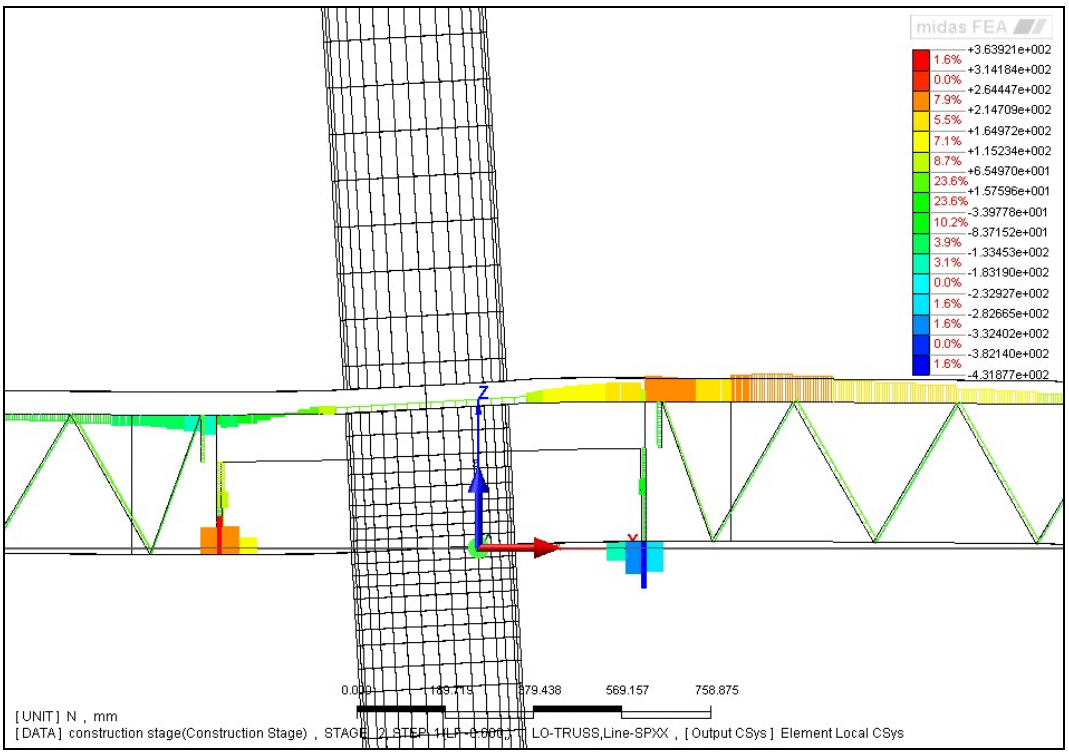

Fig. 7.27: Truss stress diagram

The bottom steel plate are yielded both in tension and compression near the joint (see Fig. 7.28). The tensile yielded region progresses along the beam further than the compressive one.

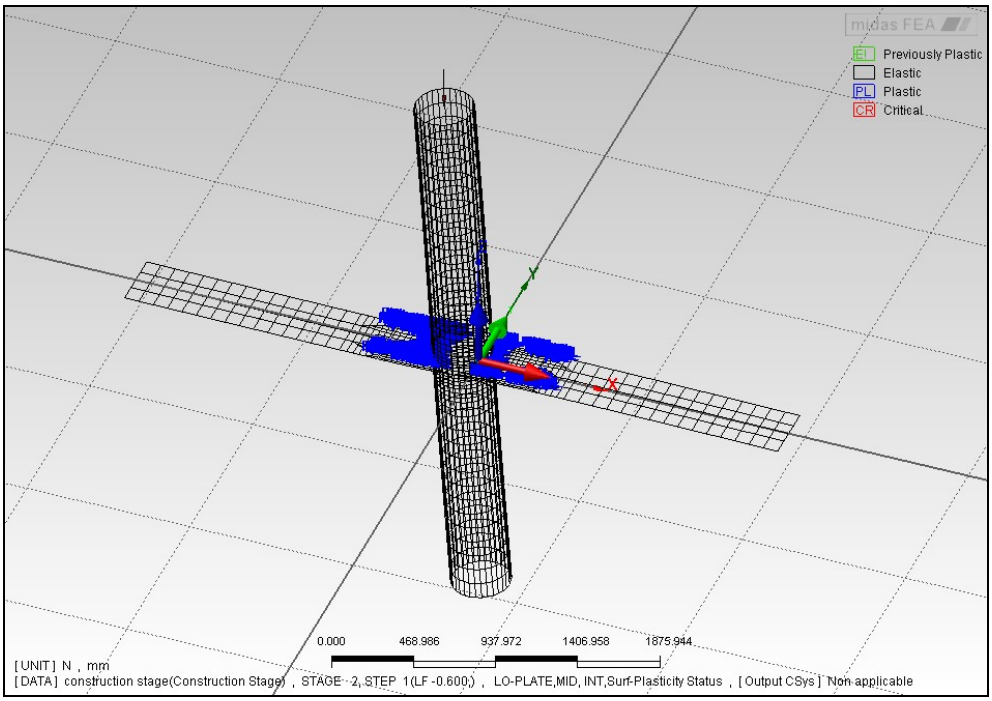

Fig. 7.28: Yielded points of the bottom plates

The horizontal normal stress contour of the vertical plate is depicted in Fig. 7.29. The stresses, increased in absolute value, change in sign and their distribution is almost opposite respect to the previous case. The plot of the vectors representing the compression principal stresses is presented in Fig. 7.30.

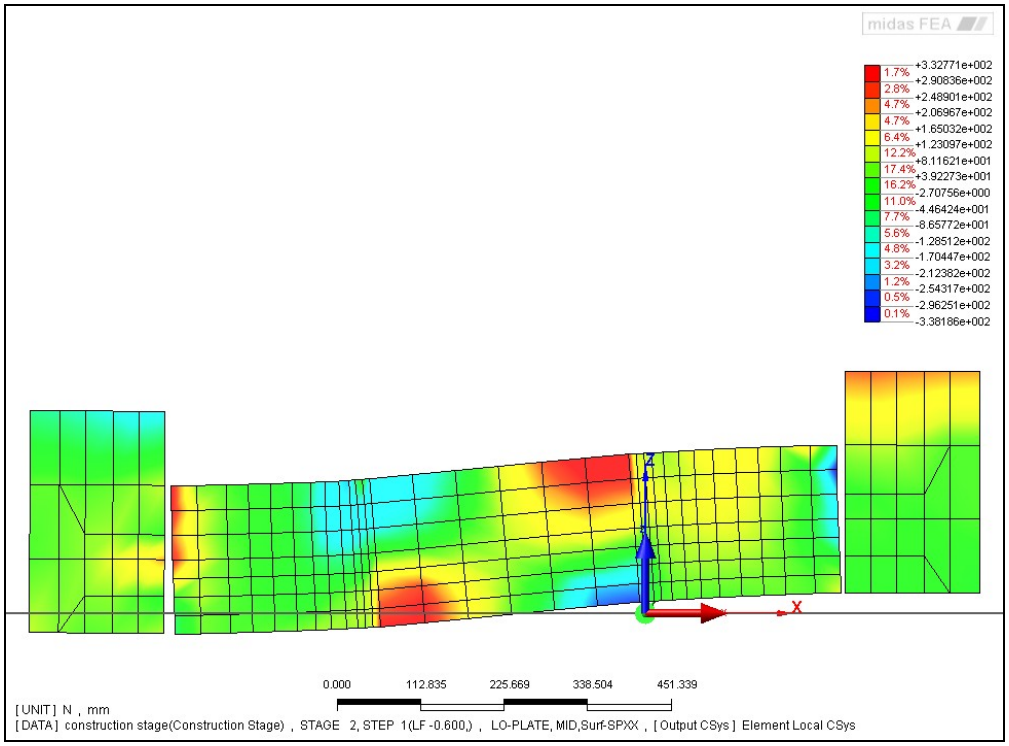

Fig. 7.29: Horizontal normal stress diagram of the vertical plate

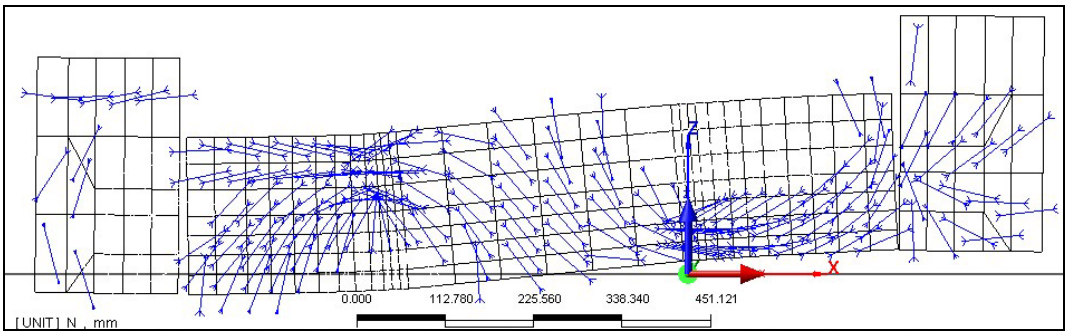

Fig. 7.30: Compressive stress vectors of the vertical plate

The consequence of the concrete stress state is summarized Fig. 7.31, where the formation of new cracks can be seen as the closure of some of the previous ones. A wide region on the upper part of the right beam has very high tensile strains.

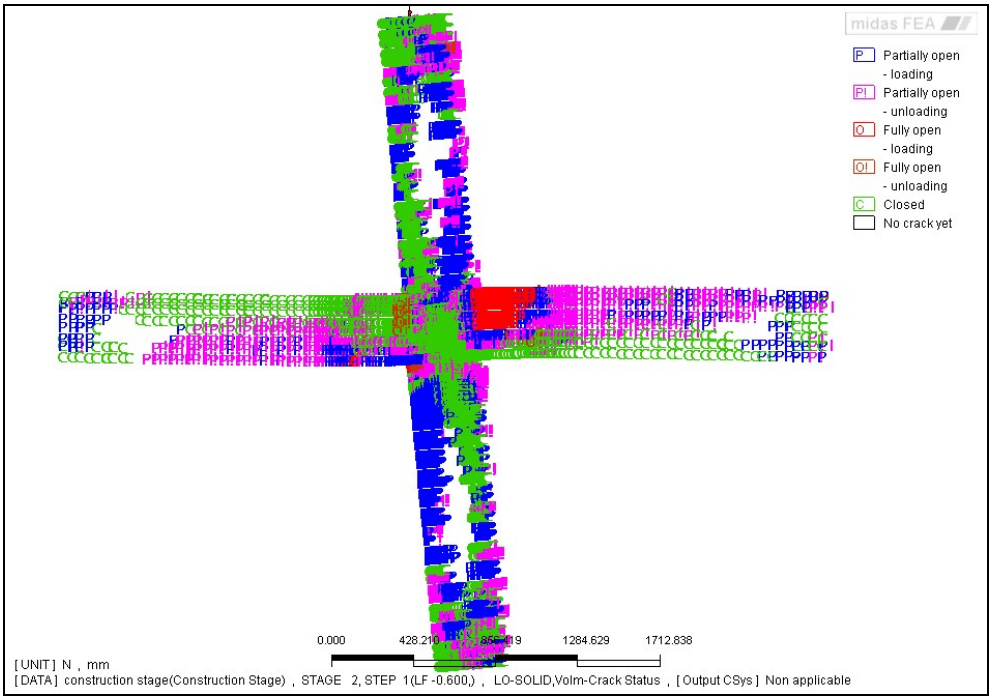

Fig. 7.31: Cracking state of the brick Gauss points

When the top displacement is reversed (+80 mm) the deformations and the stress patterns are inverted (see from Fig. 7.32 to Fig. 7.35). The top chord bars are yielded in tension and near the other face the bottom steel plate is deeply yielded. In this condition, two plastic hinges develop at each side of the joint. The stiffness of the joint is far reduced and the base shear increases very slowly. This fact can also be noted from the stresses of the vertical plate that are very close, although opposite in sign, to those of the minimum top displacement.

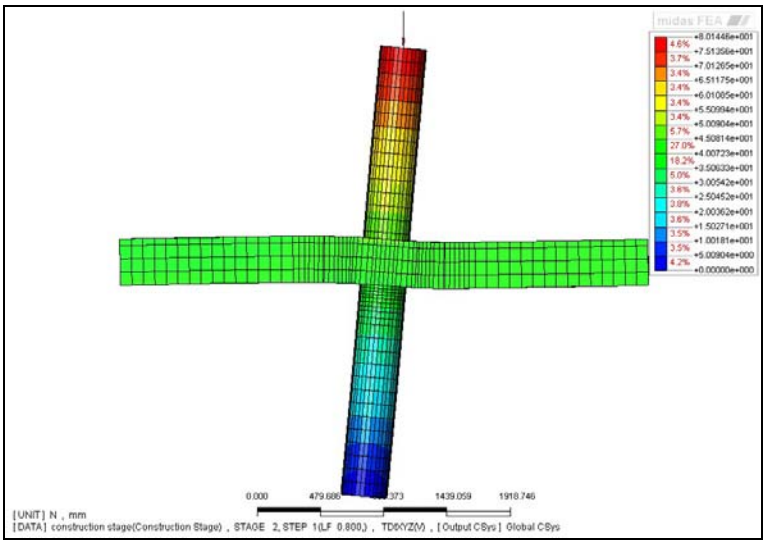

Fig. 7.32: Deformed shape at +80 mm of top displacement

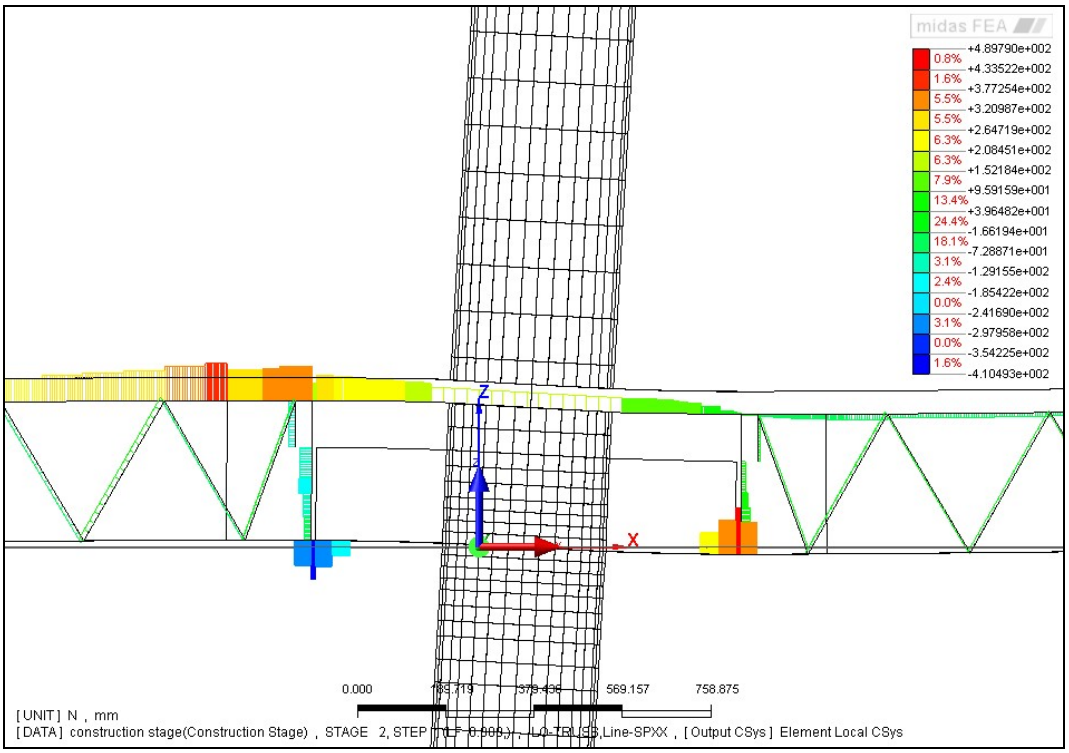

Fig. 7.33: Truss stress diagram

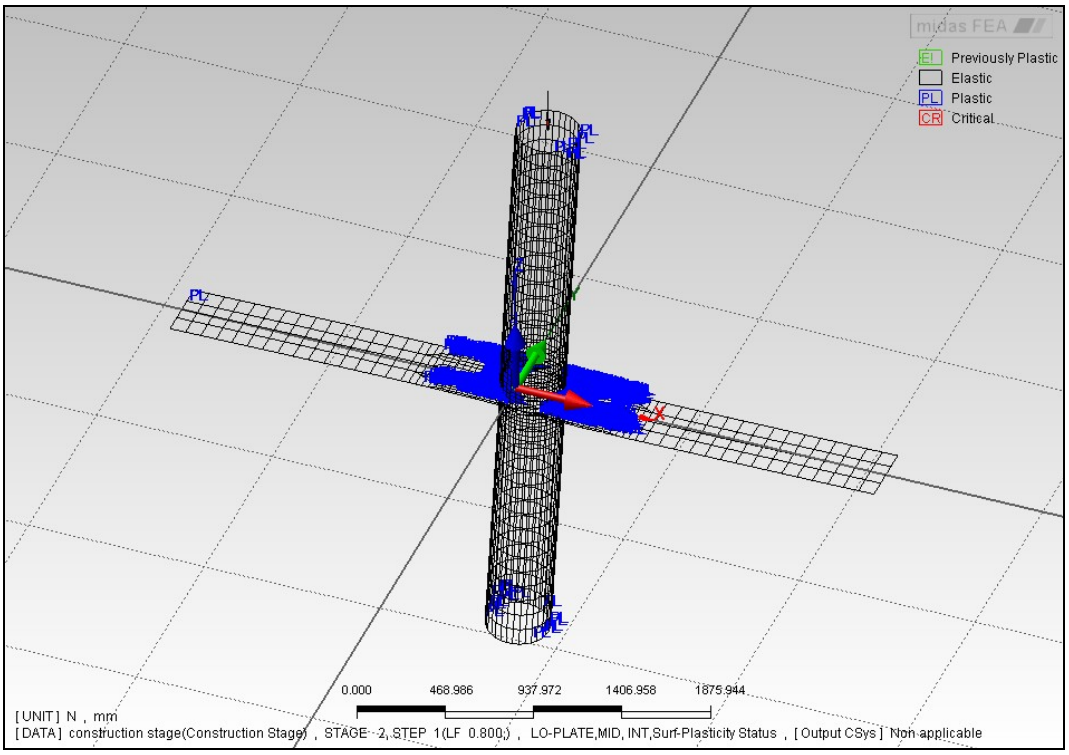

Fig. 7.34: Truss bottom plate stress diagram with yielded points

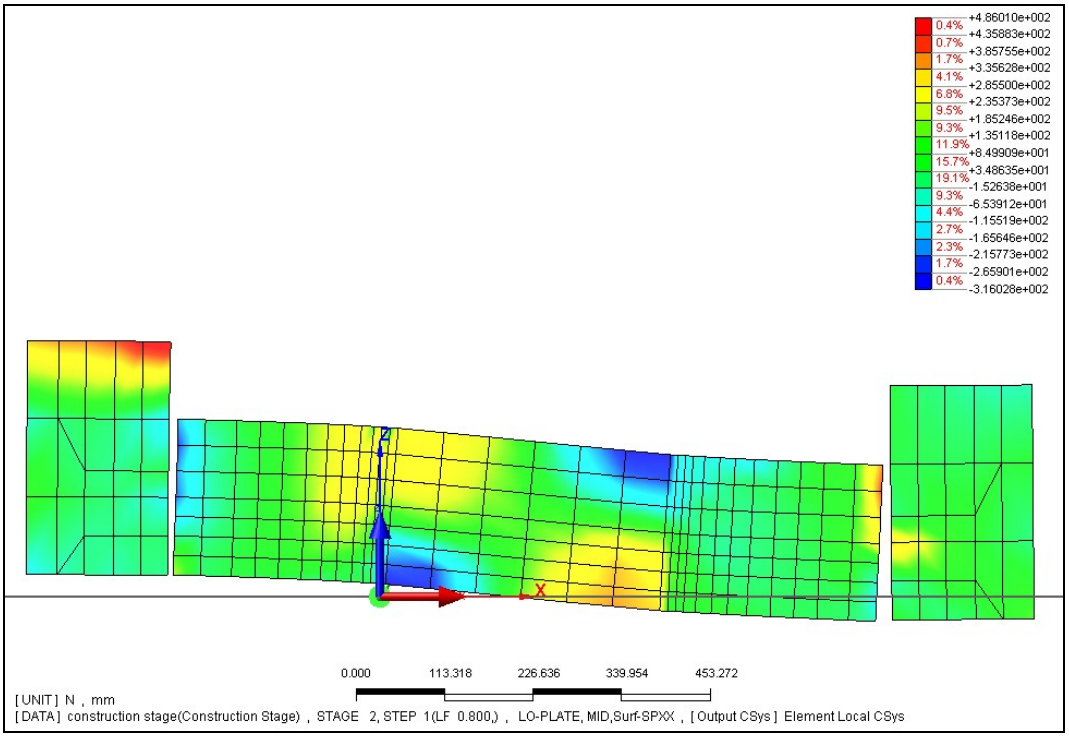

Fig. 7.35: Horizontal normal stress diagram of the vertical plate

The base shear force vs. the top displacement diagram is depicted in Fig. 7.36. After the first cycle the distinction between the elastic and the plastic range becomes more evident. The maximum base shear is about 160 kN in correspondence to a top displacement equal to

80 mm. After the load cycle reversals the stiffness and the strength of the joint decrease. When the top displacement of -85mm is imposed the program cannot converge because of the widespread damage. The final drift is about 2.5% that is lower of those had with the CSTC joints analyzed in the previous chapter.

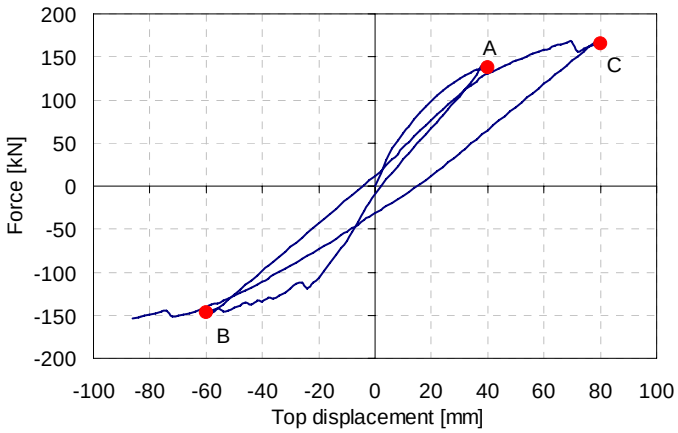

Fig. 7.36: Applied shear force vs. top displacement diagram

The deformation energy is calculated as the integral of the previous graph and it's presented in the next Fig. 7.37. It can be noticed that the joint has an high release of elastic energy during the unloading phases.

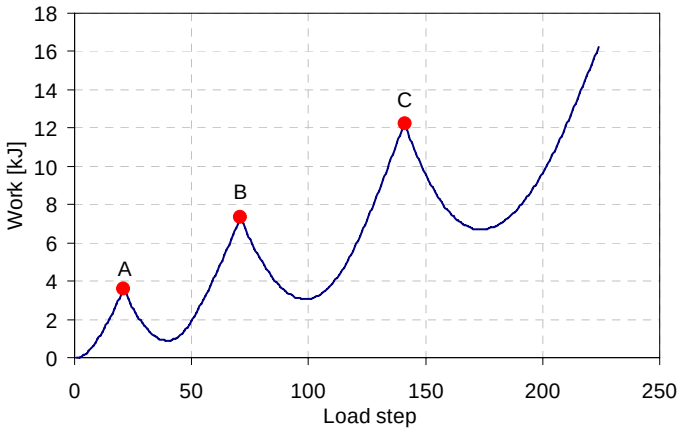

Fig. 7.37: Displacement energy diagram

7.4 Conclusions

An innovative composite beam-column joint has been studied. The joint connects composite steel truss and concrete beams and concrete filled steel tube columns. The main concept of this joint is to conserve the continuity of the column steel tube between one storey and the following one by means of blind cold connection. Some joint additional

elements, which passes through the joint to restore the beam continuity, have been proposed: the top horizontal bars and a vertical steel plate. Furthermore the lower beam plate is bolted together with an additional one welded to the external surface of the column steel tube. The connections, that require little manpower work in the construction site, are only normal, blind and welded bolts to reduce the number of operations and the working time. The concrete cast inside the column steel tube can be continuous thanks to the avoidance of any interruptions crossing the beams. The number of holes in the column steel tube is reduced to the minimum. The resulting joint is a special kind of composite steel and concrete structure in which the steel and the concrete collaborate to sustain the solicitations. In particular the joint shear force is supported by the additional vertical plate that crosses the joint.

The assessment of the joint has been made using the Eurocode 3 and 4. The verification of the joint behaviour has been done by means of numerical analyses. The FEM program MIDAS FEA has been used with different modelling solutions. Increasing the displacement amplitude, the numerical analyses by convergence problem dealing with the softening behaviour of the concrete material. The joint shows a good initial stiffness and strength even if the additional members, that cross the joint. After load cycle reversals the stiffness decays as expected because of the absence of bond within the column. Nevertheless the results show a good deformation capacity and joint strength. The novel joint can be profitably proposed for future experimental tests in order to verify the numerical results in sight of a possible application in medium-low seismicity regions.

References

1. Park JW, Kang SM, Yang SC. Experimental studies of wide flange beam to square concrete-filled tube column joints with stiffening plates around the column. *ASCE Journal of Structural Engineering* 2005, **131**: 1866-1876.
2. Swanson JA, Leon RT. Bolted steel connections: tests on T-stub components. *ASCE Journal of Structural Engineering* 2000, **126** (1): 50-56.
3. Leone S. *Sismirep Patent*, Brevetto d'invenzione, Italy, 1990.
4. Leone S. *Sismirep Patent*, Brevetto d'invenzione, Italy, 2002.
5. Di Marco R. Sperimentazione su travi continue REP con traliccio tipo TR (Experimental tests on hyperstatic REP beams with TR truss type). *Internal Report University IUAV of Venice*, 2004.
6. Sassone M, Bigaran D, Massa S. Le travi composte nel nuovo quadro normativo (The composite beams in the new code framework). *XVI CTE Congress*, Parma, 2007, 715-723.
7. Petrovich F. Un nuovo sistema strutturale per edifici multipiano in zona sismica realizzato mediante elementi tralicciati misti acciaio-calcestruzzo: analisi numerica e sperimentale (A new structural system for multi-storey building in seismic zone made by composite steel truss and concrete elements: numerical and experimental analyses). Ph.D. Thesis, University of Trieste, 2008.
8. CEN. *Eurocode 3: Design of steel structures Part 1-1: General rules and rules for buildings.* Comité Européen de Normalisation: Bruxelles, 2003.
9. CEN. *Eurocode 4: Design of composite steel and concrete structures Part 1-1: General rules and rules for buildings.* Comité Européen de Normalisation: Bruxelles, 2004.
10. MIDAS FEA, Advances Nonlinear and Detail analysis program. *Analysis reference*, 2008.
11. Thorenfeldt E., Tomaszewicz A., and Jenen JJ. Mechanical properties of high strength concrete and application in design. Proceeding Symposium, *Utilization of High Strength Concrete*, Tavanger, Norway, 1987.
12. Hordijk DA. *Local approach to fatigue of concrete*. Ph.D. Thesis, University of Delft, 1991.
13. Ricles JM, Peng SW, Lu LW. Seismic behaviour of composite concrete filled steel tube column-wide flange beam moment connections. *ASCE Journal of Structural Engineering* 2007, **130**: 223-232.

Chapter 8

Conclusions

The Composite Steel Truss and Concrete beams are composed by prefabricated steel trusses embedded in cast in place concrete. The main features of the steel trusses are that they can bear their own weight and the weight of the slabs without any provisional support during the first phase and then they can collaborate with the cast in place concrete. The recent Italian Code DMLLPP 14/01/2008 mentions the composite steel truss and concrete structures in the paragraph 4.6 that is under "*other material constructions*". It establishes that the use of this typology requires the authorization of the Italian Superior Council of Public Works and it doesn't contain any other specification. The CSTC type isn't included in any other existing construction type of Italian or International Codes and it needs particular design rules. The new research aims are the verification of their efficiency, the development of a reliable calculation method, the application of the composite steel truss beams for seismic resistant frame and the design of a joint with all the necessary good seismic performance requirements and also with the further characteristic of being easy to assemble.

Firstly it has been focused on the reinforced concrete seismic resistant frames in order to fully understand the solicitations they have to withstand and to underscored all the characteristics that can determine their behaviour in terms of stiffness, strength and ductility. In the framework of continuum damage theory, a new two-parameter damage model for concrete has been proposed. In particular, a new concrete compressive damage evolution law has been developed to evaluate the effect of confining reinforcement in RC structure better. With the aim of describing, in a unitary approach, the steel behaviour, specific steel damage indexes have been formulated, taking into account the plastic strain development and the possibility of rebar buckling. A new methodology to estimate the critical buckling load has been formulated, which turned out to be in good agreement with experimental results. An

improved and generalized definition of the global damage indexes has finally been proposed, in order to obtain powerful tools to estimate the performance and the state of a RC structure. The improved model has been implemented into a fibre research FEM code, which has been used to carry out nonlinear analyses of tests examples and of a RC concrete frame structure. In particular, the reliability of the model has been demonstrated by comparison with trusted experimental tests on RC column axially loaded and subjected to imposed transversal displacements, some of which had presented the rebar buckling. The static and dynamic nonlinear analyses of two RC frames, respectively one designed in high ductility class and one with weak-columns at the ground floor, have been carried out and the model has demonstrated its ability to describe the dynamic behaviour, the failure mechanism and the energy dissipation of both frames efficiently and accurately. In particular, the GDIs have demonstrated that they can interpret the development of the overall structural decaying correctly. The contour maps of SDIs have made it possible to evaluate the damage distribution all over the structure. The two RC frames investigated with the fibre approach have been studied with a concentrated plastic hinge approach as suggested by FEMA 356. A clear correlation between the GDIs here proposed and the Performance Level proposed by FEMA has been demonstrated for the test examples. Even though more analyses and comparisons have to be performed, especially with regard to existing buildings, the method proposed here appears to be a tool that could be used profitably for the structural seismic safety assessment, when distributed non linear models are employed. Further efforts have to be spent to extend the proposed approach in three-dimensional codes and to keep into account failure mechanism of the beams related to shear and torsion solicitations, as well as to failure of anchorage.

Then the CSTC beam mechanics have been deeply studied. Because of the lack of Italian or International Standards, the calculation methodology of the CSTC beams has to be deposited at the Italian Superior Council of Public Works by each patent owner and producer. The original calculation method of S. Leone had been developed under the Admissible Stress assessment method in the 60's. Starting from it, the CSTC beam mechanics have been analyzed and a new calculation method has been proposed as an improvement and an extension of the original one for what concerns the more wide applicability and the Limit State assessment method. Particular attention has been paid to define and correlate every Ultimate and Serviceability Limit Sates to the beam performances. The hardening of the completion concrete cast distinguishes two phases in the life of the CSTC beam that are characterized by distinct resistant sections and different mechanics. During the first phase the beam behaves as a prefabricated steel truss. In the second phase the steel truss collaborates with the hardened concrete. The mechanics of the CSTC beam have been studied for the first and second phases. More specifically the first phase truss has

only positive bending moments, whereas the second phase composite section is submitted to positive and negative bending moments that have been studied separately. For what concerns the ultimate limit states of a CSTC beam, it has been proposed an assessment method for: resistance of critical cross-sections (maximum bending moment, maximum vertical shear, supports, etc.), resistance of lateral-torsional buckling, resistance to longitudinal shear. In terms of the serviceability limit states other verifications have been suggested to check the stresses, the deformations and the concrete cracking.

The developed method has been used to predict and analyze the experimental tests carried out in the Department of Construction and Transportation of the University of Padua. Three sets of experimental tests, conduced on composite steel truss and concrete beams, have been presented and their results analyzed. In particular eight REP®-NOR beams, six ECOTRAVE® RAFTILE® and two PREREP® beams have been designed and tested. The global deformability, the bending and the shear resistant mechanisms, the global ductility, the cracking phenomena have been studied. The results have been compared to those obtained by means of the calculation method presented in the previous chapter. The beam mechanics have been confirmed and the method has demonstrated to be efficient and precise to assess the behaviour of the CSTC beams even with very different and innovative solutions. The experimental results have demonstrated the efficiency of the proposed design method and the interesting features of the studied structural type like its strength and ductility properties. Furthermore thanks to the test campaign, some general considerations on the global behaviour of the CSTC beams have been drawn. The resistance of the nude truss demonstrated to be conditioned by local failure like buckling and bar fracture. If on a hand this kind of mechanisms can be recognized only with an accurate model of the real beam, on the other the construction detail of the beam itself is very important. The welding detail, designed according to the S. Leone production rules demonstrated to be accurate since they behaved adequately in each test. Particular attention should be paid in the assembly of the steel truss limiting the eccentricities and the bending diameter for the diagonal bars. For what concerns the composite behaviour, a good ductile behaviour can be obtained by an adequate design of the steel truss and of the concrete resisting section. The shear behaviour showed particular characteristic, different from both the usual RC behaviour and the composite steel and concrete one, since it can be heavily conditioned by the shear concrete and steel resistant mechanisms. In a CSTC with the bottom steel plate the shear crack can open quite soon respect to the maximum shear resistance. This drawback seems to be overcome in the CSTC with the pre-compressed concrete base.

Then, the reinforced concrete joint mechanics have been exposed, recalling the main theory and their recent development. Two resistant mechanisms have been evaluated, the concrete strut one and the diagonal compressed field or truss one. Their contribution for the

total joint shear strength has been investigated. The theory can then explain all the Code prescriptions and be applied to generalized joint problem. The Eurocode, similar to the Italian code, and ACI 318M code provisions have been compared and the main points have been underlined. A test structural joint element has been defined and designed according to the Italian and European actual Code for seismic zone of 0.35g peak ground accelerations. By means of an improved academic program and another two commercial ones the problem of the accurate numerical analysis of reinforced concrete has been faced. Some preliminaries validation examples have been carried out comparing the numerical results with the experimental ones. Using two dimensional and three dimensional models, it has been possible to evaluate efficiently and accurately the behaviour of the designed reinforced concrete test joint. The numerical analyses have shown all the features and the issues underlined by the theory. The numerical results have been compared qualitatively and quantitatively with the ones obtained by theoretical simplified schemes showing a good agreement.

Starting from theoretical considerations some new CSTC joints have been proposed. The main aim was to reach an adequate stiffness, strength and ductility in sight of the application on seismic resistant frames. The similarity of the resisting mechanisms has permitted the extension of the RC theory to the joint shear resistant of the CSTC structural type. The calculation of the proposed joint started with the investigations of possible admissible stress distribution within the joint and it follows with their quantitative evaluations. By means of the numerical model studied and validated on the RC structures, the analysis of a designed joint have been carried out. Both two dimensional and three dimensional analysis results have been presented along with their comparison with the RC joint ones. Even if the numerical analyses have convergence difficulties for large cyclic displacements, they show the achievement of important targets as the joint stiffness, the joint strength and the joint ductility. From the comparison with the RC joint numerical results, it can be noted that, the dissipated energy being equal, the elastic energy stored in the CSTC joint is higher than the RC one. This fact turned out in a narrower hysteresis cycles of the CSTC joint. This behaviour is conditioned by the presence of the lower concrete base and by the lower chord bars of the beam trusses. A part for these conditions inherent to the CSTC structural type, the designed joint showed a good cyclic behaviour and its ductility is similar to the RC one, whereas its strength and stiffness are higher. The results confirm a good efficiency of the proposed CSTC joint. All the proposed joints can be proposed profitably for future experimental tests in order to verify the numerical results and in sight of a possible application in seismic regions.

As a final purpose, an innovative composite beam-column joint has been studied for applications in medium-low seismicity regions. The joint connects composite steel truss and

concrete beams and concrete filled steel tube columns. The main concept of this joint is to conserve the continuity of the column steel tube between one storey and the following one by means of blind cold connection. Additional elements, which passes through the joint to restore the beam continuity, have been proposed: the upper horizontal bars and a vertical steel plate. Furthermore the lower beam plate is bolted together to an additional one welded to the external surface of the column steel tube. The connections, that require little manpower work in the construction site, are only normal, blind and welded bolts to reduce the number of operations and the working time. The concrete cast inside the column steel tube can be continuous thanks to the avoidance of any interruptions crossing the beams. The number of holes in the column steel tube is reduced to the minimum. The resulting joint is a special kind of composite steel and concrete structure in which the steel and the concrete collaborate to sustain the solicitations. The assessment of the joint has been made using the Eurocode 3 and 4. The verification of the joint behaviour has been done by means of numerical analyses. Increasing the displacement amplitude, the numerical analyses are affected by convergence problem dealing with the softening behaviour of the concrete material. The joint shows a good initial stiffness and strength even if the additional members, that cross the joint. After load cycle reversals the stiffness decays as expected because of the absence of bond within the column. Nevertheless the results show a good deformation capacity and joint strength. Even this novel joint can be proposed for future experimental tests in order to verify the numerical results in sight of a possible application in medium-low seismicity regions.

Acknowledgements

The collaboration with Professor Renato Vitaliani and Researcher Roberto Scotta has been extremely enriching and stimulating. They have injected enthusiasm for the research into me. They have always thought me the scientific method with their helpfulness and attention.

The opportunity of the visit in Berkeley has been made possible thanks to Professor Filip Filippou, who has distinguished for kindness in welcoming me and for commendable support. I hope that the promising collaboration will continue profitably.

The funding of the PhD scholarship has been offered by Edis s.r.l. It has the praiseworthy merit to believe in the partnership between university research and company in order to achieve the scientific and technological progress.

The experimental tests has been carried out thanks to the effective assistance of Tecnostrutture s.r.l. that has provided the test structures and their technical support.

It has been pleasant to collaborate with the engineers Francesco Zanon, Filippo Franzolin, Mauro Roncaglia, Paolo Magaraggia, Stefano Organo, Riccardo Zen and Davide Ceccato.

The colleague, and very good friend, Giuseppe Olivato has kindly helped me to obtain the final layout of the present work.

I want to thank heartily my father Lanfranco, my brother Leonardo, my grandmother Antonia, my aunt Candida and my friend Veronique. All of them have accompanied me with their love, help and encouragement in this experience.

In the end I'd like to thank very much Enrico, Paola, Antonia, Laura, Laros, Isacco, Francesca, Andrea and Alberto for their sincere friendship.